DESIGN OF ELECTRODE COATINGS FOR BIMETALLIC WELDS

A thesis submitted in partial fulfilment
of the requirement for the award of the degree of

Doctor of Philosophy
in
Mechanical Engineering

Submitted By

DEEPAK BHANDARI

(Regd. No. 950808001)

Under the guidance of

Dr. Rahul Chhibber
Assistant Professor
Department of Mechanical Engineering
Indian Institute of Technology Jodhpur
Jodhpur.

Dr. Navneet Arora
Professor
Department of Mechanical & Industrial Engineering
Indian Institute of Technology Roorkee
Roorkee.

Dr. Rajeev Mehta
Professor
Department of Chemical Engineering
Thapar University
Patiala

DEPARTMENT OF MECHANICAL ENGINEERING
THAPAR UNIVERSITY
PATIALA-147004

April 2017

CERTIFICATE

This is to certify that the thesis entitled "Design of Electrode Coatings for Bimetallic welds", being submitted by Mr. Deepak Bhandari in fulfillment of the requirements for the degree of DOCTOR OF PHILOSOPHY to the Thapar University, Patiala is a record of the candidate's own work carried out by him under our supervision and guidance. The matter embodied in this thesis has not been submitted in part or full to any other university or institution for the award of any degree.

Rahul Chhibber

Dr. Rahul Chhibber
Assistant Professor
Department of Mechanical Engineering
Indian Institute of Technology Jodhpur
Jodhpur

Navneet Arora

Dr. Navneet Arora
Professor
Department of Mechanical and Industrial Engineering
Indian Institute of Technology Roorkee
Roorkee

Rajeev Mehta

Dr. Rajeev Mehta
Professor
Department of Chemical Engineering
Thapar University
Patiala

ACKNOWLEDGEMENT

I wish to express my sincere appreciation to those who have contributed to this thesis and supported me in one way or the other during this amazing journey.

Firstly, I would like to express my sincere gratitude to my supervisors: **Dr. Rahul Chhibber**, Assistant Professor, Department of Mechanical Engineering, Indian Institute of Technology (IIT) Jodhpur, Jodhpur, Rajasthan; **Dr. Navneet Arora**, Professor, Department of Mechanical and Industrial Engineering, Indian Institute of Technology (IIT) Roorkee, Roorkee, Uttrakhand and **Dr. Rajeev Mehta**, Professor, Department of Chemical Engineering, Thapar University, Patiala, Punjab for their continuous support of my Ph.D research work, for their motivation, patience and immense knowledge. Their guidance helped me in all the time of research and writing of this thesis.

Besides my supervisors, I would like to thank the members of my doctoral research committee for their insightful comments and encouragement which incented me to widen my research from various perspectives.

I gratefully acknowledge the Steel Authority of India Ltd. and Jindal Stainless Ltd., Hisar for providing the base materials for the research work on complimentary basis. I would also like to thank the lab staff for their help during the research work.

I would like to thank my family from the bottom of my heart who were always there as supporting pillars. I am extremely indebted to my parents for their constant unconditional support while completing this research work. I am also thankful to my wife and my kids for encouraging and supporting me in all my pursuits.

Finally, I thank God for his grace and mercy; and letting me through all the difficulties.

(DEEPAK BHANDARI)

ABSTRACT

The use of bimetallic welds between plain carbon steel and austenitic stainless steel being in nuclear power plants imposes a challenge towards the structural integrity assessment for researchers not only due to the different metallurgical zones, having a gradient in chemistry and mechanical properties but also due to the high temperature operating conditions and the temperature variations over the period of operation.

In the bimetallic welds the use of Ni-base weld metal significantly decreases the extent of carbon migration from the ferritic steel into the weld, because of the low carbon activity gradient between the ferritic steel and the weld metal, and the low diffusivity of carbon in Ni-base alloys. Hence, the Ni-base weld metals are commonly used for fabrication and repair of bimetallic weld joints. The only drawback of Ni-base weld metal is their inferior weldability compared to austenitic stainless steels, as a consequence, there are fewer welders qualified to weld with it. Further, the nuclear welds with Ni-base welds metals are also not immune to failure, and service failure of these nuclear welds have also been reported. Nucleation and propagation of creep cracks along a planar array of globular carbides formed during service have been considered responsible for many such failures.

The difference in melting temperatures of the two metals that are to be joined must always be considered. Solidification and contraction of the metal with the higher melting temperature will induce stresses in the other metal while it is in a weak, partially solidified condition. This problem may be solved by depositing one or more layers of a filler intermediate melting temperature on the face of the base metal with the higher melting temperature. This procedure is known as buttering. The weld is then made between the buttered face other base metal. The buttering layer should serve to reduce the melting temperature differential. Buttering may also be used to provide a transition between materials with substantially different coefficients of thermal expansion and to act as a barrier layer that will slow the migration of undesirable elements from the base metal to the weld metal during service at elevated temperatures. The work in this thesis is aimed at developing electrode coatings for bimetallic welds and providing a comparative assessment of the three layer and two layer approaches involving mild steel and stainless steel buttering layers.

TABLE OF CONTENTS

LIST OF TABLES

LIST OF FIGURES

CHAPTER 1
INTRODUCTION

1.0 Introduction

With the development of new alloys and the advances in their wide critical applications, there is always a need of formulation of electrode coatings for shielded metal arc welding (SMAW) process. The design and development of welding electrode coating for a weldment with good properties is often difficult due to complex interaction mechanisms taking place during welding. The design of welding electrode coatings involves expensive and time intensive experimental trials, characterizations and optimizations generally based on trial and error. The electrode coating formulations may or may not be optimum, since it is not practical to explore all combinations of compositional and process variations due to the cost and time limitations.

Bimetallic welds have been a necessity within the pressurized water reactor and boiling water reactor designs, where the heavy section low alloy steel components are connected to stainless steel primary piping systems. There are certain issues which need to be addressed while welding the bimetallic joints due to the variance in the properties of base metals. Mixture design experiments account for the dependence of response on proportionality of ingredients and involve the experimentation design of experiments on the condition that the proportions of the different ingredients in a mixture must sum to one. The purpose of experimentation with mixture design methodology is to model the measured response with some form of mathematical equation.

The work in this thesis aims to contribute towards generating a large experimental database for building a broad research base for those working in this field of electrode coating design using a much scientific mixture design methodology and design of fluxes based on phase diagrams. The comparison of two layer and three approaches provides a new dimension to fabrication of bimetallic welds.

1.1 Organization of the thesis

This thesis is organized into six chapters and the essence of each chapter is detailed below:

The **Chapter 1** outlines the introduction to the research topic and the organization of the thesis.

The **Chapter 2** provides a detailed literature survey on the investigations carried out by various researchers for the development of electrode coatings for similar and dissimilar materials and the welding processes used.

The **Chapter 3** deals with the problem formulation. The need of the research is highlighted; the research objectives are identified and the research plan is discussed.

The **Chapter 4** discusses the experimental design. It explains the use of phase diagram systems to decide the compositions of the electrode coating ingredients. It describes the mixture design methodology to develop the mixture design matrix. The chapter also discusses the manufacturing of welding electrodes and the weld characterization procedure adopted.

The **Chapter 5** presents the various results or weld responses obtained as per the testing carried out using the design matrices. The regression models of weld responses have been developed and the regression analysis has been discussed in this chapter. Multi-objective optimization has been used to derive optimized set of coating compositions.This chapter also discusses the microstructural, chemical composition analysis and mechanical behavior characterization of bimetallic welds made using two and three layer approach is described.

The **Chapter 6** presents the conclusions of the research work and suggests the scope for further research in the area.

CHAPTER 2
LITERATURE SURVEY

2.1 Introduction

This chapter presents a comprehensive literature survey related to the topic of research which includes SMAW process and its characteristics, issues related to bimetallic welds and the processes used for bimetallic joints. Design of experiment (DOE) with emphasis on extreme vertices design methodology has been discussed. The gaps in the research field and scope of research have also been identified.

2.2 Shielded Metal Arc Welding Process

Shielded metal arc welding (SMAW) process is the most widely used arc welding process all over the world because of versatility in its process, simplicity in its operation and ease of handling its equipment (Figure 2.2.1). It is being used to join wide variety of ferrous and nonferrous metals (Figure 2.2.2).

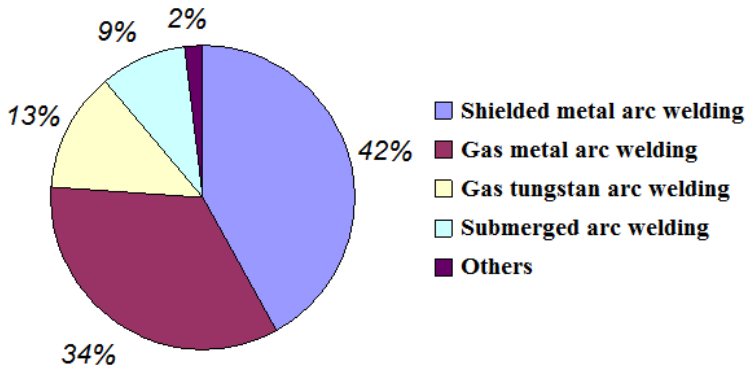

Figure 2.2.1 Pictorial depiction of percentage use of arc welding processes (Sacks and Bohnart, 2004 [131]).

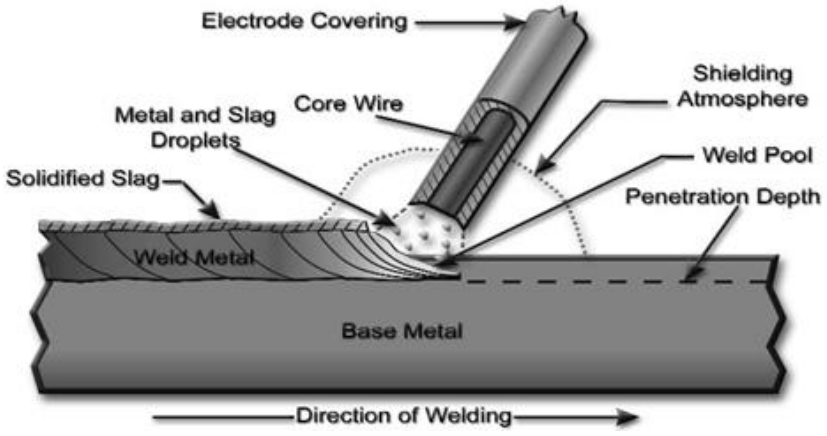

Figure 2.2.2 Shielded metal arc welding process (Schematic diagram).

2.2.1 Historical background and development

In mid-1920's, Oscar Kjellberg of Sweden produced a coated electrode by dipping short lengths of bare iron wire in thick mixtures of carbonates and silicates, and allowing the coating to dry. More improvements in applying the coating on the bare metal electrodes were achieved in the successive years by the researchers. In 1927, Langstroth and Wunder of the A.O. Smith Company developed the coated electrodes with extrusion process. Lincoln Electric Company started producing extruded coated electrodes in 1929.

2.3 Components of SMAW Process

The Figure 2.3.1 shows the electric circuit used in the SMAW process and depicts the major components used in the process. This circuit begins with the electric power source and includes the electrode welding cable, electrode holder, welding electrode and work pieces connected to the earth cable of the power source.

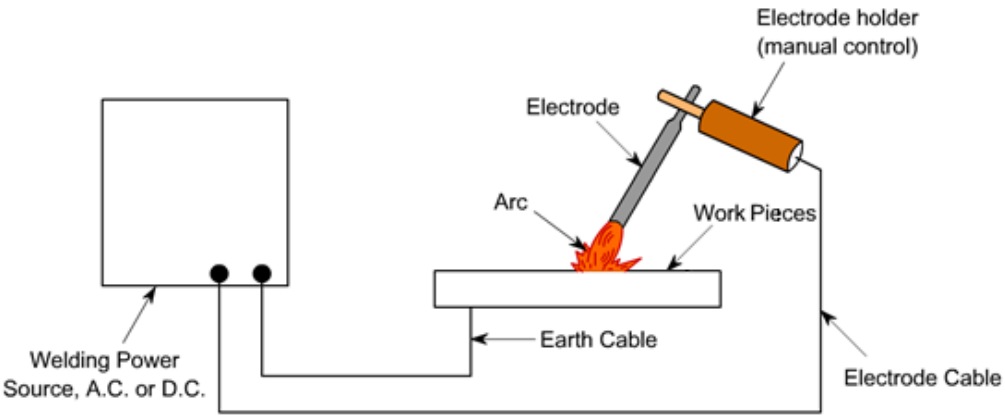

Figure 2.3.1 Circuit diagram of shielded metal arc welding process.

2.3.1 Power source

SMAW process requires electric power of relatively low voltage and high current to produce and sustain an arc capable of making a good weld. Machine designed to deliver such electric power is known as power source for arc welding. The drooping or constant current (CC) or falling characteristic type power source is used for SMAW process. The highest voltage is the open circuit voltage of the power source. Once the arc is struck the voltage rapidly falls as the gases in the arc gap become ionised and electrically conductive, the electrode heats up and the size of the arc column increases as shown in Figure 2.3.2. As the arc length changes both the voltage and welding current also change– a longer arc giving higher voltage but with a

corresponding drop in welding current and vice versa. When welding is taking place the arc length is continually changing as the welder cannot maintain a constant arc length. With a constant current power source as the arc length changes due to the welder's manipulation of the welding electrode holder there is only a small change in the welding current. The steeper the curve the smaller the change in current and a stable welding condition is achieved for weld beads of uniform in size and shape.

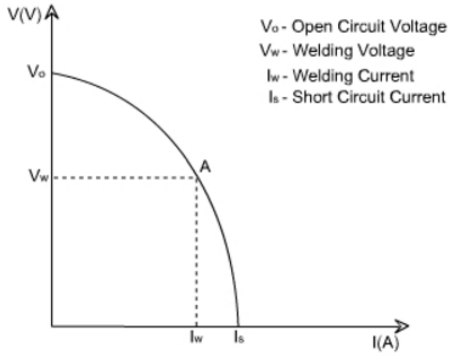

Figure 2.3.2 Volt-ampere characteristics of constant current power source.

Electrode can be operated with alternating current (AC) and direct current (DC) power source and its selection depends on the type of base metals and the electrode coatings used. For the sheet metal work, DC power source is preferred because it is easier to strike and maintain the DC arc at low currents. Figure 2.3.3 (a) to (c) show the effect of welding current on weld bead appearance. It can be seen that large amperage causes high spatter whereas low current causes sticking of the electrode and smaller penetration.

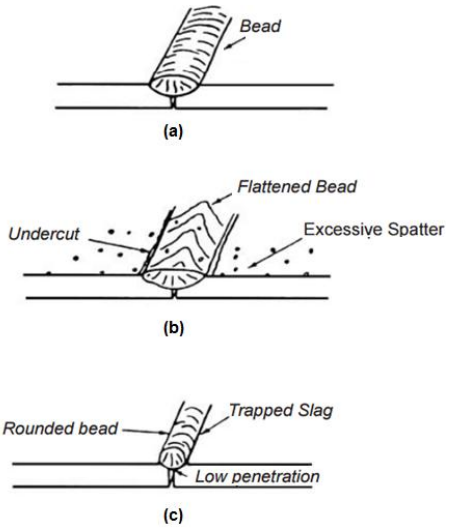

Figure 2.3.3 Schematic diagram of weld bead at different welding currents (a) correct current, (b) current too high and (c) current too low.

2.3.2 Coated electrodes

Coated welding electrodes used in SMAW process consist of only two major elements-the core wire and the flux or electrode coating. The composition of core wire is generally similar and sometimes identical to that of the base material. It also depends upon the required properties of the resulting weld. The raw material for the core wire is hot-rolled rod. It is received in large coils, cleaned, drawn down to the proper electrode diameter, straightened and cut to the proper electrode length.

American Welding Society (AWS) defines the flux or electrode coating as a material used to prevent, dissolve or facilitate removal of oxides and other undesirable substances. It comprises of a wide range of electrode coating ingredients and alloying elements having some specific function during welding. The important functions of an electrode coating can be summarized as below:

- It helps to strike and maintain the arc.
- It shields the weld metal by displacing the atmospheric oxygen and nitrogen.
- It produces slag which further protects the molten droplets in the arc and the molten weld puddle from atmospheric attack, and also provides the insulating blanket over the weld bead.
- It helps to refine the metal.
- It helps to modify the chemistry and hence the mechanical properties by providing alloying elements for the weld metal.
- It helps to reduce spatter.
- It insulates the electrode.
- It makes vertical and overhead welding possible by controlling the viscosity of the slag.

Electrode coating plays an important role in deciding the weld metal quality. It affects the weld metal physically, chemically and metallurgically. Physically, it influences the bead geometry and shape relationships, which in turn affects the load carrying capacity of the weldment. Chemically, it affects the chemistry of the weld metal, which further influences the mechanical properties like toughness, hardness, tensile strength etc. of the weld metal. Metallurgically, it determines the grain structure and hence again affects the properties of the weld metal.

2.3.3 Materials to be welded

Materials that can be welded with SMAW may be either of similar or dissimilar type. As per welding metallurgy, the coated electrode is designed to match the mechanical properties and chemical composition of the base metal as closely as possible. Quite often, the matching of the mechanical properties is the major consideration, and therefore the weld-metal chemistry varies to some reasonable extent from the base-metal chemistry.

2.4 Electrode Coating Ingredients and Their Functions

Arc Stabilizers: Air is not sufficiently conductive to maintain a stable arc. So to provide a conductive path for the flow of current, arc stabilizers like titanium compounds, potassium compounds, and calcium compounds are used in flux coatings.

Slag Formers: These ingredients are used primarily to give body to the slag and impart properties such as slag viscosity, surface tension, and melting point. Silica, CaO, fluorspar and magnetite are materials of this type.

Alloying Elements: Alloying elements such as molybdenum, chromium, nickel, manganese and others impart specific mechanical properties to the weld metal.

Binding Agents: Soluble silicates such as sodium and potassium silicates are used in the electrode coating as binding agents. They form a plastic mass of coating material capable of being extruded and baked. They are also used to make coating nonflammable and avoid premature decomposition.

Gas Forming Materials: Common gas forming materials used are the carbohydrates, hydrates, and carbonates. These materials evolve carbon dioxide (CO_2), carbon monoxide (CO) etc. at the high temperature of the welding arc.

Slipping Agents: These are used for easy extrusion. Common slipping agents include glycerin, china clay, talc, mica, bentonite clay.

2.5 Types of Electrode Coatings

The operational characteristics of welding electrodes arc stability, slag formation, slag detachability, interfacial tension, deposition rate depth of penetration, metal deposition rate and positional capability are greatly influenced by the chemical composition of the electrode coatings on the electrode. Depending on the types of electrode coating, the electrodes can be of cellulosic, rutile and basic types.

Cellulosic type of electrodes contain a high proportion of cellulose in the coating and are characterized by a deeply penetrating arc with rapid burn-off rate thus giving high welding speeds. Weld deposits have fluid slag with poor slag detachability. These electrodes are easy to use in any position, have reasonably good mechanical properties but higher risks of hydrogen assisted cracking.

Rutile electrodes contain a high proportion of titanium oxide (rutile) in the coating. Titanium oxide assists in easy arc ignition, smooth arc operation and low spatter. These electrodes are general purpose electrodes with good welding properties. They can be used with AC and DC power sources and in all positions. They exhibit good bead profile through the viscous slag and ease slag removal characteristics.

Basic electrodes have high proportion of calcium carbonate (limestone) and calcium fluoride (fluorspar) in the coatings. These coating ingredients reduce the slag viscosity. These electrodes are also fast-freezing which assists welding in the vertical and overhead position. These electrodes show higher weld quality, good mechanical properties and resistance to cracking.

2.6 Design and Development of Electrode Coatings

Bhandari et al., 2012, 2016 [12, 13] have studied the effect of composition of electrode coatings on weld metal chemistry & mechanical behavior of bimetallic welds. The ability to design and optimize welding electrode coatings in a reliable and efficient manner is very crucial for any welding industry to remain competitive in a global marketplace. With the development of new alloys and the advances in their critical applications, there is always a need of formulation of electrode coatings in SMAW process.

Researchers have tried to examine the percentage composition variations in electrode coating ingredients, nature of chemical reactions and element transfer mechanisms during arc welding processes. The individual as well as interaction behaviour of electrode coating ingredients during welding must be established for obtaining high quality weld.

Thus, the physicochemical properties of the electrode coating ingredients such as the bulk density, flowability, hygroscopic nature, melting point, surface tension, viscosity and electrical conductivity that affect the weld pool chemistry significantly are of

utmost importance in the design and development of welding electrodes. Some of the important operational characteristics of electrodes coatings and physicochemical properties are discussed in the following sub-sections.

2.6.1 Slag formation

Slag is a layer of glassy and various crystalline phases formed over the weld. It is highly required that the slag should remain in molten state and cover the molten weld pool throughout the time the weld pool is in liquid state. To accomplish this, the formulation of electrode coatings are designed in such a manner that their composite melting temperature remain below the melting temperature of the weld metal so as to provide the protective shielding around the molten weld pool. The density of slag is kept lower than the molten weld in order to float above the molten metal and avoid the slag entrapment in the weld metal (Natalie et al., 1986 [113]; Jackson et al., 1973 [60]).

The slag viscosity must be adequate in the weld metal melting temperature range to completely cover and protect the molten weld pool during welding. Slag viscosity significantly influences the operability of the welding electrode (Kalisz, 2013 [74]). It also affects the adhesion of the slag to the metal. Slag viscosity is of great importance because if it is too low, slag can flow in front of the weld pool and cause operability problems. It will also result in the formation of small pockets of weld metal which have been exposed to atmosphere because the molten slag move away from the top of the weld bead. Too high slag viscosity retards the diffusion rate and slag-metal reactions at the weld-slag interface (Belton et al., 1963 [5]). It may result in entrapment of gases and contribute to various surface defects like pocking. So, the viscosity of slag must be sufficient enough to provide impermeability to atmospheric gases and non-metallic inclusions in the weld; and to prevent slag from running away from the molten weld pool and flowing in front of arc.

The slag viscosity also affects the weld bead morphology. High viscosity tends to confine the weld pool, thus increasing the heat input for a given area and resulting in deeper penetration (Kuzmenko, 1985 [93]). The electrode coating that generates more viscous slag is preferred for vertical and overhead welding to assist in reinforcing and protecting the weld pool while that of low viscosity is desirable for high welding

speed. Tarlinsku, 1980 [148] suggested the suitable range of slag viscosity for the satisfactory welds between 22-35 poise at the temperature range of 1450-1550°C.

The electrode coating that possess silica (SiO_2) exhibits high viscosity due to the formation of three dimensional tetrahedron network structure of silicate ions (SiO_4^{4-}) in the slag (Liu et al., 1994 [100]). The silicate tetrahedron consists of four nearly close packed oxygen atoms surrounding a small silicon atom. These SiO_4^{4-}- tetrahedra can share corners with each other forming networks. The bonds shared between these tetrahedra are high strength bonds and cause silica melts to exhibit a high viscosity. When a divalent metal oxide is added to this silicate network, the metal ion will form weak bonds between the silicate tetrahedrons and further disrupt the network, causing the viscosity to decrease. The bond strength between the metal ions and the silica tetrahedra will vary depending on the metal oxide added (Schwemmer and Olson, 1979 [133]). Fluorides tend to decrease the viscosity of the slag by ionizing and breaking down the network of silicate ions (Weymueller, 1981 [157]).

It has been reported by Ferrera and Olson, 1975 [46] that manganese oxide decreases the slag viscosity. De Rissone et al., 2002 [35] revealed that calcium oxide in electrode coatings decrease the slag viscosity. It was also observed that the slag becomes more thick and redundant at the higher amounts of calcium oxide while its lower levels assisted in the formation of well shaped beads.

2.6.2 Slag detachability

Slag detachability is the ease with which the slag can be detached from the weld metal after solidification. It affects the integrity of multi-pass weldments and the productivity of the welding process. Slag detachability is dependent on the physical and chemical properties of the ingredients of the electrode coatings. The difference between the coefficient of thermal expansion of the slag and the metal is an important factor to be considered for the slag removal (Vornovitskii, 1973, 1975 [153, 154]). For good slag detachability, it is desirable to have a slag with coefficient of thermal expansion different from that of the weld metal. It has been reported that more is this difference, better will the slag detachability (Nadkarni, 1988 [111]).

Slag detachability is affected by the differential thermal contraction during welding. The differential thermal contraction is the temperature difference between slag and

the weld metal at their bonding interface. High differential thermal contraction and relatively slow cooling rates to optimize slag detachability.

Rutile based electrode coating produces slag that exhibits good detachability while the While in basic flux systems the slag removal is more difficult. An increase in the alumina, zirconia and corundum in the coating composition has shown improved slag detachability (Bennett, 1970[6]). The calcium fluoride shows the deleterious effect on detachability due to cuspidine formation and its interaction with silica. Slag containing spinels and cordierite glass phase been reported to be difficult to remove.

2.6.3 Interfacial tension

It is the surface tension at interface of molten slag and the weld metal. It influences the protection of the weld pool from atmospheric contamination. Too high interfacial tension causes the undercut in weld thus affecting the quality of the weld. Too low interfacial tension, results in extensive spreading of the molten slag on metal substrate which may cause poor slag detachability (Hazlett, 1957 [58]). Low value of surface tension promotes better bead profile of weld metal and good separation of slag from molten metal. It has also been found that high interfacial tension causes an increase in penetration depth in weld. Komapov, 1983 [84]) investigated the effects of surface tension of steels and fluxes on shape of deposited metal.

2.6.4 Arc stability

The stability of the welding arc which is produced by a SMAW electrode is very important for creating sound welds. It affects the initiation and maintenance of welding arc during welding and even the weld bead morphology (Patchett, 1974 [126]). If the welding electrode melts inconsistently, it will cause sporadic metal transfer which leads to increased defects and discontinuities (Gaal, 2012 [49]). The most unfavourable results of poor arc stability are spatters which are problematic in terms of material losses, extension of production times due to cleaning, as well as unaesthetic appearance (Suban and Tusek, 2003 [141]). The various weld defects due to low arc stability has been highlighted by (Niagaj, 2002 [114]).

The arc stability of the welding process is affected by numerous parameters. When an electrode is eccentric, the filler metal core wire is not centered in the electrode coating causing the thinner side of the coating to burn away faster and the arc to blow out on that side. This causes the arc to widen and wander producing an unacceptable weld

bead. Arc stability is very vital in alternating current (AC) power source as the welding arc is extinguished and re-established a number of times per second (Sham and Liu, 2014 [134]).

The arc stability of the welding arc is dependent on the ionization potential or ionization energy of the atoms within the arc plasma. The ionization energy is the energy required to remove one electron from an isolated, gas-phase atom, when this atom is not hooked up to others like in a solid or a liquid phase. The welding electrodes that have lower ionization potential produces more stable arc because the electrons are emitted at lower energies (Sham and Liu, 2014 [134]). Some ingredients like potassium silicate, sodium silicate, rutile and potassium titanate improve the electric conductivity in the arc region to improve the arc ignition and stabilization of the arc (Natalie et al., 1986 [113]). Potassium silicate used as a binder in the electrode coating, also plays a critical role in the stabilization of the arc in AC power source applications because of lower value (4.34eV) of ionization energy of potassium. Sodium ionizes at 5.14eV and is preferably used as the binder for arc stabilizer of DC applications where the arc is not extinguished and re-established as in the case of AC applications (Liu et al., 1994 [100]).

Hazlett and Parker, 1956 [57] found that weld made under a lime based coating resulted in smooth running arcs with high stability. Ferrera and Olson, 1975 [46] studied the MnO-SiO_2-CaO phase system and observed that the additions of calcium oxide (CaO) to the manganese silicate flux could improve the arc stability. The effect of CaO with the addition of wollastonite (calcium silicate containing 50% CaO/50% SiO_2) in the electrode coating to improve arc stability has also been reported by De Rissone et al., 1997 [34]. The addition of alloying elements like magnesium improves the arc stability (Farias et al., 1997 [45]). It has also been reported that the addition of fluorides of calcium and magnesium causes arc instability (Witting, 1980 [158]) while potassium oxalate and lithium carbonate enhances the arc stability (Nadkarni, 1988 [111]).

2.6.5 Electrode deposition rate

The electrode deposition rate helps to estimate the deposition efficiency by comparing the weight of weld metal to weight of the welding electrode. The higher current and addition of alloy powders in coating result in higher electrode deposition rate. The use

of higher deposition rate electrodes decreases the total cost as labour costs decrease with its use.

2.6.6 Weld metal chemistry

Weld metal chemistry is an important factor in determining the mechanical and metallurgical properties of the weld (Davis, 1977 [33]; Kou, 2002 [86]; Palm, 1972 [116]; Polar, 1991 [127]; Tuliani, 1972 [150]). The final weld deposit composition is the end-point of a complex interplay of various physical and chemical factors (North et al., 1978 [115]). The overall weld metal chemistry is controlled by the composition of the metal droplets that enter the weld pool and by the amount of dilution of the weld pool by the base plates.

There are four separate zones at which the thermochemical reactions take place namely the melted electrode tip, the detached droplet, the molten weld pool immediately below the arc, and the solidifying weld pool behind the arc. Researchers had investigated microstructure development during solidification of stainless steel alloys (Bhaduri et al., 1988 [11]; Kacar and Baylan, 2004 [73]). These reactions tend to move the weld metal chemistry in the direction of chemical equilibrium. The most important chemical considerations include the control of oxygen, oxidation losses of alloy elements, and the pickup of elements from the slag. The main source of oxygen during welding is the decomposition of electrode coatings ingredients. In the high temperature environment near the arc, it is suggested that all oxides are susceptible to decomposition and produce oxygen.

$$SiO_2 \rightarrow SiO(g) + 1/2O_2(g) \quad (2.6.1)$$

$$MnO \rightarrow Mn(g) + 1/2O_2(g) \quad (2.6.2)$$

Presence of oxygen in arc environment not only increases chances of oxide inclusion formation tendency but also affects the element transfer efficiency from electrode to weld pool due to oxidation of alloying elements as shown in Figure 2.6.1. Melting of electrode and coating and then transfer of the elements from the electrode across the arc zone causes the oxidation of some of the highly reactive elements which may be removed in form of slag (NPTEL, [115a]). Thus transfer of especially reactive elements to weld pool is reduced which in turn affects the weld metal composition and so mechanical and other performance characteristics of weld.

$$Mn + O \rightarrow MnO \quad (2.6.3)$$

$Si+2O \rightarrow SiO_2$ (2.6.4)

$Ti+2O \rightarrow TiO_2$ (2.6.5)

$2Al+3O \rightarrow Al_2O_3$ (2.6.6)

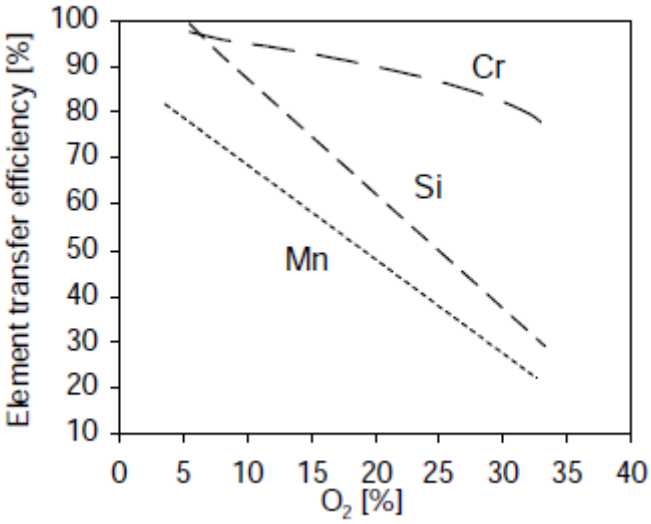

Figure 2.6.1 Variation of element transfer with oxygen content of weld (NPTEL, [115a]).

The electrochemical reactions also occur only at the melted electrode tip and in the molten weld pool immediately below the arc. The electrochemical reactions occur due to ionic conduction of a portion of the welding current through the molten slag layer. Kozyrev et al., 2015, 2016a, 2016b [87-89] have investigated some aspects of oxidation reduction reactions under carbon bearing flux welding. Butler, 1967 [14] studied SAW characteristics of CaO-TiO_2–SiO_2 system. Blander and Olson, 1986 [14] postulated electrochemical mechanism reactions that occur when direct current is used in welding. Chai and Eagar, 1981 [25] presented a thermodynamic model of the equilibrium existing between the slag and the weld metal during submerged arc welding. The model was applied to neutral fluxes containing less than 20% CaF_2. The developed model was capable of predicting gain or loss of both Mn and Si over a wide range of base plate, electrode and flux compositions.

Chai and Eagar, 1982 [24] in their study highlighted that oxygen in steel weld causes a number of problems including porosity, loss of fracture toughness and reduced ductility. They have shown that CaF_2 tend to reduce the amount of oxygen in the weld. The stability of metal oxides during welding decreases in the following order: CaO, K_2O, Na_2O, TiO_2, Al_2O_3, MgO, SiO_2, MnO. Higher the stability of the fluxes,

lesser will be the decomposition into oxides, thereby providing lesser levels of O_2 in weld-metal.

Mitra et al., 1984 [106] studied the transfer of Cr, Si, Mn, P, S, C, Ni, and Mo between the slag and the weld pool for submerged arc welds made with calcium silicate and manganese silicate fluxes. Seven alloy steel electrodes with varying amount of chromium from 1.37 to 26.31% were used and four different fluxes with varying ingredients CaO, SiO_2, TiO_2, Cr_2O_3, MnO and CaF_2 were developed. The manganese silicate flux produced lower residual sulfur while the calcium silicate fluxes were more effective for the removal of phosphorus from the welds. The effective oxygen reaction temperature lies between 1700^oC and 2000^oC for all elements studied. Evidence of Cr and Mn loss by metal vaporization was also reported. Lime silicate fluxes produced weld metal with a much higher Cr content than manganese silicate flux. The Mn content of the weld metal depends mainly on the amount of manganese oxide in the flux and the initial Mn content of the electrode. Correa, 2010, 2012, 2013 [39-41] studied the effect of weld metal chemistry on stress corrosion cracking behavior of AISI 444 ferritic stainless steel weldments in boiling chloride solution. He investigated the mechanical and microstrutural characterization of weldments of ferritic stainless steel AISI 444 using austenitic stainless steels filler metals.

The chemical reactions taking place between slag and the metal during welding result in compositional changes that affect the properties of the weld (Mitra et al., 1991a, 1991b, 1991c [106-108]; Christensen, 1953 [28]). In the first part, Mitra et al. evaluated and reassessed the existing theories of slag-metal reactions during welding. In second part, a kinetic model was proposed to describe the transfer of alloying elements and to predict the weld metal composition. The authors pointed out that chemical interaction between the slag and weld metal can be understood by dividing the process into three stages comprising reactions within the droplets, within the diluted weld pool, and within the solidifying weld pool. The compositional differences between single pass and multiple pass weld beads could be better explained with the developed kinetic model. It was further reported that the final weld metal oxygen content depends on the weld solidification time along with the type of flux used. Finally, the third part discussed the verification of the kinetic model theory through different experiments.

Paniagua-Mercado et al., 2005, 2007, 2011 [119-121] had worked on chemical and physical properties of fluxes and their influence on microstructure and mechanical properties of submerged arc welds. Researchers (Yusufzai, 2012 [159]) have worked on utilization of waste material for flux design and development.

2.6.7 Metal transfer

Metal transfer is the transfer of molten metal from the tip of the welding electrode to the weld pool. Depending on the welding conditions, there are different ways in which the transfer of metal takes place. These ways are referred to as the modes of metal transfer. The mode of metal transfer is dependent upon the cumulative effect of the different forces acting on the metal droplets. These forces are the gravitational force, electromagnetic force, surface tension and drag force. In SMAW process, due to low current densities employed, the metal transfer takes place mainly by three modes namely short circuit, globular and projected sprays (Parmar, 2008 [124]).

Short circuit transfer occurs, when welding current is very low but high enough to have stable arc and arc gap is small. The molten metal droplet grows slowly at the tip of the electrode and then as soon as drop touches weld pool, short-circuiting takes place. Due to narrow arc gap, molten drop does not attain a size big enough to fall down under gravitational force. Globular metal transfer results when welding current is low but higher than that for short circuit transfer and arc gap is large enough so molten metal droplets can grow slowly with melting of the electrode tip. Drop continues to grow until gravitational force on drop exceeds the surface tension force. At high current, fine metal droplets are propelled across the arc towards the weld pool and spray transfer becomes the predominant mechanism (Liu and Siewert, 1989 [99]). High welding current density results in high melting rate and greater electromagnetic forces. Various metal transfer modes are shown in Figure 2.6.2.

The transfer mode of liquid metal from the electrode tip to the weld pool is often difficult to establish without special experimental techniques because of the fume and slag present (Brandi et al., 1991 [17]). The electrode temperature during welding affects the metal transfer and weld deposit properties. There are many causes for the electrode heating which include the electrical resistance of the electrode, Joule heating the heat of the plasma (Waszink and Piena, 1985 [156]). The heating of the electrode changes the metal droplet transfer size across the arc. At low heating, alloying

elements in the small droplets are easily oxidized to form oxide inclusions and removed from the weld pool as slag. High heating causes larger droplets so the alloying elements are not as easily oxidized, resulting in their higher content in the weld metal (Bracarense and Liu, 1993 [16]).

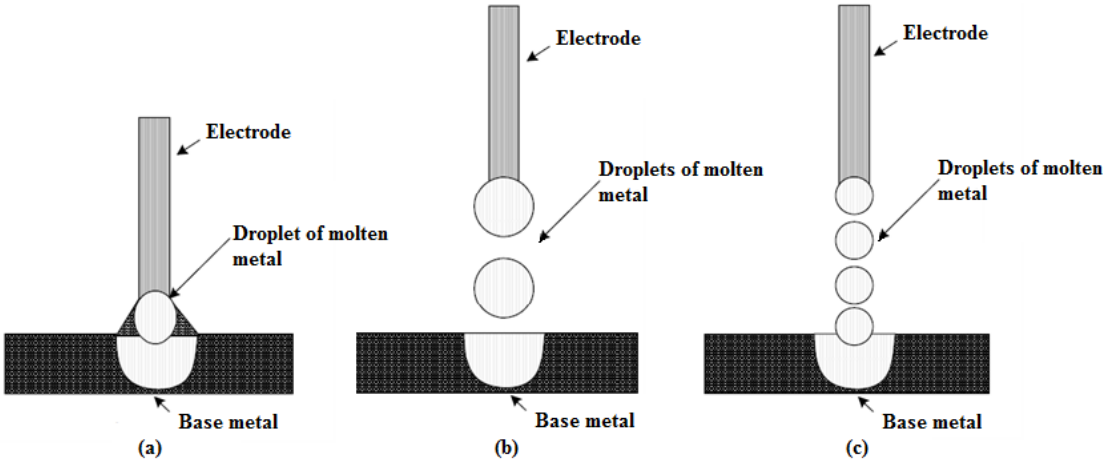

Figure 2.6.2 Metal transfer modes (a) short-circuiting, (b) globular and (c) projected spray.

Yusufzai et al., 2012 [160] investigated the effect of process parameters of gas metal arc welding on dilution in cladding of stainless steel on mild steel. Khan et al., 2011, 2014 [77, 78] studied burst investigation in Zircaloy-4 claddings in inert environment and reviewed failure studies in claddings.

Kanjilal et al., 2004 [76] have developed a quantitative model and verified it to predict weld metal chemistry in terms of flux ingredients at constant heat input using statistical design for mixture. Kanjilal et al., 2006 [75] performed a series of experiments using agglomerated fluxes, prepared by varying the ingredients CaO, MgO, CaF_2 and Al_2O_3. The researchers (Chandel, 1998 [26]; Pandey, 1994 [118]) studied the effect of welding process parameters on the weld metal composition.

2.6.8 Alloying elements

Evans, 1992 [44] established that the transfer of a small amount of titanium into the weld (of the order of 30 ppm) for the fixed 1.4% Mn level in the basic low-hydrogen iron-powder type electrode modified the as-deposited and the reheated microstructures of the weldments. Both the hardness and the tensile properties of the weldments increased with increasing titanium content while two optima impact

toughness values were exhibited, first at 30 ppm of Ti and second in the region of 200 ppm.

Evans, 1993 [43] developed the basic low-hydrogen iron powder-type electrodes (E7018) with the alloying elements titanium in the range from 0 to 3.6% (with 0, 0.4, 1.2, 2.4 and 3.6% levels that could yield 5, 40, 90, 150 and 220 ppm of Ti in the weld deposits respectively) and manganese varying from 0.6 to 1.8%. The weldments microstructure and properties were investigated. It was realized that a delicate balance between Ti and Mn contents must be attained to get their full benefit to weld properties. A complex interaction effect was found between the two elements and titanium showed the marked influence at the higher levels of manganese. The impact toughness was optimized at 35 ppm of Ti and 1.4% Mn. It was remarked that the required increase in hardenability, achieved by manganese to trigger the titanium effect, can also be generated by other major alloying elements.

Surian, 1997 [146] investigated the three rutile electrodes ANSI/AWS A5.1-91 E7024 type, with the addition of 0, 2 and 4% magnesium (Mg) metal powder to the coating at the expense of iron powder, in such a way as to obtain the same levels of Mn and Si in the deposits. Mg powder was chosen for the investigations as it acts a strong deoxidant and is able to decrease oxygen content in weld deposits. It was found that the all-weld-metal oxygen content decreased and impact toughness improved with the increase in magnesium addition in the coatings. Operational behavior was not worsened. Diffusible hydrogen also decreased with the incremental increases in Mg content in electrode coatings. No variation in hardness and tensile properties were reported.

Surian et al., 1999 [145] worked on AWS A5.5-811 E10018M2, E11018M2 and E12018M2 SMAW-type electrodes with the aim to study the behaviour of different alloying elements such as manganese, carbon and chromium on the heat input, the mechanical properties and the microstructure of the weld. The weld metal composition leading to optimum combination of tensile strength and toughness was found. At constant heat input, an increase in Mn, C or Cr individually produced an increase of ultimate tensile strengths and hardness values. Maximum toughness was obtained for Mn content varying between 1.0% and 1.5% at the lowest value of C in the absence of Cr. It was also observed that toughness decreased significantly as C

increased. Manganese and carbon promoted the formation of acicular ferrite, as revealed by microstructural examination at low magnification with the light microscope. The alloying elements in the welding electrode coatings affect the mechanical properties and microstructure of the weld (Surian, 2005 [147]). ANSI/AWS A5.5-96 E10018/11018/12018M type electrodes were chosen for the investigations. The objective of their work was to study the effect of alloying elements Mo, Ni, C and Mn in the ANSI/AWS A5.5-96 E10018/11018/12018M type electrodes on various mechanical, chemical and microstructural properties of the weldments. Eight low-hydrogen iron powder electrodes with coating factor 1.65 were designed and developed by varying the alloying elements in the electrode coatings with four levels (0, 0.25, 0.50, and 0.90%) of Mo, two levels of Mn (1% and 1.5%) and one level of Ni (1.8%). It was observed that hardness and tensile strengths increased as Mo content increased. A progressive refinement of the microstructure was observed in the columnar regions with the increase in Mo and Mn contents. Impact toughness values corresponding to 1% Mn were larger than those of 1.5% Mn, but this difference became smaller as the Mo content increased and was found to be maximum for 1.5% Mn at 0.25% Mo combination of alloying elements. Matsushita, 2000 [103] worked on hydrogen control in steel weld metal by means of fluoride additions in welding flux.

2.7 Extrusion Process for Manufacturing of Electrodes

After deciding the exact percentage composition of electrode coating ingredients, they are carefully weighed and blended in a dry state so as to make the homogeneous mixture. After mixing the binder in the mixture, briquettes are made with the help of briquetting press. The briquettes are fit into a large cylinder in the extrusion press. The coating is extruded over the core wires which are fed through the extrusion press. The diameter of the core wire of an electrode refers to electrode diameter (d). Diameter of electrode with coating (D) with respect to that of core wire (d) is used to characterize the coating thickness as shown in Figure 2.7.1. The ratio of electrode diameter with coating and core diameter is called coating factor.

It is required that the coating thickness must be uniform. If the coating is not concentric to the core wire, it can cause the poor arc direction which results in poor shielding and in inconsistent weld beads with lack of penetration.

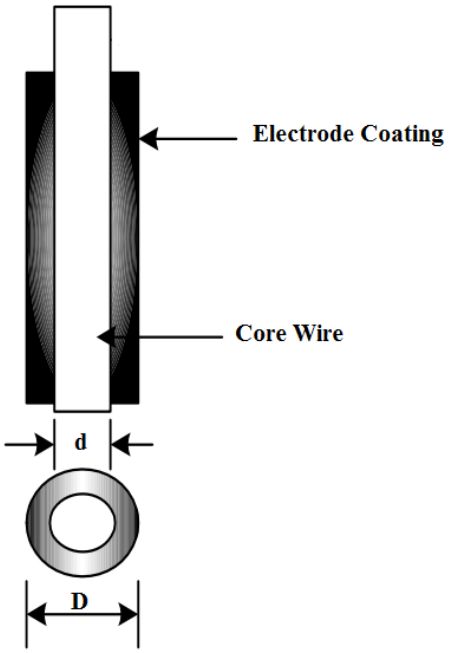

Figure 2.7.1 Schematic diagram of coated welding electrode.

2.8 Need of Bimetallic Welds

Bimetallic welds (BMWs) between low alloy steel components and stainless steel are widely used in nuclear power plants (Haas, 1982 [51]; Klueh and King, 1982 [81]; Klueh et al., 1983 [82]; Maruyama, 2003 [102]; Price, 1982[128]).

For pressurised water reactor, the BMWs, which are of particular interest, are those attaching the piping system to the various nozzles of the reactor pressure vessel (RPV), steam generators and pressuriser (Chhibber et al., 2006 [27]; Blumer et al., 1984 [15]). A sketch of a Combustion Engineering hot-leg surge nozzle shown in Figure 2.8.1 depicts the bimetallic weld between the surge line and the hot-leg surge nozzle. The material of surge line is stainless steel while the hot-leg is made of carbon steel. Thermal sleeves are installed and hot-leg surge nozzles to protect the nozzle wall from thermal transients, which could develop high thermal stresses (IAEA Report, 2003 [59]).

BMWs between ferritic low alloy steels such as SA 508 and austenitic stainless steels such as AISI types 304, 316, etc., as shown in Figure 2.9 are used widely in steam generators of the power plants (Tucker and Eberle, 1956 [149]; Slaughter, 1964 [138]). The requirement of high corrosion resistance, higher creep strength and suitable mechanical behavior at elevated temperatures such as in final stages of super heaters and reheaters, has led to the extensive use of austenitic stainless steels such as

SS 304, SS 304L, 316L,etc. in nuclear power plants (Kiyohoara et al., 2002 [80]; Buckthorpe, 1997, 2002 [18,19]). The use of carbon and low alloy steels, due to their low cost and relatively good mechanical strength, is preferred particularly in the construction of reactor pressure vessels and tubes for use in low temperature sections of nuclear power plants (Arora et al., 2011 [4]; Hadraba, 2009, 2011a, 2011b [52-54]).

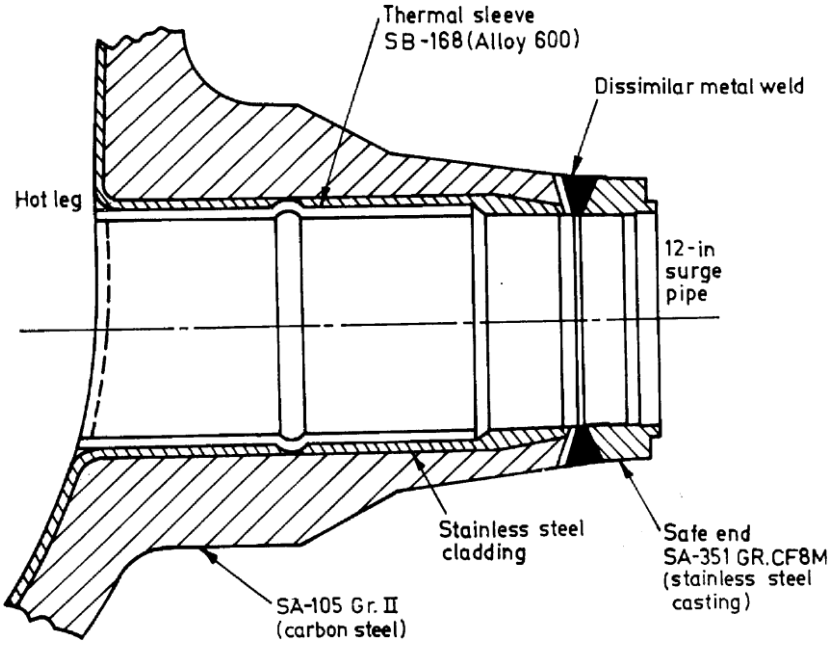

Figure 2.8.1 Typical combustion engineering surge nozzle at the hot leg (IAEA Report, 2003 [59]).

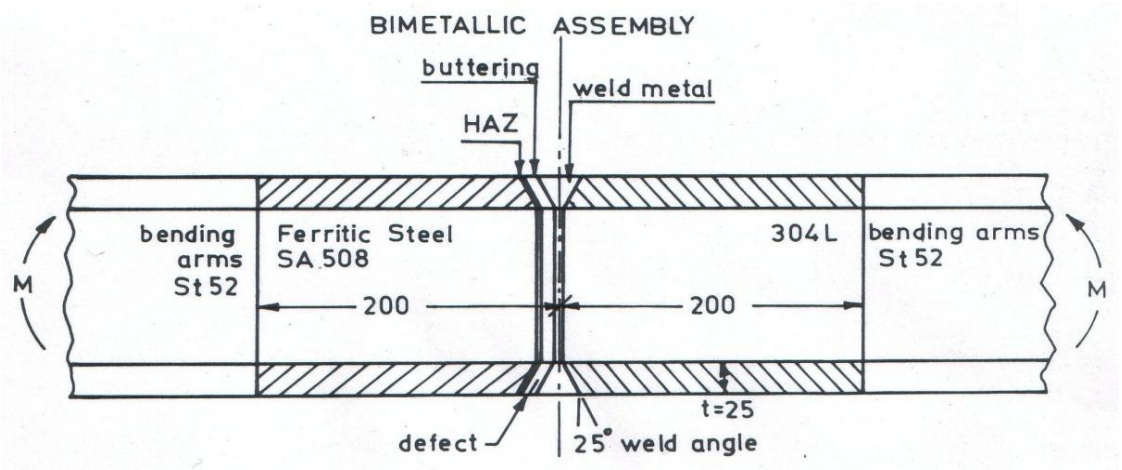

Figure 2.9.0 Ferritic- austentitc bimetallic weld configuration with a buttering layer and different zones (Schwalbe et al., 2004 [132]).

2.9 Issues Related to Bimetallic Welds

2.9.1 Metallurgical problems

The BMWs represent regions or zones with metallurgical discontinuities as shown in Figure 2.9.1. The regions critical for the performance of the BMW (Figure 2.9.1), are the coarse grained heat affected zone (CGHAZ), carbon depleted zone (CDZ), fully austenitic zone (FAZ), the fusion line and its immediate vicinity, and the first buttering layer. Degradation of fusion zone toughness is related to the formation of coarse upper-bainitic CGHAZ micro- structure, as well as a narrow martensitic layer as a result of carbon migration from the ferritic steel towards the austenitic material during welding as suggested by Laukkanen et al., 2001 [96]. The other two zones are the carbon depleted zone and fully austenitic zone.

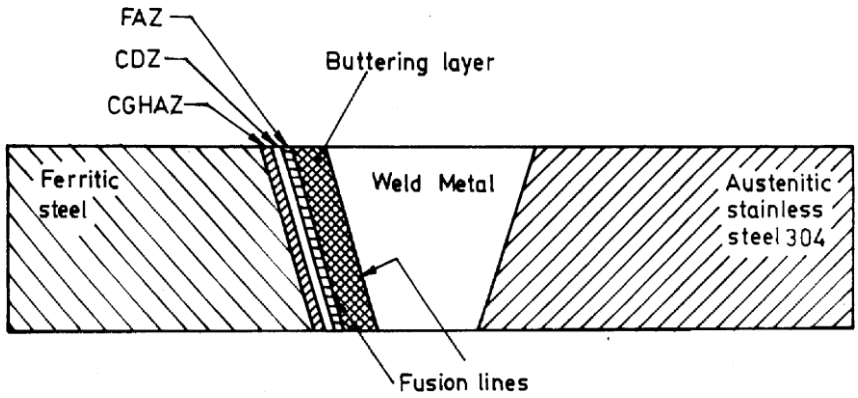

Figure 2.9.1 Bimetallic weld assembly (Chhibber et al., 2006 [27]).

2.9.2 Thermal fatigue

The usual heat-up and cool-down cycles further impose thermal strain on the BMW having stainless steel as filler metal because the thermal expansion coefficients for SS is about 30 percent higher than that for ferritic steel.

2.9.3 Residual stresses

BMWs between ferritic and austenitic steels exhibit a strong residual stress field, both in as welded condition and after PWHT. Knowledge of the residual stress is an essential input to the structural integrity analysis of the joint, particularly where there is a locally embrittled region near the interface (Leggatt and Olden, 2001 [98]).

2.9.4 Atmospheric corrosion

In 1997, in France more than 1000 BMWs (using SS buttering and ferritic-SS weld) were analysed and 50 of them were found to be affected by intergranular degradation on the outer surface in the buttering and close to the ferritic to SS buttering interface.

2.9.5 Solidification cracking (hot cracking)

Hot cracking has been observed in the BMWs that join the hot leg pipes to the RPV nozzle. The hot leg pipes are large diameter, thick wall pipes. Typically, an Inconel weld metal is used to join the ferritic pressure vessel steel to the stainless steel pipe. The austenitic welds, which have 4–10 vol% of delta ferrite and fine dendrites, are resistant to hot cracking, stress and severe impacts during service conditions (Kacar and Baylan, 2004 [73]; Meola et al., 2004 [104]).

2.10 Welding of Bimetallic Joints

In their study King et al., 1977 [79] proposed that joint stress could be reduced considerably by using a transition material alloy 800H with an intermediate coefficient of thermal expansion between the 2-1/4 Cr-1Mo ferritic steel and the type 316 austenitic stainless steel. Various filler metals corresponding to types 309, 312, 347 and 16-8-2 were evaluated for joining alloy 800H to type 316 stainless steel and their relative merits/demerits were highlighted. Weldability studies showed that type 16-8-2 weld metal was the least fissure sensitive while type 347 was the most susceptible to hot cracking. Although type 312 showed little cracking but it contained a relatively large amount of delta ferrite which could transform to sigma phases during high-temperature service.

Lundin, 1982 [101] has revealed areas in which research and evaluation efforts need to be undertaken to better define the transition joint problem. The diffusion of carbon in nickel-based alloys is comparatively lower than in steels. Thus, when the Ni based alloys are used for the joining of the ferritic steels to austenitic stainless steels, the extent of carbon migration from the ferritic steels into the Ni based weld metals is significantly reduced due to decrease in carbon activity gradient and low diffusion coefficient of carbon in nickel-base alloys (Viswanathan et al., 1982 [152]). Although the use of Ni based welding consumables (welding electrodes/fillers) offers improved weld performance, but still service failures in these joints have been reported. It is

realized that bimetallic joints using Ni based welding consumables are not immune to failure.

In bimetallic joints with Ni-base weld metal, the failure predominantly occurs due to cracking along the weld metal/ferritic steel interface (Roberts et al., 1985 [130]). Klueh and King, 1982 [81] performed the metallographic observations on failed and unfailed joints to explain the interface microstructure and subsequent failure mode. It was recommended that transition pieces with intermediate coefficients of thermal expansion between the two dissimilar steels and transition pieces that minimize carbon transfer could be investigated for extending weld joint lifetime.

Tucker and Eberle, 1956 [149] summarized the factors that contribute to dissimilar alloy weld failure as cyclic thermal stresses, low oxidation resistance of the low-alloy ferritic steel, carbon migration and the metallurgical deterioration caused by elevated temperature service. Bhaduri et al., 1990, 1994, 1988, 1989 [8-11] carried out the investigations on transition metal joints between chromium-molybdenum (Cr-Mo) ferritic steel and austenitic stainless steel widely used in the steam generators of power plants. The investigators highlighted the various failure causes of bimetallic joints using Ni-base weld metals and instead of austenitic SS weld metals. They proposed an improved trimetallic transition metal configuration of austenitic stainless steel (SS304)/ Alloy 800/ ferritic steel (2.25Cr-lMo). For the type 304 SS/Alloy 800 joint, a comparative evaluation of Inconel 182 and 16-8-2 welding consumables has been carried by the authors. 16-8-2 consumable was declared better over Inconel 182 for welding the joint between SS304 and Alloy 800 due to its various advantages which includes its lower tendency for micro fissuring along with the reduced mismatch in the coefficient of thermal expansion across the joint. Also the choice of 16-8-2 welding consumable, involve only a marginal penalty on the elevated temperature mechanical properties of the joint.

A significant number of weld failures occur in the heat affected zone (HAZ) region on the ferritic steel side of dissimilar weld joints (Kumar et al., 2015 [90]). Residual stresses present in the weld joint are one of the main factors, responsible for these failures. The dissimilar joints between 2.25Cr-1Mo ferritic steel and AISI 316 stainless steel with and without buttering layer using Inconel-82 on the ferritic steel side have been studied by Joseph et al., 2005 [72]. The buttered ferritic steel pipe was

joined to stainless steel pipe using a conventional manual TIG welding process with Inconel-82 filler metal. The X-ray diffraction (XRD) technique was used to measure the residual stress profiles across these weld-joints. Their study indicated that residual stresses present at the HAZ of the ferritic steel are reduced significantly with the buttering layer.

Pan et al., 1994 [117] studied the weld interface in dissimilar alloys of austenitic and pearlitic steel joined by arc welding process. The weld characterization was done by SEM, TEM and EDAX techniques and weld analysis was focused on diffusion of Cr and Ni from weld metal into the base metal, and migration of carbon from base metal into weld metal.

Researchers have also tried to explore laser beam welding, electron beam welding and adhesive bonding for dissimilar transition joints (Arora et al., 2014 [3]; Da Silva 2013, 2015 [31, 32]). Sun, 1996 [144]) discussed about the feasibility of producing ferritic/austenitic dissimilar metal joints by laser beam process. In comparison to other fusion welding processes, a focused beam used in Laser beam welding maintains a deeply penetrating weld pool and enables through thickness welds to be made rapidly in a single pass. The other advantages include low energy input, a small heat affected zone, less residual stresses and distortion. The dissimilar base material combination examined was low alloy Cr-Mo steel 13CrMo44 and austenitic stainless steel AISI 347. Microstructural characterization revealed that weld metal produced with filler wire Inconel 625 possesses fully austenitic microstructure, while the weld metal produced without filler has a mixed microstructure containing austenite and martensite. The heat affected zone in low alloy steel possesses martensite structure near the fusion line in both the cases but its size is small when the weld is produced with filler wire. The results of this evaluation indicate that satisfactory bimetallic joints in terms of weldability and room temperature mechanical properties can be produced with laser beam welding process.

Lee, 2000 [97] investigated effect of welding parameters on size of heat affected zone of submerged arc weld. Celik and Alsaran, 1999 [23] studied the GTAW weldments of ferritic steel (St37-2) and an austenitic stainless steel (AISI 304) by using an austenitic filler metal.

Sireesha et al., 2000a, 2000b [136-137] presented a comparative evaluation of welding consumables for dissimilar welds between 316LN austenitic stainless steel and Alloy 800. Four consumables examined were 316, 16-8-2, Inconel 82 and Inconel 182. The comparative evaluation was made on the basis of hot cracking tests; estimation of mechanical properties and coefficient of thermal expansion. The weld samples were prepared using shielded arc welding with Inconel 182 and 316 consumables and gas tungsten arc welding with 16-8-2 and Inconel 82 filler wires. The coefficient of thermal expansion coefficients of Inconel 182 lies in between the both base metals and therefore it is better suited than the other welding consumables. The 16-8-2 filler material resulted in the lowest susceptibility to solidification cracking while the other Inconel welding consumables were superior from the mechanical property view point.

Sireesha et al., 2002 [135] discussed the thermal cycling of transition joints between modified 9Cr–1Mo steel and Alloy 800. This is part of a trimetallic transition joint involving Alloy 800–316LN austenitic stainless steel for steam generator application. The welding consumables used were Inconel 82 and Inconel 182. Gas tungsten arc welding was used for root pass of the joint with Inconel 82 and manual metal arc welding with Inconel 182 was applied for subsequent passes to complete the bimetallic transition joint. It has been shown that, during thermal cycling following the typical post-weld tempering treatment at 760°C for 2 hours, no carbon diffusion occurs from the ferritic steel towards the weld metal. A hardness increase at the ferritic steel/weld metal interface was reported.

Sudha et al., 2002 [143] discussed about the dissimilar weldments between low-Cr and high-Cr ferritic steel used in a number of steam generator circuits. Weldments of 9Cr-1Mo and 2¼Cr-1Mo steel were prepared using plates of 12.5mm thickness by shielded metal arc welding process using 9Cr-1Mo as the electrodes. Carbon migration occurs across the weld interface from low-alloy ferritic steel to high-alloy ferritic steel during exposure to high temperature. Diffusion of carbon driven by the activity gradient across the weld interface resulted in the formation of a soft zone in the low-Cr side and a carbide-rich hard zone in the high-Cr side of the weld interface. The authors also discussed the width of these zones and the effect of post weld heat treatment. It was suggested that hardness and width of both soft as well as hard zone decreases with increasing the time of heat treatment. The presence of carbides in hard

zone was justified with TEM micrographs. In their study Sudha et al., 2006 [142] reported the microstructure and microchemistry of hard and soft zones in a dissimilar weldment subjected to post weld heat treatments.

Srinivasan et al., 2006 [140] investigated the joining of carbon steel to duplex stainless steel using shielded metal arc welding, with E2209 and E309 electrodes. Hasanbasoglu and Kacar, 2007 [56] studied the resistance spot welding for the dissimilar materials AISI 316L austenitic stainless steel and DIN EN 10130-99 (7114 grade) interstitial free steel.

Jenga et al., 2005 [62] studied the microstructure and corrosion of dissimilar weldments of Alloy 690 and SUS 304L with various additions of niobium (Nb) (0.1, 1.03, 2.49, and 3.35% by weight) in the flux of coated electrodes. Labanowski, 2007 [94] studied the mechanical properties and corrosion resistance of dissimilar stainless steels between UNS31803 and AISI316L welded with submerged arc welding. Anawa and Olabia, 2008 [1] successfully applied CO_2 continuous laser welding process for joining dissimilar AISI 316 stainless-steel and AISI 1009 low carbon steel plates.

Srinivasan et al., 2008 [139] investigated the use of autogenous gas tungsten arc welding to produce a dissimilar weld between ferritic and austenitic stainless steels and carried out a mechanical property evaluation of these welds. The dissimilar metal welds are expected to show the spatial variation in mechanical properties joining the low alloy steel because of the existence of different materials and chemistry variation within welds (Jang, 2008 [61]). To investigate these variations, the dissimilar metal welds joining the low alloy steel and stainless steel were fabricated by gas tungsten arc welding (Inconel 82 filler wire) and shielded metal arc welding (Inconel 182 welding electrodes) processes.

Dehmolaeia et al., 2008 [37] investigated dissimilar welds with four different filler materials. Naffakh et al., 2009 [112] carried out the work to characterize welding of AISI 310 austenitic stainless steel to Inconel 657 nickel–chromium superalloy. Four types of filler materials; Inconel 82, Inconel A (1% Si, 3% Mn, 12% Fe, 15% Cr, 1.5% Mo, 2.5% Nb, 0.5% Cu and remaining % Ni), Inconel 617 and 310 austenitic stainless steels were used to produce welds. The comparative performance evaluation of welds was based on hot-cracking tests and estimation of mechanical properties.

Inconel A showed the least susceptibility to hot cracking, highest strength and total elongation. The weld metals failed by ductile fracture except Inconel 617, which exhibited mixed fracture mode. Inconel 82 and 310 SS weld metals exhibited higher tendency to solidification cracking.

Another combination of dissimilar weld joint i.e. 403SS/304L(N)SS was studied by Das et al., 2009 [30] to evaluate the performance of various filler metals and phenomenon of auto tempering of heat affected zone (HAZ) of 403SS base metal. The application of this combination of bimetallic joint is in the nuclear power plants where the austenitic stainless steel 304L(N) SS pipes are joined with the martensitic 403 SS end fittings of the reactor. Welds were prepared by gas tungsten arc welding process using ERNiCr-3, ER308L and ER309L three different filler metals. Firstly the buttering layer of filler metals was applied on 403 SS and then these buttered 403 SS plates were joined to 304L(N) SS base plates. The experimental analysis show the presence of delta ferrite content (3-8FN) in welds made with stainless steel filler metals.

Wang et al., 2011 [155] studied the bimetallic joint between 16MnR low alloy high strength steel and 2205 duplex stainless steel welded using shielded metal arc welding (SMAW) and tungsten inert gas arc welding (GTAW). The welds produced with GTAW process showed better corrosion resistance in chloride solution as compared to SMAW process. Microstructures also indicated the uniform distribution of austenite and acicular ferrite structures in the weld metal. Kurt, 2007 [92] investigated the interface morphology of diffusion bonded dissimilar stainless steel and medium carbon steel couples. The author has attempted diffusion bonding to eradicate the problems associated with fusion welding processes.

Rathod et al., 2016 [129] suggested a Ni-Fe alloy buffer layer in buttering the ferritic steel for the dissimilar welds between SA508Gr.3Cl.1 and SS304LN. The joints (with and without buffer layer in buttering) were fabricated using gas tungsten arc welding and shielded arc welding processes. The metallurgical and mechanical investigations of four dissimilar welds were carried out. The carbon did not migrate from the ferritic steel to the Ni-Fe alloy (buffer layered buttering) due to the absence of chromium.

2.11 Design of Experiment

Many researchers (Benyounisa et al., 2008 [7]; Castillo, 1996 [22]; Fussel, 2012 [47]; Gunaraj, 1999 [50]; Kumar et al., 2016 [91]; Murugana, 2005 [109]; Murugananth, 2004 [110]) have used DOE for process parameter optimization for different welding processes.

2.11.1 Design of mixture experiments

Jindal et al., 2013, 2014a, 2014b, 2015 [68-71] tried to explore mixture design methodology for flux design in submerged arc welding process. Panigarhi et al., 2008a, 2008b [122, 123] has worked on mixture design of ternary systems of fly-ash-sand bricks and developed model for prediction of compressive strength of developed mixture.

Several classical mixture design approaches are available (Cornell, 2002 [29]; Anderson and McLean, 1974 [2]). There are standard mixture designs for fitting standard models, such as Simplex-Lattice designs and Simplex-Centroid designs. When mixture ingredients are subject to additional constraints, such as a maximum and/or minimum value for each ingredient, designs are referred to as constrained mixture designs or extreme-vertices designs. The general form of the constrained mixture problem is.

$x_1 + x_2 + ... + x_q = 1$

$L_i \leq x_i \leq U_i$, for i = 1, 2,..., q

with $L_i \geq 0$ and $U_i \leq 1$.

where L_i is the lower bound for the i-th component and U_i the upper bound for the i-th component.

2.11.2 Mixture design space

The main distinction between factorial experiments and mixture experiments is the construction of their design space. The design space of a factorial experiment is the set of possible combinations of its independent variables or components. The design space of a mixture experiment is the set of possible combinations of the relative proportion of each component, which usually add up to a certain value. Figure 2.11.1 illustrates the distinction between factorial design space and mixture design space for three different components.

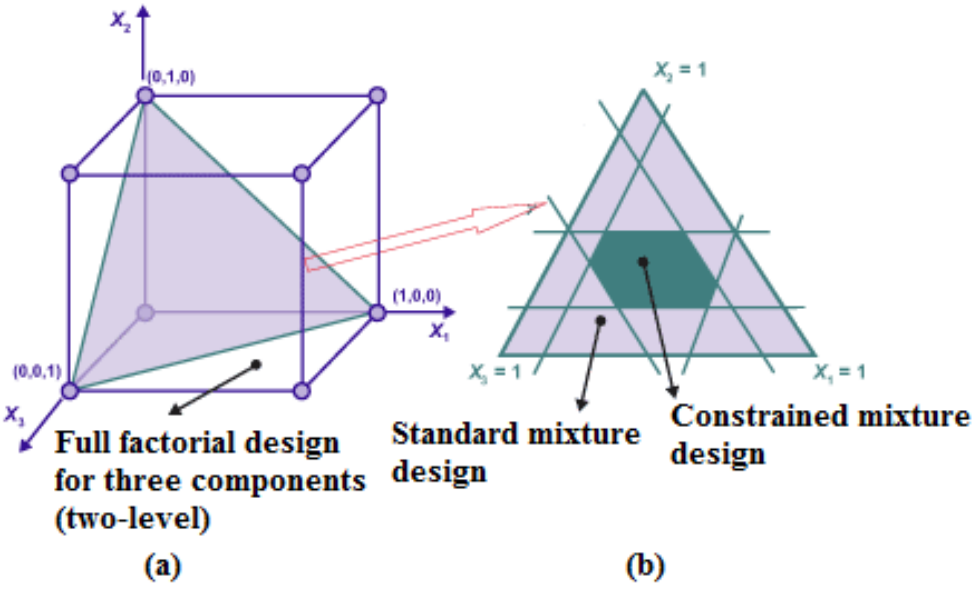

Figure 2.11 (a) Factorial design space and (b) mixture design space.

The plane where the sum of the three factors sum to one, is a triangle-shaped slice. The standard mixture design space for three ingredients is shown as a triangle-shaped slice (area) inside the cube of Figure 2.11.1 (a). Simplex-lattice designs and simplex centroid designs are fitting models for the standard mixture design. The constrained mixture design space is shown as a polygonal area in the triangle in Figure 2.11(b). Extreme vertices designs are fitting models for the constrained mixture design. The mixture design space for four-ingredient mixture experiment requires another dimension in simplex geometry in the form of a tetrahedron.

2.12 Gaps and Opportunities

It has been found from literature survey that extensive research has been done on welding electrode coatings and there exists a large set of experimental data relating the process, weld metal composition, and mechanical properties. Some theoretical and computational models have been developed to describe individual as well as some of the complex interactions taking place during welding. Traditionally the formulations of welding electrode coatings involve expensive and time intensive experimental trials, characterizations and optimizations based on trial and error. The electrode coating formulations may or may not be optimum, since it is not practical to explore all combinations of compositional and process variations due to the cost and time limitations. There is nearly a total absence of applied research to extend this knowledge to the design and optimization of welding electrode coatings.

The literature review also throws light on the various issues related the bimetallic welds and reveals that the investigations are mainly focused on nickel based welding consumables using gas tungsten arc welding process. The use of nickel base alloy as filler metal is no longer considered as the final solution for unexpected failures due to incidences of hot cracking of bimetallic welds under cyclically shifted temperature environment. The use of conventional stainless steel welding fillers for achieving the desired delta ferrite content and microstructural evolution in solidified weld metal of bimetallic welds has been highlighted to prevent hot cracking of welds in the various research findings.

From the literature survey it can be concluded that there are very limited research findings available related to the design of welding electrode coatings using conventional stainless steel welding fillers for SMAW process for the joining of bimetallic welds.

CHAPTER 3
PROBLEM FORMULATION

3.1 Need for Research

- From the literature survey it is clearly evident that the formulations of welding electrode coatings are based on trial and error method and practical experience. So there is need to apply the design of experiments to reduce the number of trails for the design of electrode coatings systematically and scientifically.
- It is documented that austenitic welds with 4–10 vol% delta ferrite are resistant to hot cracking, stress and severe impacts during service conditions. Work needs to be carried out to explore the use of stainless steel welding fillers with the SMAW electrode coatings for the application of bimetallic welds.
- In bimetallic welds, base metals have different elemental compositions so work (deposition of buttering or intermediate layer) needs to be carried out to reduce this elemental composition gradient across the joint.

3.2 Research Objectives

Based on the need of research as identified from literature review, the current research proposal aims to develop a generalized methodology

- To design the welding electrode coatings for ferritic-austenitic bimetallic welds; and
- To develop predictive mathematical models for weld metal chemistry and mechanical properties of bimetallic welds,

3.3 Research Plan

3.3.1 Design of electrode coatings

The electrode coating ingredients along with their range had to be selected on the basis of their physiochemical properties. The design matrices of the formulations of electrode coatings were to be created using extreme vertices design methodology.

3.3.2 Experimentation

Welding electrodes were needed to be developed with the coatings formulations as per design matrices. The trial runs had to be conducted to decide the welding current

and voltage. The weld coupons of bimetallic joints were to be fabricated using the designed electrodes and then, the various tests had to be conducted.

3.3.3 Regression analysis

The mathematical regression models were required to be developed using the experimental data of various weld responses. Regression analysis had to be performed to check the adequacy of the developed models.

3.3.4 Multi response optimization

Multi response optimization using composite desirability optimization technique had to be implemented to achieve optimized set of design parameters.

3.3.5 Confirmatory experiments

Confirmatory experiments were to be conducted to validate the developed mathematical regression models of various weld responses.

The flow chart of the research plan being followed is shown in Figure 3.1. The successful completion of the research work would provide an efficient and reliable methodology for the design and development of welding electrode coatings for bimetallic welds. The research would help to contribute to competitiveness in the Indian welding industry and will have significant impact on the shipbuilding, construction, heavy machine, power generation, and oil and gas industries.

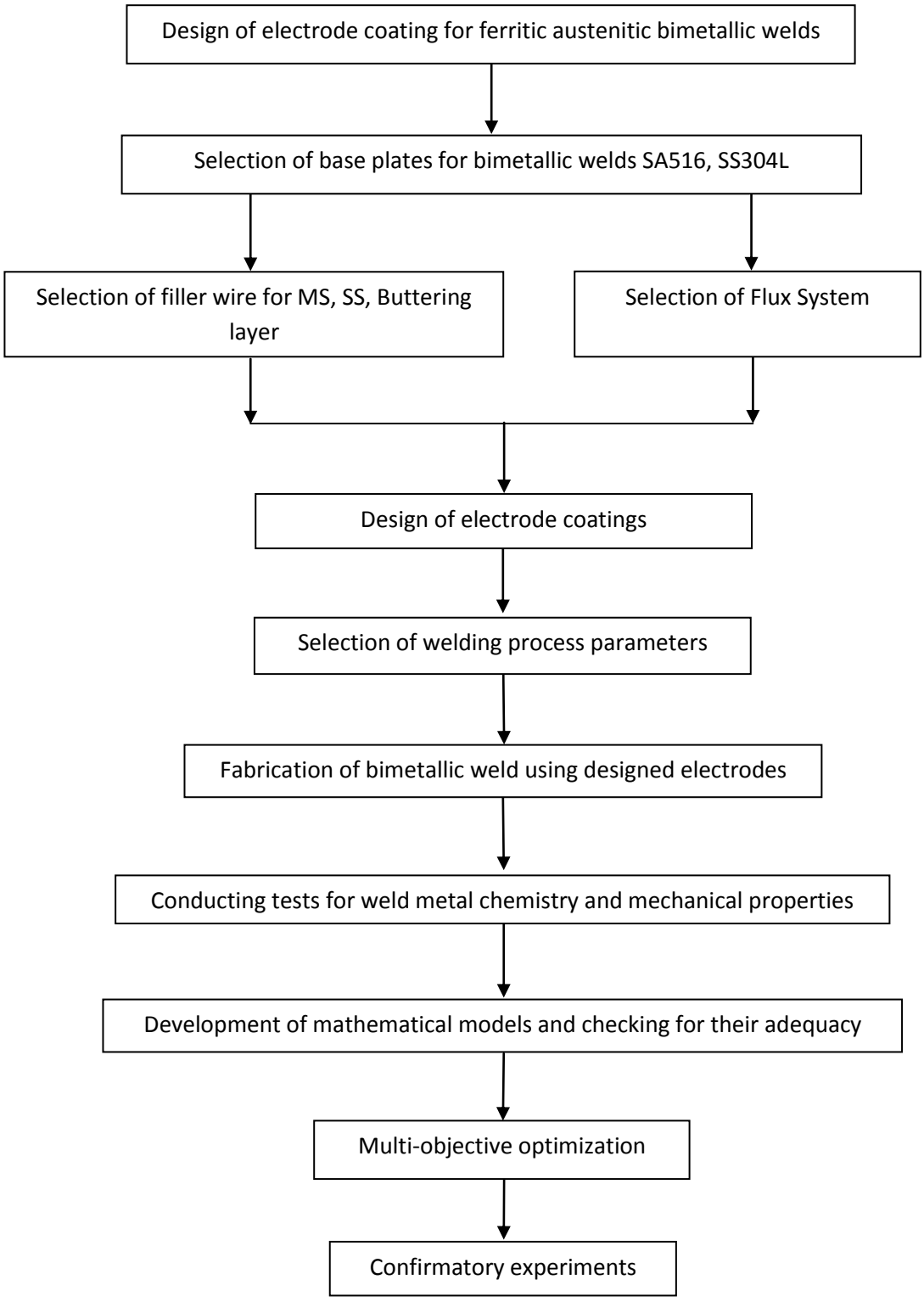

Figure 3.1 Flow chart of research plan.

CHAPTER 4
EXPERIMENTAL DESIGN

This chapter gives detailed information on the experimental design and procedures adopted in the research work. The use of two layer and three layer approaches for fabrication of bimetallic welds has been discussed. The design matrices for welding electrode coating formulations based on three different phase diagram were developed. The welding trials for the selection of welding parameters are explained. Finally, the procedure followed for weld characterization has been reported.

4.1 Use of Two and Three Layer Bimetallic Weld Methodologies

In two layer procedure for the bimetallic welds, first of all, the layer of buttering material (6 mm thickness) is applied to the end of the ferritic steel. The SS309L stainless steel filler core wire was used for applying the buttering layer by developing buttering layer electrode. This layer of buttering is over-alloyed with chromium and nickel content in order to compensate the dilution resulting from the diffusion to the base metal. The complete bimetallic joint was fabricated between the buttered ferritic steel SA516 grade 70 and the stainless steel SS304L base plates using stainless steel electrodes made using SS308L core wire. For both the buttering layer and the final weld joint, the welding electrodes were designed and developed on the basis of phase diagram systems using extreme vertices design methodology.

In the present research work, three layer bimetallic weld methodology has also been used. Three different types of welding electrodes have been proposed for the three types of layers between ferritic steel SA516 grade 70 and austenitic stainless steel SS304L to complete the bimetallic joint. The motive of applying one additional layer over the two layer approach was to reduce further the compositional variation between the base metals.

The first type of electrodes were designed and developed based on CaO-CaF_2-SiO_2 ternary phase diagram system and nickel as an additional electrode coating ingredient with mild steel filler wires. These electrodes were used for applying the first layer of buttering on the edge of ferrite steel and named as mild steel (MS) buttering electrodes. The purpose of developing these electrodes was to reduce the compositional gradient at the interface of ferritic steels.

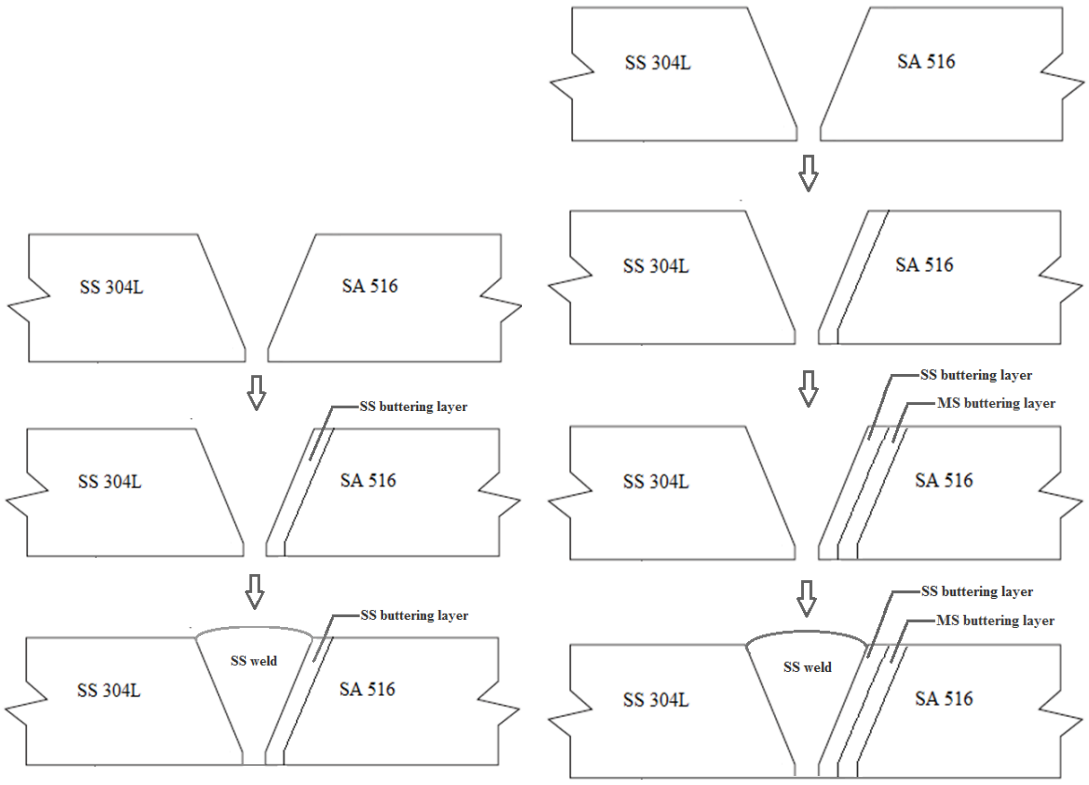

Figure 4.1 Schematic diagram of the two and three layer bimetallic weld methodology.

In the next step, the other two different types of electrodes with different stainless steel filler core wires (SS309L and SS308L) were designed and developed on the basis of phase diagram systems. The second layer of buttering on the MS buttered ferritic steels was applied with SS309L developed electrodes. The steel was named as MS/SS buttered ferritic steel and the SS309L electrodes were designated as SS buttering electrodes. Finally bimetallic welds were made between the MS/SS buttered ferritic steels and the austenitic stainless steels by applying the third layer of weld using SS308L developed electrodes designated as weld electrodes.

For both the two layer and three layer bimetallic methodologies, the $CaO\text{-}TiO_2\text{-}SiO_2$ ternary phase system was used to design and develop one set of stainless steel electrodes i.e. (SS309L and SS308L). In another set of experimentation, second set of stainless steel based electrodes were designed by combining the observations of two ternary phase diagram systems namely $CaO\text{-}SiO_2\text{-}TiO_2$ system and $CaO\text{-}SiO_2\text{-}Al_2O_3$ system.

4.2 Design of Experiment

4.2.1 Extreme vertices design

The coating formulations of welding electrodes were designed using extreme vertices design as suggested by McLean and Anderson (Cornell, 2002 [29]; Anderson and Mclean, 1974 [2]). The method suggests that constrained mixture design for a mixture of k ingredients having both lower and upper bounds on some or all of ingredients may be represented mathematically as follows (Jindal et al, 2013 [63]):

$$0 \le \alpha_i \le x_i \le \beta_i \le 100 \tag{4.2.1}$$

$$\sum_{i=1}^{k} x_i = 100 \tag{4.2.2}$$

Where, *i=1, 2, 3…, k* and; α_i *and* β_i are the lower and upper limits of constraints on the x_i which is the percentage composition of i^{th} ingredient in the mixture.

When there are no lower and upper bounds on the ingredients of a mixture, the geometric description of the confined design space is easy to define and consists of all points on or inside the boundaries of a regular (k-1)-dimensional simplex. So the experimental mixture design space of k dimensions is reduced to a (k-1) dimensional simplex.

For three ingredients mixture system (k=3), the three dimensional design space (cube) is reduced to a two dimensional simplex (equilateral triangle) and for k=4, it is a tetrahedron as shown in Figures 4.2.1 and 4.2.2, respectively.

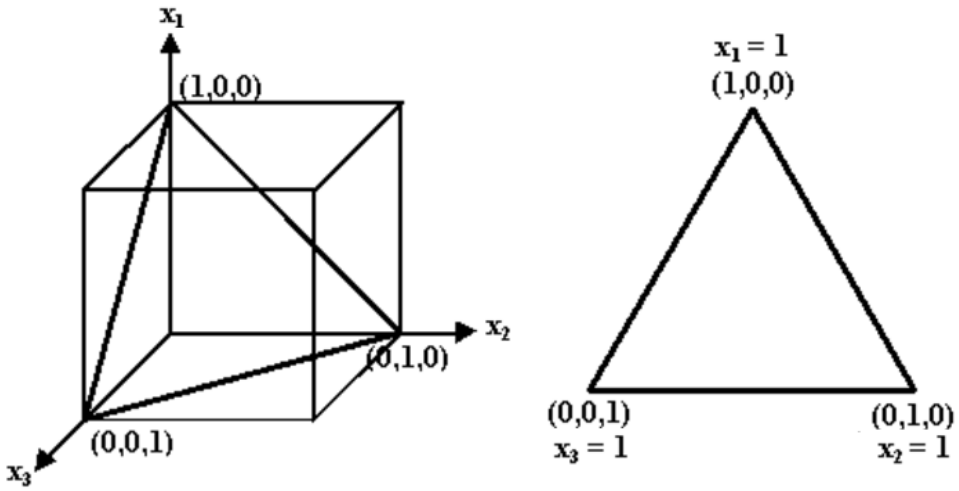

Figure 4.2.1 Three ingredient simplex region (Cornell, 2002 [29]).

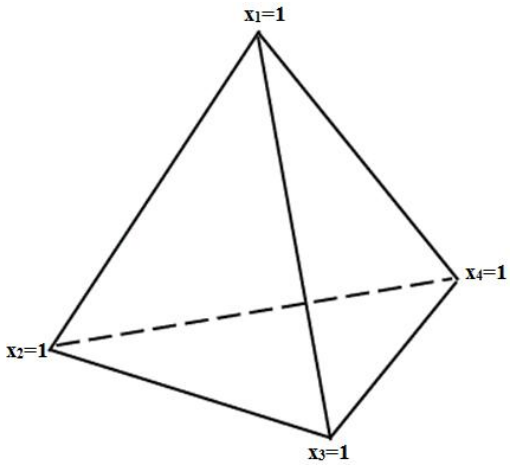

Figure 4.2.2 Four ingredients tetrahedron (Cornell, 2002 [29]).

The confined design space is also not so difficult to define even when only one or two ingredients of the mixture are restricted. It takes the form of hyper-polyhedron or convex polyhedron for the mixture having more number of constraints with both lower as well as upper bounds.

To model the response surface of measured properties over the polyhedron region (confined design space) defined by Eq. (4.2.1and 4.2.2), the various design points are specified. The design points represent the various vertices and centroids of the faces of the polyhedron. To obtain the vertices of polyhedron, first of all the possible combinations (as in two-level factorial method) of proportions of k-1 ingredients using their lower and upper bound limits, are listed. The proportions of the one ingredient are left blank. This procedure produces 2^{k-1} points. The same process is repeated for all the ingredients by keeping alternatively the proportions of one ingredient blank in the list. It will generate a total list of $k.2^{k-1}$ possible combinations. The proportions of the left out ingredients in the list are specified in a manner satisfying their lower and upper bound limits as well as the condition that the sum of all ingredients must be 100% or unity. In this way, the vertices of the polyhedron are obtained. In the next step, the centroids of the various the two-dimensional faces are found by grouping the vertices of the polyhedron. The overall centroid of the polyhedron is obtained by averaging all the vertices of the polyhedron. These design points comprise the complete design matrix for experimentation. The observations of output responses are obtained from which the estimates of the input parameters in the standard mixture design regression models can be calculated.

The output response characteristic for a mixture with k ingredients can be given in the form of second order regression model as:

$$Y = \sum_{i=1}^{k} b_i x_i + \sum_{i<j} \sum^{k} b_{ij} x_i x_j \quad (4.2.3)$$

Here, b_i and b_{ij} represent least square model regression coefficients. The terms $b_i x_i$ and $b_{ij} x_i x_j$ are the individual and interaction effects of the various ingredients of electrode coatings respectively. These types of regression models are without intercept terms and classic terms such as $x_1^2$and are known as Scheffe type models.

4.3 Design of Mild Steel (MS) Buttering Electrode

The basic requirement while deciding the percentage composition of various electrode coating ingredients is that their composite melting point temperature must be lower than that of the core wire and base metals because the electrode flux coating should melt before the core wire and base metals and should remain in the molten state even during the solidification of weld. Considering these important aspects, the phase diagrams of various systems are analyzed and percentage compositions of electrode coating ingredients are broadly decided. Then the range of these electrode coating ingredients is further narrowed, based on the research findings in the relevant literature (Bhandari et al., 2012, 2016 [12, 13]).

The ternary phase diagram represents the projection of the liquidus surface of the three component system with the help of contour plots depicting the temperature intervals onto the base of the triangle. In the present work, the CaO-CaF_2-SiO_2 ternary phase diagram system (Figure 4.3.1) has been chosen to design and develop the mild steel based coated electrodes. The CaO-CaF_2-SiO_2 based basic electrode coatings have the ability to produce low oxygen content and thus better mechanical properties. The region just adjacent to the lower composite melting point (around 1100°C) on the ternary phase diagram was selected to decide the broad range of CaO, CaF_2 and SiO_2 electrode coating ingredients. In order to accommodate some specific ingredients in the coatings to facilitate the development of coated electrodes during extrusion process, the estimated upper and lower weight limits of the CaO, CaF_2 and SiO_2 electrode coating ingredients were scaled down to a total of 65%.

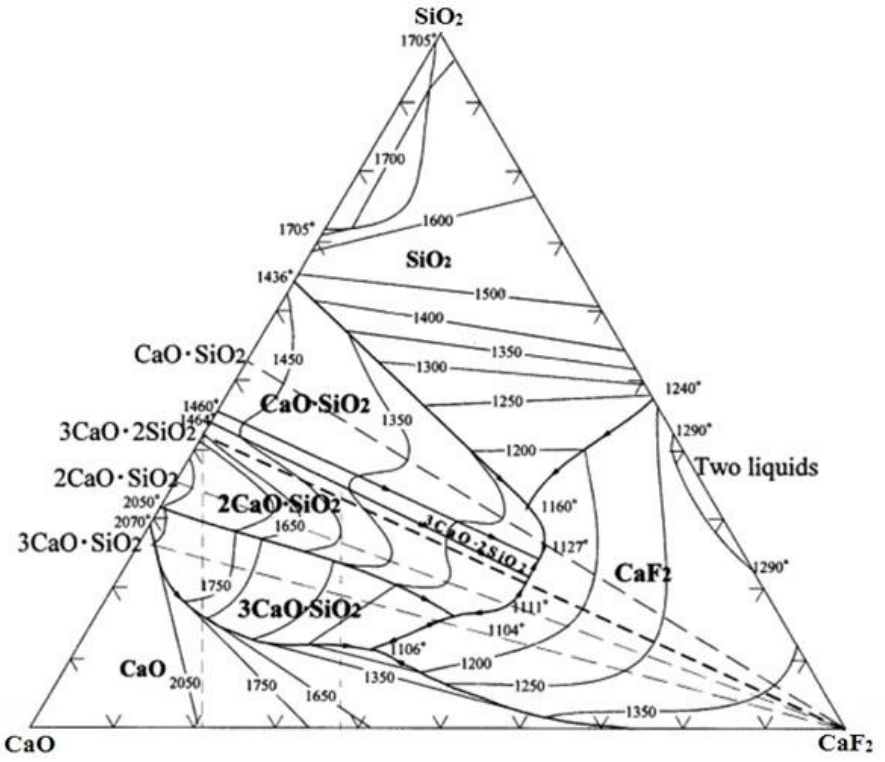

Figure 4.3.1 Experimental ternary phase diagram of CaO-CaF_2-SiO_2 system (Kalisz, 2013 [74]).

As mentioned earlier, the purpose of developing the mild steel based electrode was to reduce the compositional gradient in bimetallic welds and the developed electrode was to be applied for first layer of buttering on the ferritic steel so it was decided to include nickel (Ni) in the compositions of electrode coatings to achieve this specific task. Nickel acts an austenitic stabilizer and helps to reduce the carbon migration due to the compositional variance in the different base metals. The carbon has the tendency to move due to the gradient in the chromium levels of base metals. The upper and lower limits of percentage composition of the four ingredients of CaO, CaF_2, SiO_2 and Ni are shown collectively in Eq. (4.3.1) and their total sum of the weight composition is given in Eq. (4.3.2):

$20 \leq CaO(x_1) \leq 35$

$20 \leq CaF_2(x_2) \leq 35$

$8 \leq SiO_2(x_3) \leq 15$

$1 \leq Ni(x_4) \leq 8$ (4.3.1)

$\sum_{i=1}^{4} x_i = 65$ (4.3.2)

The various design points (vertices and centroids) of the polyhedron specified by the constraints on the proportions of four ingredients (Eq. (4.3.1 and 4.3.2)) were decided using extreme vertices design methodology and presented in Table 4.3.1. The resulting mixture design confined space within the tetrahedron in the form of polyhedron along with the design point designations is shown in Figure 4.3.2.

Table 4.3.1 Design matrix of electrode coating formulations of MS buttering electrode

Expt. No.	Nature of mixture design point	Ingredients of electrode coatings (Percentage Composition)			
		CaO	CaF_2	SiO_2	Ni
1	Vertex	20	22	15	8
2	Overall centroid	25.5	25.5	10.5	3.5
3	Vertex	35	21	8	1
4	Centroid	22.75	22.75	11.5	8
5	Vertex	20	35	9	1
6	Centroid	22.75	22.75	15	4.5
7	Vertex	20	29	15	1
8	Centroid	20	30	11	4
9	Centroid	26.67	26.67	10.67	1
10	Vertex	35	20	9	1
11	Vertex	21	35	8	1
12	Centroid	26.67	26.67	8	3.67
13	Vertex	20	29	8	8
14	Centroid	30	20	11	4
15	Vertex	29	20	15	1
16	Vertex	20	35	8	2
17	Vertex	35	20	8	2
18	Centroid	35	20.33	8.33	1.33
19	Centroid	20.33	35	8.33	1.33
20	Vertex	29	20	8	8
21	Vertex	22	20	15	8

The polyhedron can be assumed to be consisting of twelve vertices of hexagonal prism (design points 1, 3, 5, 7, 10, 11, 13, 15, 16, 17, 20, 21), eight centroids of its various faces (design points 4, 6, 8, 9, 12, 14, 18, 21) and one overall body centroid (design point 2).

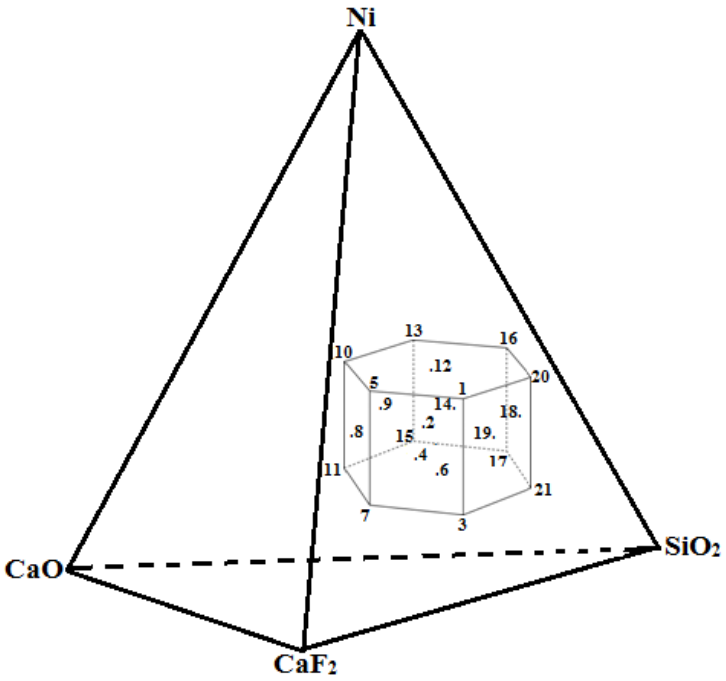

Figure 4.3.2 Confined design space within the tetrahedron.

4.4 Design of Stainless Steel Electrodes Based on CaO-TiO_2-SiO_2 System

For the design of stainless steel electrodes, a ternary phase diagram of CaO-TiO_2-SiO_2 system as shown in Figure 4.4.1 was used to design electrode coating compositions by selecting points from the ternary phase diagram (points marked with X in Figure 4.4.1). These points were selected so as to obtain a lower composite melting point of the slag (around 1365°C) and predominantly perovskite phase which imparts good slag detachability due to relatively different coefficient of thermal expansion in comparison to the weld metal. The upper and lower weight limits of the three electrode coating ingredients TiO_2, SiO_2 and CaO were estimated.

In order to accommodate other essential electrode coating ingredients which amount to around 20% by weight of the complete composition, the estimated upper and lower weight limits were scaled down to a total of 80%. Further in order to decrease the composite melting point of the coating an amount of CaF_2 upto 10 % was added by replacing CaO. The upper and lower limits of percentage composition of the four components TiO_2, SiO_2, CaO and CaF_2 are shown in Eq. (4.4.1) and their sum total which is 80% of the total weight of the composition is shown in Eq. (4.4.2):

$50 \leq TiO_2\,(x_1) \leq 55$

$5 \leq CaO\,(x_2) \leq 15$

$10 \leq SiO_2\,(x_3) \leq 20$

$0 \leq CaF_2\,(x_4) \leq 10$ (4.4.1)

$\sum_{i=1}^{4} x_i = 80$ (4.4.2)

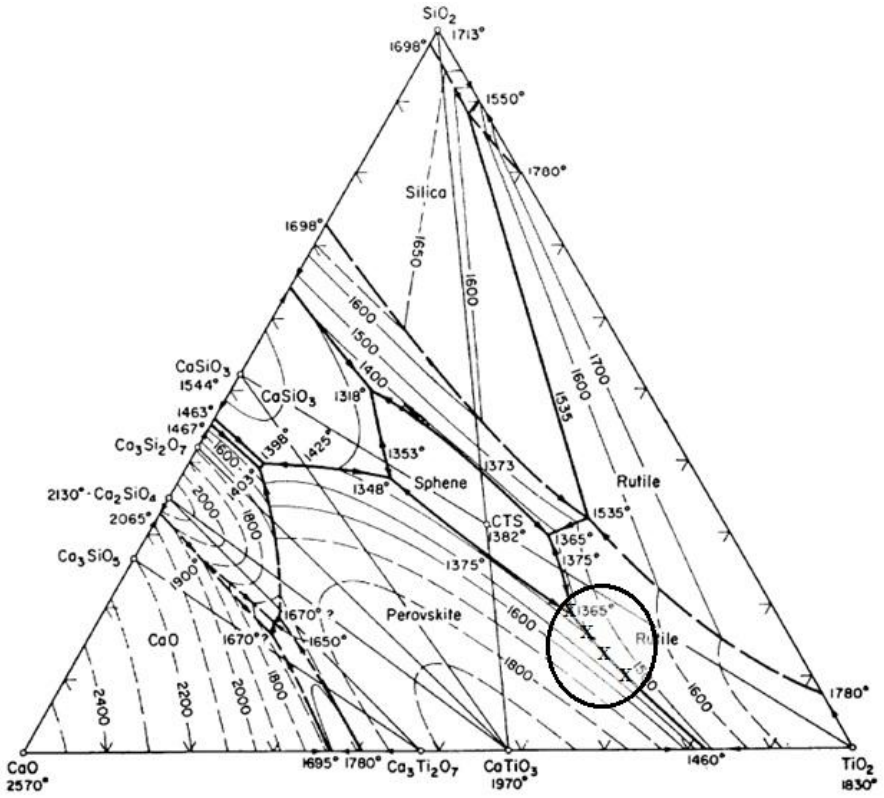

Figure 4.4.1 Experimental phase diagram of CaO-TiO_2-SiO_2 system (De Vries, 1955 [36]).

Eighteen sets of electrode coating compositions were designed by varying the composition of four coating ingredients; TiO_2, SiO_2, CaO, CaF_2 by using extreme vertices mixture design methodology as shown in Table 4.4.1 The mixture design space consists of nine vertices of bi-truncated triangular bi-pyramid, six centroids of trapezoidal faces, two centroids of triangular faces and one overall body centroid as shown in Figure 4.4.2.

Hence total eighteen designed experiments were to be performed, expt. no. 7-10 and expt. no. 14-18 represent nine vertices, expt. no. 2-6 and expt. no. 11-13 represent eight centroids of various faces while expt. no. 1 represent overall centroid of polyhedron.

Table 4.4.1 Design matrix for electrode coating formulations (SS electrodes based on CaO-TiO_2-SiO_2 system)

Expt. No.	Nature of polyhedron points	Ingredients of electrode coatings (Percentage composition)			
		TiO_2	CaO	SiO_2	CaF_2
1	Centroid	51.7	9.4	14.4	4.4
2	Centroid	51.7	15	11.7	1.7
3	Centroid	52.5	5	16.3	6.3
4	Centroid	52.5	11.3	16.2	0
5	Centroid	52.5	11.3	10	6.2
6	Centroid	51.7	6.7	20	1.7
7	Vertex	50	10	10	10
8	Vertex	55	5	20	0
9	Vertex	50	5	15	10
10	Vertex	50	15	10	5
11	Centroid	50	10	15	5
12	Centroid	55	8.3	13.3	3.3
13	Centroid	51.7	6.7	11.7	10
14	Vertex	55	5	10	10
15	Vertex	55	15	10	0
16	Vertex	50	10	20	0
17	Vertex	50	15	15	0
18	Vertex	50	5	20	5

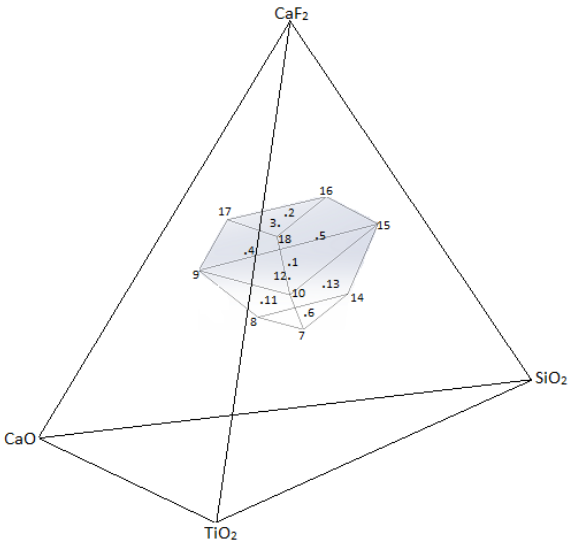

Figure 4.4.2 Polyhedron designed on the basis of mixture design methodology.

4.5 Design of Stainless Steel Electrodes Based on $CaO\text{-}SiO_2\text{-}Al_2O_3\text{-}TiO_2$ System

Two ternary phase diagrams of $CaO\text{-}SiO_2\text{-}TiO_2$ and $CaO\text{-}SiO_2\text{-}Al_2O_3$ system as shown in Figure 4.5.1(a) and (b) were used to design electrode coating compositions by selecting points from the ternary phase diagrams (points marked with X in Figure 4.5.1(a) and (b)). The points in $CaO\text{-}SiO_2\text{-}TiO_2$ system (Figure 4.5.1(a)) were selected so as to obtain a lower composite melting point of the slag (around 1348°C) and predominantly perovskite phase which imparts good slag detachability due to relatively different coefficient of thermal expansion in comparison to the weld metal. These selected compositions of CaO and SiO_2 were then marked in $CaO\text{-}SiO_2\text{-}Al_2O_3$ system (Figure 4.5.1(b)) and the points were chosen at the lower composite melting point of the slag (around 1282°C). The upper and lower weight limits of the electrode coating ingredients CaO, SiO_2, Al_2O_3 and TiO_2 were estimated.

In order to accommodate other essential electrode coating ingredients which amount to around 25% by weight of the complete composition, the estimated upper and lower weight limits were scaled down to a total of 75%. The upper and lower limits of percentage composition of the four electrode coating ingredients i.e. CaO, SiO_2, Al_2O_3 and TiO_2 are given in Eq.(4.5.1) and their sum total which is 75% of the total weight of the composition is shown in Eq.(4.5.2):

$$15 \leq CaO \leq 35$$
$$15 \leq SiO_2 \leq 35$$
$$8 \leq Al_2O_3 \leq 18$$
$$10 \leq TiO_2 \leq 35 \quad (4.5.1)$$
$$\sum_{i=1}^{4} x_i = 75 \quad (4.5.2)$$

For the development of welding electrodes, total 21 sets of electrode coating formulations were designed on the basis of mixture design methodology by varying the composition of four major ingredients i.e. CaO, SiO_2, Al_2O_3 and TiO_2 as shown in Table 4.5.1. The mixture design confined space of electrode coating formulations consists of twelve vertices of hexagonal prism, eight centroids of its various faces and one overall body centroid as shown in Figure 4.5.2.

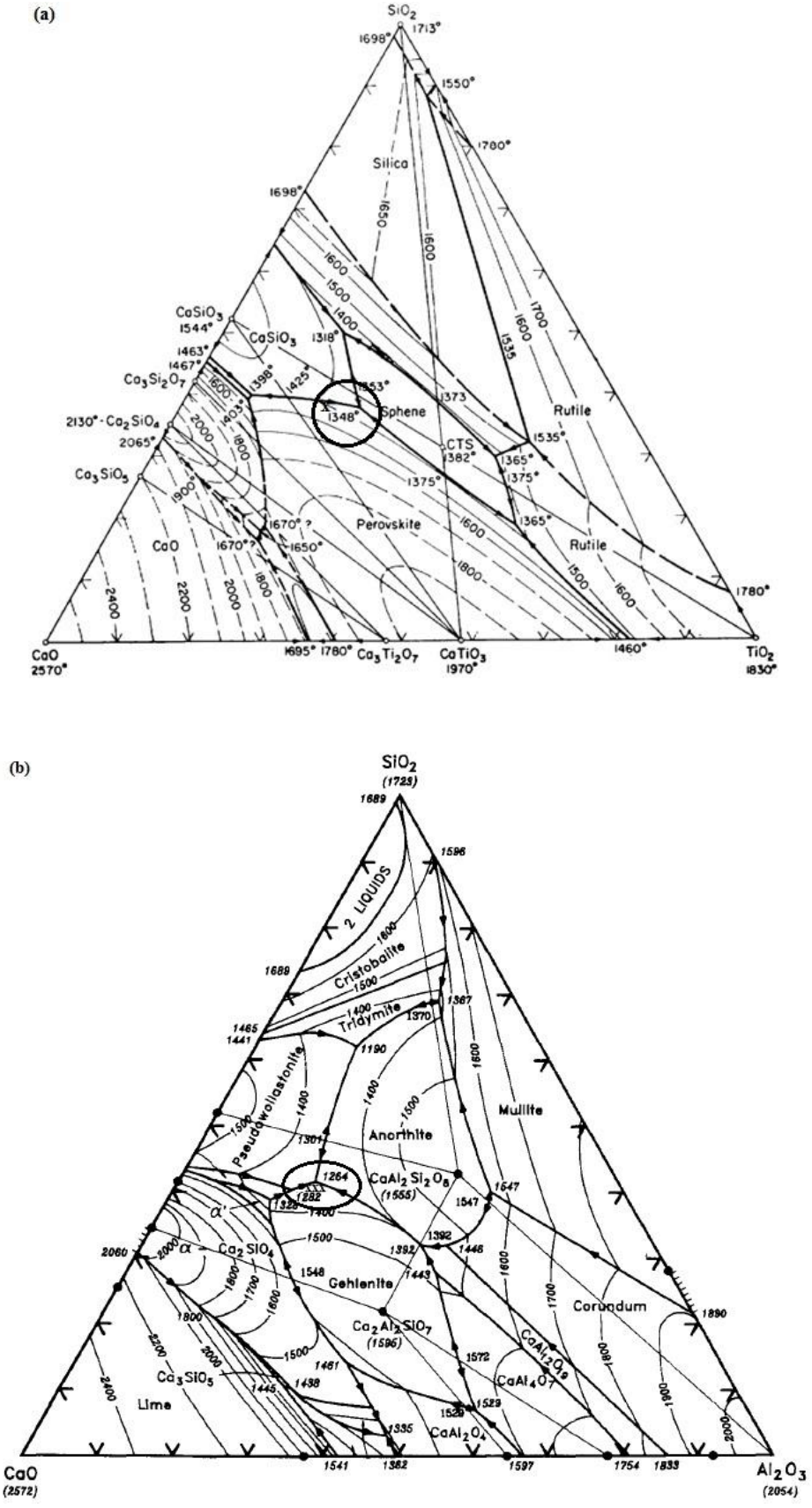

Figure 4.5.1 Experimental phase diagram of (a) CaO-SiO_2-TiO_2 system (De Vries, 1955 [36]) (b) CaO-SiO_2-Al_2O_3 system (Eriksson and Pelton, 1993 [42]).

Table 4.5.1 Design matrix of electrode coating formulations (SS electrodes based on CaO-SiO_2-Al_2O_3-TiO_2 system)

Expt. No.	Nature of mixture design point	Ingredients of electrode coatings			
		CaO	SiO_2	Al_2O_3	TiO_2
1	Vertex	15	32	18	10
2	Centroid	23.17	23.17	8	20.67
3	Vertex	15	15	18	27
4	Vertex	15	17	8	35
5	Vertex	15	35	15	10
6	Vertex	22	35	8	10
7	Centroid	24.83	15	12.83	22.33
8	Centroid	25.67	25.67	13.67	10
9	Vertex	35	15	8	17
10	Vertex	35	15	15	10
11	Centroid	35	17.33	10.33	12.33
12	Centroid	15	24.83	12.83	22.33
13	Vertex	15	35	8	17
14	Centroid	20.67	20.67	18	15.67
15	Centroid	15.67	15.67	8.67	35
16	Centroid	22.17	22.17	11.83	18.83
17	Vertex	17	15	8	35
18	Centroid	17.33	35	10.33	12.33
19	Vertex	35	22	8	10
20	Vertex	15	15	10	35
21	Vertex	32	15	18	10

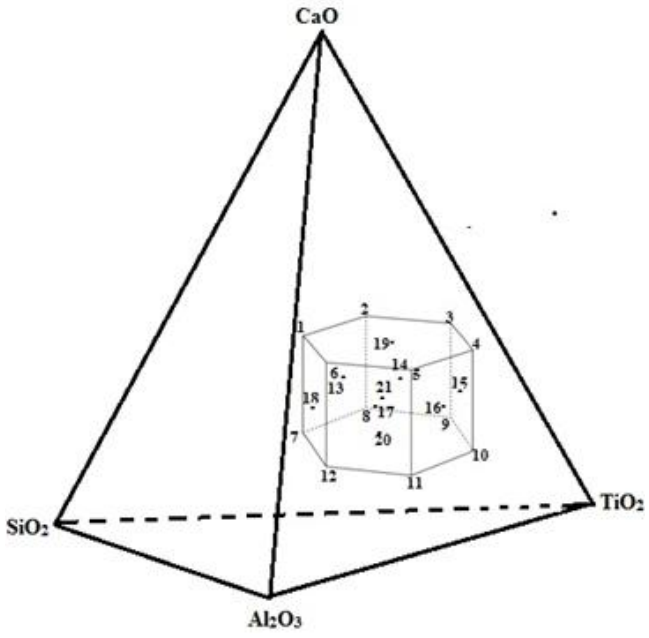

Figure 4.5.2 Mixture design points in 3D space.

4.6 Experimentation

4.6.1 Manufacturing of coated electrodes

The different welding electrodes were manufactured in welding electrode manufacturing plant. The welding electrode manufacturing plant consists of wire straightening & cutting machine, dry mixer, wet mixer, briquetting press, extrusion plant, concentricity tester and electrode baking oven as shown in Figure 4.6.1. The electrode extrusion plant further has wire feeder, extruder and conveyor.

The various ingredients of welding electrode coatings were weighed as described/formulated in design matrices (Tables 4.3.1, 4.4.1 and 4.5.1) and then mixed properly with dry mixer. The liquid silicate binder was then added to the dry mixture, followed by further mixing in the wet mixer. With the help of briquetting press the mixture was compressed and cylindrical briquettes were made. The coiled core wires were straightened and cut into the desired lengths. Also some core wires of desired length were purchased directly as shown in Figure 4.6.2. The core wires of dimensions diameter 3.15 mm and length 350 mm were placed into the feeder. The briquettes were then fed into the cylindrical barrel of the extruder and hydraulic pressure was applied to push the coating mixture towards extruder die. The core wires were fed into the extruder die with the help of wire feeder. The coating mixture was coated on the core wire when it came out of the extruder die and placed on the conveyor. With the help of rotating wheels, some portion of coating was removed from one end of the electrode from where it was to be hold in the electrode holder. The coating from the opposite end was also removed to facilitate the electrical contact for arc initiation. The electrode was checked for eccentricity with the concentricity tester. The concentricity of the coated electrodes was ensured by adjusting the various bolts with which the die was attached to the extruder. The extruded electrodes using mild steel core wire were kept at room temperature for air drying for one day and then baked at 200°C for one hour and allowed to cool to room temperature in oven itself. The stainless steel electrodes on the other hand were air dried for one day and then baked at 400°C for one hour in the drying oven and then allowed to cool to room temperature in the oven itself.

(a) Wire cutting machine

(b) Wire feeder

(c) Wet mixer

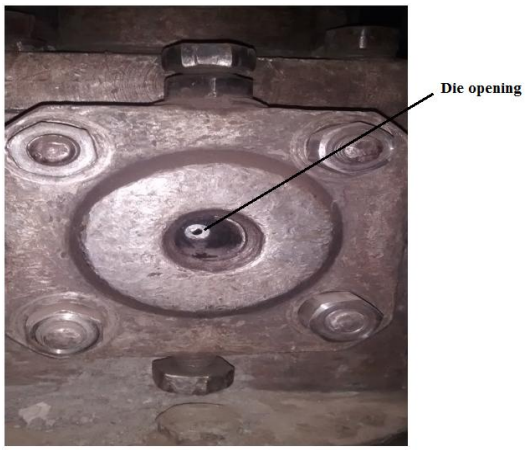

(d) Extrusion die

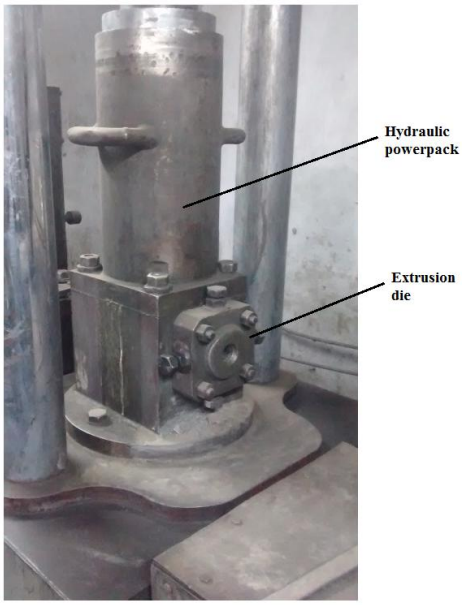

(e) Extruder

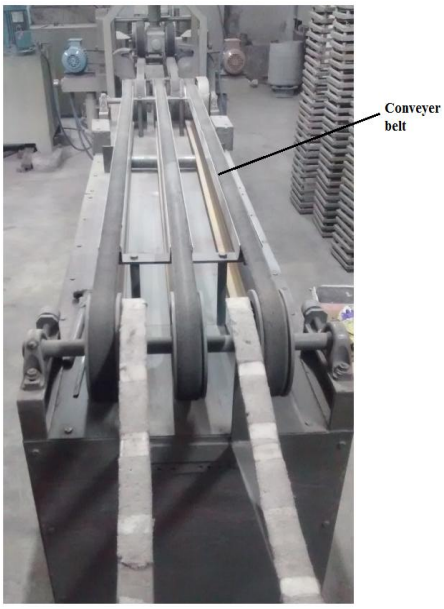

(f) Conveyor system

Figure 4.6.1 Components of electrode manufacturing plant.

Figure 4.6.2 Core wires used for the development of coated electrodes.

The mild steel coating formulations as given in Table 4.3.1 were extruded with mild steel core wire. For the development of stainless steel electrodes, SS308L and SS309L filler core wires were used for each set of electrode coating formulation (Table 4.4.1 and 4.5.1). The core wires used in the manufacturing process are shown in Figure 4.6.2.

4.6.2 Welding trials for welding process parameters.

The welding trials were conducted to decide the welding process parameter i.e. welding current for the developed coated electrodes. For the mild steel electrode, the coating formulation no. 2 (Table 4.3.1 and Figure 4.6.3(a)) represents the overall centroid of the design matrix. This electrode was selected for the bead on plate welding trails to decide the welding current for the mild steel electrodes. The bead on plate trials were conducted with DC electrode positive polarity and the welding speed was tried to maintain at 2 mm/s. The broad qualitative observations were made and marked in the Table 4.6.1. The current value 115A depicted better qualitative observations in terms of arc stability, slag detachability and bead appearance and was chosen for further investigations of mild steel electrodes.

The two characteristics of the weld bead are the bead height and width, as shown in Figure 4.6.4. These characteristics are important to assure that the weld joint is properly filled, with a minimum of defects, particularly in multi-pass weldments. If the bead height is too large, it becomes very difficult to make subsequent weld passes that will have good fusion. The more peaked and narrow the weld bead, the greater the chance that poor fusion may occur.

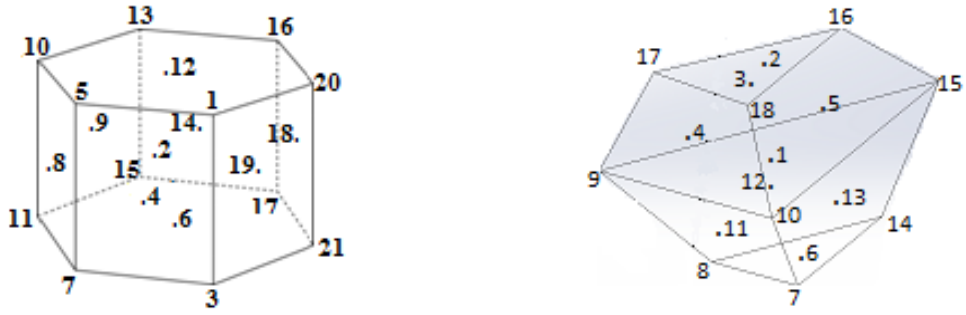

(a) (b)

Figure 4.6.3 Mixture design space.

Table 4.6.1 Qualitative observations of mild steel electrode (coating formulation no. 2)

S.No.	Current (Ampere)	Arc stability	Slag detachability	Bead appearance
1	105	Fair	Fair	Poor
2	110	Fair	Fair	Good
3	115	Good	Fair	Good
4	120	Fair	Fair	Good

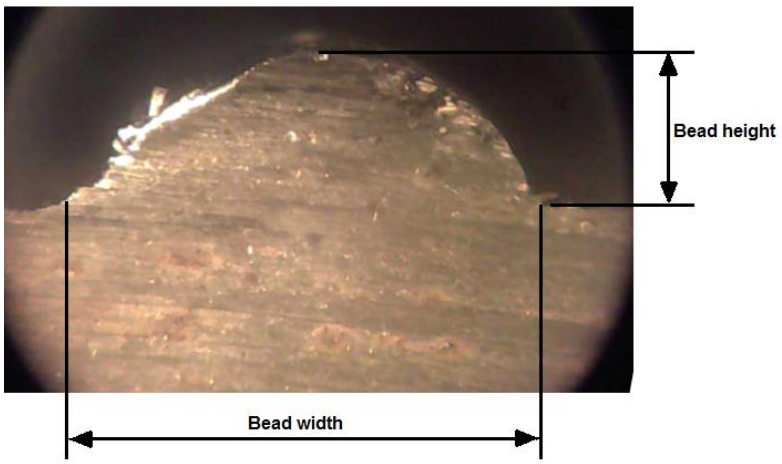

Figure 4.6.4 Weld bead profile at current 115A for mild steel electrode (coating formulation no. 2).

The same procedure was repeated for the stainless steel electrodes also so as to find out the welding current. The stainless steel coated electrodes (both SS 308L and SS309L) based on CaO-TiO_2-SiO_2 system with coating formulation no. 1 (Table 4.4.1 and Figure 4.6.3(b)) representing the overall centroid of design matrix were chosen

for the bead on plate welding trails to decide the welding current. The trials were conducted with DC electrode positive polarity while keeping the welding speed at 2 mm/s. On the basis of observed behavior of electrodes, the current value range 95A was found out to be comparatively better than the other trials as shown in Table 4.6.2.

Table 4.6.2 Qualitative observations of stainless steel electrodes (coating formulation no. 1) based on CaO-TiO_2-SiO_2 system

S.No.	Current (Ampere)	Arc stability	Slag detachability	Bead appearance
1	80	Poor	Fair	Poor
2	85	Fair	Good	Fair
3	90	Fair	Good	Good
4	95	Fair	Good	Excellent

After repeating the same process for the stainless steel electrodes based on CaO-SiO_2-Al_2O_3-TiO_2 system (coating formulation no.16), the current value 95A was found out to be better process parameters (Table 4.6.3).

Table 4.6.3 Qualitative observations of stainless steel electrodes based on CaO-SiO_2-Al_2O_3-TiO_2 system (coating formulation no. 16)

S.No.	Current (Ampere)	Arc stability	Slag detachability	Bead appearance
1	80	Fair	Fair	Poor
2	85	Fair	Fair	Fair
3	90	Fair	Good	Good
4	95	Good	Good	Good

4.6.3 Fabrication of weld pads with mild steel electrodes

For the bimetallic welds, the base plates were of SA516 ferritic steel and SS304L austenitic stainless steel materials. The chemical composition of base metals as determined by atomic absorption spectrometer is presented in Table 4.6.4. First of all the investigations were made to find out the optimized electrode coating composition of MS electrode which was aimed to be used as the first buttering layer electrode on the ferritic steel SA516 base plates in the proposed three layer bimetallic weld methodology.

Table 4.6.4 Chemical composition of base metals

Material	%Cr	%C	% Si	%Mn	% P	% S	% Mo	% Ni	% N_2	% Cu
SS304L	18.2	0.025	0.5	1.6	0.045	0.030	-	8.5	0.10	-
SA516	-	0.19	0.3	1.1	0.03	0.030	0.08	-	-	0.3

The weld pads on SA516 base plates were fabricated with the mild steel electrodes so as to investigate the role of electrode coating ingredients on various weld responses. The welding current was taken as 115A and the welding speed was around 2 mm/s. For weld quality analysis, the various test specimens were prepared from the weld pads. After undergoing through the weld characterization (discussed later in this chapter), regression analysis and optimization, the optimized electrode coating formulation was found out (to be discussed in Chapter 5). The electrode with this optimized composition was manufactured to act as the MS buttering layer electrode in the fabrication of three layer of bimetallic welds.

4.6.4 Preparation of bimetallic weld coupons

For experimentation, the large size SA516 ferritic steel and SS304L austenitic stainless steel plates were provided by Steel Authority of India Ltd and JSL Ltd. respectively on complimentary basis. The SS304L austenitic stainless steel plate of size 800x300x32mm is shown in Figure 4.6.5. The plates were cut into sizes of 300x80x32 mm dimensions as shown in Figures 4.6.6 (a) and (b). For weld coupons, the edges of plates were prepared for making V-grooves of 60° as shown in Figure 4.6.7 and described in Table 4.6.5.

Figure 4.6.5 SS304L plate (800x300x32mm).

(a) (b)

Figure 4.6.6 Base plates for weld coupon (a) SA516 (b) SS304L (300x80x32 mm).

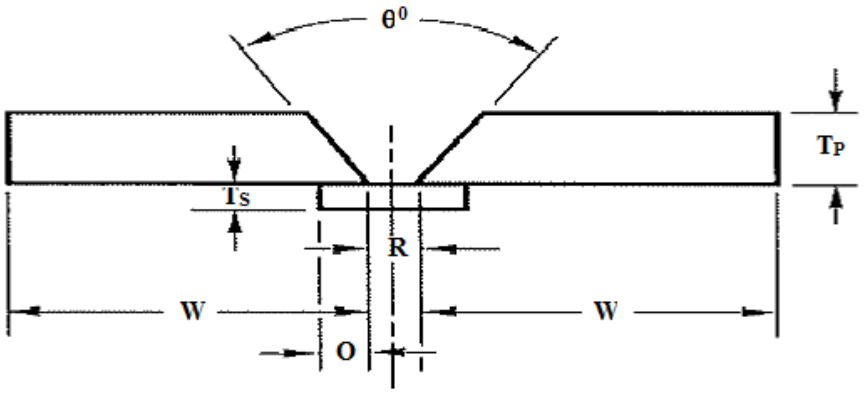

(a)

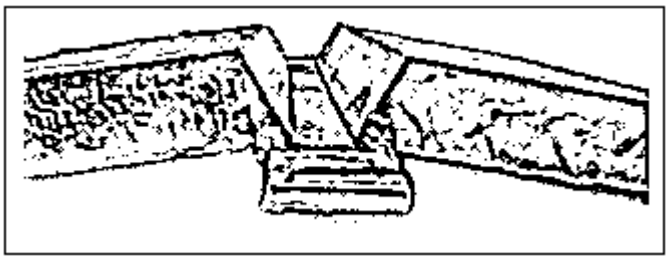

(b)

Figure 4.6.7 Weld coupon.

Table 4.6.5 Description of weld coupon

S.No.	Description	Dimension (mm)
1.	Plate width (W)	80
2.	Plate thickness (T_P)	32
3.	Strip thickness (T_S)	6
4.	Root gap (R)	16
5.	Overlap (O)	7
6.	Groove angle (θ°)	60°

The SMAW welding setup used for the welding of bimetallic joints is shown in Figure 4.6.8. In the two layer bimetallic methodology, the weld coupons were prepared by firstly applying the buttering layer with the SS309L developed electrodes on the edges of SA516 ferritic steel plates and then subsequently the bimetallic weld coupons were prepared between the buttered plates and the SS304L austenitic stainless steel plates.

In three layer bimetallic methodology, the optimized MS buttering electrode was used to apply the first layer of buttering on the SA516 base plates. The SS309L stainless steel electrodes based on both $CaO\text{-}TiO_2\text{-}SiO_2$ and $CaO\text{-}SiO_2\text{-}Al_2O_3\text{-}TiO_2$ systems were used separately for buttering the mild steel buttered SA516 plates. Then SS308L electrodes (of the same type of coating composition of SS309L) were subsequently used to butt weld the MS/SS buttered SA516 plates with SS304L plates by using optimum welding parameters with DC electrode positive polarity so as to make the bimetallic welds. The welding speed was maintained constant at 2 mm/s. Each coating formulation as given in Tables 4.4.1 and 4.5.1 was extruded on both SS309L and SS308L filler wires. So both SS309L and SS308L coated electrodes might be termed as one set in which the SS309L electrode was to be used for the buttering and SS308L electrode of same electrode coating formulation was to be used for making the final weld between the MS/SS buttered SA516 ferrite steel and the SS304L austenitic stainless steel. The Figure 4.6.9 (a) to (d) shows the different stages of welding of bimetallic joints.

Ultrasonic testing is a non destructive testing (NDT) method, in which sound waves of high frequency are introduced in to the material being inspected to detect internal flaws and to study the properties of material. The sound waves travel into the material with some loss of energy due to attenuation and are reflected as interfaces. In most of the applications, the reflected beam is detected and analyzed to define the presence and location of defect and for quantitative evaluation. Defect like cracks, shrinkage cavities, lack of fusion, pores and bonding faults which act like metal gas interface can be easily detected by this method. Inclusions and other inhomogenities in the metal can also be detected due to partial reflection or scattering of the ultrasonic waves. The bimetallic weld plates were ultrasonically inspected as shown in figure 4.6.9 (e). Ultrasonic inspection is mostly carried out at frequencies between 1 and 25 MHz. The inspection system includes, An electronic flaw detector having a sweep

circuit, pulse generator, clock circuit and a cathode ray tube and a transducer (probe or search unit) having a piezoelectric crystal that emits a beam of ultrasonic waves when burst of alternating voltage are applied to it.

Figure 4.6.8 SMAW welding setup used.

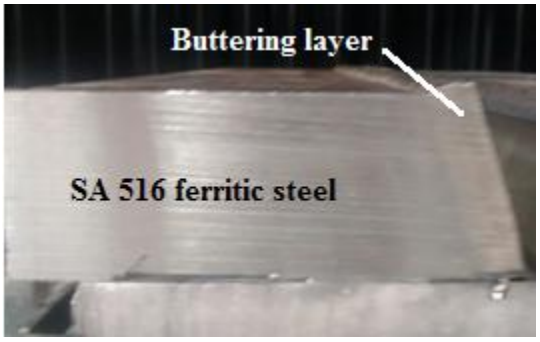

(a)

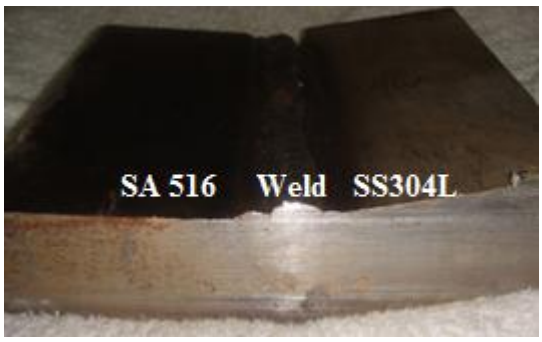

(b)

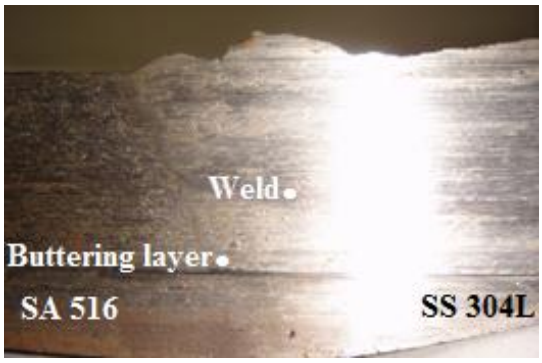

(c)

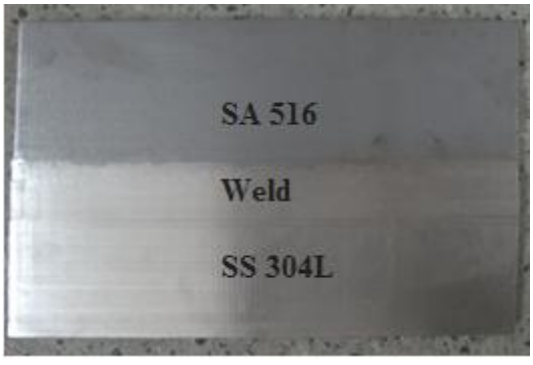

(d)

(e)

Figure 4.6.9 (a) Buttering layer on SA516 plate, (b) bimetallic weld coupon, (c) front edge of bimetallic weld, (d) top view of machined bimetallic weld coupon and (e) ultrasonic inspection of bimetallic weld plate.

4.6.5 Weld Characterization

The chemical composition analysis of welds was determined using optical emmision spectrometer. The various test specimens were cut from the welded coupons and weld pads for the mechanical behavior analysis. The weld plate showing the location of various test specimens is shown in Figure 4.6.10.

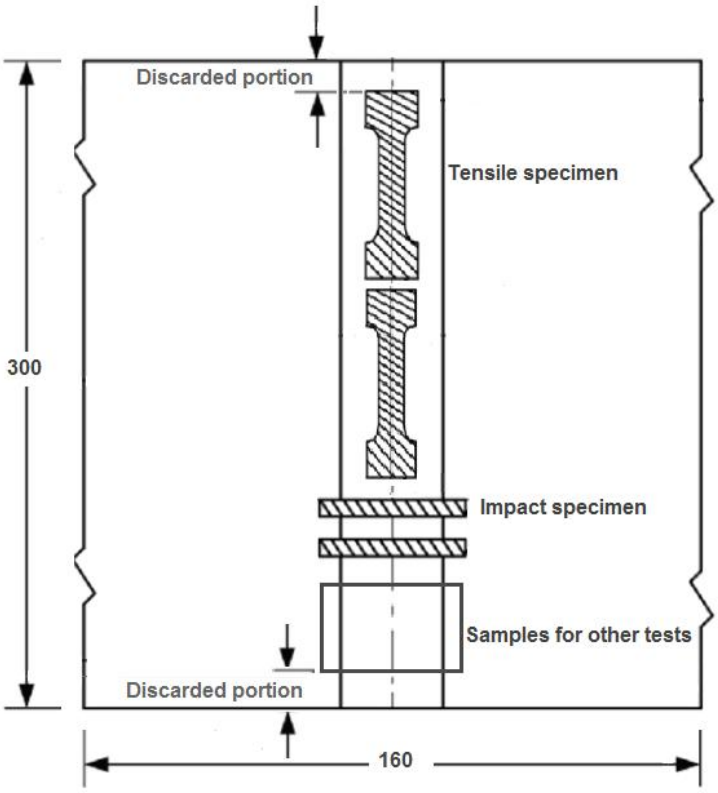

Figure 4.6.10 Weld plate showing the location of various test specimens (all dimensions are in mm).

Tensile tests as per ASTM E8M on all weld tensile specimens were performed on computerized UTM (Model-5982 of Instron) as shown in Figure 4.6.11 and ultimate tensile strength (UTS) along with percentage elongation was observed.

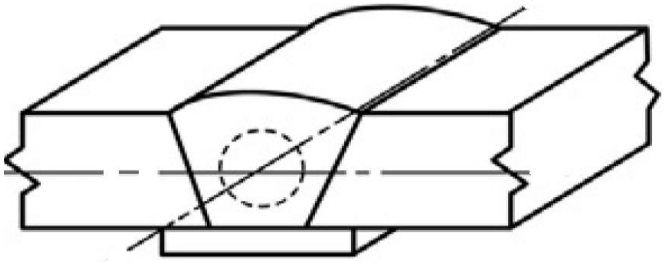

(a)

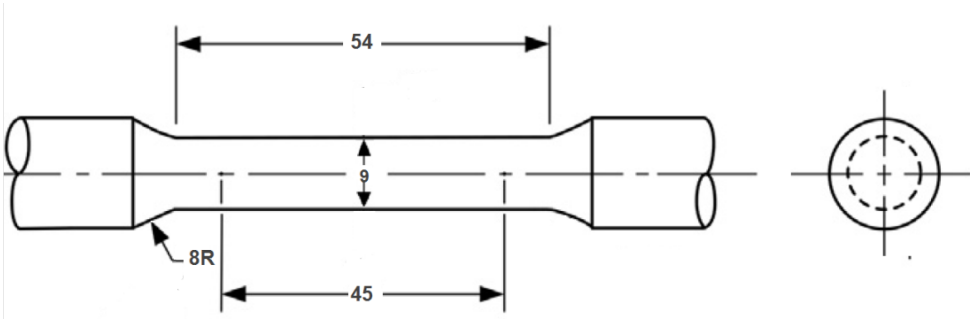

(b)

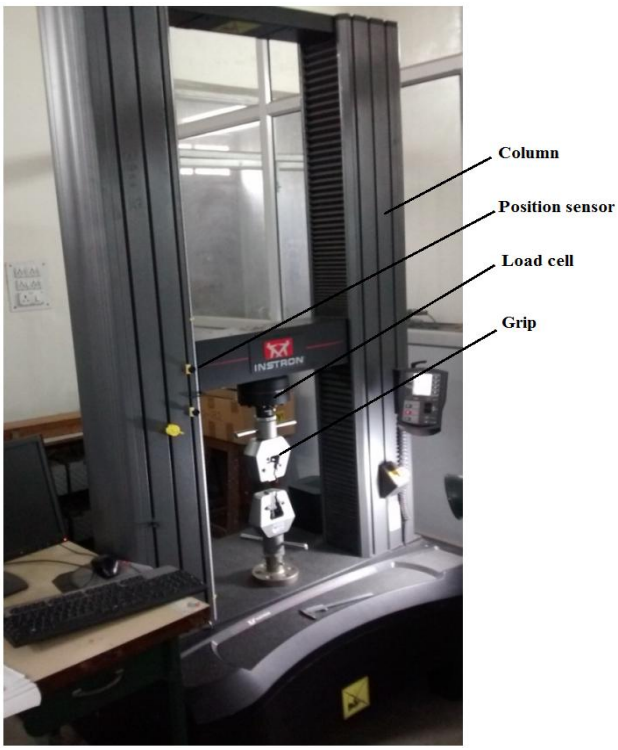

(c)

Figure 4.6.11 (a) Orientation of tensile specimen, (b) specifications of standard tensile specimen (ASTM E8M) (all dimensions are in mm) and (c) UTM (Model-5982 of Instron).

Charpy V- notch impact test was performed on impact specimens having specifications ASTM E23-07AE1 (Figure 4.6.12) on impact testing machine (Model-FIT30 of Batliboi) at room temperature. Microhardness measurement was carried on Omnitech microhardness tester (Model MVH-S-AUTO) as shown in Figure 4.6.13.

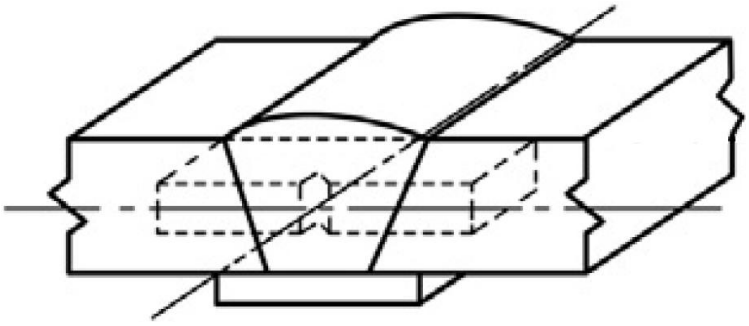

(a)

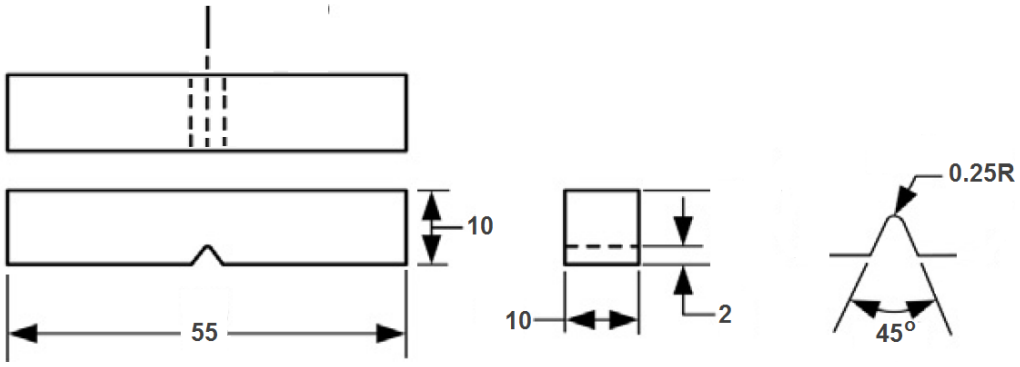

(b)

Figure 4.6.12 (a) Orientation of impact specimen and (b) specifications of standard impact specimen (ASTM E23) (all dimensions are in mm).

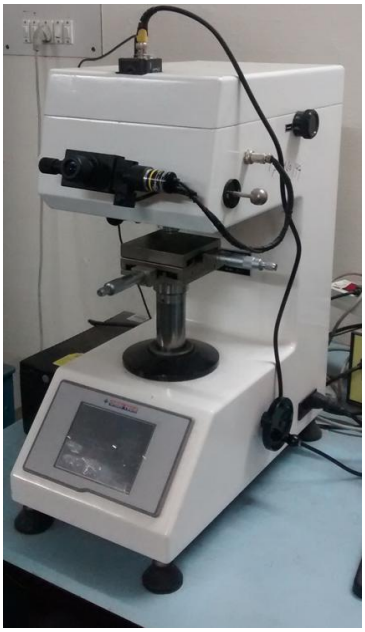

(a)

(b)

Figure 4.6.13 (a) Microhardness tester and (b) test specimen.

To measure the diffusible hydrogen content, mercury method was used. Filler material was deposited on to a standard test coupon in a manner that ensures control of pertinent variables to produce a representative specimen for analysis. Subsequent storage and handling of the specimen is controlled to prevent premature loss of hydrogen. Finally, the specimen is transferred to a gas collection apparatus (mercury method) held for a period of 72 hours at a temperature sufficient to quantitatively release the diffusible hydrogen into a burette. The amount of hydrogen collected is determined by measuring the displaced volume (mercury method). Finally, quantification of the mass of deposited metal or volume of fused weld metal enables calculations of diffusible hydrogen in deposited metal.

Corrosion test was carried out to measure the corrosion rate of specimens made from deposition pads using MS buttering layer electrodes. To assess the corrosion resistance of specimens, immersion test (ASTM G1) was carried out. Specimens were prepared, cleaned with acetone and then immersed in the 3.5% NaCl solution. The corrosion rate was obtained as follows:

Corrosion rate (mm/year) = (87.6*W) / (D*A*T)
Where, W = weight loss in milligrams,
D = metal density in g/cm^3,
A = area of weld specimen in cm^2, and
T = time of exposure of specimen in hours

The metallographic examination of the welded samples was conducted on Dewinter optical microscope (DMI Premium). The weld specimens were polished for microstructural examination. The mild steel specimens were etched with 2% nital solution while the etching of stainless steel specimens were carried out with and then etched by the acetic glyceregia etchant (5 ml glycerine + 10 ml acetic acid + 10 ml HNO_3 + 15 ml HCl). For the measurement of inclusion size, linear analysis technique in quantitative metallography was adopted. The straight lines were drawn on the print image of the micrographs. The length of all intercepts was summated and the ratio of the summated length to the calibrated optical scale length was evaluated to find the size of the inclusions. The calibrated optical scale on the microscope is the actual distance between two points on an optical image.

The ferrite number represents the volume content of delta ferrite which is responsible for preventing solidification cracking in welds. It was measured using WRC 92 diagram (Kotecki and Siewert, 1992[85]) shown in Figure 4.6.14 and ferritescope. The WRC 92 diagram uses chromium equivalent (Cr_{eq}=Cr+Mo+0.7Nb) and nickel equivalent (Ni_{eq}=Ni+35C+20N+0.25Cu) to calculate the ferrite number.

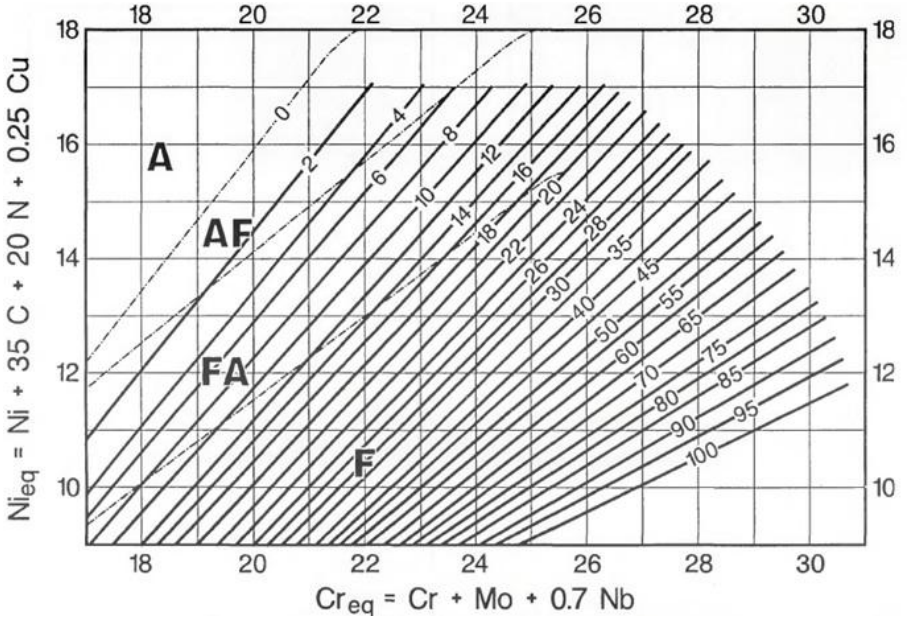

Figure 4.6.14 WRC 92 diagram (Kotecki and Siewert, 1992 [85]).

CHAPTER 5
RESULTS AND DISCUSSION

This chapter deals with the development of the regression models on the basis of results obtained from experimentation and characterization of bimetallic weld coupons. The developed regression models have been checked for adequecy using analysis of variance (ANOVA) and also discussed. This chapter also analyses and discusses the results obtained through the experimentation.

5.1 Development of Regression Models (Mild Steel Electrodes)

The results of weld metal chemistry analysis are given in Table 5.1.1. The quadratic regression models of these weld responses have been developed in terms of percentage composition of individual electrode coating ingredients (CaO, CaF_2, SiO_2 and Ni) along with their binary mixtures and are given below:

%Ni = -0.073742CaO - 4.22449E-004CaF_2 - 0.89745SiO_2 + 0.77899Ni + 0.023142 CaO.SiO_2 + 0.017730CaF_2.SiO_2 - 0.015801CaF_2.Ni + 0.019224SiO_2.Ni (5.1.1)

%P = -1.02981E-004CaO - 2.65661E-004CaF_2 - 7.9795E-003SiO_2 + 5.46824E-003Ni + 1.78768E-004CaO.SiO_2 - 8.58256E-005CaO.Ni + 2.01430E-004CaF_2.SiO_2 (5.1.2)

%S = +6.75878E-004CaO + 1.04239E-003CaF_2 + 0.012934SiO_2 + 0.048732Ni - 2.67960E-004CaO.SiO_2 - 8.79692E-004CaO.Ni - 2.92074E-004CaF_2.SiO_2 - 8.13678E-004CaF_2.Ni - 1.15577E-003SiO_2.Ni (5.1.3)

%C = +3.03388E-003CaO + 3.61996E-003CaF_2 - 1.09569E-004SiO_2 + 0.059539Ni - 1.38966E-004CaO.CaF_2 - 1.17374E-003CaO.Ni - 1.03441E-003CaF_2.Ni - 8.17685E-004SiO_2.Ni (5.1.4)

%Mn = +0.042942CaO + 0.016006CaF_2 - 0.037389SiO_2 + 0.45457Ni - 0.012274CaO.Ni - 7.19330E-003CaF_2.Ni (5.1.5)

%Si = +2.96050E-003CaO + 1.30248E-003CaF_2 + 7.11400E-003SiO_2 + 0.021669Ni - 2.53949E-004CaO.SiO_2 - 4.37208E-004CaO.Ni - 3.96394E-004CaF_2.Ni (5.1.6)

Table 5.1.1 Chemical composition analysis of weld pads of mild steel electrodes

Expt.	%Ni	%P	%S	%C	%Mn	%Si
1	3.50	0.020	0.020	0.086	1.05	0.154
2	1.70	0.020	0.005	0.059	0.84	0.120
3	0.30	0.016	0.017	0.073	1.30	0.117
4	3.80	0.028	0.016	0.078	1.05	0.127
5	0.45	0.017	0.019	0.078	1.10	0.123
6	2.00	0.020	0.010	0.065	0.85	0.120
7	0.35	0.015	0.021	0.079	0.83	0.134
8	1.70	0.023	0.007	0.068	0.80	0.122
9	0.55	0.017	0.017	0.069	1.30	0.118
10	0.40	0.013	0.015	0.070	1.40	0.110
11	0.47	0.015	0.018	0.080	1.20	0.120
12	1.50	0.019	0.008	0.058	1.20	0.110
13	2.90	0.032	0.024	0.080	1.10	0.130
14	2.20	0.019	0.006	0.060	0.95	0.116
15	0.50	0.012	0.019	0.070	0.90	0.110
16	0.80	0.017	0.017	0.080	0.81	0.118
17	0.70	0.012	0.013	0.059	1.30	0.112
18	0.60	0.015	0.012	0.068	1.36	0.112
19	0.70	0.015	0.018	0.078	1.00	0.120
20	3.80	0.025	0.016	0.065	0.88	0.120
21	3.95	0.022	0.021	0.082	1.00	0.150

The results of other weld responses i.e. ultimate tensile strength (UTS), impact toughness, macrohardness, diffusible hydrogen content and corrosion rate are summarized in Table 5.1.2. The developed quadratic regression models of these weld responses are as follows:

$$UTS = +3.58086CaO + 8.63573CaF_2 - 29.71837SiO_2 + 11.38299Ni + 1.09819CaO.SiO_2 + 0.55125CaF_2.SiO_2 + 0.28368CaF_2.Ni + 0.97845SiO_2.Ni \quad (5.1.7)$$

$$\text{Impact toughness} = +2.54610CaO + 1.65079CaF_2 - 0.17142SiO_2 + 1.13513Ni + 0.12273CaO.Ni + 0.11510CaF_2.SiO_2 + 0.13442CaF_2.Ni \quad (5.1.8)$$

Macrohardness = +2.40245CaO + 3.46397CaF_2 - 0.80086SiO_2 + 1.77842Ni - 0.04852CaO.CaF_2 - 0.11779CaO.SiO_2 + 0.07046CaF_2.Ni + 0.13231SiO_2.Ni (5.1.9)

Diffusible hydrogen content = -0.20272CaO - 0.30460CaF_2 - 0.32004SiO_2 - 0.78784Ni + 0.023926CaO.CaF_2 + 0.021198CaO.Ni + 0.024781CaF_2.SiO_2 + 0.044305SiO_2.Ni (5.1.10)

Corrosion rate = +1.96840E-003CaO + 1.86179E-003CaF_2 + 7.01305E-004SiO_2 + 8.51538E-003Ni - 5.65870E-005CaO.CaF_2 - 1.89148E-004CaO.Ni - 1.59320E-004CaF_2.Ni - 1.94885E-004SiO_2.Ni (5.1.11)

Table 5.1.2 Results of various weld responses of mild steel electrodes

Expt. No.	Ultimate tensile strength (MPa)	Impact toughness (NM)	Macrohardness (HVN)	Diffusible hydrogen content (ml per 100 gms	Corrosion rate (mm/y)
1	590	174	168	5.8	0.052
2	540	162	160	6.7	0.058
3	485	148	150	6.4	0.068
4	595	178	168	5.0	0.052
5	510	152	155	7.0	0.069
6	540	164	160	6.4	0.057
7	480	154	150	7.0	0.067
8	552	167	162	6.8	0.061
9	505	152	152	7.2	0.067
10	503	148	154	5.4	0.070
11	515	152	155	7.4	0.068
12	535	166	158	6.6	0.060
13	610	185	172	4.0	0.055
14	555	164	163	5.5	0.062
15	505	145	154	5.1	0.070
16	520	154	158	6.3	0.064
17	515	155	156	5.0	0.065
18	500	155	153	5.9	0.069
19	510	152	155	6.5	0.069
20	580	182	165	5.0	0.053
21	585	175	170	5.2	0.053

5.1.1 Regression analysis

It was observed while analysing the quadratic regression models that there were many insignificant terms in the models. Therefore, model reduction using the backward elimination process was performed to improve the each model (Eq. (5.1.1 to 5.1.11)). It eliminates the insignificant terms in order to adjust the fitted quadratic model while maintaining the hierarchy of model. Tables 5.1.3 and 5.1.4 show the results of ANOVA after backward elimination.

Table 5.1.3 ANOVA results of regression models of weld metal chemistry after backward elimination (mild steel electrodes)

Weld response	Source	Sum of squares	DF	Mean square	F value	P value	Status
%Ni	Model	33.80547	7	4.829353	729.59	< 0.0001	Signi.
	Linear	32.7355	3	10.91183	1648.5	< 0.0001	
	$CaO.SiO_2$	0.254503	1	0.254503	38.44	< 0.0001	
	$CaF_2.SiO_2$	0.149726	1	0.149726	22.619	0.0004	
	CaF_2.Ni	0.534334	1	0.534334	80.724	< 0.0001	
	SiO_2.Ni	0.131413	1	0.131413	19.853	0.0006	
	Residual	0.08605	13	0.006619			
	Total	33.89152	20	R-Squared	0.9974		
	Std.Dev.	0.081359		Adj R-Squared	0.9960		
	Mean	1.565238		Pred R-Squared	0.9914		
	C.V.	5.197849		Adeq Precision	71.373		
%P	Model	0.000496	6	8.27E-05	33.481	< 0.0001	Signi.
	Linear Mixture	0.000378	3	0.000126	51.034	< 0.0001	
	$CaO.SiO_2$	4.54E-05	1	4.54E-05	18.367	0.0008	
	CaO.Ni	1.61E-05	1	1.61E-05	6.5209	0.0230	
	$CaF_2.SiO_2$	5.65E-05	1	5.65E-05	22.898	0.0003	
	Residual	3.46E-05	14	2.47E-06			
	Total	0.000531	20	R-Squared	0.934		
	Std.Dev.	0.001571		Adj R-Squared	0.9069		
	Mean	0.018667		Pred R-Squared	0.8221		
	C.V.	8.418529		Adeq Precision	20.465		
%S	Model	0.000545	8	6.81E-05	28.796	< 0.0001	Signi.
	Linear Mixture	0.0005	3	0.00017	70.30	1.0000	
	$CaO.SiO_2$	3.14E-05	1	3.14E-05	13.2	0.0034	
	CaO.Ni	0.000338	1	0.000338	143.1	< 0.0001	
	$CaF_2.SiO_2$	3.73E-05	1	3.73E-05	15.775	0.0019	

	CaF_2.Ni	0.00029	1	0.00029	122.43	< 0.0001	
	SiO_2.Ni	0.000347	1	0.000347	146.69	< 0.0001	
	Residual	2.84E-05	12	2.37E-06			
	Total	0.000573	20	R-Squared	0.9504		
	Std.Dev.	0.001538		Adj R-Squared	0.9174		
	Mean	0.01519		Pred R-Squared	0.7194		
	C.V.	10.12411		Adeq Precision	18.688		
%C	Model	0.00149	7	0.000213	29.049	< 0.0001	Signi.
	Linear	0.000527	3	0.000176	23.961	< 0.0001	
	CaO. CaF_2	6.87E-05	1	6.87E-05	9.3722	0.0091	
	CaO.Ni	0.000621	1	0.000621	84.749	< 0.0001	
	CaF_2.Ni	0.000482	1	0.000482	65.822	< 0.0001	
	SiO_2.Ni	0.000231	1	0.000231	31.466	< 0.0001	
	Residual	9.53E-05	13	7.33E-06			
	Total	0.001585	20	R-Squared	0.9399		
	Std.Dev.	0.002707		Adj R-Squared	0.9075		
	Mean	0.071476		Pred R-Squared	0.8765		
	C.V.	3.787109		Adeq Precision	17.781		
%Mn	Model	0.586912	5	0.117382	9.4259	0.0003	Signi.
	Linear	0.267864	3	0.089288	7.1693	0.0033	
	CaO.Ni	0.237477	1	0.237477	19.068	0.0006	
	CaF_2.Ni	0.081571	1	0.081571	6.5497	0.0218	
	Residual	0.186812	15	0.012454			
	Total	0.773724	20	R-Squared	0.7585		
	Std.Dev.	0.111598		Adj R-Squared	0.6780		
	Mean	1.058095		Pred R-Squared	0.5578		
	C.V.	10.54707		Adeq Precision	10.917		
%Si	Model	0.002515	6	0.000419	21.554	< 0.0001	Signi.
	Linear	0.001841	3	0.000614	31.560	< 0.0001	
	$CaO.SiO_2$	0.000141	1	0.000141	7.2505	0.0175	
	CaO.Ni	0.000271	1	0.000271	13.952	0.0022	
	CaF_2.Ni	0.000219	1	0.000219	11.262	0.0047	
	Residual	0.000272	14	1.94E-05			
	Total	0.002787	20	R-Squared	0.9023		
	Std.Dev.	0.00441		Adj R-Squared	0.8604		
	Mean	0.122048		Pred R-Squared	0.6447		
	C.V.	3.613058		Adeq Precision	16.816		

DF- degree of freedom; Signi.- significant

Table 5.1.4 ANOVA results of regression models of various weld responses after backward elimination (mild steel electrodes)

Weld response	Source	Sum of squares	DF	Mean square	F value	P value	Status
Ultimate tensile strength	Model	28964.02	7	4137.718	135.2246	< 0.0001	Signi.
	Linear	27733.54	3	9244.515	302.1196	< 0.0001	
	$CaO.SiO_2$	573.1068	1	573.1068	18.72968	0.0008	
	$CaF_2.SiO_2$	144.7353	1	144.7353	4.730089	0.0487	
	CaF_2.Ni	172.2187	1	172.2187	5.62827	0.0338	
	SiO_2.Ni	340.4185	1	340.4185	11.1252	0.0054	
	Residual	397.7852	13	30.59886			
	Total	29361.81	20	R-Squared	0.986452		
	Std. Dev.	5.531624		Adj R-Squared	0.979157		
	Mean	534.7619		Pred R-Squared	0.966737		
	C.V.	1.034409		Adeq Precision	37.37036		
Impact toughness	Model	2797.278	6	466.2129	158.0621	< 0.0001	Signi.
	Linear	2721.681	3	907.2268	307.5809	< 0.0001	
	CaO.Ni	20.99137	1	20.99137	7.11679	0.0184	
	$CaF_2.SiO_2$	28.96192	1	28.96192	9.819079	0.0073	
	CaF_2.Ni	25.64384	1	25.64384	8.694137	0.0106	
	Residual	41.29378	14	2.949556			
	Total	2838.571	20	R-Squared	0.985453		
	Std. Dev.	1.717427		Adj R-Squared	0.979218		
	Mean	161.1429		Pred R-Squared	0.961723		
	C.V.	1.065779		Adeq Precision	38.15709		
Macro-hardness	Model	850.2274	7	121.4611	76.18799	< 0.0001	Signi.
	Linear	782.5473	3	260.8491	163.6209	< 0.0001	
	$CaO.CaF_2$	8.852184	1	8.852184	5.552645	0.0348	
	$CaO.SiO_2$	29.71476	1	29.71476	18.63896	0.0008	
	CaF_2.Ni	10.63199	1	10.63199	6.66905	0.0228	

	SiO_2.Ni	18.48114	1	18.48114	11.59253	0.0047	
	Residual	20.72497	13	1.594228			
	Total	870.9524	20	R-Squared	0.976204		
	Std. Dev.	1.262628		Adj R-Squared	0.963391		
	Mean	158.9524		Pred R-Squared	0.902143		
	C.V.	0.794343		Adeq Precision	28.68002		
Diffusible hydrogen content	Model	15.48085	7	2.211551	18.6793	< 0.0001	Signi.
	Linear	8.978679	3	2.992893	25.27871	< 0.0001	
	$CaO.CaF_2$	2.152519	1	2.152519	18.1807	0.0009	
	CaO..Ni	0.962287	1	0.962287	8.12771	0.0136	
	$CaF_2.SiO_2$	1.315185	1	1.315185	11.10837	0.0054	
	SiO_2.Ni	2.072185	1	2.072185	17.50218	0.0011	
	Residual	1.539146	13	0.118396			
	Total	17.02	20	R-Squared	0.909568		
	Std. Dev.	0.344087		Adj R-Squared	0.860874		
	Mean	6		Pred R-Squared	0.686708		
	C.V.	5.734782		Adeq Precision	15.38797		
Corrosion rate	Model	0.000842	7	0.00012	67.6214	< 0.0001	Signi.
	Linear	0.00079	3	0.000263	148.0242	< 0.0001	
	$CaO.CaF_2$	1.14E-05	1	1.14E-05	6.404704	0.0251	
	CaO.Ni	1.61E-05	1	1.61E-05	9.07054	0.0100	
	CaF_2.Ni	1.14E-05	1	1.14E-05	6.435269	0.0248	
	SiO_2.Ni	1.31E-05	1	1.31E-05	7.366799	0.0177	
	Residual	2.31E-05	13	1.78E-06			
	Total	0.000865	20	R-Squared	0.97327		
	Std. Dev.	0.001333		Adj R-Squared	0.958877		
	Mean	0.062333		Pred R-Squared	0.927844		
	C.V.	2.139093		Adeq Precision	21.46858		

DF- degree of freedom; Signi.- significant

The p values less than 0.0001 for nearly all the weld responses as given in Tables 5.1.3 and 5.1.4 indicate that the models are significant i.e. the terms in the models have significant effect on the response and there are very low chances of error occurrence due to noise. The coefficient of determination ((R-squared) for all the weld responses approaches unity and it predicts that the response models fit better to the actual data and shows less difference between the predicted and actual values. Figures 5.1.1 and 5.1.2 depict the variation of predicted values with the actual values of various weld responses. The lower values of coefficient of variation (C.V.) and higher values of Adequate Precision (Tables 5.1.3 and 5.1.4) indicate the adequacy of developed models. Hence, the developed regression models can be used to navigate the design space and predict the various weld responses.

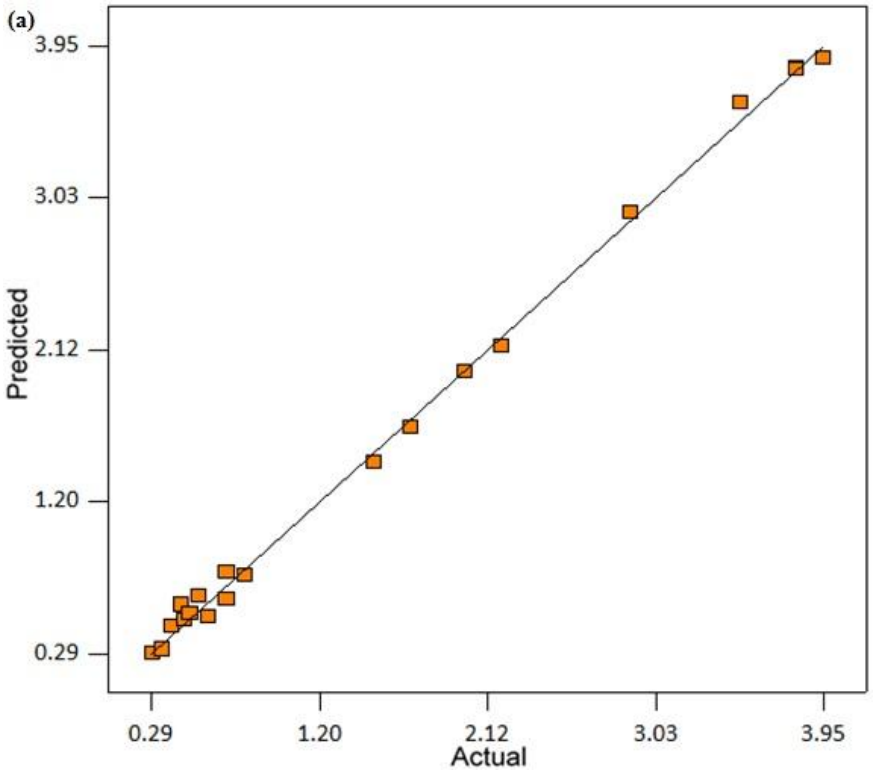

(a) %Ni

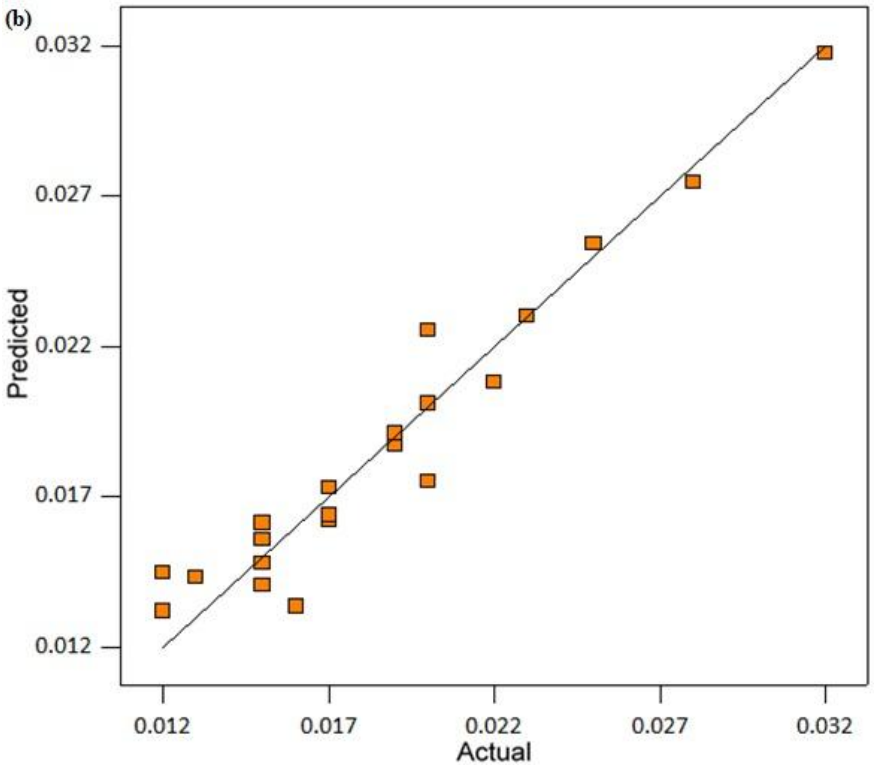
(b)
0.032
0.027
0.022
0.017
0.012
Predicted
0.012
0.017
0.022
0.027
0.032
Actual

(b) %P

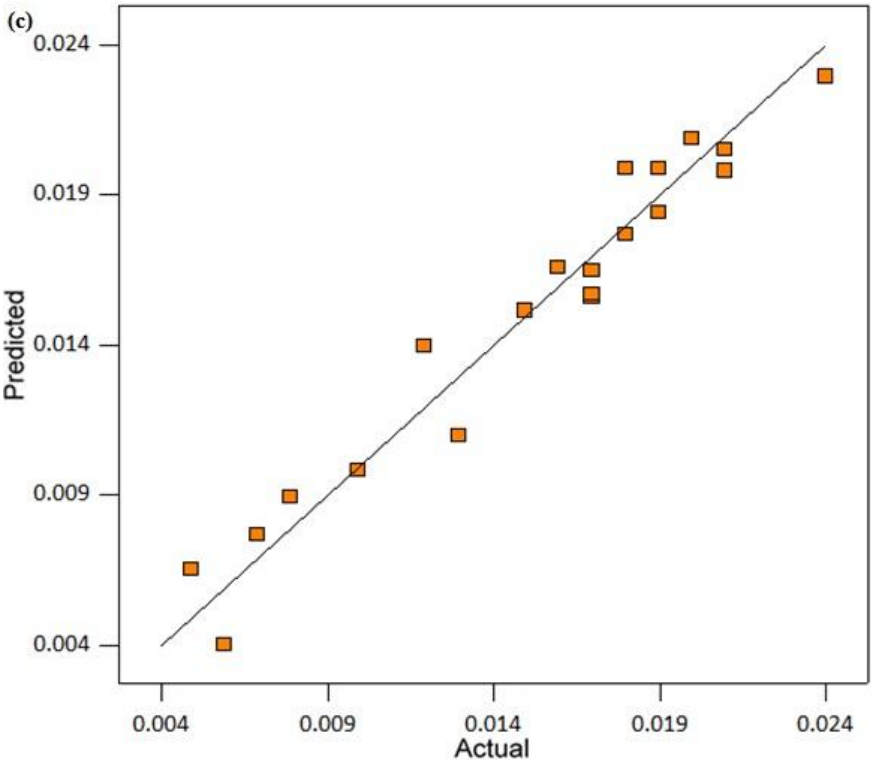
(c)
0.024
0.019
0.014
0.009
0.004
Predicted
0.004
0.009
0.014
0.019
0.024
Actual

(c) %S

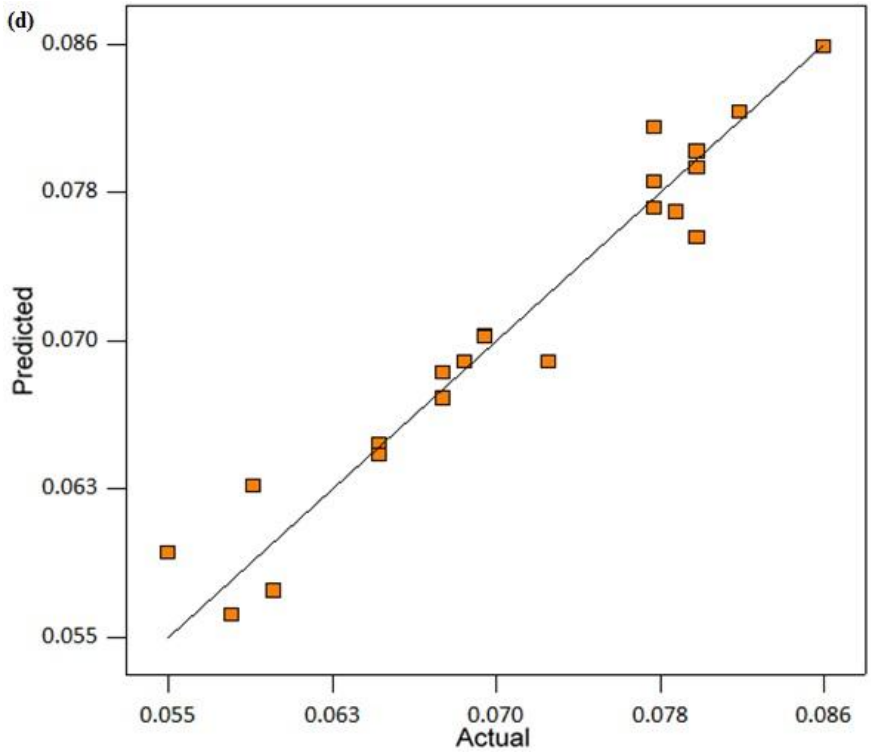
(d)
0.086
0.078
0.070
0.063
0.055
Predicted
0.055
0.063
0.070
0.078
0.086
Actual

(d) %C

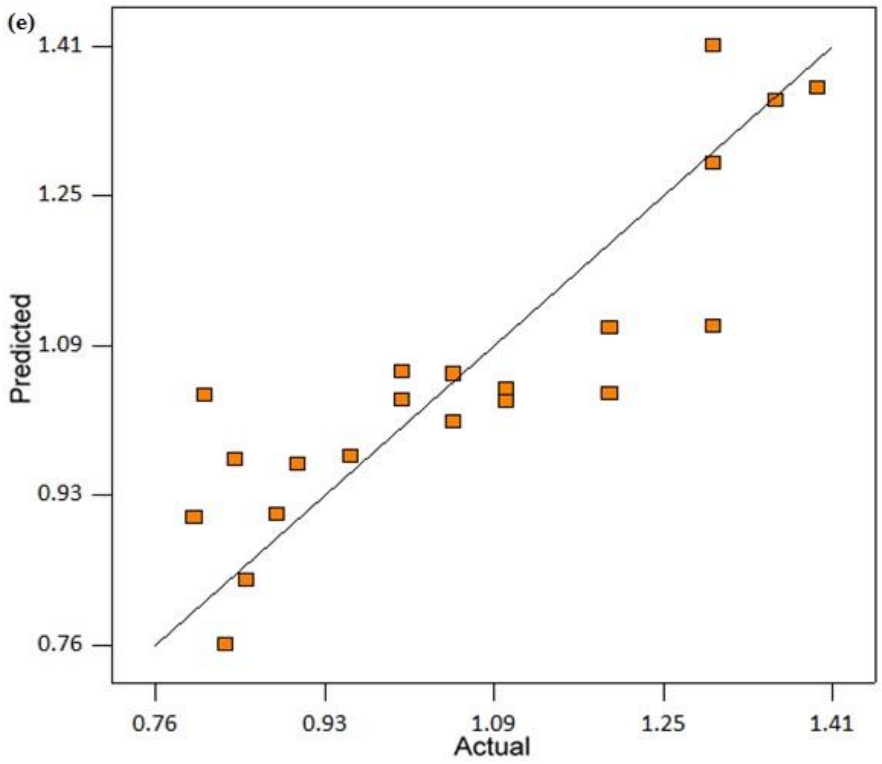
(e)
1.41
1.25
1.09
0.93
0.76
Predicted
0.76
0.93
1.09
1.25
1.41
Actual

(e) %Mn

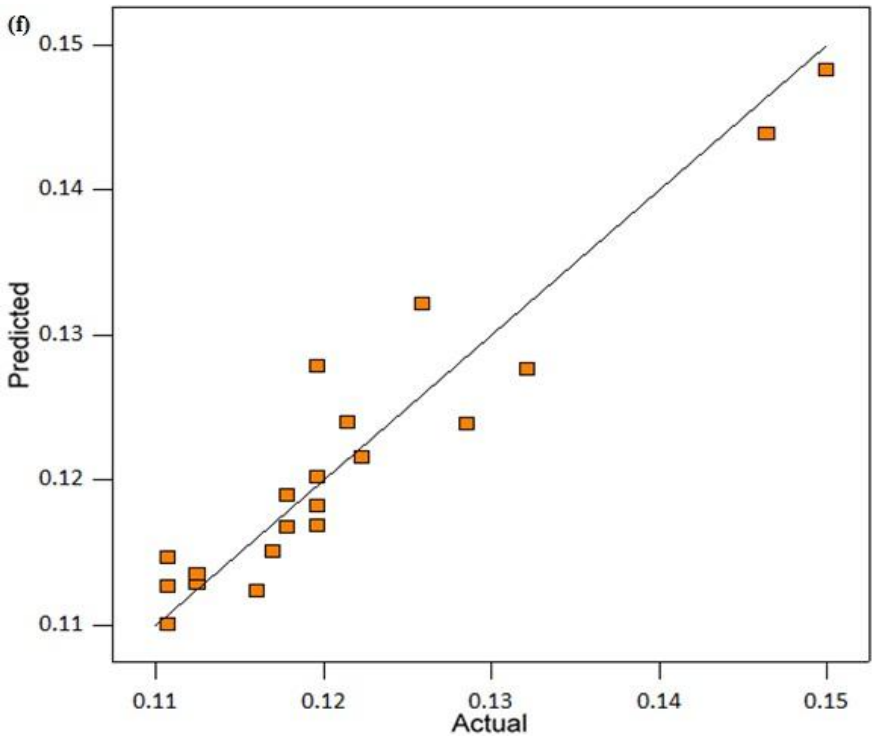

(f) %Si

Figure 5.1.1 Predicted versus actual plots of various weld responses (a) %Ni, (b) %P, (c) %S, (d) %C, (e) % Mn and (f) %Si.

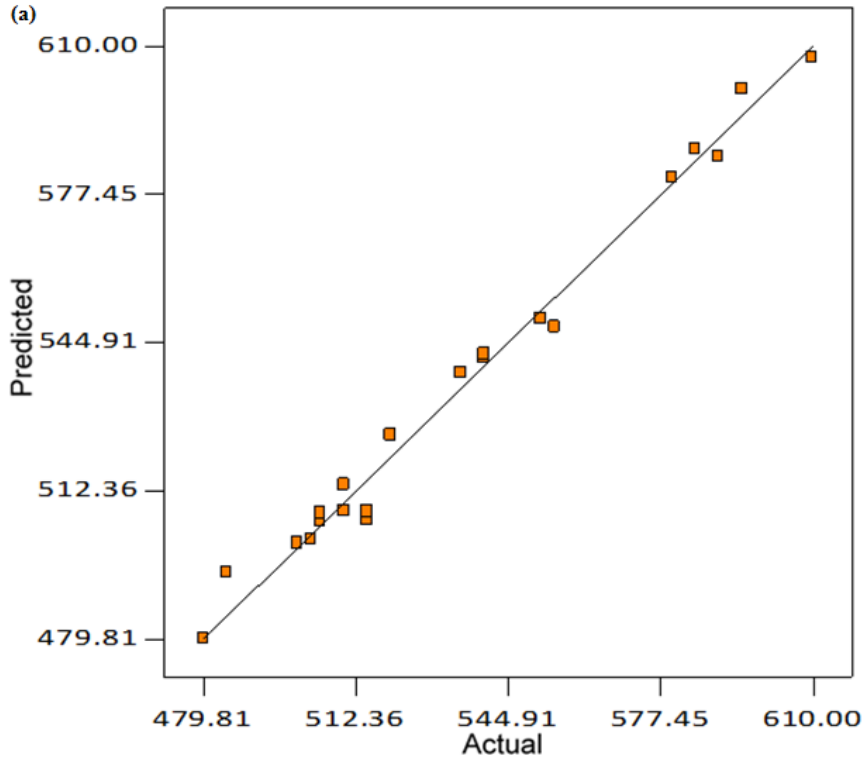

(a) Ultimate tensile strength

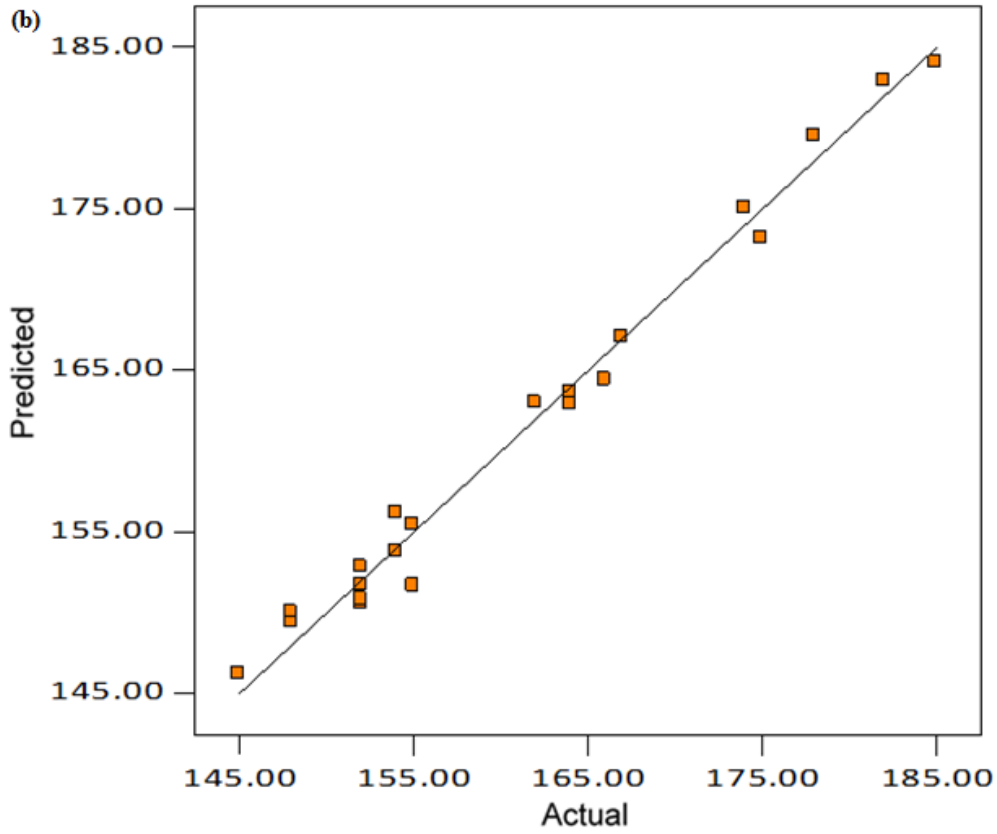

(b) Impact toughness

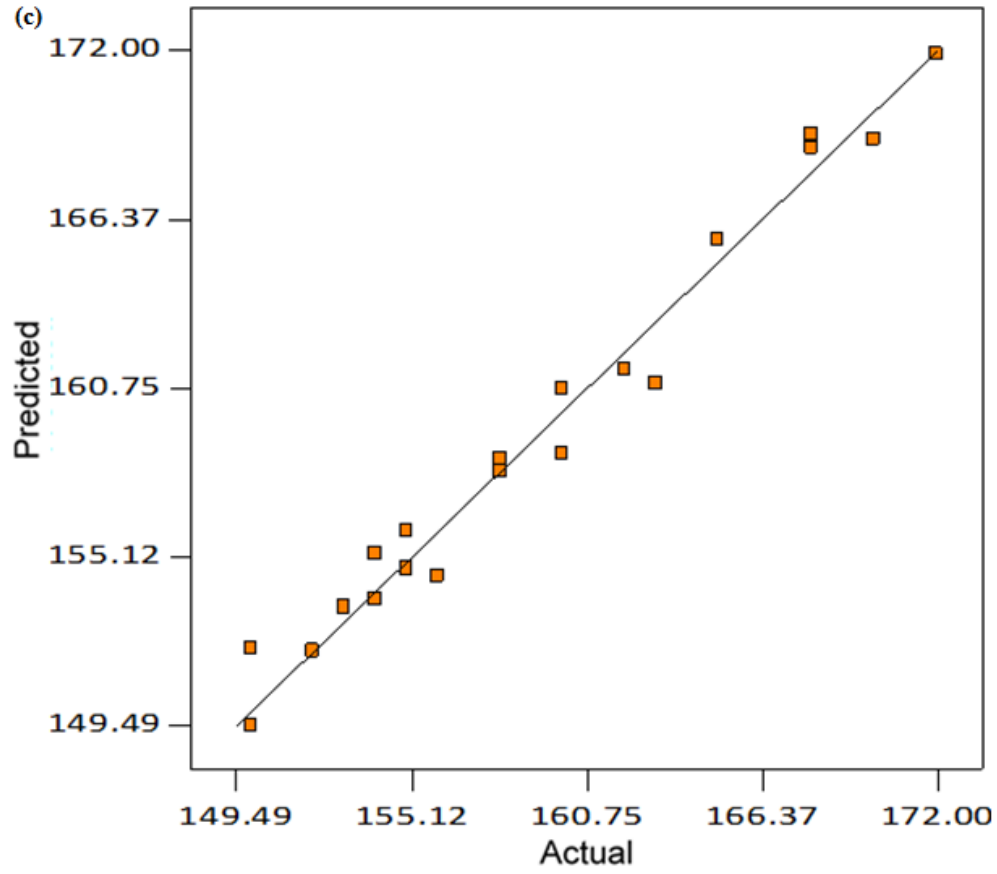

(c) Macrohardness

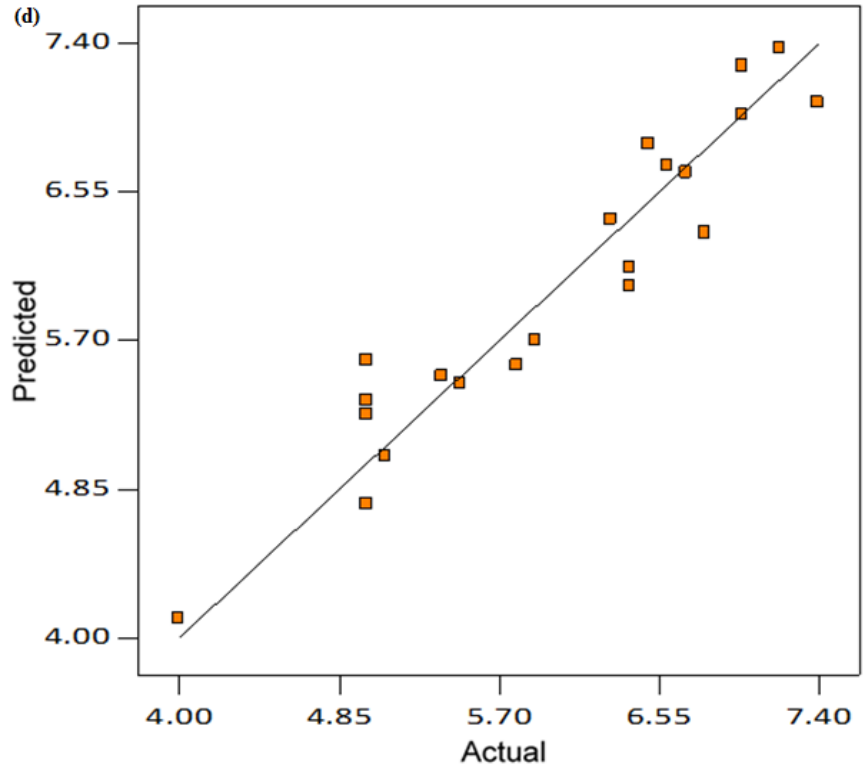

(d) Diffusible hydrogen content

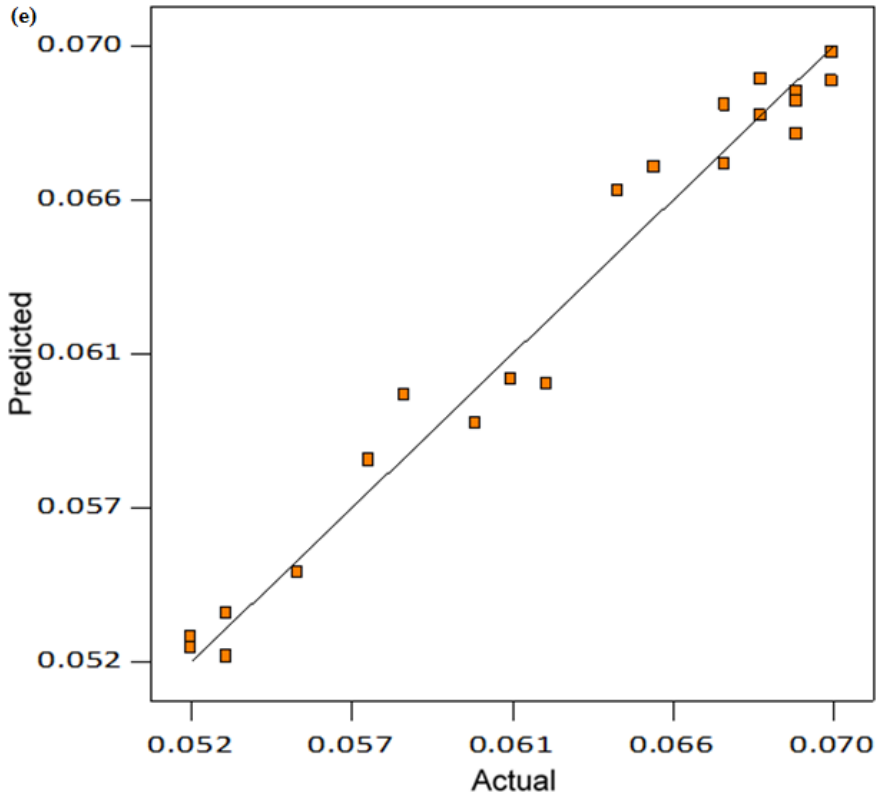

(e) Corrosion rate

Figure 5.1.2 Predicted versus actual plots of various weld responses (a) ultimate tensile strength, (b) impact toughness, (c) macrohardness, (d) diffusible hydrogen content and (e) corrosion rate.

5.2 Discussion of Mild Steel Coated Electrodes

5.2.1 Effect of electrode coating ingredients on weld metal chemistry

It is observed from the regression analysis that amount of nickel content in weld metal is increased with the increase in its percentage composition in welding electrode coatings. CaO, CaF_2 and SiO_2 show decreasing effect whereas the interaction binary effects of SiO_2 and other ingredients depict an increasing trend on the nickel as well as phosphorous content of weld. CaO and CaF_2 promote the oxidation of phosphorous resulting in formation of phosphorous pentoxide and lower its activity coefficient in the slag thereby decreasing phosphorous content in the weld as per the following reaction (Mitra and Eagar, 1991a, 1991b, 1991c [106-108]):

$$4P+5O_2 \rightarrow 2P_2O_5 \qquad (5.2.1)$$

The individual effect of all the ingredients is positive on the sulphur content of weld whereas their interaction binary effects of the ingredients are negative which may be attributed to the formation of sulphides during slag-metal reactions. From the regression analysis it has been observed that SiO_2 and all the binary mixtures of CaO i.e. $CaO.CaF_2$ and CaO.Ni have significant decreasing effect on the carbon content of weld metal probably due to the oxidation of carbon to its oxides. Regression analysis shows that the manganese content in weld is decreasing with the increase in SiO_2 in the electrode coatings. Higher SiO_2 results in higher MnO concentration in the slag which causes lower manganese content in the weld (Palm, 1972 [116]). The characteristic of CaO that it decreases the density of slag, have assisted in the transfer of manganese across the slag-metal interface.

From the regression analysis of the experimental weld chemistry data, it has been observed that silicon content in weld metal has increased with the increase in SiO_2 content in the electrode coating composition. This could be explained from the fact that Si^{4+} metallic cation from slag is reduced and increases the silicon content in the weld pool-slag interface during electrode positive polarity (Kou, 2002 [86]). The accompanying reaction is shown:

$$Si^{4+}\ (slag) + 4e^- \rightarrow Si\ (metal) \qquad (5.2.2)$$

The decreasing effect of CaO and its binary mixture $CaO.SiO_2$ on the silicon content of weld, may be attributed to the decrease in the activity of SiO_2 in slag-metal

reactions by CaO due to the formation of SiO_4^{4-} complex ions as per the following reactions (Palm, 1972 [116]):

$$CaO \rightarrow Ca^{2+} + O^{2-} \quad (5.2.3)$$

$$SiO_2 + 2O^{2-} \rightarrow SiO_4^{4-} \quad (5.2.4)$$

5.2.2 Effect of electrode coating ingredients on ultimate tensile strength

It is observed that individual electrode coating ingredients CaO, CaF_2 and Ni tend to increase the ultimate tensile strength of weld while SiO_2 shows the opposing trend. Higher SiO_2 in electrode coating formulations results in higher silicon and dissolved oxygen along with lower manganese and carbon content in the weld metal. CaF_2 and its binary mixture $CaF_2.SiO_2$ increase the UTS by controlling the oxygen levels in the weld. The binary effect of $CaO.SiO_2$ is to increase the tensile strength as the activity of SiO_2 is reduced due to the formation of SiO_4^{4-} complex ions. Both the binary mixtures of Ni i.e. CaF_2.Ni and SiO_2.Ni show increasing effect on UTS because the presence of the nickel makes the weld metal more resistant to cracking.

5.2.3 Effect of electrode coating ingredients on impact toughness

The individual effect of CaO and CaF_2 in electrode coatings is to increase the impact toughness of weld. CaO increases the impact toughness by increasing the basicity of the electrode coatings which is also reported in literature (De Rissone, 2002 [35]). CaF_2 increases the fluidity during slag metal reactions which results in better weld coverage and easy escape of gases from the weld (Weymueller, 1981 [157]). SiO_2 leads to higher oxygen and lower manganese content in the weld metal which further causes the decrease in its impact toughness. Nickel along with its binary mixtures CaO.Ni and CaF_2.Ni have a tendency the increase the impact toughness of weld by acting as a ferrite strengthener and promoting the grain refinement.

5.2.4 Effect of electrode coating ingredients on macrohardness

It is seen that the electrode coating ingredients CaO, CaF_2 and Ni tend to increase the macrohardness values in weld. SiO_2 causes the decrease in manganese and carbon content of weld thereby decreasing its macrohardness. The decreasing hardness effect of binary mixtures $CaO.CaF_2$ and $CaO.SiO_2$ indicates that during slag metal reactions, after a certain level, CaO tends to pick carbon from the weld.

5.2.5 Effect of electrode coating ingredients on diffusible hydrogen content

All the individual electrode coating ingredients CaO, CaF_2, SiO_2 and Ni decrease the diffusible hydrogen content in weld metal. CaO increases the basicity and produces a gaseous shield low in H_2, thereby decreasing hydrogen content in welds. The fluorine in CaF_2 reacts with hydrogen to form insoluble HF compound which escapes into the atmosphere and results in reduction in weld metal hydrogen content (Du Plessis, 2007 [38]). The dissociation of SiO_2 during complex weld reactions increases the oxygen content which reacts with hydrogen and hence leads to decrease in its levels. SiO_2 combines with CaF_2 to form SiF_4 which further functions as a shielding gas and reduces the partial pressure of hydrogen in the arc (Du Plessis, 2007 [38]). The binary mixtures CaO.CaF_2, CaO.Ni, CaF_2.SiO_2 and SiO_2.Ni showed increasing effect on diffusible hydrogen content of weld metal.

5.2.6 Effect of electrode coating ingredients on corrosion rate

The results show that the individual electrode coating ingredients CaO, CaF_2, SiO_2 and Ni have increasing effect on the corrosion rate of weld whereas the binary mixtures of Ni i.e. CaO.Ni, CaF_2.Ni and SiO_2.Ni represent the decreasing trend. The binary effects of other electrode coating ingredients are not significant.

5.2.7 Contour surface plots of various weld responses

The contour plots depicting predicted values of various weld responses for different proportions of electrode coating ingredients CaO, CaF_2, SiO_2 and constant Ni = 3.5% are shown in Figures 5.2.1 and 5.2.2. The variation of a particular weld response with respect to electrode coating ingredients can be easily observed from these contour curves as each curve on the surface plot shows the constant value of that weld response.

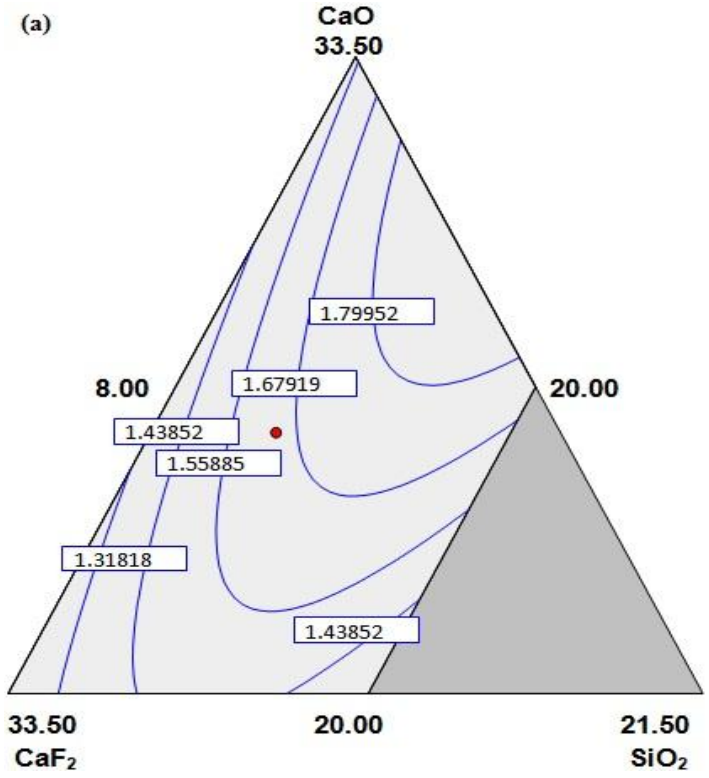
(a)
CaO
33.50
1.79952
8.00
1.67919
20.00
1.43852
1.55885
1.31818
1.43852
33.50
CaF2
20.00
21.50
SiO2

(a) %Ni

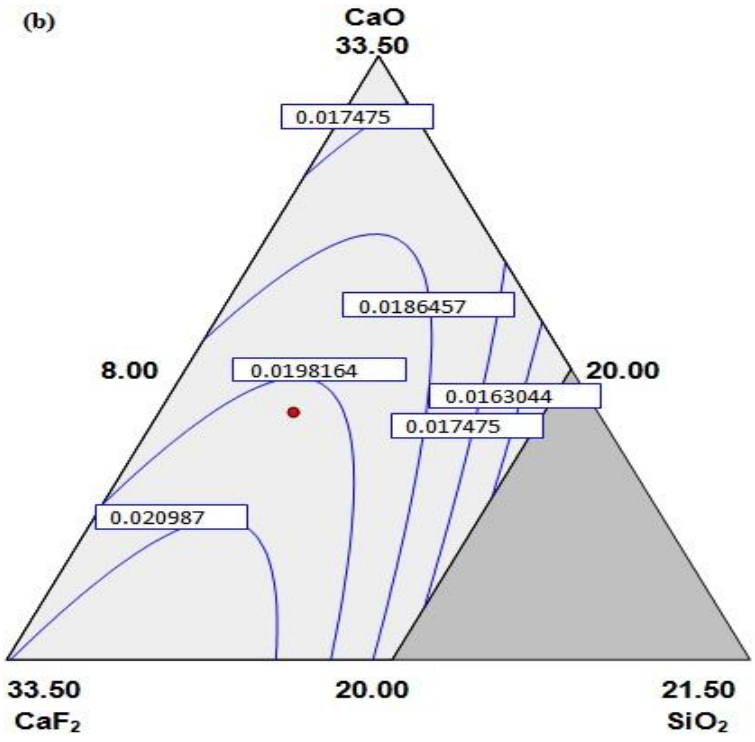
(b)
CaO
33.50
0.017475
0.0186457
8.00
0.0198164
20.00
0.0163044
0.017475
0.020987
33.50
CaF2
20.00
21.50
SiO2

(b) %P

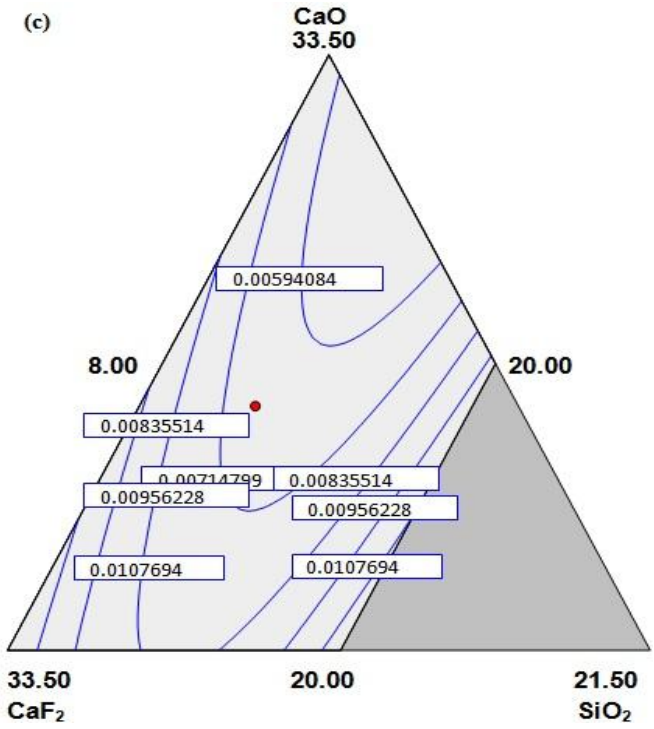
(c)
CaO
33.50
0.00594084
8.00
20.00
0.00835514
0.00714799
0.00835514
0.00956228
0.00956228
0.0107694
0.0107694
33.50
CaF2
20.00
21.50
SiO2

(c) %S

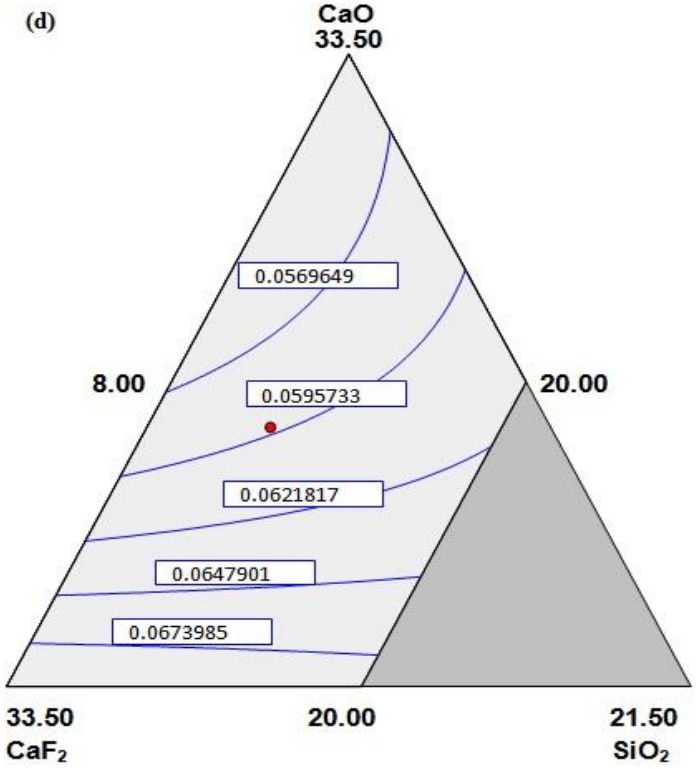
(d)
CaO
33.50
0.0569649
8.00
20.00
0.0595733
0.0621817
0.0647901
0.0673985
33.50
CaF2
20.00
21.50
SiO2

(d) %C

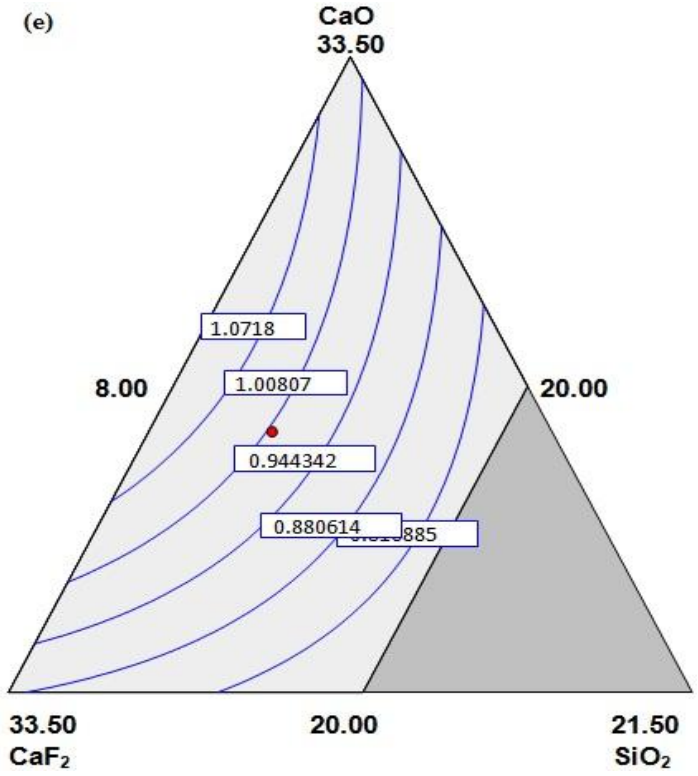

(d) %Mn

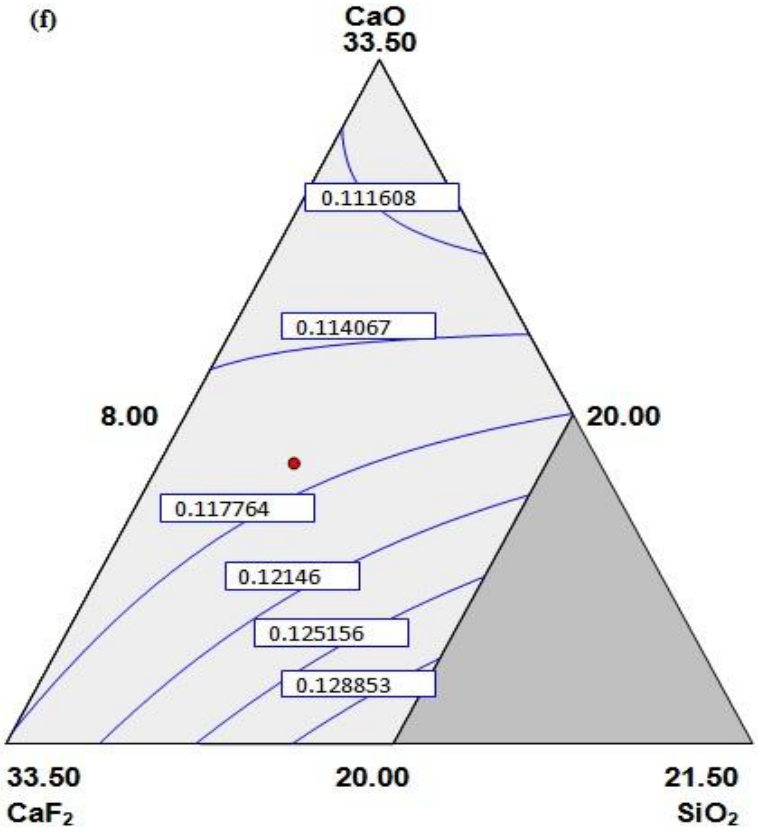

(e) Si

Figure 5.2.1 Contour surface plots of various weld responses (a) %Ni, (b) %P, (c) %S, (d) %C, (e) % Mn and (f) %Si.

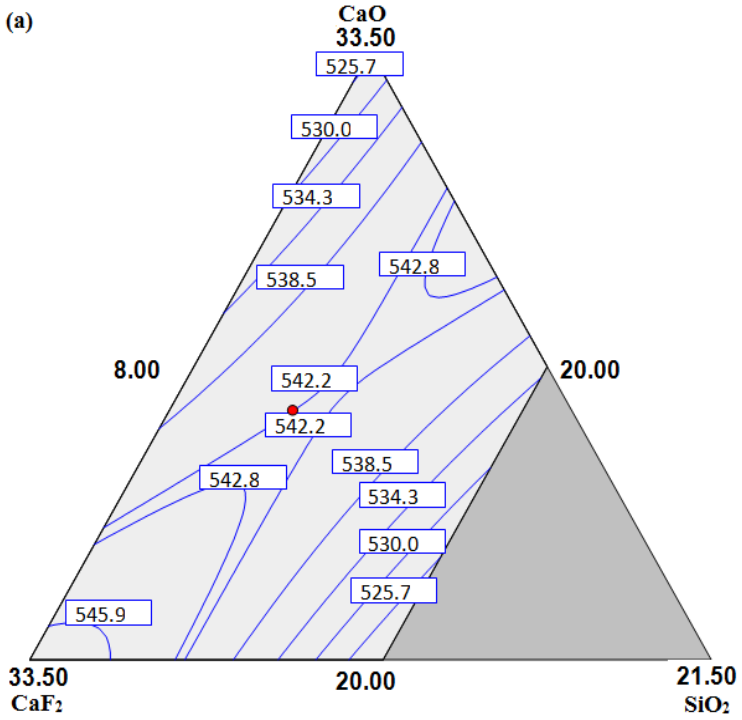

(a) Ultimate tensile strength

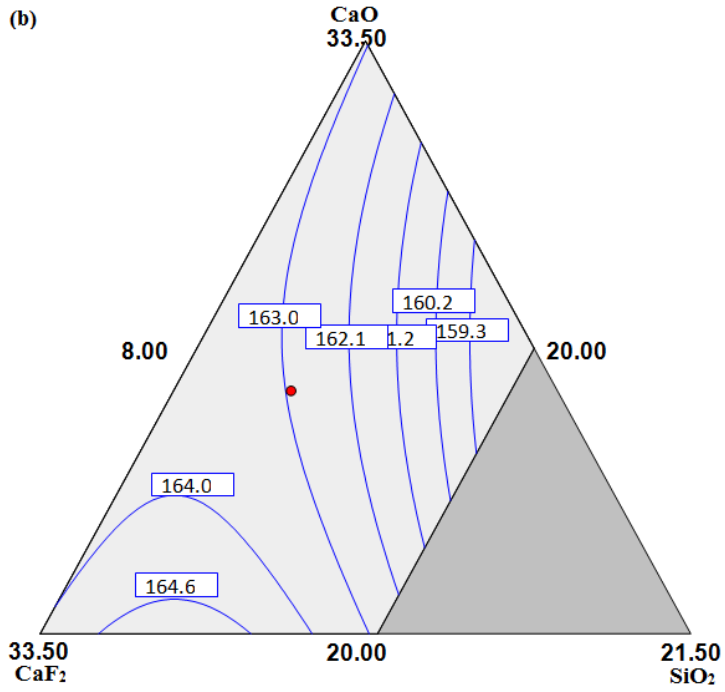

(b) Impact toughness

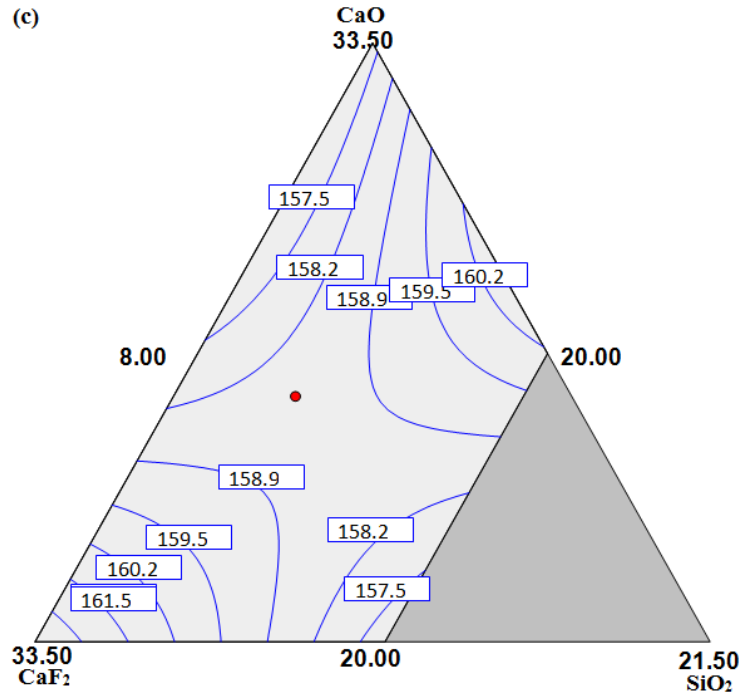

(c) Macrohardness

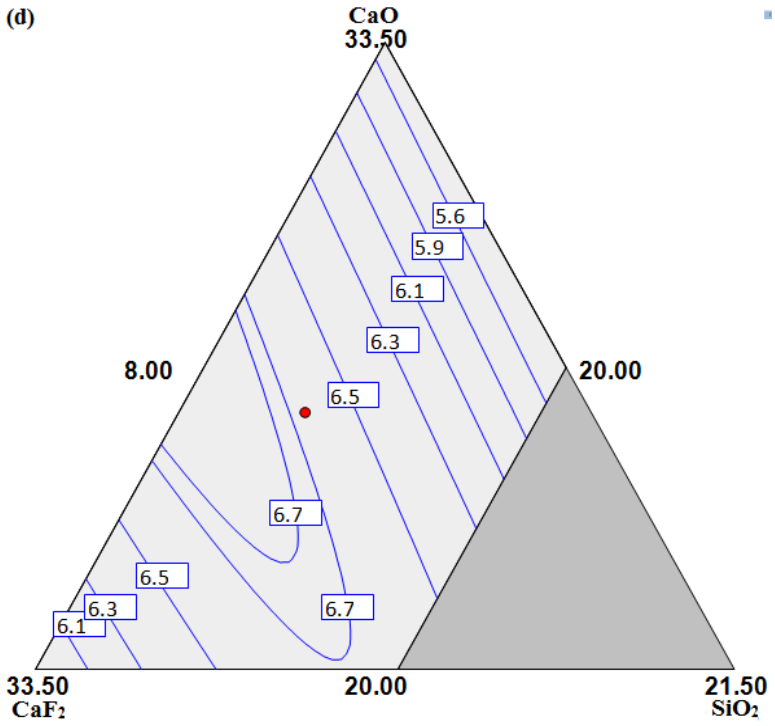

(d) Diffusible hydrogen content

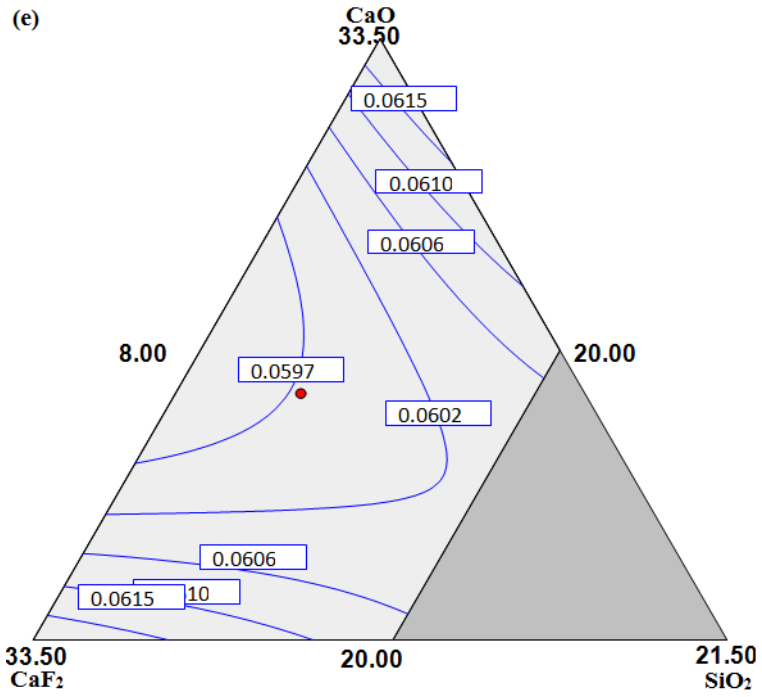

(e) Corrosion rate

Figure 5.2.2 Contour surface plots of various weld responses (a) ultimate tensile strength, (b) impact toughness, (c) macrohardness, (d) diffusible hydrogen content and (e) corrosion rate.

5.2.8 Microstructural analysis

The optical micrographs of various weld samples were taken. Figure 5.2.3(a) shows the optical micrograph of base metal SA516. It shows ferritic and pearlitic structure. It can be seen from micrograph as shown in Figure 5.2.3(b) that weld sample of experiment no. 13 has fine grained acicular ferrite structure. This weld sample has higher Ni content in welding electrode coating formulations which improves the grain refinement in weld. Smaller grain size causes the dislocations to have lesser space to move before these can reach grain boundaries. The difficulty in dislocations movement results in the decrease in plastic deformation and thereby increasing ultimate tensile strength of weld and also improving its corrosion resistance. The grain boundary makes the crack propagation difficult and hence enhances the impact toughness. The coarse grain structure was observed for the weld sample of experiment no. 7 as shown in Figure 5.2.3(c). This experiment was conducted with welding electrodes having 1% of Ni content in coating formulation. Due to increase in grain size of this weld sample, all the mechanical properties such as ultimate tensile

strength, impact toughness and hardness get adversely affected which have been reported in Table 4. The micrograph as shown in Figure 5.2.3(d) depict the improvement in grain size of weld sample no. 6 as the amount of Ni in electrode coatings has been increased to 4%.

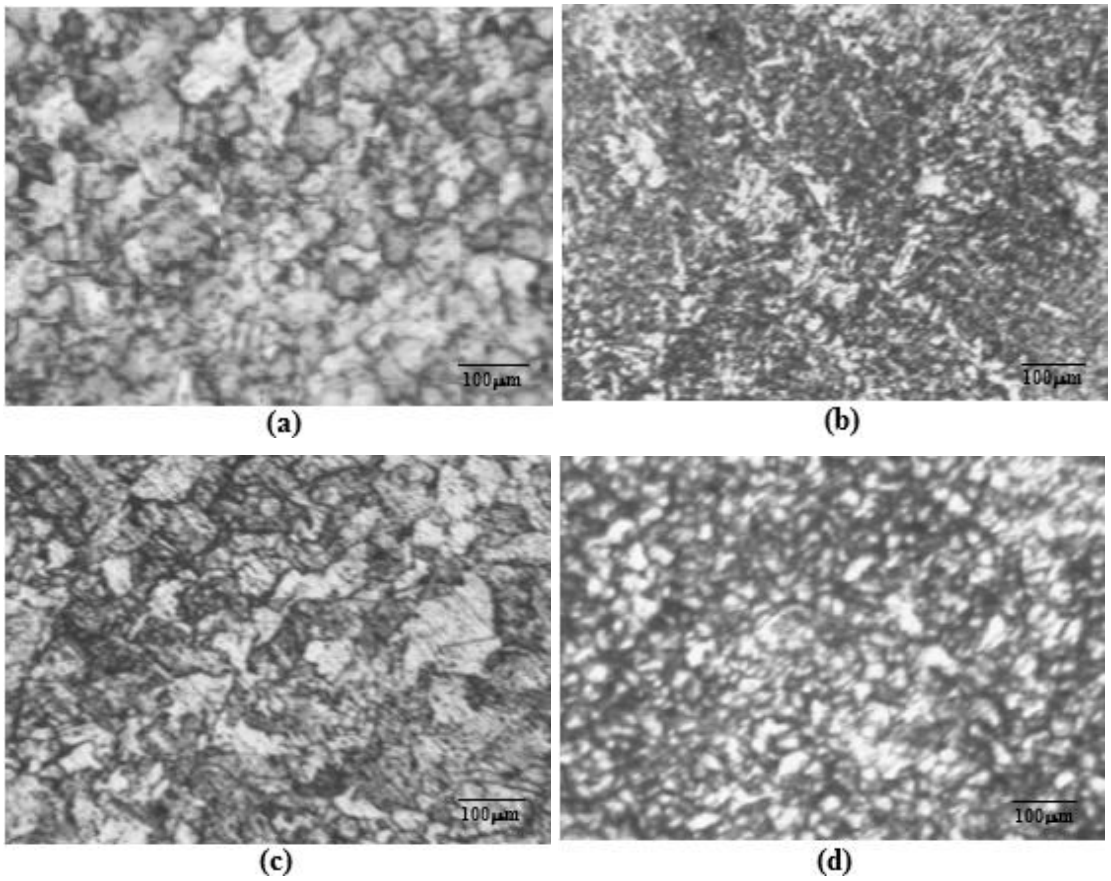

Figure 5.2.3 Optical micrographs of (a) base metal, (b) weld sample (expt. no. 13), (c) weld sample (expt. no. 7) and (d) weld sample (expt. no. 6).

5.2.9 Model validation

The developed regression models of various weld responses were validated by using three randomly selected welding electrode coating formulations for conducting the confirmatory experiments. The experimental results along with predicted values are summarized in Table 5.2.1 and it is found that percentage error (%) for weld responses is nearly 5% in almost all the cases.

5.2.10 Multi objective optimization

The simultaneous optimization of more than one weld response is a multi objective, multi variable non-linear optimization problem. Derringer and Suich, 1980 proposed a multi objective optimization method that makes use of desirability function which is actually the transformation of response variable into a value. Overall or composite

desirability (D) is the weighted geometric mean of individual desirability of various responses. Thus, the simultaneous optimization of several responses gets reduced to optimizing a single response. Weights are fixed according to the importance of an objective function in the multi objective optimization. The composite desirability (Harington, 1965 [55]; Castillo, 1996 [22]) is given by:

$$D = \left(d_1^{w_1} . d_2^{w_2} . d_3^{w_3} ..... d_n^{w_n} \right)^{\frac{1}{(w_1 + w_2 + w_3 ..... + w_n)}} \tag{5.2.5}$$

$$D = \left(\prod_i^n d_i^{w_i} \right)^{\frac{1}{\sum_i^n w_i}} \tag{5.2.6}$$

Here n is number of weld responses, d_i is desirability of a particular weld response and w_i is the weight factor satisfying the conditions $0 \leq w_i \leq 1$ and $(w_1 + w_2 + w_3 + ... + w_n) = 1$

Table 5.2.2 shows the three multi objective optimized solutions with equal weights to all the weld responses. The optimized solutions have been obtained for the optimization of ultimate tensile strength, impact toughness, corrosion rate along with the target values of macrohardness and diffusible hydrogen content.

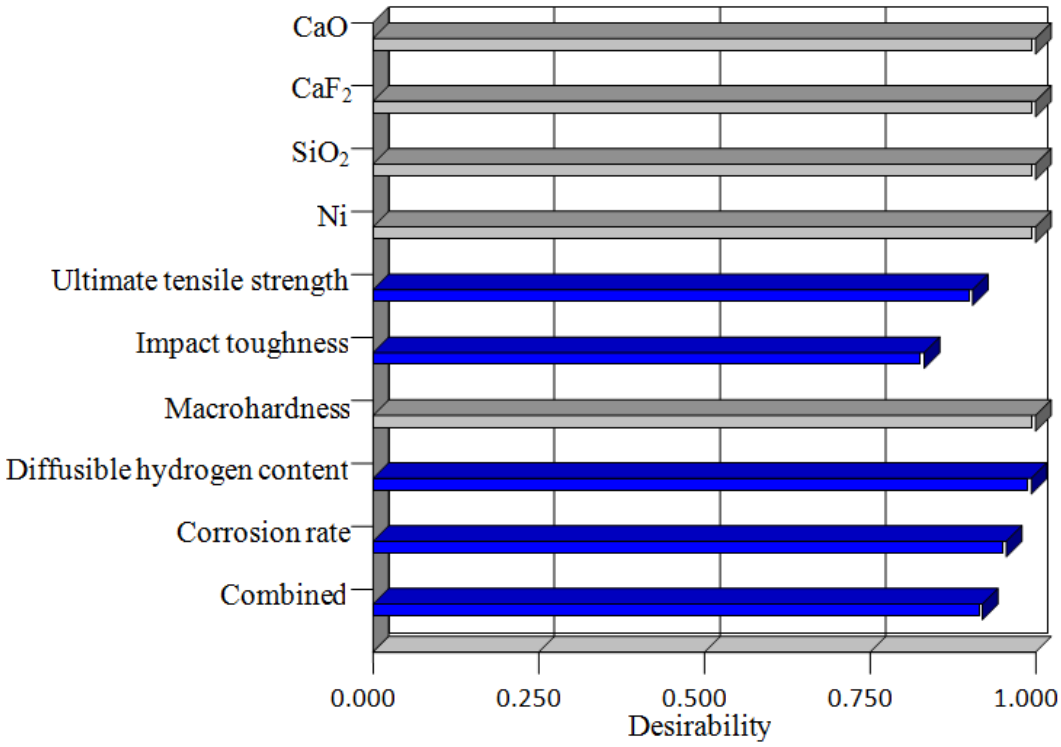

Figure 5.2.4 Graphical demonstration of variation of desirability of optimized solution.

The graphical demonstration of desirability of optimized solution no. 1 is presented in Figure 5.2.4. It represents the variation in the desirability function of individual weld responses along with the composite desirability of complete solution. This optimum composition of electrode coating was selected for the three layer bimetallic weld methodology so as to apply the first layer of mild steel buttering on the edge of SA516 ferritic steel.

Table 5.2.1 Percentage error during confirmatory experiments in weld responses

Electrode coating formulation				Predicted value					Actual value					Error (%)				
CaO	CaF_2	SiO_2	Ni	UTS	IT	MH	DHC	CR	UTS	IT	MH	DHC	CR	UTS	IT	MH	DHC	CR
20	30	10	5	567	171	164	5.8	0.058	596	180	160	5.4	0.061	5.1	5.0	2.7	6.8	4.6
27	20	10	8	594	180	168	4.9	0.053	618	188	177	5.2	0.05	4.1	4.3	5.5	5.5	5.7
21	28	15	1	483	153	150	6.8	0.067	510	160	155	6.3	0.062	5.7	4.6	3.5	7.4	7.5

UTS=Ultimate tensile strength (MPa); IT= Impact toughness (J); MH= Macrohardness (HVN); DHC= Diffusible hydrogen content (ml per 100 gm of weld metal); CR= Corrosion rate (mm/y) and Error (%) = (Actual value- Predicted value)*100/ (Predicted value)

Table 5.2.2 Electrode coating formulations for optimized weld responses

S.No	Electrode coating formulation				Ultimate tensile strength (MPa)	Impact toughness (J)	Macrohardness (HVN)	Diffusible hydrogen content (ml per 100 gm of weld metal)	Corrosion Rate (mm/y)	Composite Desirability
	CaO	CaF_2	SiO_2	Ni						
1.	20.9	23.3	12.8	8.0	597.9	178.4	169.5	5.4	0.053	0.92
2.	21.3	23.4	12.4	7.8	597.4	178.4	169.2	5.4	0.053	0.90
3.	29.8	20.4	8.0	6.9	567.5	179.0	163.6	5.1	0.055	0.79

5.3 Development of Regression Models (Stainless Steel Electrodes Based on $CaO\text{-}TiO_2\text{-}SiO_2$ System) with Two Layer Methodology

The results of weld metal chemistry and ferrite number of bimetallic welds are given in Table 5.3.1 and Table 5.3.2. The elements Mo, Nb, N and Cu have not been considered in the calculatons of ferrite number since they were not found in the elemental composition analysis of the weld metal. The Table 5.3.3 shows the results of mechanical behaviour i.e. mean values of ultimate tensile strength (UTS), percentage elongation, impact toughness and microhardness of bimetallic welds.

Table 5.3.1 Results of weld metal chemistry of bimetallic welds based on $CaO\text{-}TiO_2\text{-}SiO_2$ system

Expt. No.	%C	%Cr	%Ni	%Mn	%Si
1	0.039	18.2	10.2	1.29	0.66
2	0.041	18.8	10.8	1.32	0.60
3	0.038	18.0	9.8	1.24	0.71
4	0.039	18.0	10.2	1.28	0.68
5	0.040	18.3	10.6	1.32	0.60
6	0.036	17.9	9.7	1.22	0.76
7	0.040	18.6	10.2	1.30	0.60
8	0.036	17.8	9.8	1.21	0.79
9	0.038	18.0	9.9	1.24	0.67
10	0.039	18.9	10.1	1.30	0.58
11	0.038	18.1	9.9	1.26	0.67
12	0.040	18.0	10.5	1.32	0.61
13	0.040	18.2	10.6	1.35	0.58
14	0.042	18.0	10.8	1.36	0.56
15	0.040	18.5	10.3	1.34	0.58
16	0.036	18.0	9.7	1.20	0.79
17	0.040	18.4	10.4	1.28	0.64
18	0.036	17.9	9.7	1.20	0.80

Table 5.3.2 Results of ferrite number of bimetallic welds based on $CaO\text{-}TiO_2\text{-}SiO_2$ system

S.No.	Cr_{eq}	Ni_{eq}	Cr_{eq}/Ni_{eq}	Ferrite Number (FN)		Solidification mode
				WRC 92 diagram	Ferritescope	
1	18.2	11.5	1.58	3.8	4.4	FA
2	18.8	12.2	1.53	4.1	5	FA
3	18.0	11.2	1.61	4	5.4	FA
4	18.0	11.5	1.57	3.4	4.4	FA
5	18.3	12.0	1.52	2.8	3.8	FA
6	17.9	11.0	1.62	3.9	4.9	FA
7	18.6	11.6	1.60	5	6	FA
8	17.8	11.1	1.60	3.6	2.5	FA
9	18.0	11.2	1.61	4	5	FA
10	18.9	11.4	1.66	6.5	8	FA
11	18.1	11.2	1.61	4.3	5.3	FA
12	18.0	11.9	1.51	2.2	3.2	FA
13	18.2	12.0	1.52	2.8	4	FA
14	18.0	12.3	1.46	1.2	2.8	FA
15	18.5	11.7	1.58	4.5	5.5	FA
16	18.0	11.0	1.63	4.3	5	FA
17	18.4	11.8	1.57	4.2	6	FA
18	17.9	10.9	1.64	4.3	5.3	FA

Cr_{eq}- chromium equivalent; Ni_{eq}- nickel equivalent; FA- ferritic-austentic

With the help of observed values of weld responses in terms of weld metal chemistry and mean values of mechanical properties from experimentation of bimetallic welds, the regression equations developed in terms of percentage composition of individual electrode coating ingredients (TiO_2, CaO, SiO_2 and CaF_2) and their combined binary mixtures are shown below:

Ferrite number = $0.30219TiO_2$ $+2.80055CaO$ $+1.68831SiO_2$ $+2.91560CaF_2$ $-0.053655TiO_2.CaO$ $-0.037643TiO_2.SiO_2$ $-0.068601TiO_2.CaF_2$ $-0.040899CaO.SiO_2$ $+5.31504E\text{-}004CaO.CaF_2$ $-6.07293E\text{-}004SiO_2\,CaF_2$ (5.3.1)

Table 5.3.3 Weld responses in terms of mechanical properties of bimetallic welds based on CaO-TiO_2-SiO_2 system

Expt. No.	Ultimate tensile strength (MPa)	Percentage elongation (%)	Impact toughness (Nm)	Microhardness (VHN)
1	543	41	190	207
2	512	48	193	200
3	560	39	188	209
4	540	41	190	206
5	538	42	192	204
6	599	34	185	215
7	590	36	193	212
8	560	39	181	210
9	602	33	185	216
10	528	44	196	203
11	520	46	192	201
12	531	43	186	205
13	600	34	184	214
14	635	30	183	220
15	520	46	188	202
16	551	40	188	208
17	530	43	194	205
18	608	31	186	218

$$\%C = -3.45848E\text{-}004TiO_2 -1.92703E\text{-}003CaO -4.44418E\text{-}003SiO_2 -3.70678E\text{-}003CaF_2 +7.63366E\text{-}005TiO_2.CaO +1.17991E\text{-}004TiO_2.SiO_2 +1.21107E\text{-}004TiO_2.CaF_2 +2.98572E\text{-}005\ CaO.SiO_2 -2.94313E\text{-}005CaO.CaF_2 -1.95355E\text{-}006SiO_2.CaF_2 \quad (5.3.2)$$

$$\%Cr = 0.15275TiO_2 +0.57158CaO -0.065489SiO_2 +0.25065CaF_2 -1.20834E\text{-}003TiO_2.CaO +8.28302E\text{-}003TiO_2.SiO_2 +2.76426E\text{-}003TiO_2.CaF_2 -9.01903E\text{-}003CaO.SiO_2 -4.63856E\text{-}003CaO.CaF_2 -2.10618E\text{-}003SiO_2.CaF_2 \quad (5.3.3)$$

$$\%Ni = -0.046897TiO_2 - 0.43790CaO - 0.76268SiO_2 - 0.85806CaF_2 + 0.017482TiO_2\ CaO + 0.022402\ TiO_2.SiO_2 + 0.027384TiO_2.CaF_2 + 3.32524E\text{-}003CaO.SiO_2 - 5.49400E\text{-}003CaO.CaF_2 - 2.55451E\text{-}003SiO_2.CaF_2 \quad (5.3.4)$$

$$\%Mn = 4.10868E\text{-}003TiO_2 - 0.058285CaO - 0.060226SiO_2 - 0.043474CaF_2 + 1.87252E\text{-}003TiO_2.CaO + 1.72805E\text{-}003TiO_2.SiO_2 + 1.80495E\text{-}003TiO_2.CaF_2 + 6.56884E\text{-}004CaO.SiO_2 - 3.23355E\text{-}004CaO.CaF_2 - 1.32243E\text{-}004SiO_2.CaF_2 \quad (5.3.5)$$

$$\%Si = 2.09601E\text{-}003TiO_2 - 0.024444CaO + 0.065774SiO_2 - 3.77788E\text{-}003CaF_2 + 7.80922E\text{-}004\ TiO_2.CaO - 5.84280E\text{-}004TiO_2.SiO_2 + 2.66337E\text{-}004TiO_2.CaF_2 - 1.02472E\text{-}003CaO.SiO_2 + 5.18298E\text{-}004CaO.CaF_2 - 6.94227E\text{-}004SiO_2.CaF_2 \quad (5.3.6)$$

$$\text{Ultimate tensile strength (UTS)} = 0.64901TiO_2 - 14.32443CaO + 42.87580SiO_2 + 16.03307\ CaF_2 + 0.75983TiO_2.CaO - 0.30822TiO_2.SiO_2 + 0.63538TiO_2.CaF_2 - 1.23431CaO.SiO_2 - 1.31982CaO.CaF_2 - 1.84658\ SiO_2.CaF_2 \quad (5.3.7)$$

$$\text{Percentage elongation} = 1.45298\ TiO_2 + 4.33194CaO - 4.31768SiO_2 - 0.25451CaF_2 - 0.12096TiO_2.CaO + 0.036531TiO_2.SiO_2 - 0.095955TiO_2.CaF_2 + 0.15694CaO.SiO_2 + 0.16899CaO.CaF_2 + 0.24239SiO_2.CaF_2 \quad (5.3.8)$$

$$\text{Impact toughness} = 1.63377TiO_2 + 3.83673CaO - 1.17934SiO_2 - 4.34618CaF_2 + 9.27859E\text{-}005TiO_2.CaO + 0.083293TiO_2.SiO_2 + 0.11849TiO_2.CaF_2 + 0.042462CaO.SiO_2 + 0.10906CaO.CaF_2 + 0.10185SiO_2\ CaF_2 \quad (5.3.9)$$

$$\text{Microhardness} = 2.30374TiO_2 + 2.41427CaO - 10.19632SiO_2 + 6.02979CaF_2 + 0.032341TiO_2.CaO - 0.11025TiO_2.SiO_2 + 0.031173TiO_2.CaF_2 - 0.18971CaO.SiO_2 - 0.22026CaO.CaF_2 - 0.26621SiO_2.CaF_2 \quad (5.3.10)$$

5.3.1 Regression analysis

The developed regression equations have been analyzed using analysis of variance (ANOVA) as shown in Tables 5.3.4 and 5.3.5. The Table 5.3.4 shows the analysis of regression equations of weld metal chemistry while the analysis of regression equations of mechanical behaviour of bimetallic welds is given in Table 5.3.5. The coefficient of determination i.e. R-square values (Tables 5.3.4 and 5.3.5) for the developed regression models are nearly equal or greater than 84% which indicate that predicted values are in close agreement with the actual values of various weld responses as shown in Figures 5.3.1 and 5.3.2.

Table 5.3.4 Analysis of regression equations using ANOVA (F-test) of weld metal chemistry of bimetallic welds

Weld response	Source	Sum of squares	DF	Mean square	F value	P value	R square
%Si	Model	0.105628	9	0.011736	43.39895	< 0.0001	0.97
	Linear	0.098484	3	0.032828	121.3905	< 0.0001	
	TiO_2.CaO	0.001076	1	0.001076	3.978002	0.0812	
	TiO_2.SiO_2	0.001042	1	0.001042	3.854648	0.0852	
	TiO_2.CaF_2	8.81E-06	1	8.81E-06	0.032594	0.8612	
	CaO.SiO_2	0.002177	1	0.002177	8.048387	0.0219	
	CaO.CaF_2	0.001301	1	0.001301	4.8108	0.0596	
	SiO_2.CaF_2	0.00154	1	0.00154	5.694627	0.0441	
	Residual	0.002163	8	0.00027			
	Total	0.107792	17				
%Mn	Model	0.042236	9	0.004693	13.8666	0.0006	0.94
	Linear	0.040405	3	0.013468	39.79559	< 0.0001	
	TiO_2.CaO	0.000436	1	0.000436	1.287409	0.2894	
	TiO_2.SiO_2	0.000371	1	0.000371	1.096423	0.3257	
	TiO_2.CaF_2	0.000405	1	0.000405	1.196177	0.3059	
	CaO.SiO_2	0.000483	1	0.000483	1.428574	0.2662	
	CaO.CaF_2	0.000117	1	0.000117	0.346167	0.5725	
	SiO_2.CaF_2	1.96E-05	1	1.96E-05	0.057899	0.8159	
	Residual	0.002707	8	0.000338			
	Total	0.044944	17				
%Cr	Model	1.792764	9	0.199196	29.19133	< 0.0001	0.97
	Linear	1.662887	3	0.554296	81.22967	< 0.0001	
	TiO_2.CaO	0.000181	1	0.000181	0.026588	0.8745	
	TiO_2.SiO_2	0.008525	1	0.008525	1.249365	0.2961	
	TiO_2.CaF_2	0.00095	1	0.00095	0.139146	0.7188	
	CaO.SiO_2	0.091142	1	0.091142	13.35649	0.0065	
	CaO.CaF_2	0.024108	1	0.024108	3.53297	0.0970	
	SiO_2.CaF_2	0.00497	1	0.00497	0.728388	0.4182	

	Residual	0.05459	8	0.006824			
	Total	1.847354	17				
%Ni	Model	1.928458	9	0.214273	4.534487	0.0223	0.84
	Linear	1.381416	3	0.460472	9.744596	0.0048	
	TiO_2.CaO	0.137977	1	0.137977	2.919895	0.1259	
	TiO_2.SiO_2	0.162359	1	0.162359	3.435879	0.1009	
	TiO_2.CaF_2	0.193184	1	0.193184	4.0882	0.0778	
	CaO.SiO_2	0.012389	1	0.012389	0.262185	0.6225	
	CaO.CaF_2	0.03382	1	0.03382	0.71571	0.4221	
	SiO_2.CaF_2	0.007312	1	0.007312	0.15473	0.7043	
	Residual	0.378033	8	0.047254			
	Total	2.306491	17				
%C	Model	5.5E-05	9	6.11E-06	16.50126	0.0003	0.94
	Linear	0.000047	3	1.57E-05	42.31657	0.0000	
	TiO_2.CaO	7.24E-07	1	7.24E-07	1.955863	0.1995	
	TiO_2.SiO_2	1.73E-06	1	1.73E-06	4.672708	0.0626	
	TiO_2.CaF_2	1.82E-06	1	1.82E-06	4.922756	0.0573	
	CaO.SiO_2	2.73E-06	1	2.73E-06	7.377262	0.0264	
	CaO.CaF_2	9.71E-07	1	9.71E-07	2.621513	0.1441	
	SiO_2.CaF_2	4.28E-09	1	4.28E-09	0.01155	0.9171	
	Residual	2.96E-06	8	3.7E-07			
	Total	5.79E-05	17				
Ferrite number	Model	18.57784	9	2.064204	5.300166	0.01400	0.86
	Linear	12.58423	3	4.194744	10.77066	0.00350	
	TiO_2.CaO	1.357736	1	1.357736	3.4862	0.09884	
	TiO_2.SiO_2	1.176079	1	1.176079	3.019767	0.12046	
	TiO_2.CaF_2	1.584791	1	1.584791	4.0692	0.07840	
	CaO.SiO_2	1.874268	1	1.874268	4.812475	0.05957	
	CaO.CaF_2	0.000317	1	0.000317	0.000813	0.97800	
	SiO_2.CaF_2	0.000413	1	0.000413	0.001061	0.97480	
	Residual	3.115682	8	0.38946			
	Total	21.69352	17	2.064204			

DF- degree of freedom

Table 5.3.5 Analysis of regression equations using ANOVA (F-test) of various mechanical properties of bimetallic welds

Weld response	Source	Sum of squares	DF	Mean square	F value	P value	R square
UTS	Model	21273	9	2363.666	9.674201	0.0020	0.92
	Linear	13659.78	3	4553.261	18.63595	0.0006	
	TiO_2.CaO	71.74186	1	71.74186	0.293631	0.6027	
	TiO_2.SiO_2	11.80471	1	11.80471	0.048315	0.8315	
	TiO_2.CaF_2	50.16541	1	50.16541	0.205321	0.6625	
	CaO.SiO_2	1707.063	1	1707.063	6.986804	0.0296	
	CaO.CaF_2	1951.784	1	1951.784	7.988419	0.0223	
	SiO_2.CaF_2	3820.653	1	3820.653	15.63747	0.0042	
	Residual	1954.614	8	244.3268			
	Total	23227.61	17				
Percentage elongation	Model	436.5763	9	48.50848	7.204033	0.0053	0.89
	Linear	278.0217	3	92.67389	13.76307	0.0016	
	TiO_2.CaO	11.81803	1	11.81803	1.755105	0.2218	
	TiO_2.SiO_2	0.165834	1	0.165834	0.024628	0.8792	
	TiO_2.CaF_2	1.144129	1	1.144129	0.169916	0.6910	
	CaO.SiO_2	37.59771	1	37.59771	5.583667	0.0457	
	CaO.CaF_2	41.99755	1	41.99755	6.23709	0.0371	
	SiO_2.CaF_2	65.83137	1	65.83137	9.77667	0.0141	
	Residual	53.86813	8	6.733517			
	Total	490.4444	17				
Impact toughness	Model	279.3894	9	31.04327	11.7951	0.0010	0.93
	Linear	219.8125	3	73.27085	25.83976	0.0002	
	TiO_2.CaO	1.07E-06	1	1.07E-06	4.06E-07	0.9995	
	TiO_2.SiO_2	0.862091	1	0.862091	0.327557	0.5828	
	TiO_2.CaF_2	1.744681	1	1.744681	0.662903	0.4391	
	CaO.SiO_2	12.02026	1	12.02026	4.567182	0.0651	
	CaO.CaF_2	23.32622	1	23.32622	8.862956	0.0177	
	SiO_2.CaF_2	21.62363	1	21.62363	8.216048	0.0209	

	Residual	21.05502	8	2.631878			
	Total	300.4444	17				
Microhardness	Model	553.1598	9	61.4622	7.325867	0.0050	0.89
	Linear	337.3068	3	112.4356	13.40154	0.0017	
	TiO_2.CaO	0.129972	1	0.129972	0.015492	0.9040	
	TiO_2.SiO_2	1.510426	1	1.510426	0.180032	0.6825	
	TiO_2.CaF_2	0.12075	1	0.12075	0.014393	0.9075	
	CaO.SiO_2	60.32635	1	60.32635	7.190482	0.0279	
	CaO.CaF_2	74.35784	1	74.35784	8.862938	0.0177	
	SiO_2.CaF_2	79.40761	1	79.40761	9.464835	0.0152	
	Residual	67.11801	8	8.389751			
	Total	620.2778	17				

DF- degree of freedom

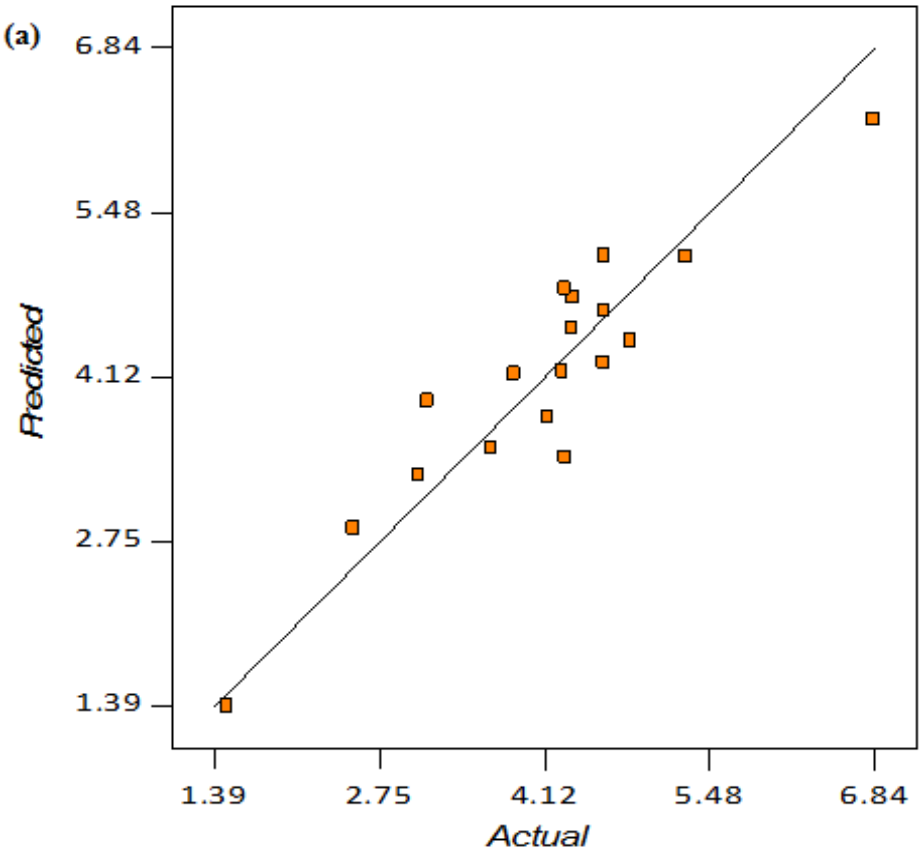

(a) Ferrite number

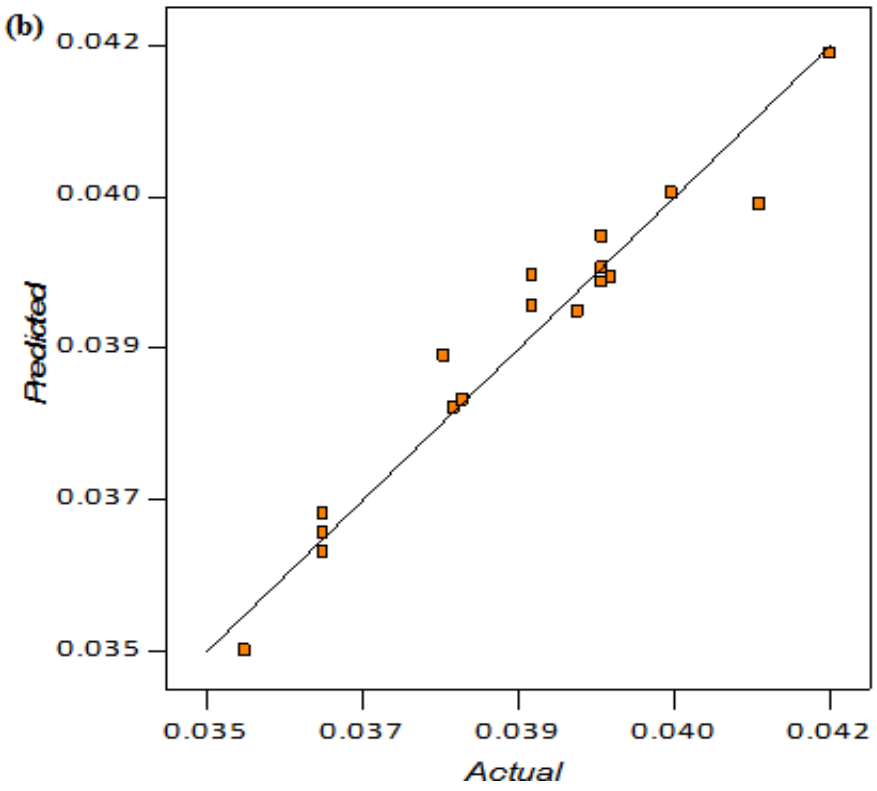
(b)
0.042
0.040
0.039
0.037
0.035
Predicted
0.035
0.037
0.039
0.040
0.042
Actual

(b) %C

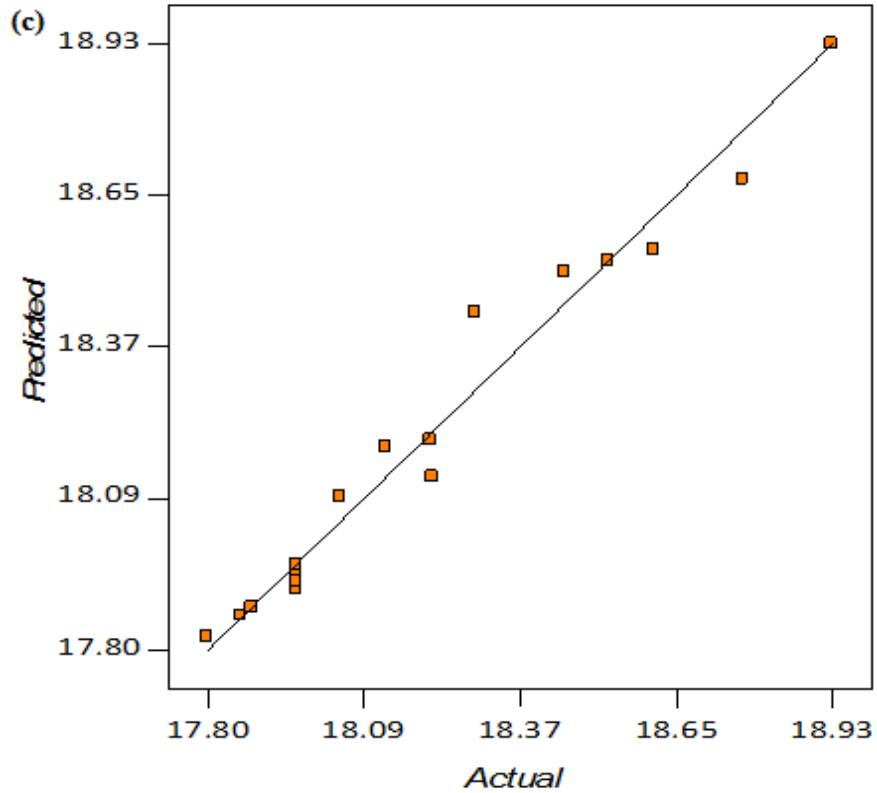
(c)
18.93
18.65
18.37
18.09
17.80
Predicted
17.80
18.09
18.37
18.65
18.93
Actual

(c) %Cr

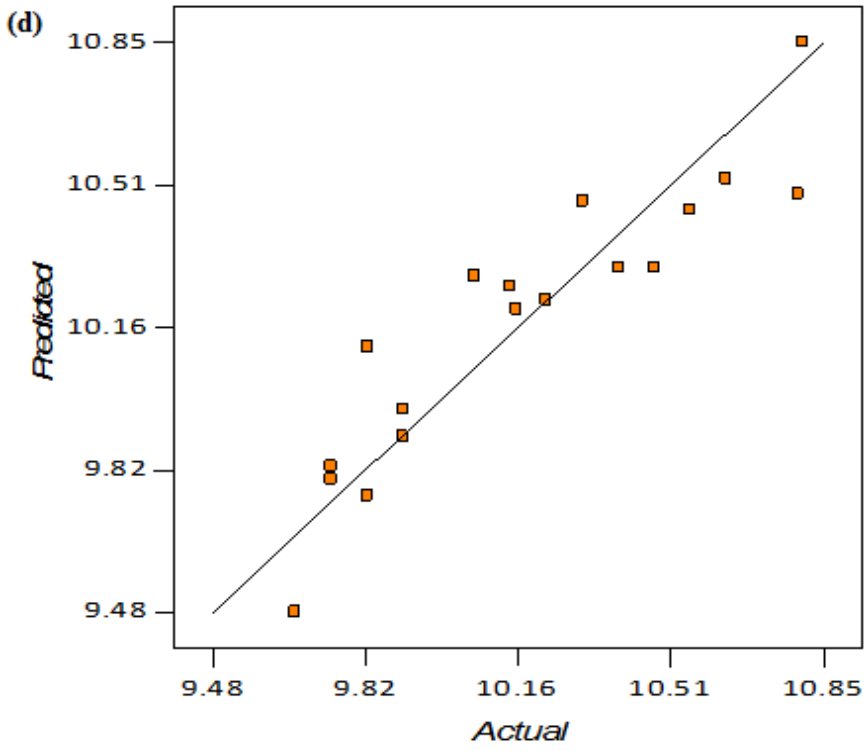
(d)
10.85
10.51
10.16
9.82
9.48
Predicted
9.48
9.82
10.16
10.51
10.85
Actual

(d) %Ni

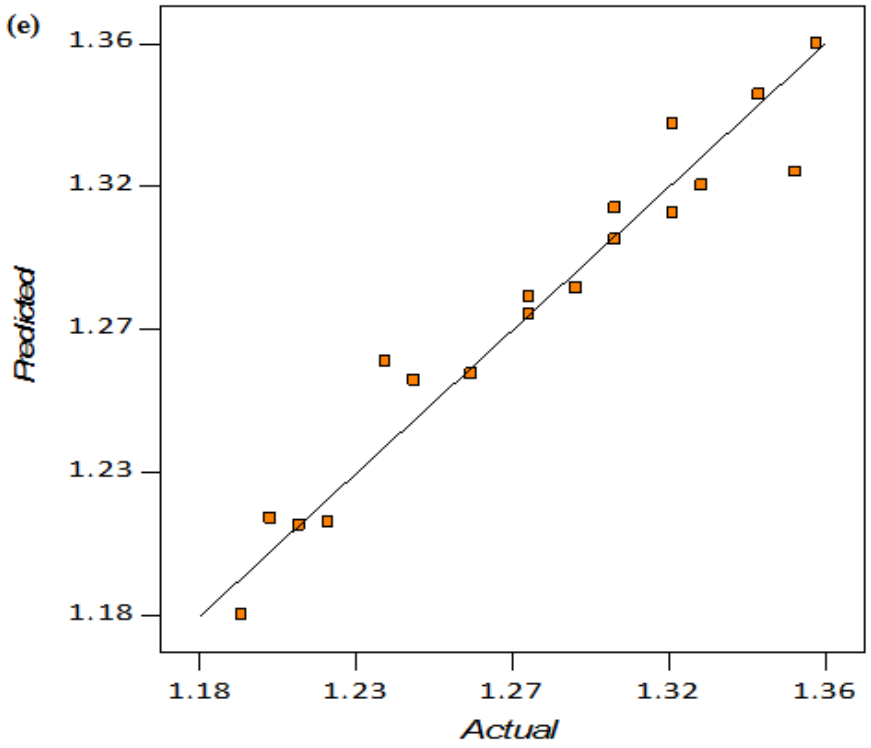
(e)
1.36
1.32
1.27
1.23
1.18
Predicted
1.18
1.23
1.27
1.32
1.36
Actual

(e) %Mn

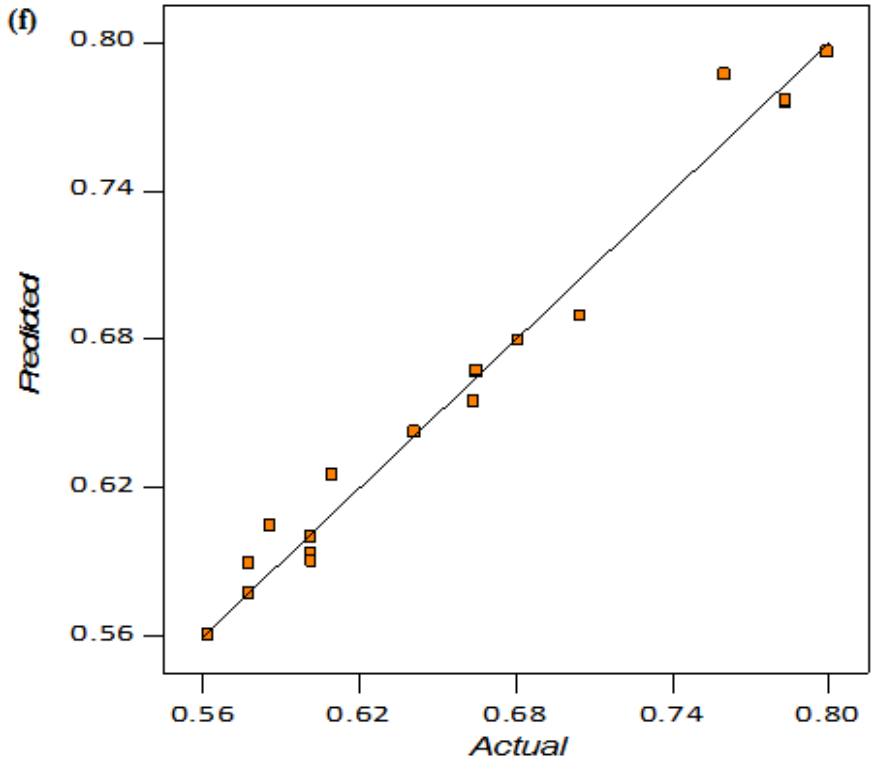

(f) %Si

Figure 5.3.1 Predicted versus actual values of various weld responses of bimetallic welds (a) ferrite number, (b) %C, (c) %Cr, (d) %Ni, (e) %Mn and (f) %Si.

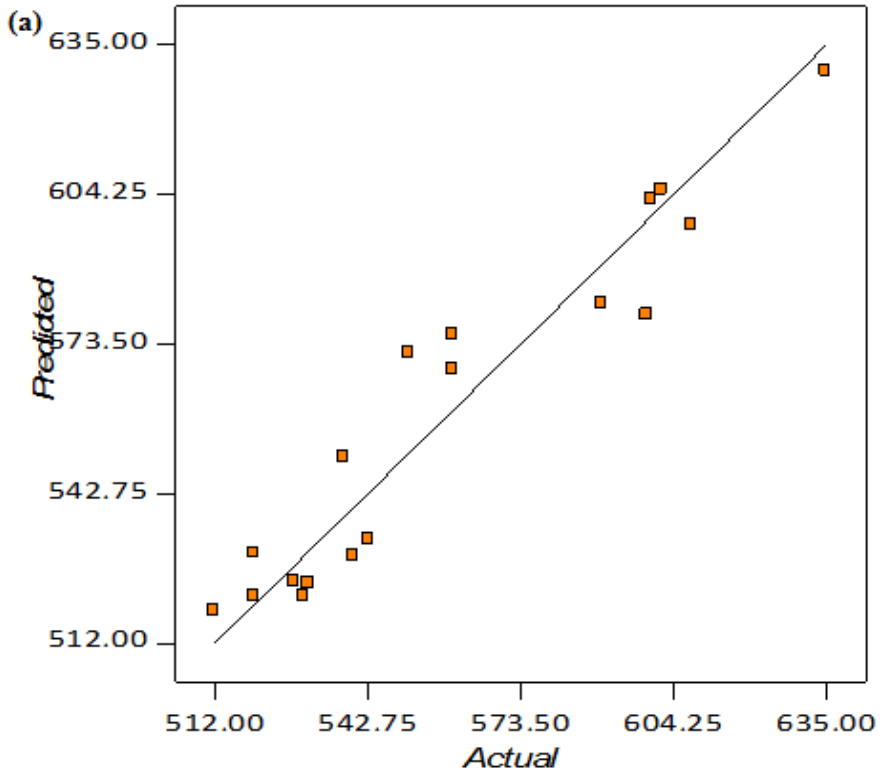

(a) Ultimate tensile strength

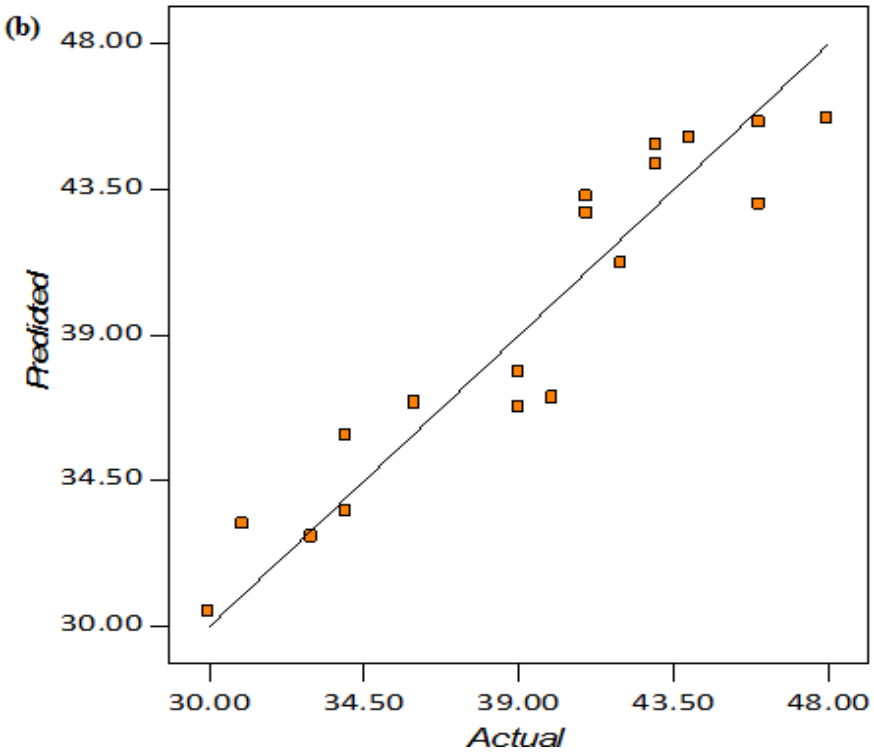

(b) Percentage elongation

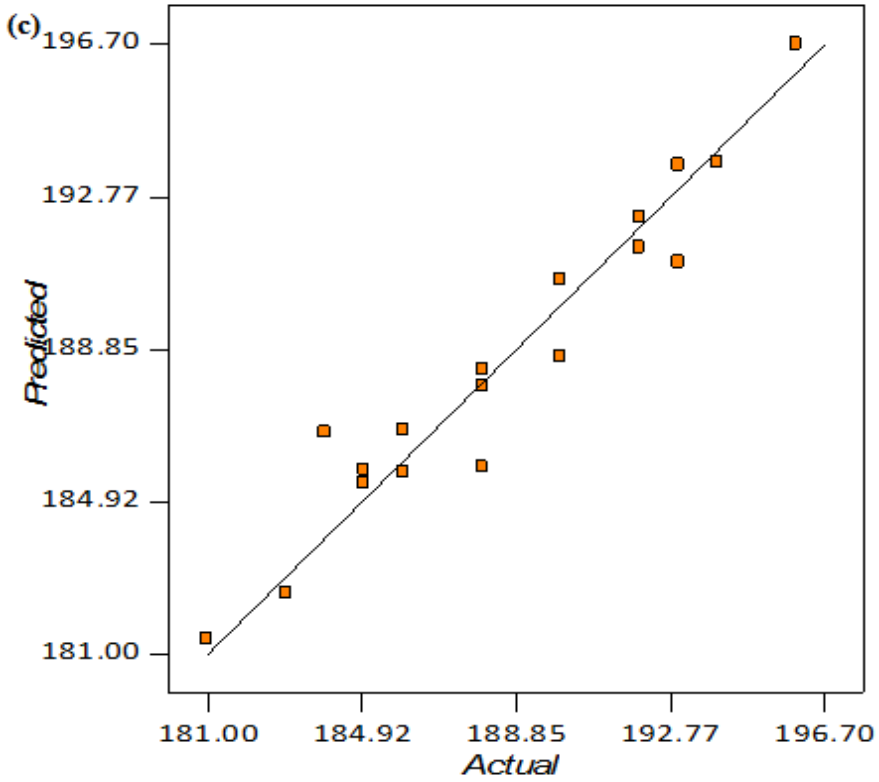

(c) Impact toughness

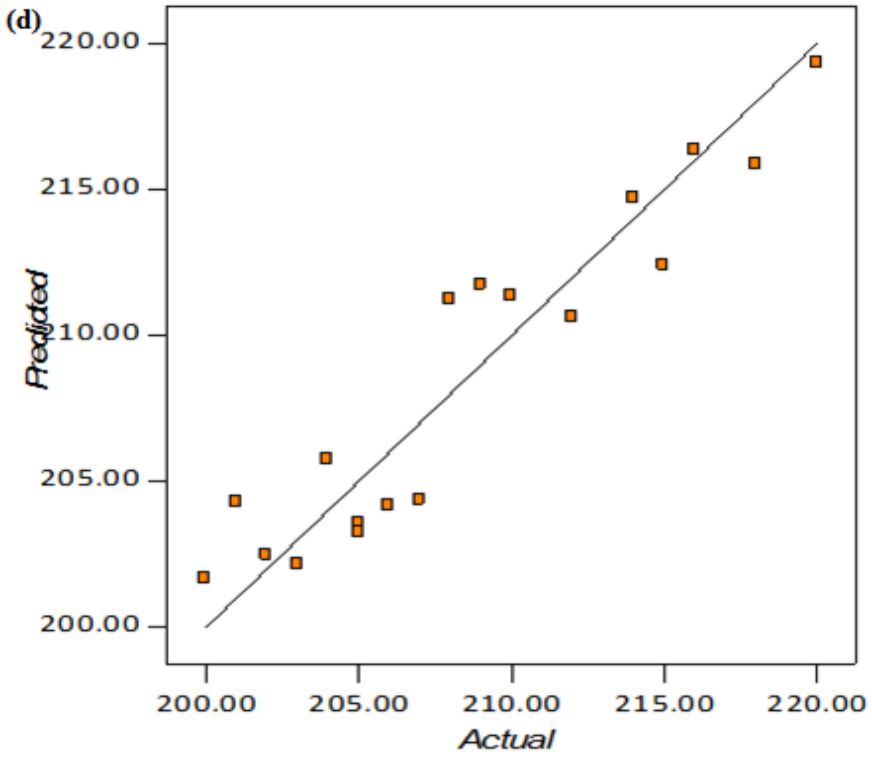

(d) Microhardness

Figure 5.3.2 Predicted versus actual values of various mechanical properties of bimetallic welds (a) ultimate tensile strength, (b) percentage elongation, (c) impact toughness and (d) microhardness.

5.4 Discussion of Two Layer Bimetallic Welds Fabricated with Stainless Steel Electrodes Based on CaO-TiO_2-SiO_2 System

5.4.1 Effect of electrode coating ingredients on weld metal chemistry

From the regression analysis of the experimental weld chemistry data, it is observed that silicon content in weld metal is increased with the increase in SiO_2 content in the electrode coating composition. This can be explained from the fact that Si^{4+} metallic cation from slag is reduced and increases the silicon content in the weld pool-slag interface during electrode positive polarity (Kou, 2002 [86]).

The regression analysis shows that CaO content and its binary mixture CaO.SiO_2 tend to decrease the silicon content of weld metal which can be attributed to the decrease in the activity of SiO_2 in slag-metal reactions by CaO due to the formation of SiO_4^{4-} complex ions as per the following reactions (Palm, 1972 [116]):

$CaO \rightarrow Ca^{2+} + O^{2-}$ (5.4.1)

$SiO_2 + 2O^{2-} \rightarrow SiO_4^{4-}$ (5.4.2)

The three dimensional tetrahedron network structure of silicate ions (SiO_4^{4-}) consists of four close packed oxygen atoms surrounding a small silicon atom. These SiO_4^{4-}-tetrahedra can share corners with each other forming networks. The bonds shared between these tetrahedra are high strength bonds (Schwemmer and Olson 1979 [133]).

The transfer of manganese to weld metal composition largely depends upon the manganese content of electrode core wire and electrode coating compositions. The manganese content in weld is decreased with the increase in SiO_2. The increase of SiO_2 in the electrode coatings results in a higher MnO concentration in the slag which causes lower manganese content in the weld (Palm, 1972 [116]). From the regression analysis, it is observed that the CaF_2 content in electrode coatings decrease the weld metal manganese content. This is coherent with the fact that the addition of CaF_2 decreases the extent of manganese transfer from the coatings and core wire to the weld metal and manganese is lost from the weld metal to the slag as reported by (Kou, 2002 [86]).

It is found that electrode coating ingredients TiO_2, CaO and CaF_2 tends to increase the chromium content of weld metal, while SiO_2 behaves in a negative manner. The free oxygen available after the dissociation of SiO_2 combines with chromium to form chromium oxide, resulting in decrease in chromium content of weld metal. The regression analysis results show the decrease of nickel content in weld metal with increase of various electrode coating ingredients. These results are consistent with those in the reference (Kou, 2002 [86]), however the reason for this is not very clear.

The individual flux ingredients CaO, CaF_2, TiO_2 and SiO_2 show the decreasing trend on the carbon in weld metal composition. The basic oxide CaO has a strong tendency to dissociate and release oxygen at high fusion temperature. The increase of SiO_2 in the electrode coatings also results in higher oxygen content in the weld. The oxygen released during these slag-metal reactions from various electrode coating ingredients, further combines with carbon to form its oxides and thereby decreasing the carbon content of weld metal composition. Figure 5.4.1 shows contour plots for predicted values of weld metal content of bimetallic welds at different proportions of electrode coating ingredients TiO_2, CaO, SiO_2 and with constant CaF_2= 4.29%.

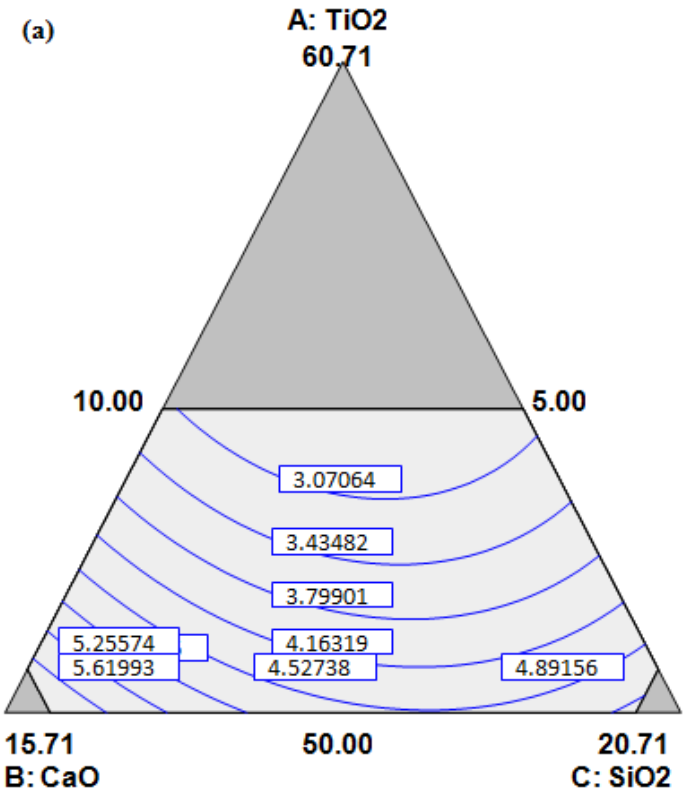

(a) Ferrite number

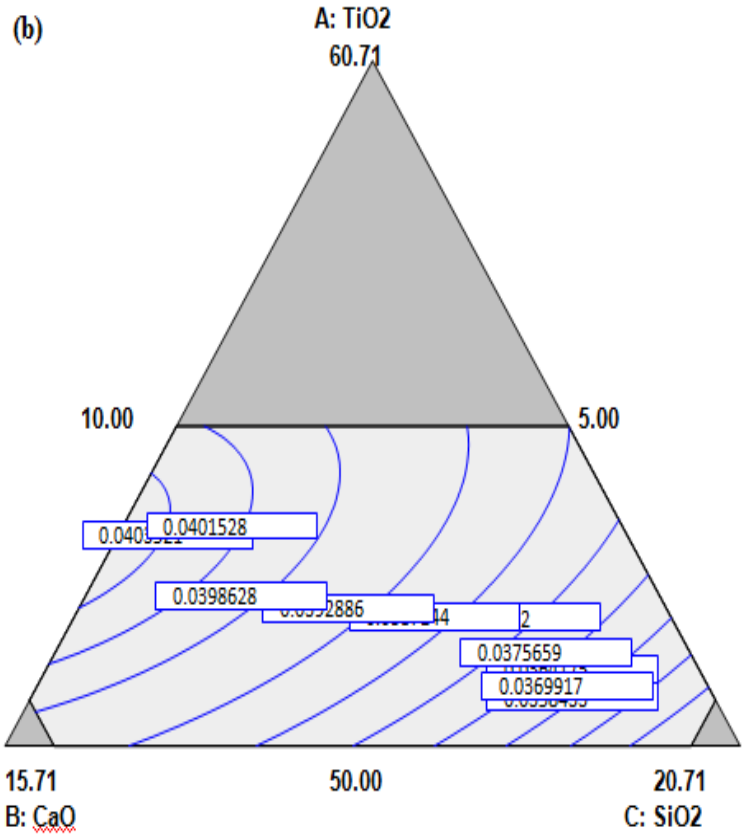

(b) %C

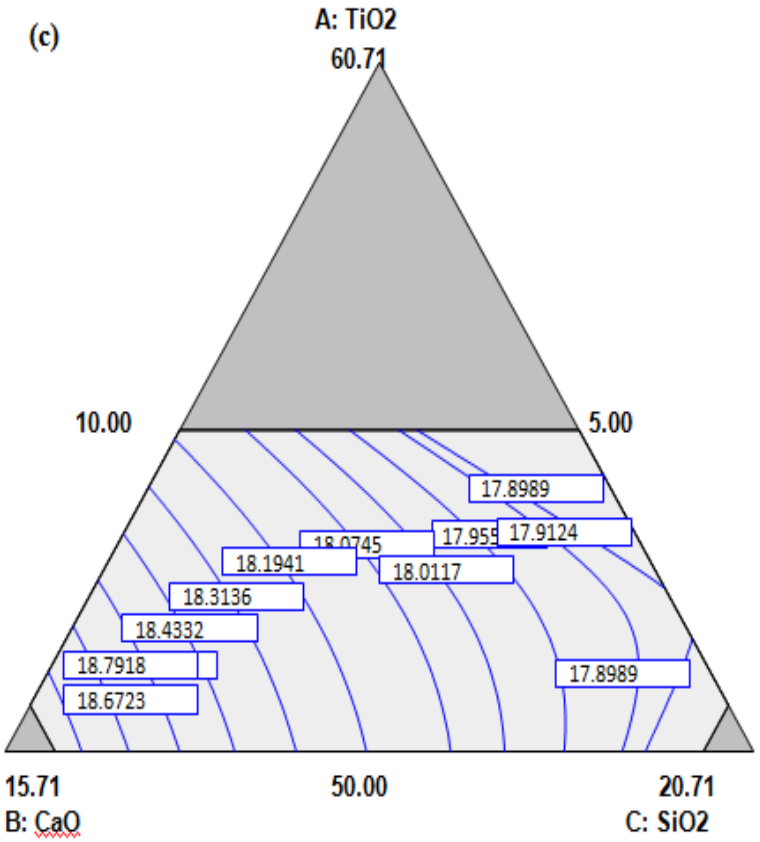
(c)
A: TiO2
60.71
10.00
5.00
17.8989
17.9124
18.1941
18.0117
18.3136
18.4332
18.7918
18.6723
17.8989
15.71
50.00
20.71
B: CaO
C: SiO2

(c) %Cr

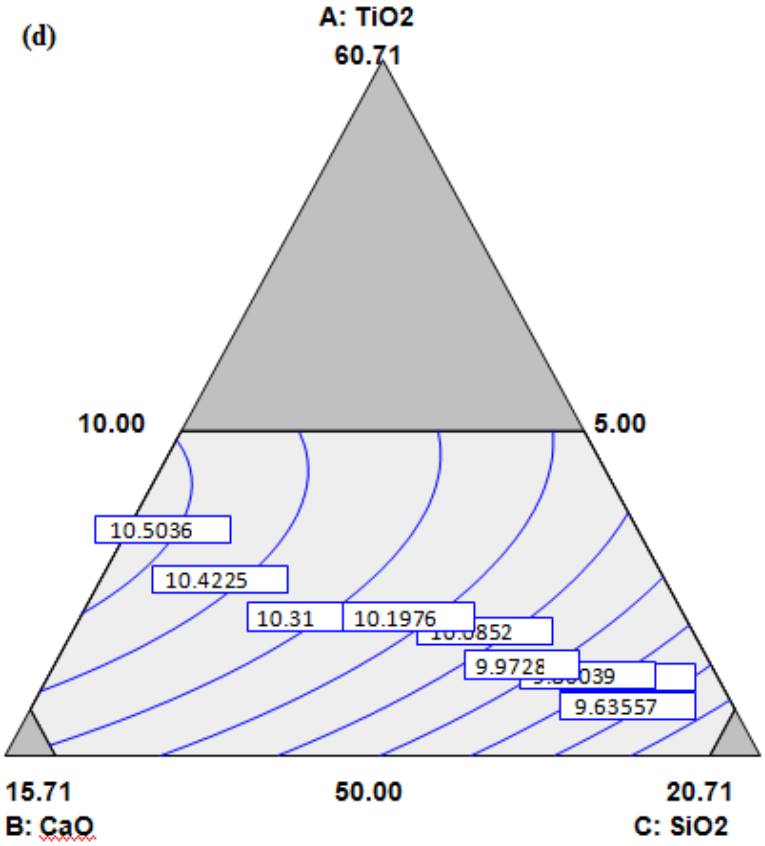
(d)
A: TiO2
60.71
10.00
5.00
10.5036
10.4225
10.31
10.1976
9.9728
9.63557
15.71
50.00
20.71
B: CaO
C: SiO2

(d) %Ni

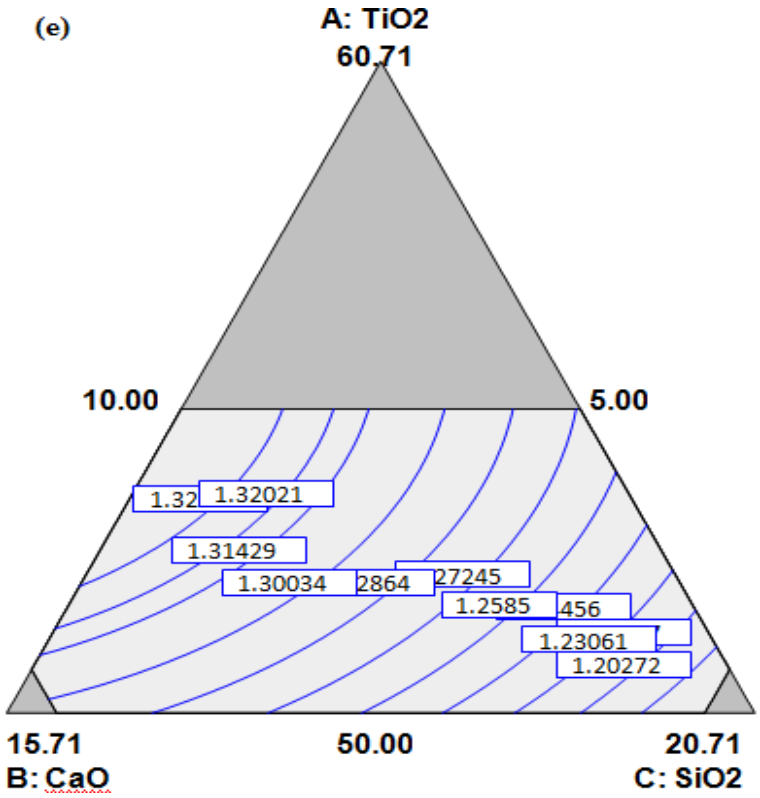

(e) %Mn

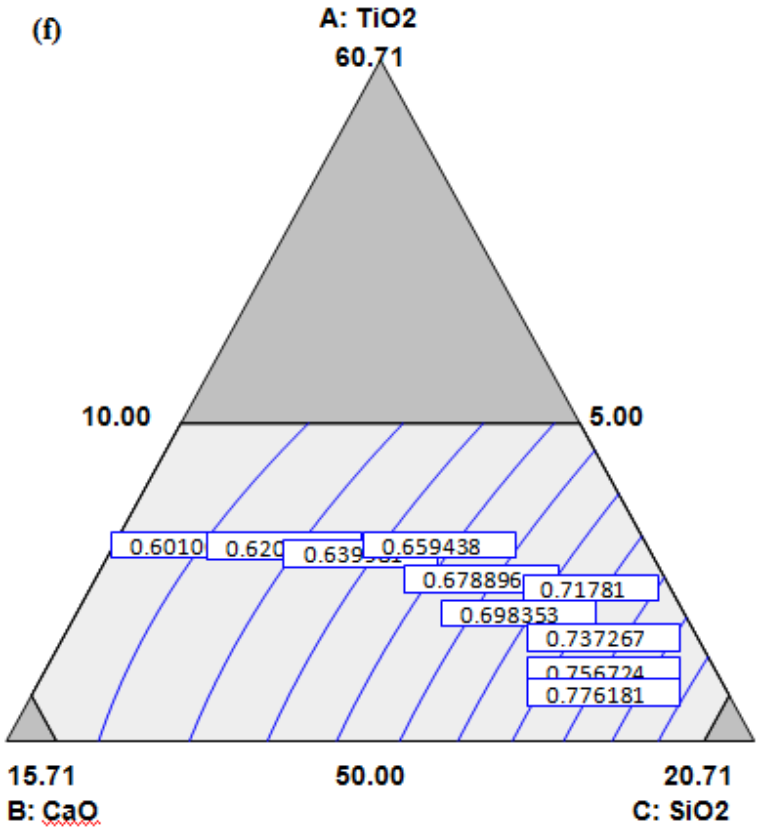

(f) %Si

Figure 5.4.1 Contour surface plots of various bimetallic weld responses (a) ferrite number, (b) %C, (c) %Cr, (d) %Ni, (e) %Mn and (f) %Si.

5.4.2 Effect of electrode coating ingredients on weld metal mechanical properties

It is observed from the regression analysis that TiO_2, SiO_2 and CaF_2 tend to increase the ultimate tensile strength of weld while CaO decreases it. The significant (decreasing) effect of binary mixtures $CaO.SiO_2$, $CaO.CaF_2$ and $SiO_2.CaF_2$ can be seen from the lower p values of these mixtures (Table 5.3.5). The interaction effects of TiO_2 with other electrode coating ingredients are not significant.

The impact toughness of weld increased with increasing TiO_2 content as TiO_2 acts as a grain refiner and also reduces the oxygen content of weld metal which is also reported by Kohno et al., 1982 [83]. SiO_2 in the electrode coatings leads to a higher silicon and oxygen content and a lower manganese content in the weld metal (Palm, 1972 [116]). This dissolved oxygen causes a decrease in impact toughness of bimetallic welds. From the regression analysis CaO shows an increasing effect on impact toughness of welds.

It is observed that the individual effect of TiO_2, CaO and CaF_2 electrode coatings is on increasing the microhardness of the welds. SiO_2 shows a decreasing trend by increasing the oxygen level in weld pool which further combines with carbon to form its oxides. The regression analysis shows the significant decreasing effect of binary mixtures $CaO.SiO_2$, $CaO.CaF_2$ and $SiO_2.CaF_2$ on the observed microhardness values as shown by the lower calculated p values of these binary mixtures in Table 5.3.5.

The contour plots for various mechanical properties i.e. ultimate tensile strength, percentage elongation, impact toughness and microhardness at different proportions of electrode coating ingredients TiO_2, CaO, SiO_2 with constant CaF_2= 4.29% are shown in Figure 5.4.2.

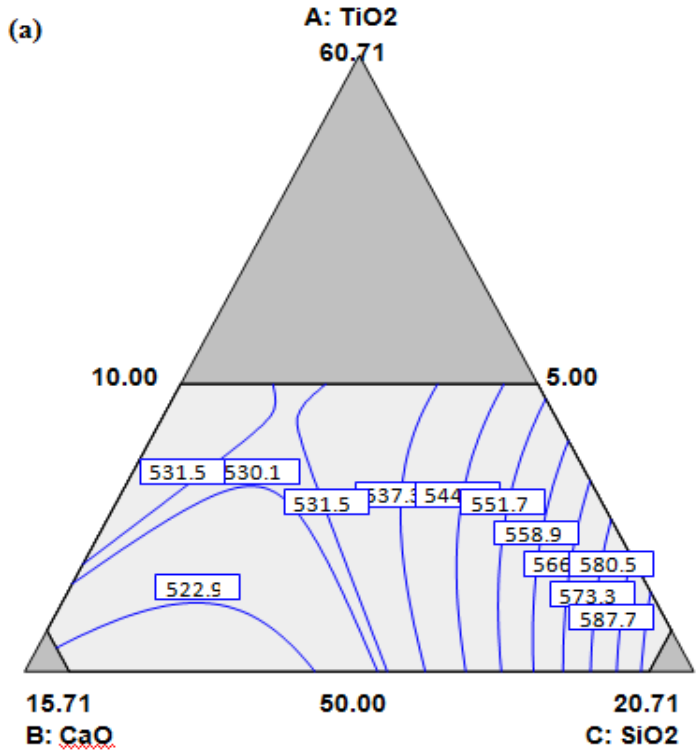

(a) Ultimate tensile strength

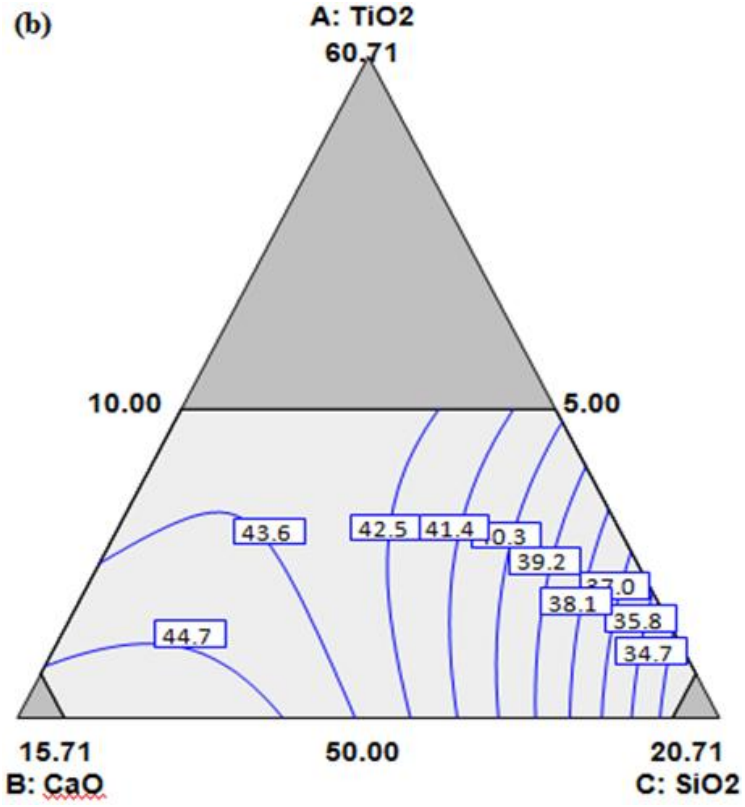

(b) Percentage elongation

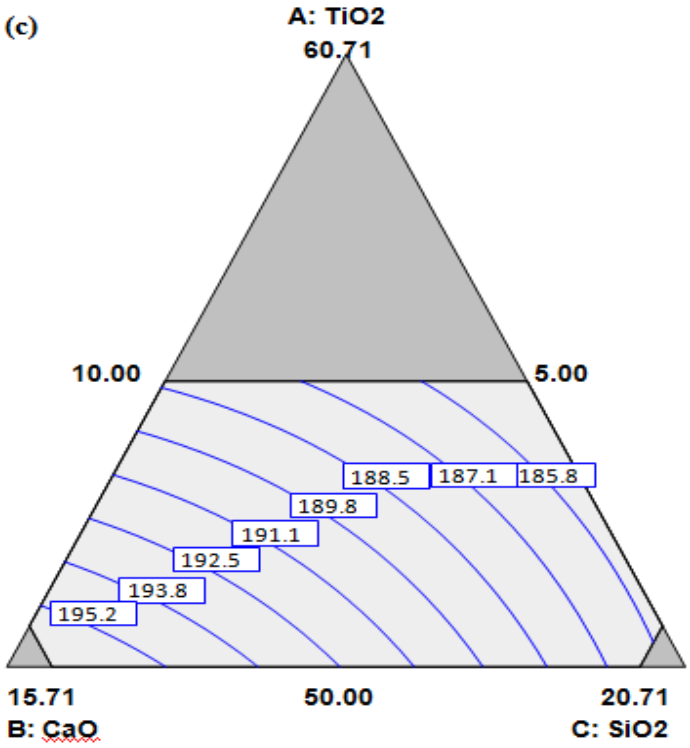

(c) Impact toughness

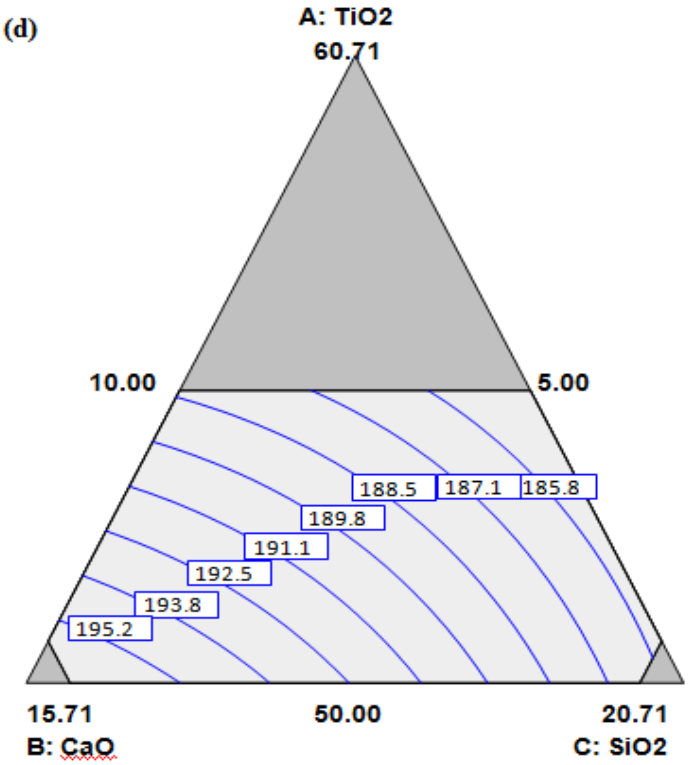

(d) Microhardness

Figure 5.4.2 Contour surface plots for various mechanical properties of bimetallic welds (a) ultimate tensile strength, (b) percentage elongation, (c) impact toughness and (d) microhardness.

5.4.3 Microstructure analysis

Figure 5.4.3 shows the typical microstructures of various weld metal specimens. The microstructures comprise of austenite (fcc) with varying amount of delta ferrite (bcc) indicating the primarily solidifications mode as ferritic–austenitic (FA). The delta ferrite at the dendrite cores also known as skeletal ferrite or vermicular ferrite (VF) is clearly visible in the microstructures of welds. It helps in minimizing the hot cracking of austenitic stainless steel matrix (Bystram, 1969).

The large inclusions (I) of size nearly 6μm are present on grain boundaries in microstructure of experiment no. 8 as shown in Figure 5.4.3(a) which adversely affects the mechanical strength and impact toughness along with ductility of weld whereas increased average microhardness value is obtained. The Figure 5.4.3(b) shows the weld microstructure derived from experiment no 7. It shows dispersed structure of very small size spherical-shaped inclusions of maximum size 0.4μm inside the grains that increase the ultimate tensile strength, impact toughness and average microhardness values whereas decreasing the ductility as observed from mechanical property test data (Table 5.3.3).

The weld microstructure obtained from experiment no. 13 as shown in Figure 5.4.3(c) shows the small size inclusions of size 1μm dispersed along the grains at the grain boundaries. This also results in relatively higher strength, toughness and microhardness values while lowering the ductility of the weld and also contributes towards the anisotropic behaviour in these welds.

The Figure 5.4.3(d) shows sparcely distributed intermediate size inclusions (maximum size 3μm) in the microstructure of weld sample of experiment no. 15. The observed values of lower ultimate tensile strength, microhardness and intermediate impact toughness along with higher ductility can be attributed to the absense of particle induced strengthening mechanism as shown by the microstructure.

The changes in the weld microstructures and the resultant mechanical peoperties can be attributed to the slag-metal reactions occuring due to the interaction of different ingredients with the weld metal resulting in element transfer and different weld chemistry.

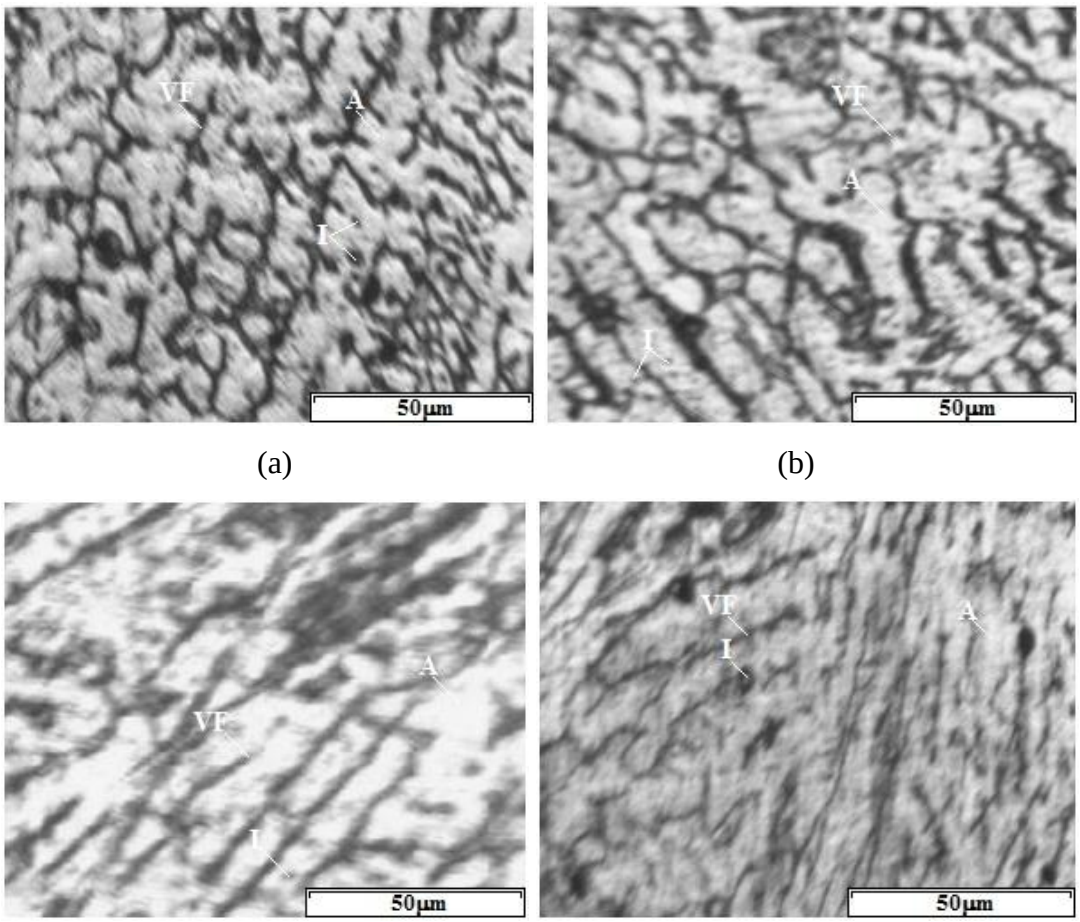

(a) (b)

(c) (d)

Figure 5.4.3 Microstructures of various weld specimen (a) expt. no. 8 (b) expt. no. 7 (c) expt. no. 13 (d) expt. no. 15 (VF-vermicular ferrite; I-inclusion; A-austenite).

5.4.4 Model validation

The developed regression models were validated by using three randomly selected welding electrode coating formulations for conducting the confirmatory experiments. The results are summarized in Table 5.4.1 and from the experimental values; it is observed that error (%) for each weld response is less than 5% in most of the cases.

5.4.5 Multi objective optimization

Here six optimized solutions with equal weight to ultimate tensile strength, impact toughness and microhardness along with the defined range of ferrite number have been found out at different levels of desirability as shown in Table 5.4.2. The range of ferrite number was decided on the observation that the delta ferrite number in the range from 3 to 8 percent helps in minimizing the hot cracking of austenitic stainless steel matrix. The first optimum electrode coating composition (Table 5.4.2) was then

selected for the three layer bimetallic weld approach for applying the second layer of buttering with SS309L electrodes on the mild steel buttered SA516 ferritic steel plates and then making the final bimetallic joint with SS304L after using the SS309L electrodes and finally comparing the results with those obtained with two layer approach.

Table 5.4.1 Error (%) in weld responses

Electrode coating formulation				Predicted value				Actual value				Error (%)			
A	B	C	D	UTS	%E	IT	MH	UTS	%E	IT	MH	UTS	%E	IT	MH
51	5	20	4	594.6	33.7	185.3	215.1	620	36	192	204	4.10	6.40	3.62	5.16
55	5	15	5	552.7	40.2	184.5	208.7	532	37	180	203	3.89	8.64	2.44	2.73
50	15	10	5	524.7	45.1	196.7	202.1	550	42	188	212	4.60	7.31	4.42	4.90

A-TiO_2, B-CaO, C-SiO_2, D-CaF_2, UTS-ultimate tensile strength (MPa), %E-percentage elongation (%), IT-impact toughness (Nm), MH-microhardness (VHN), Error (%) = (Actual value- Predicted value) x100/(Actual value)

Table 5.4.2 Electrode coating formulations for optimized weld responses

S.No.	TiO_2	CaO	SiO_2	CaF_2	Ultimate tensile strength (MPa)	Percentage elongation (%)	Impact toughness (Nm)	Micro-hardness (VHN)	Ferrite number	Composite desirability
1	50.2	9.8	10.0	10.0	584.9	36.5	190.7	211.1	4.9	0.95
2	51.5	8.2	10.3	10.0	599.8	34.3	188.3	213.5	3.6	0.95
3	50.0	10.0	20.0	0.0	571.5	37.1	188.3	211.2	4.2	0.93
4	53.5	9.3	10.0	7.2	567.1	38.8	188.8	208.6	3.0	0.93
5	50.0	7.2	20.0	2.9	578.5	36.0	187.5	212.5	4.7	0.93
6	50.0	12.6	17.4	0.0	538.0	42.1	191.3	205.9	4.3	0.91

5.5 Development of Regression Models of Buttering region (Stainless Steel Electrodes Based on CaO-TiO_2-SiO_2 System) with Two Layer Methodology

The metal chemistry, ferrite number and microhardness tests were also conducted at the buttering layer of bimetallic welds and the results are shown in Table 5.5.1.

Table 5.5.1 Results of metal chemistry, ferrite number and microhardness of buttering layer of bimetallic welds based on CaO-TiO_2-SiO_2 System

Expt. No.	%C	%Cr	%Ni	%Mn	%Si	Ferrite number	Microhardness
1	0.0752	18.64	9.17	1.31	0.50	4.6	222
2	0.0757	19.28	9.50	1.35	0.42	5.9	215
3	0.0731	18.48	9.10	1.27	0.63	4.4	228
4	0.0752	18.56	9.24	1.33	0.51	4.1	221
5	0.0766	18.80	9.60	1.34	0.45	3.9	222
6	0.0731	18.24	8.89	1.26	0.61	4.1	230
7	0.0766	19.12	9.31	1.33	0.46	5.7	227
8	0.0731	18.32	8.96	1.24	0.63	4.2	225
9	0.0738	18.56	9.03	1.29	0.52	4.8	231
10	0.0752	19.44	9.22	1.29	0.45	7.1	218
11	0.0745	18.64	9.03	1.29	0.52	5.0	218
12	0.0759	18.40	9.52	1.34	0.47	2.9	220
13	0.0776	18.72	9.59	1.34	0.45	3.6	229
14	0.0794	18.48	9.87	1.38	0.43	2.0	240
15	0.0759	19.04	9.60	1.38	0.45	4.8	217
16	0.0731	18.27	9.00	1.24	0.63	4.0	226
17	0.0759	18.96	9.45	1.34	0.50	4.9	220
18	0.0717	18.40	8.82	1.24	0.64	4.9	233

With the help of observed values of test results, the regression equations developed in terms of percentage composition of individual electrode coating ingredients (TiO_2, CaO, SiO_2 and CaF_2) and their combined binary mixtures are shown below:

%C = +4.48964E-004TiO_2 -6.71765E-004CaO -2.64516E-003SiO_2 -1.30590E-003CaF_2 +4.79051E-005TiO_2.CaO +8.18653E-005TiO_2.SiO_2 +7.80357E-005TiO_2.CaF_2 +2.36618E-005CaO.SiO_2 -2.82940E-005CaO.CaF_2 -3.17866E-005SiO_2.CaF_2 (5.5.1)

%Cr = +0.14984TiO_2 +0.71151CaO -0.20095SiO_2 +0.31646CaF_2 -3.04904E-003TiO_2.CaO +0.011290TiO_2.SiO_2 +1.98343E-003TiO_2.CaF_2 -0.010377CaO.SiO_2 -6.97178E-003CaO.CaF_2 -8.79732E-004SiO_2.CaF_2 (5.5.2)

%Ni = +0.088961TiO_2 -0.097726CaO -0.094245SiO_2 -0.26655CaF_2 +5.40323E-003TiO_2.CaO +4.27124E-003TiO_2.SiO_2 +0.010637TiO_2.CaF_2 +2.34522E-003CaO.SiO_2 -5.50016E-003CaO.CaF_2 -3.88139E-003SiO_2.CaF_2 (5.5.3)

%Mn = +9.65009E-003TiO_2 -0.066181CaO -0.037210SiO_2 -1.98289E-003CaF_2 +1.76606E-003TiO_2.CaO +1.07422E-003TiO_2.SiO_2 +8.62358E-004TiO_2.CaF_2 +1.17309E-003CaO.SiO_2 -7.34136E-004CaO.CaF_2 -2.63006E-005SiO_2.CaF_2 (5.5.4)

%Si = +0.014446TiO_2 +0.048464CaO +0.10824 SiO_2 +0.033037CaF_2 -1.07218E-003TiO_2.CaO -1.95268E-003TiO_2.SiO_2 -9.57789E-004TiO_2.CaF_2 -1.31363E-003CaO.SiO_2 +1.39424E-004CaO.CaF_2 -5.58419E-004SiO_2.CaF_2 (5.5.5)

Ferrite number =-0.15127TiO_2 +2.26260CaO -0.75198SiO_2 +1.32657CaF_2 -0.024967TiO_2.CaO +0.025109TiO_2.SiO_2 -0.022391TiO_2.CaF_2 -0.043823CaO.SiO_2 -7.93720E-03CaO.CaF_2 +0.010041SiO_2.CaF_2 (5.5.6)

Microhardness = +2.62599TiO_2 +2.51911CaO +12.57733SiO_2 -0.39527CaF_2 +0.028716TiO_2.CaO -0.15548TiO_2.SiO_2 +0.15449TiO_2.CaF_2 -0.19498CaO.SiO_2 -0.19991CaO.CaF_2 -0.27181SiO_2.CaF_2 (5.5.7)

5.5.1 Regression Analysis

The developed regression equations have been analyzed using analysis of variance (ANOVA) as shown in Tables 5.5.2 and 5.5.3. The coefficient of determination i.e. R-square values for the developed regression models are nearly equal or greater than 94% which indicate that predicted values are in close agreement with the actual values of various weld responses as shown in Figures 5.5.1 (a) to (g)

Table 5.5.2 Analysis of regression equations using ANOVA (F-test) of buttering layer metal chemistry of bimetallic welds

Weld response	Source	Sum of squares	DF	Mean square	F value	P value	R square
%C	Model	5.48E-05	9	6.09E-06	28.20833	< 0.0001	0.96
	Linear	5.03E-05	3	1.68E-05	77.6265	< 0.0001	
	TiO_2.CaO	2.85E-07	1	2.85E-07	1.321369	0.2835	
	TiO_2.SiO_2	8.33E-07	1	8.33E-07	3.858877	0.0851	
	TiO_2.CaF_2	7.57E-07	1	7.57E-07	3.506287	0.0980	
	CaO.SiO_2	6.27E-07	1	6.27E-07	2.906806	0.1266	
	CaO.CaF_2	8.97E-07	1	8.97E-07	4.156322	0.0758	
	SiO_2.CaF_2	1.13E-06	1	1.13E-06	5.245776	0.0512	
	Residual	1.73E-06	8	2.16E-07			
	Total	5.65E-05	17				
%Cr	Model	2.071711	9	0.23019	46.77752	< 0.0001	0.97
	Linear	1.87824	3	0.62608	127.2273	< 0.0001	
	TiO_2.CaO	0.001155	1	0.001155	0.234755	0.6410	
	TiO_2.SiO_2	0.01584	1	0.01584	3.218885	0.1105	
	TiO_2.CaF_2	0.000489	1	0.000489	0.09934	0.7607	
	CaO.SiO_2	0.120658	1	0.120658	24.51929	0.0011	
	CaO.CaF_2	0.054461	1	0.054461	11.06721	0.0104	
	SiO_2.CaF_2	0.000867	1	0.000867	0.176218	0.6857	
	Residual	0.039368	8	0.004921			
	Total	2.111078	17				
%Ni	Model	1.425072	9	0.158341	16.27368	0.0003	0.94
	Linear	1.34818	3	0.449393	46.18681	< 0.0001	
	TiO_2.CaO	0.003628	1	0.003628	0.372852	0.5584	
	TiO_2.SiO_2	0.002267	1	0.002267	0.23299	0.6422	
	TiO_2.CaF_2	0.014058	1	0.014058	1.444873	0.2637	
	CaO.SiO_2	0.006163	1	0.006163	0.63337	0.4491	
	CaO.CaF_2	0.033896	1	0.033896	3.483708	0.0989	
	SiO_2.CaF_2	0.01688	1	0.01688	1.734864	0.2243	
	Residual	0.077839	8	0.00973			
	Total	1.502911	17				

%Mn	Model	0.034621	9	0.003847	17.46312	0.0002	0.95
	Linear	0.031851	3	0.010617	48.19779	< 0.0001	
	TiO_2.CaO	0.000388	1	0.000388	1.759454	0.2213	
	TiO_2.SiO_2	0.000143	1	0.000143	0.650952	0.4431	
	TiO_2.CaF_2	9.24E-05	1	9.24E-05	0.419509	0.5353	
	CaO.SiO_2	0.001542	1	0.001542	6.999806	0.0295	
	CaO.CaF_2	0.000604	1	0.000604	2.741445	0.1364	
	SiO_2.CaF_2	7.75E-07	1	7.75E-07	0.003518	0.9542	
	Residual	0.001762	8	0.00022			
	Total	0.036383	17				
%Si	Model	0.083459	9	0.009273	57.73091	< 0.0001	0.94
	Linear	0.080424	3	0.026808	166.8938	< 0.0001	
	TiO_2.CaO	0.000143	1	0.000143	0.88931	0.3733	
	TiO_2.SiO_2	0.000474	1	0.000474	2.949714	0.1242	
	TiO_2.CaF_2	0.000114	1	0.000114	0.70967	0.4240	
	CaO.SiO_2	0.001934	1	0.001934	12.03724	0.0084	
	CaO.CaF_2	2.18E-05	1	2.18E-05	0.135598	0.7222	
	SiO_2.CaF_2	0.000349	1	0.000349	2.175196	0.1785	
	Residual	0.001285	8	0.000161			
	Total	0.084744	17				

DF-degree of freedom

Table 5.5.3 Analysis of regression equations using ANOVA (F-test) of buttering layer ferrite number and microhardness

Weld response	Source	Sum of squares	DF	Mean square	F value	P value	R square
Ferrite number	Model	20.90887	9	2.323207	18.0847	0.0002	0.95
	Linear	18.35545	3	6.118482	47.62853	< 0.0001	
	TiO_2.CaO	0.077461	1	0.077461	0.602987	0.4598	
	TiO_2.SiO_2	0.078344	1	0.078344	0.609858	0.4573	
	TiO_2.CaF_2	0.062301	1	0.062301	0.484974	0.5059	
	CaO.SiO_2	2.151761	1	2.151761	16.7501	0.0035	
	CaO.CaF_2	0.070589	1	0.070589	0.549487	0.4797	
	SiO_2.CaF_2	0.112963	1	0.112963	0.879346	0.3758	
	Residual	1.027701	8	0.128463			
	Total	21.93657	17				

Microhardness	Model	692.9545	9	76.99494	20.88707	0.0001	0.95
	Linear	516.7258	3	172.2419	46.72553	< 0.0001	
	TiO_2.CaO	0.102466	1	0.102466	0.027797	0.8717	
	TiO_2.SiO_2	3.003831	1	3.003831	0.814874	0.3931	
	TiO_2.CaF_2	2.965912	1	2.965912	0.804588	0.3959	
	CaO.SiO_2	42.59548	1	42.59548	11.55524	0.0094	
	CaO.CaF_2	44.77741	1	44.77741	12.14715	0.0083	
	SiO_2.CaF_2	82.78354	1	82.78354	22.45739	0.0015	
	Residual	29.48999	8	3.686249			
	Total	722.4444	17				

DF-degree of freedom

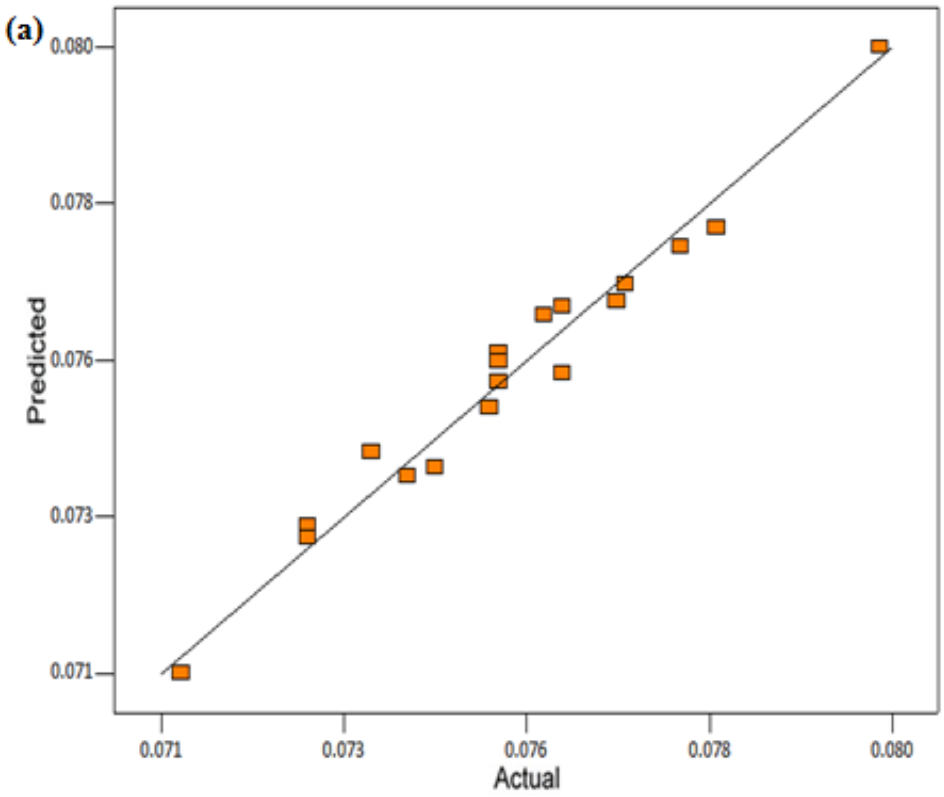

(a) %C

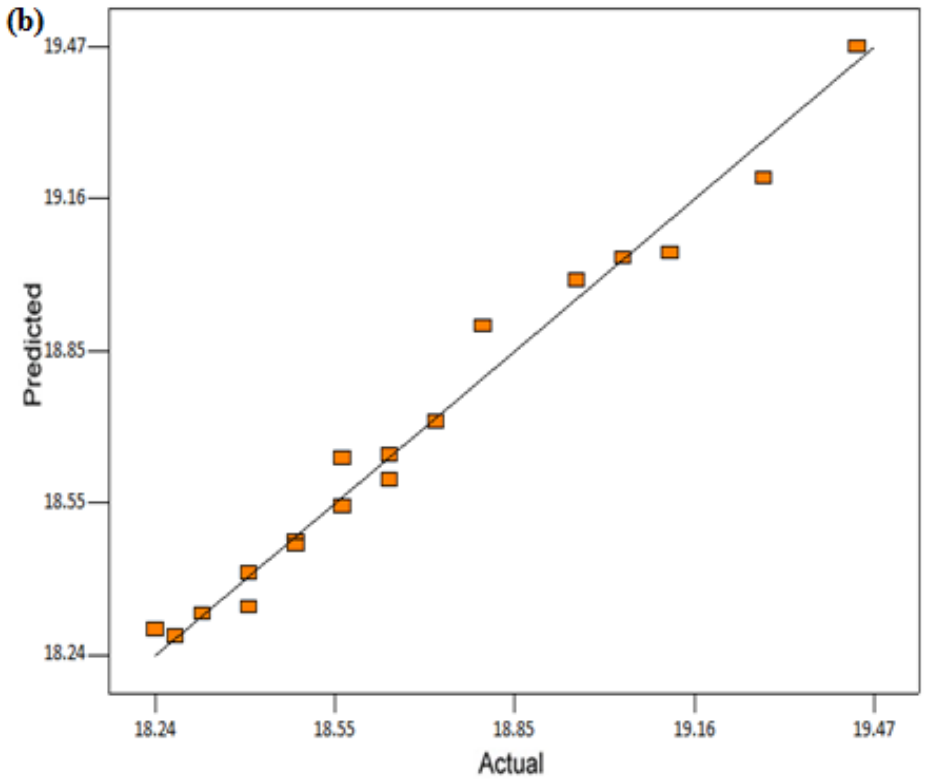
(b)
19.47
19.16
18.85
18.55
18.24
Predicted
18.24
18.55
18.85
19.16
19.47
Actual

(b) %Cr

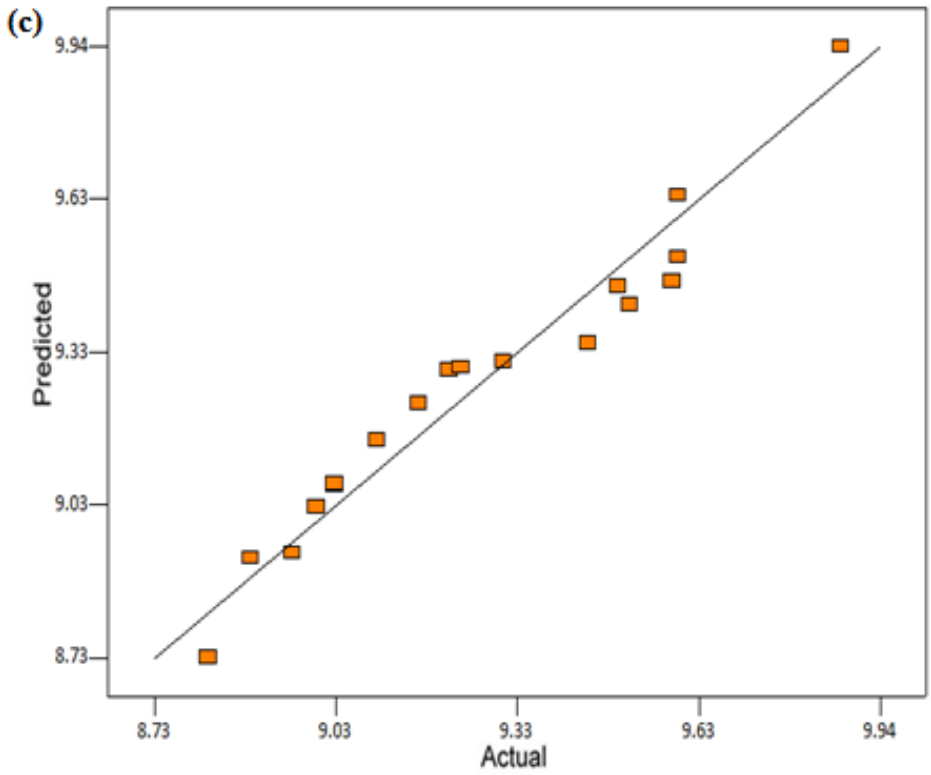
(c)
9.94
9.63
9.33
9.03
8.73
Predicted
8.73
9.03
9.33
9.63
9.94
Actual

(c) %Ni

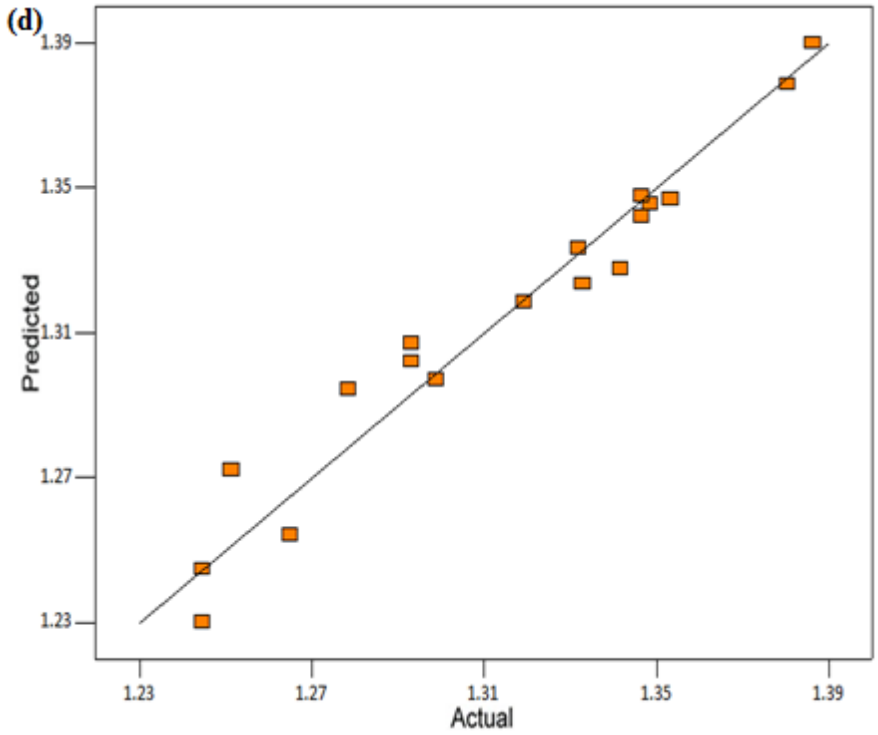
(d)
1.39
1.35
1.31
1.27
1.23
Predicted
1.23
1.27
1.31
1.35
1.39
Actual

(d) %Mn

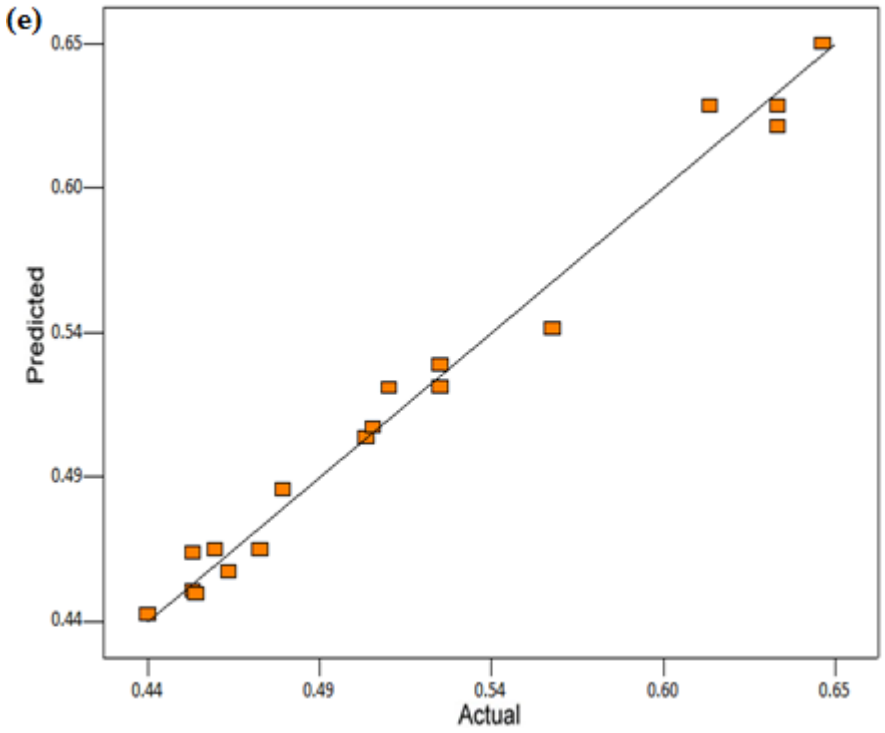
(e)
0.65
0.60
0.54
0.49
0.44
Predicted
0.44
0.49
0.54
0.60
0.65
Actual

(e) %Si

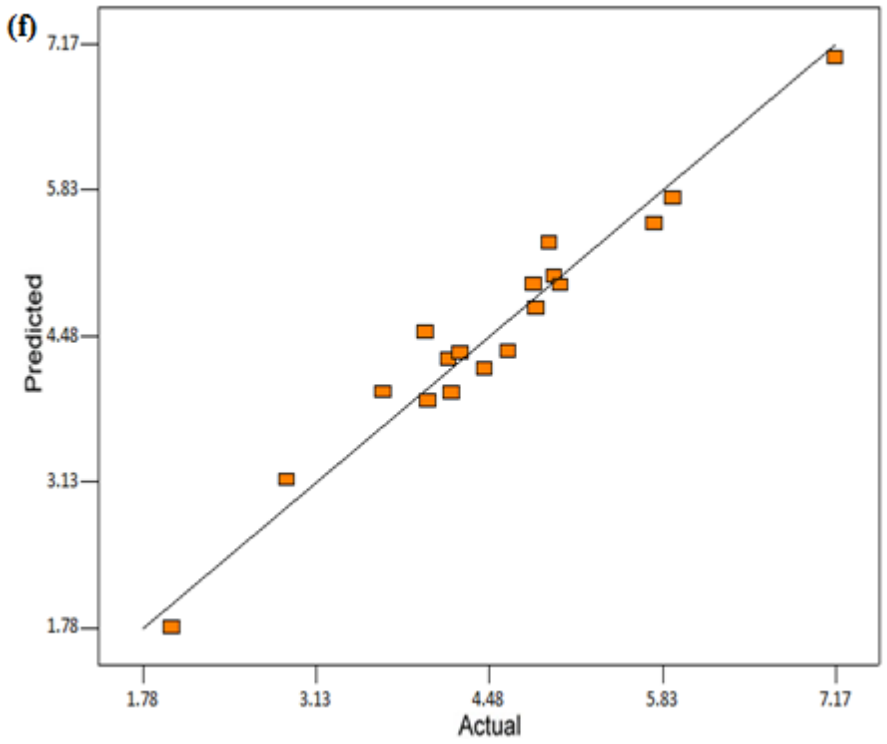

(f) Ferrite number

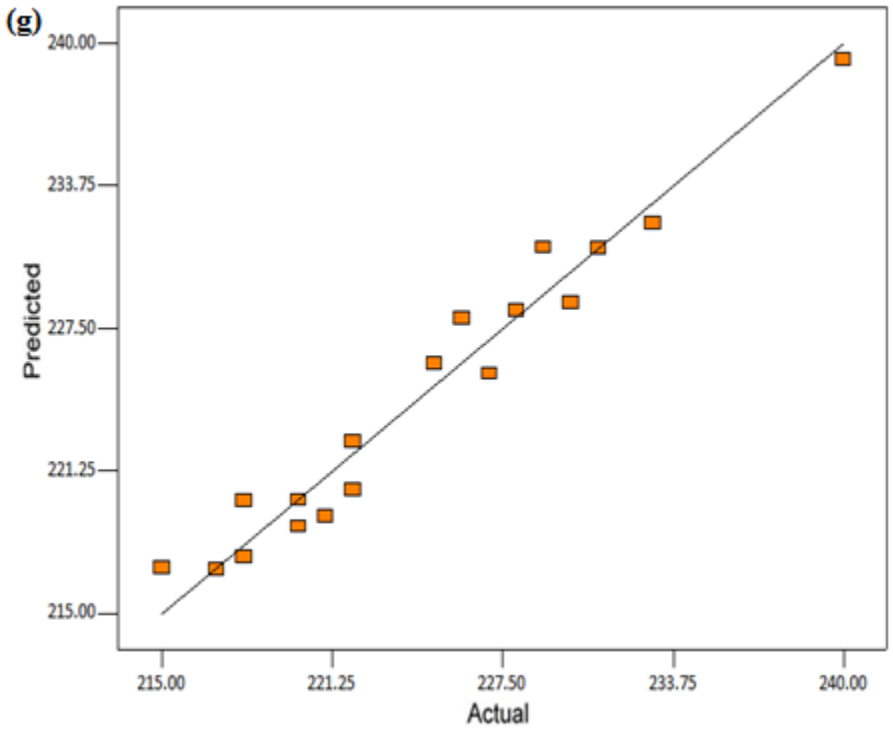

(g) Microhardness

Figure 5.5.1 Predicted versus actual values of various weld responses of buttering region (a) %C, (b) %Cr, (c) %Ni, (d) %Mn, (e) %Si, (f) ferrite number and (g) microhardness.

5.6 Discussion of Buttering Region Two Layer Bimetallic Welds Fabricated with Stainless Steel Electrodes Based on CaO-TiO_2-SiO_2 System

5.6.1 Effect of electrode coating ingredients on weld responses of buttering layer

It is observed from regression analysis that silicon content in buttering layer is significantly increased with the increase in SiO_2 in electrode coatings as SiO_2 dissociates into Si and O_2. The interaction effect of CaO.SiO_2 decreases the silicon content in buttering layer composition as CaO decreases the activity of silica in slag metal reactions. It has also been reported by Palm (1972)[116] in references. Regression analysis also shows that other binary interaction effects of SiO_2 depict decreasing effect on buttering layer silicon content. The increase of SiO_2 in the electrode coatings causes the higher MnO and FeO concentration in the slag which results in a lower Mn content in the buttering layer. The additions of CaO and CaF_2 in electrode coatings decrease the manganese content in buttering layer region.

It is found that electrode coating ingredients TiO_2, CaO and CaF_2 tends to increase the chromium content of buttering layer, while SiO_2 behaves in a negative manner. The free oxygen in the electrode coatings recombines with chromium from the buttering layer. The SiO_2 reduced to form silicon and chromium oxide, resulting in a decrease chromium content of buttering layer. The regression results show the decrease of nickel content in buttering layer with increase of various electrode coating ingredients except TiO_2. The ingredients CaO, CaF_2 and SiO_2 tend to decrease the carbon in buttering layer composition. The oxygen released during the slag-metal reactions from various electrode coating ingredients, further combines with carbon to form its oxides and thereby decrease in carbon content of buttering layer composition. Regression results show that the all the coating ingredients except SiO_2 increase the ferrite number thereby promote the delta ferrite content in the welds.

5.6.2 Contour surface plots for various properties

The contour surface plots showing predicted values of chemical composition of various elements, ferrite number and microhardness of buttering region for different proportions of electrode coating ingredients TiO_2, CaO, SiO_2 with constant CaF_2= 4.29% are shown in Figure 5.6.1 (a) to (g).

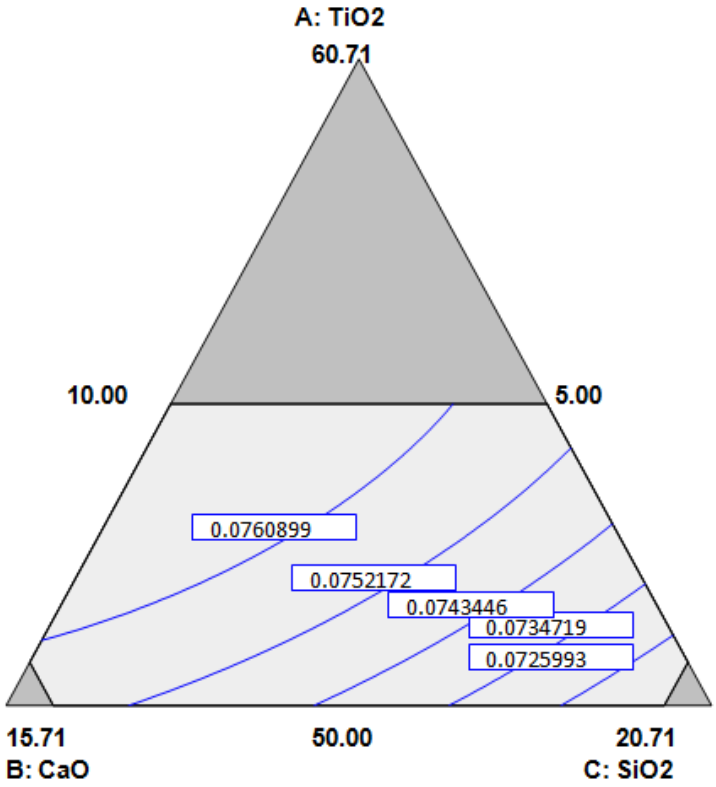
A: TiO2
60.71
10.00
5.00
0.0760899
0.0752172
0.0743446
0.0734719
0.0725993
15.71
B: CaO
50.00
20.71
C: SiO2

(a) %C

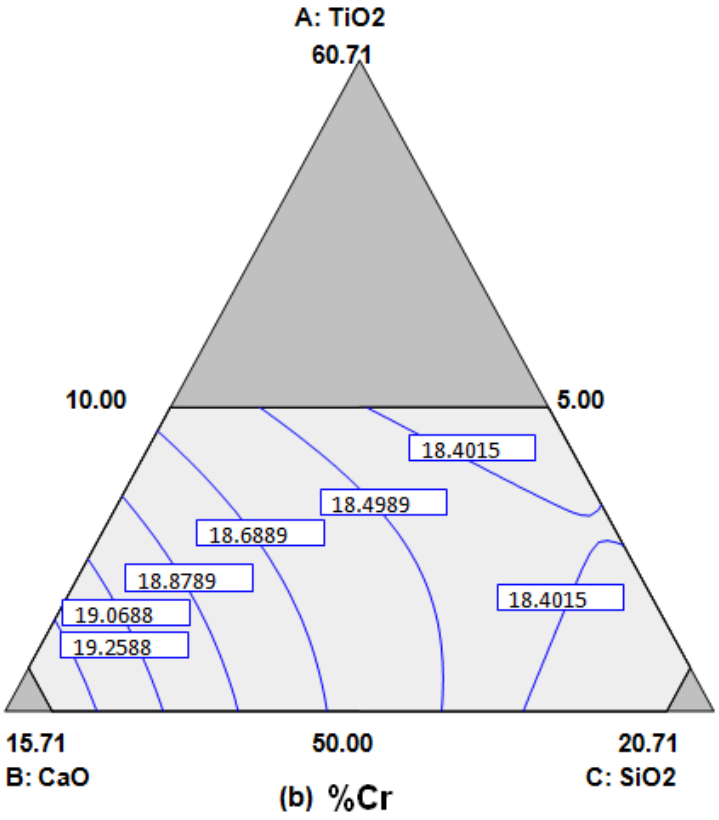
A: TiO2
60.71
10.00
5.00
18.4015
18.4989
18.6889
18.8789
19.0688
19.2588
18.4015
15.71
B: CaO
50.00
20.71
C: SiO2

(b) %Cr

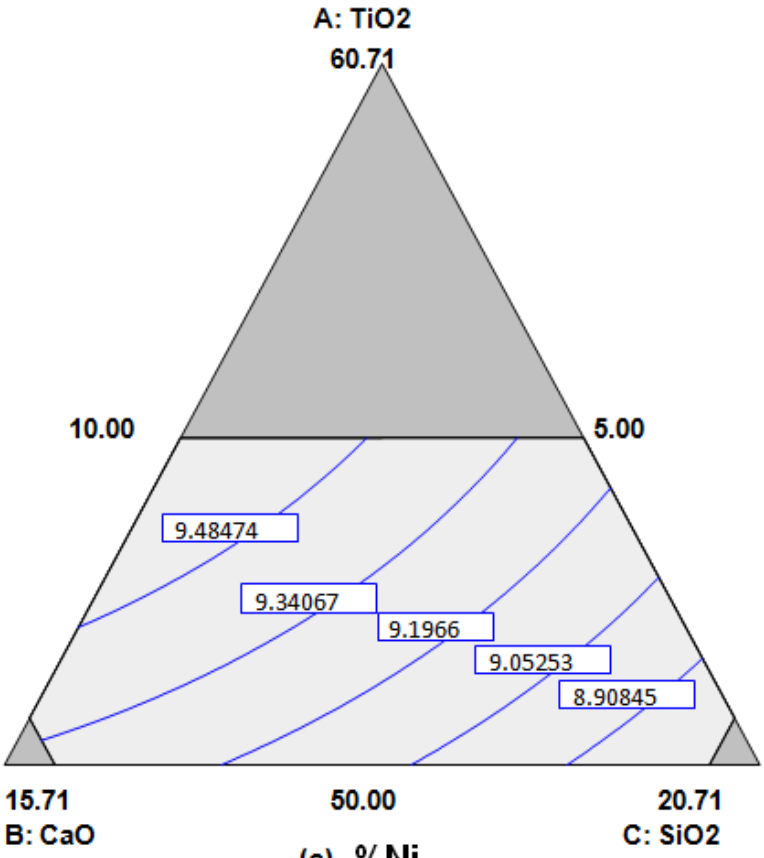
A: TiO2
60.71
10.00
5.00
9.48474
9.34067
9.1966
9.05253
8.90845
15.71
B: CaO
50.00
20.71
C: SiO2

(c) %Ni

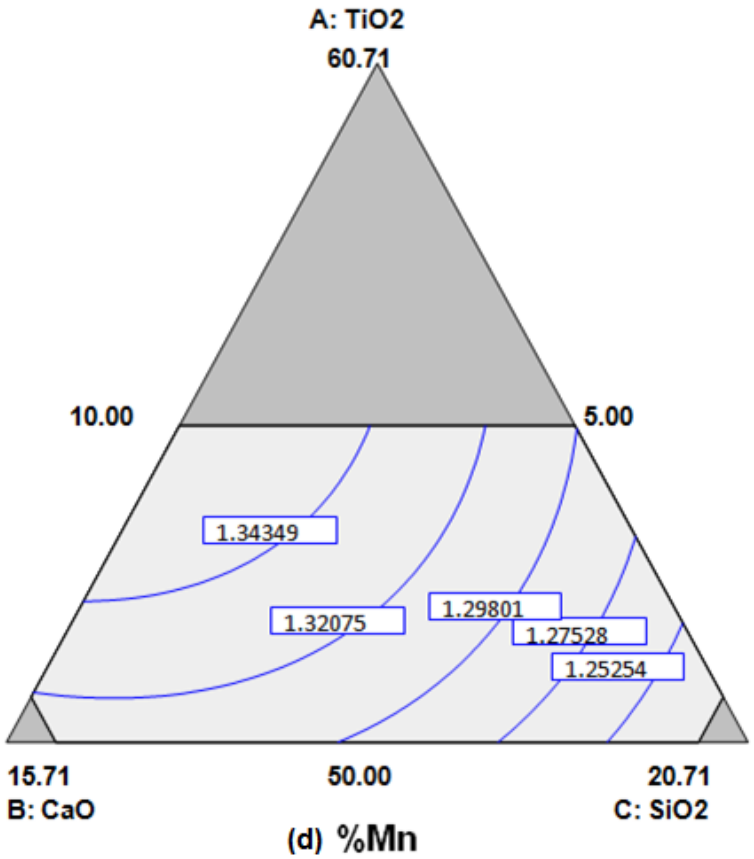
A: TiO2
60.71
10.00
5.00
1.34349
1.32075
1.29801
1.27528
1.25254
15.71
B: CaO
50.00
20.71
C: SiO2

(d) %Mn

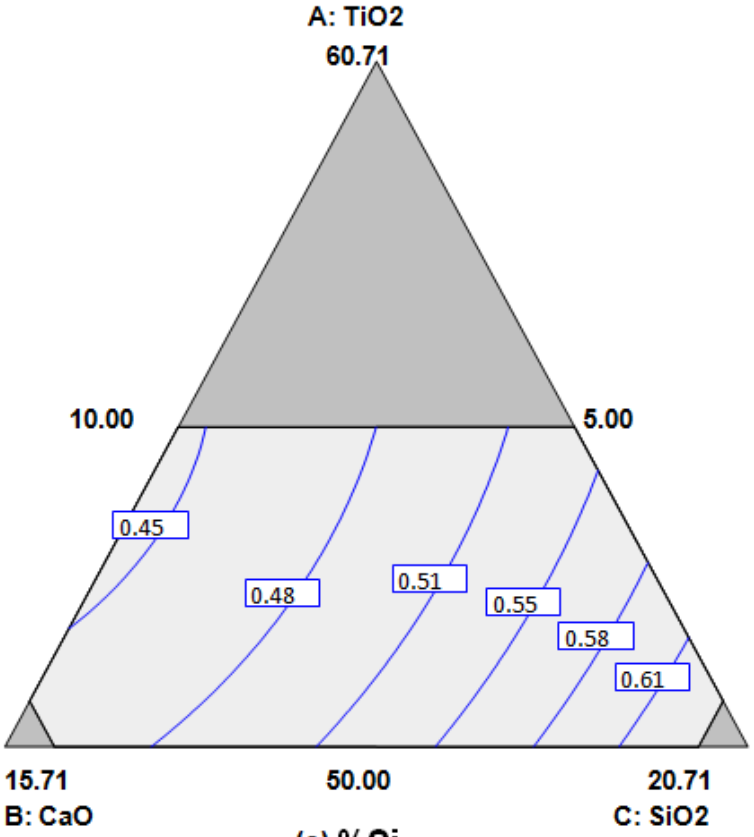

(e) %Si

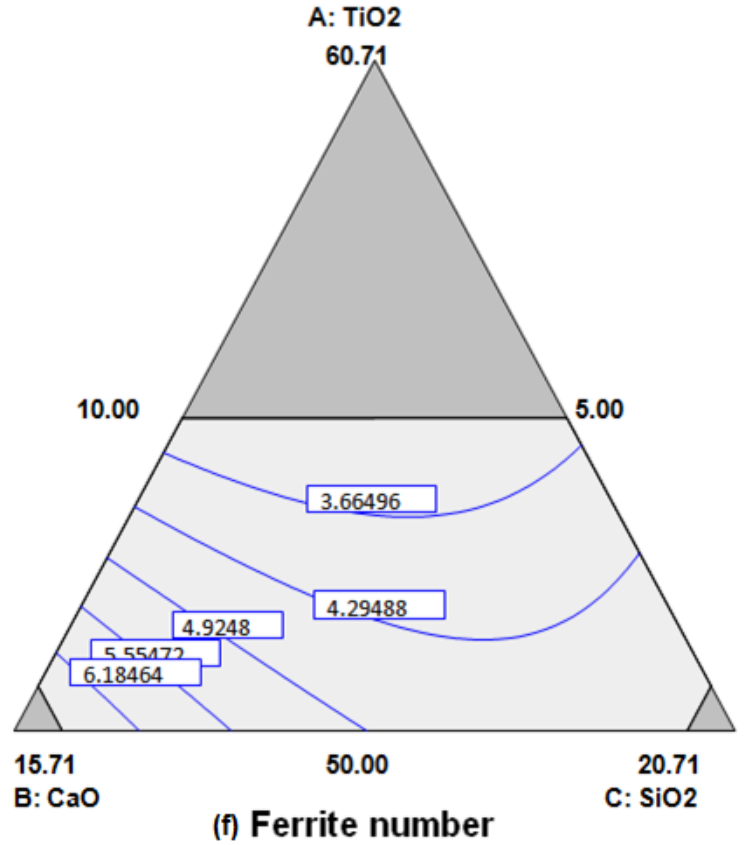

(f) Ferrite number

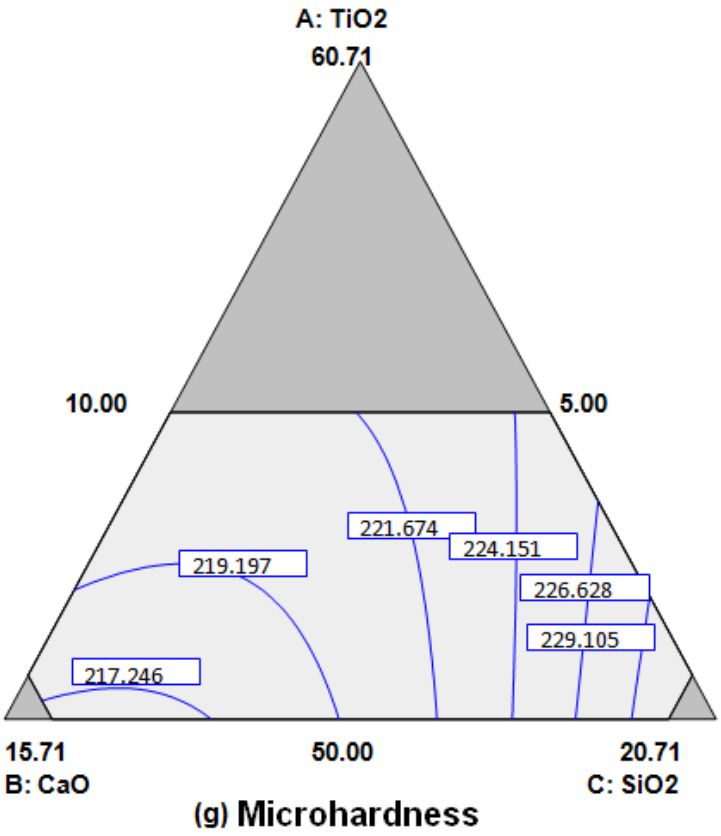

Figure 5.6.1 Contour surface plots of various weld responses of buttering region (a) %C, (b) %Cr, (c) %Ni, (d) %Mn, (e) %Si, (f) ferrite number and (g) microhardness.

5.6.3 Microstructural analysis

The microstructures of expt no. 14 are given in Figure 5.6.2 (a) and (b). The interface of SA516 and buttering layer is shown in Figure 5.6.2 (a). The carbide precipitates are visible near to the interface and the coarse grained region is also seen on the SA516 side. Figure 5.6.2 (b) shows the buttering layer and weld interface. Due to the carbon migration from the SA516 towards weld zone, the microhardness of the buttering (Table 5.5.1) as well as the bimetallic weld (Table 5.3.3) specimen fabricated with the electrode coating formulation or expt. no. 14 has increased.

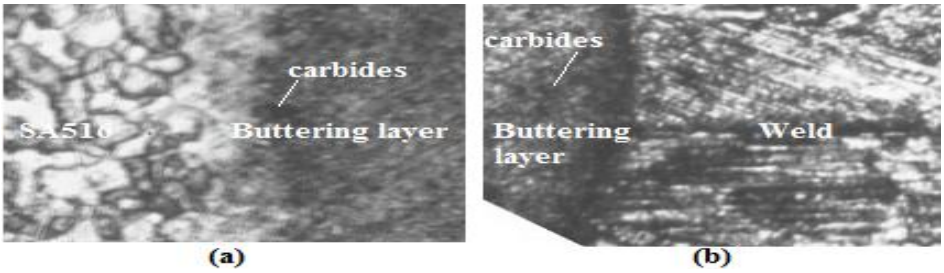

Figure 5.6.2 Microstructure of (a) SA516 and buttering layer interface and (b) buttering layer and weld interface.

5.7 Development of Regression Models (Stainless Steel Electrodes Based on $CaO\text{-}SiO_2\text{-}Al_2O_3\text{-}TiO_2$ System) with Two Layer Methodology

The chemical composition analysis of bimetallic welds between SS304L and SA516 base plates using stainless steel electrodes based on $CaO\text{-}SiO_2\text{-}Al_2O_3\text{-}TiO_2$ system is presented in Table 5.7.1. The results of ferrite number of bimetallic welds are given in Table 5.7.2. It was measured using WRC 92 diagram and ferritescope.

Table 5.7.1 Results of chemical composition analysis of bimetallic welds

Expt. No.	%Si	%Mn	%Cr	%Ni	%C
1.	0.74	1.22	17.89	11.01	0.043
2.	0.66	1.28	18.13	10.76	0.039
3.	0.58	1.36	18.80	10.20	0.039
4.	0.59	1.32	18.53	10.36	0.042
5.	0.79	1.20	17.72	10.92	0.042
6.	0.76	1.22	17.89	10.84	0.038
7.	0.59	1.34	18.69	10.20	0.039
8.	0.69	1.26	18.05	10.76	0.040
9.	0.58	1.35	18.93	9.96	0.038
10.	0.58	1.34	18.77	10.12	0.037
11.	0.62	1.32	18.93	9.94	0.036
12.	0.68	1.28	18.13	10.76	0.042
13.	0.79	1.22	17.80	10.75	0.042
14.	0.64	1.29	18.37	10.52	0.037
15.	0.58	1.33	18.61	10.28	0.041
16.	0.67	1.28	18.29	10.60	0.039
17.	0.57	1.34	18.53	10.36	0.040
18.	0.79	1.21	17.80	10.78	0.040
19.	0.61	1.30	18.53	10.36	0.037
20.	0.58	1.34	18.71	10.10	0.040
21.	0.59	1.32	18.77	10.32	0.036

Table 5.7.2 Results of ferrite number of bimetallic welds

S.No.	Cr_{eq}/Ni_{eq}	Ferrite Number (FN)		Solidification mode
		WRC 92 diagram	Ferritescope	
1	1.43	0.4	1.4	FA
2	1.50	2.0	2.8	FA
3	1.63	6.0	5.1	FA
4	1.57	3.5	4.2	FA
5	1.43	0.1	1.0	AF
6	1.47	2.0	1.2	FA
7	1.62	4.8	6.1	FA
8	1.49	1.8	3.3	FA
9	1.68	6.0	7.1	FA
10	1.64	5.5	6.3	FA
11	1.69	6.5	8.0	FA
12	1.48	1.2	2.1	FA
13	1.46	0.8	1.4	FA
14	1.55	3.0	3.7	FA
15	1.59	5.8	4.7	FA
16	1.53	3.9	2.9	FA
17	1.57	4.8	4.0	FA
18	1.46	0.8	1.5	FA
19	1.59	3.0	4.6	FA
20	1.63	5.6	4.9	FA
21	1.62	5.0	6.1	FA

FA- ferritic–austenitic; AF- austenitic–ferritic

Using observed values of weld responses in terms of weld metal chemistry and ferrite number of bimetallic welds from experimentation; the regression equations developed in terms of percentage composition of individual electrode coating ingredients (CaO, SiO_2, Al_2O_3 and TiO_2) along with their binary mixtures are given below:

$$\%Si = +4.04422E\text{-}003CaO +0.017454SiO_2 -0.013988Al_2O_3 +2.49793E\text{-}003TiO_2 - 1.11440E\text{-}004CaO.SiO_2 +5.04078E\text{-}004CaO.Al_2O_3 +1.03496E\text{-}004CaO.TiO_2 + 2.94528E\text{-}004SiO_2.Al_2O_3 +3.6037E\text{-}005SiO_2.TiO_2 +4.02535E\text{-}004Al_2O_3.TiO_2 \quad (5.7.1)$$

%Mn = +0.021001CaO +0.016057SiO_2 +0.019860Al_2O_3 +0.018283TiO_2 -9.53390E-005CaO.SiO_2 -9.29543E-005CaO.Al_2O_3 -1.31870E-005CaO.TiO_2 -1.41419E-004SiO_2.Al_2O_3 -6.93336E-005SiO_2.TiO_2 +1.34948E-004Al_2O_3.TiO_2 (5.7.2)

%C = +7.51876E-004CaO +4.62297E-004SiO_2 -3.46136E-004Al_2O_3 +6.28307E-004TiO_2 -1.18236E-005CaO.SiO_2 +5.25483E-006CaO.Al_2O_3 -8.54690E-006CaO.TiO_2 +3.20295E-005SiO_2.Al_2O_3 +6.80004E-006SiO_2.TiO_2 +6.00484E-006Al_2O_3.TiO_2 (5.7.3)

%Cr = +0.32031CaO +0.26073SiO_2 +0.29669Al_2O_3 +0.26276TiO_2 -2.23586E-003CaO.SiO_2 -2.31987E-003CaO.Al_2O_3 -1.23546E-003CaO.TiO_2 -1.91595E-003SiO_2.Al_2O_3 -1.28083E-003SiO_2.TiO_2 +7.20638E-004Al_2O_3.TiO_2 (5.7.4)

%Ni = +0.061107CaO +0.090519SiO_2 +0.25153Al_2O_3 +0.12546TiO_2 +3.29774E-003CaO.SiO_2 -6.36647E-004CaO.Al_2O_3 +1.36212E-003CaO.TiO_2 -2.58481E-004SiO_2.Al_2O_3 +1.98687E-003SiO_2.TiO_2 -3.89615E-003Al_2O_3.TiO_2 (5.7.5)

Ferrite number = +0.52331CaO +0.27173SiO_2 +0.19945Al_2O_3 +0.13827TiO_2 -0.018550CaO.SiO_2 -0.010112CaO.Al_2O_3 -6.20395E-003CaO.TiO_2 -8.84869E-003SiO_2.Al_2O_3 -9.19775E-003SiO_2.TiO_2 +3.35071E-003Al_2O_3.TiO_2 (5.7.6)

The results of mechanical behaviour i.e. mean values of ultimate tensile strength, impact strength and microhardness of bimetallic welds are given in Table 5.7.3

The developed regression models for the observed values of mechanical properties are as follows:

Ultimate tensile strength = +6.08053CaO +6.45533SiO_2 +12.07737Al_2O_3 +4.55110TiO_2 +0.080256CaO.SiO_2 -0.015857CaO.Al_2O_3 +0.20590CaO.TiO_2 -0.17961SiO_2.Al_2O_3 +0.010147SiO_2.TiO_2 -0.017502Al_2O_3.TiO_2 (5.7.7)

Impact toughness = +2.55896CaO +1.82496SiO_2 -0.95017Al_2O_3 +0.99801TiO_2 -0.017044CaO.SiO_2 +0.062746CaO.Al_2O_3 +0.055321CaO.TiO_2 +0.088543SiO_2.Al_2O_3 +0.040415SiO_2.TiO_2 +0.055386Al_2O_3.TiO_2 (5.7.8)

Microhardness = +3.11522CaO +2.91312SiO_2 +2.72309Al_2O_3 +3.41162TiO_2 -0.016704CaO.SiO_2 -0.035678CaO.Al_2O_3 -0.055393CaO.TiO_2 +0.038850SiO_2.Al_2O_3 +0.012474SiO_2.TiO_2 -0.017878Al_2O_3.TiO_2 (5.7.9)

Table 5.7.3 Weld responses in terms of mechanical properties of bimetallic welds

Expt. No.	UTS (MPa)	Impact toughness (Nm)	Microhardness (VHN)
1.	520	181	221
2.	590	189	200
3.	570	178	204
4.	560	180	207
5.	525	180	219
6.	560	176	207
7.	608	192	191
8.	567	182	205
9.	620	195	186
10.	600	190	188
11.	610	193	190
12.	545	185	212
13.	540	180	218
14.	580	185	200
15.	565	180	205
16.	580	188	200
17.	573	184	203
18.	532	181	217
19.	595	185	195
20.	570	180	204
21.	598	188	190

5.7.1 Analysis of regression models

The developed regression models have been analyzed using t-test and F-test i.e. analysis of variance (ANOVA). The significance of regression coefficients (b_i and b_{ij}) have been tested by comparing their t value with tabulated t values at 95% significance level. The Table 5.7.4 shows the analysis of regression equations of weld metal content of bimetallic welds while the analysis of regression equations of mechanical behaviour of bimetallic welds is presented in Table 5.7.5. The Tables 5.7.6, 5.7.7 and 5.7.8 depict the t-test analysis for significance of regression coefficients of regression models of various weld responses.

Table 5.7.4 Analysis of regression equations using ANOVA (F-test) of weld metal content of bimetallic welds

Weld response	Source	Sum of squares	DF	Mean square	F value	P value	Status
%Si	Model	0.121884	9	0.013543	243.5456	< 0.0001	Signi.
	Residual	0.000612	11	5.56E-05			
	Total	0.122496	20	R-Squared	0.995007		
	Std. Dev.	0.007457		Adj R-Squared	0.990921		
	Mean	0.652271		Pred R-Squared	0.977657		
	CV	1.143232		Adeq Precision	41.65752		
%Mn	Model	0.050658	9	0.005629	305.088	< 0.0001	Signi.
	Residual	0.000203	11	1.84E-05			
	Total	0.050861	20	R-Squared	0.99601		
	Std. Dev.	0.004295		Adj R-Squared	0.992745		
	Mean	1.291719		Pred R-Squared	0.984692		
	CV	0.332523		Adeq Precision	49.8981		
%C	Model	7.29E-05	9	8.09E-06	9.782688	0.0004	Signi.
	Residual	9.1E-06	11	8.27E-07			
	Total	8.2E-05	20	R-Squared	0.888938		
	Std. Dev.	0.00091		Adj R-Squared	0.79807		
	Mean	0.03943		Pred R-Squared	0.567264		
	CV	2.306997		Adeq Precision	9.440938		
%Cr	Model	3.182276	9	0.353586	62.52626	< 0.0001	Signi.
	Residual	0.062205	11	0.005655			
	Total	3.244481	20	R-Squared	0.980827		
	Std. Dev.	0.0752		Adj R-Squared	0.965141		
	Mean	18.37417		Pred R-Squared	0.928873		
	CV	0.409269		Adeq Precision	22.43672		
%Ni	Model	2.026763	9	0.225196	23.97828	< 0.0001	Sign.
	Residual	0.103308	11	0.009392			
	Total	2.130071	20	R-Squared	0.9515		
	Std. Dev.	0.096911		Adj R-Squared	0.911818		

	Mean	10.47217		Pred R-Squared	0.810802		
	CV	0.925411		Adeq Precision	15.63313		
Ferrite number	Model	75.32857	9	8.369842	36.47992	< 0.0001	Signi.
	Residual	2.523806	11	0.229437			
	Total	77.85238	20	R-Squared	0.967582		
	Std. Dev.	0.478996		Adj R-Squared	0.941058		
	Mean	3.747619		Pred R-Squared	0.880296		
	CV	12.78134		Adeq Precision	18.09278		

DF- degree of freedom; Signi.- significant

Table 5.7.5 Analysis of regression equations using ANOVA (F-test) of mechanical properties

Weld response	Source	Sum of squares	DF	Mean square	F value	P value	Status
Ultimate tensile strength	Model	15892.1	9	1765.789	84.76826	< 0.0001	Signi.
	Residual	229.1386	11	20.83078			
	Total	16121.24	20	R-Squared	0.985787		
	Std.Dev.	4.564075		Adj R-Squared	0.974157		
	Mean	571.8095		Pred R-Squared	0.941889		
	CV	0.798181		Adeq Precision	32.57569		
Impact toughness	Model	548.6184	9	60.9576	54.36458	< 0.0001	Signi.
	Residual	12.33402	11	1.121274			
	Total	560.9524	20	R-Squared	0.978012		
	Std. Dev.	1.058902		Adj R-Squared	0.960022		
	Mean	184.381		Pred R-Squared	0.916537		
	CV	0.574301		Adeq Precision	27.77454		
Micro-hardness	Model	2185.334	9	242.8149	121.4938	< 0.0001	Signi.
	Residual	21.98436	11	1.998578			
	Total	2207.318	20	R-Squared	0.99004		
	Std.Dev.	1.413711		Adj R-Squared	0.981891		
	Mean	202.9569		Pred R-Squared	0.945979		
	CV	0.696557		Adeq Precision	35.28195		

DF- degree of freedom; Signi.-significant

Table 5.7.6 Analysis of regression coefficients of weld responses (%Si, %Mn, %C) using t-test

Predictor	% Si		%Mn		%C	
	t value	Status	t value	Status	t value	Status
CaO	2.95	Significant	26.63	Significant	4.50	Significant
SiO_2	12.75	Significant	20.36	Significant	2.76	Significant
Al_2O_3	-1.95	Significant	4.24	Significant	-0.34	Not Significant
TiO_2	2.69	Significant	34.21	Significant	5.55	Significant
$CaO.SiO_2$	-2.03	Significant	-3.01	Significant	-1.86	Significant
$CaO.Al_2O_3$	3.10	Significant	-0.99	Not Significant	0.26	Not Significant
$CaO.TiO_2$	1.98	Significant	-0.43	Not Significant	-1.34	Not Significant
$SiO_2.Al_2O_3$	1.81	Significant	-1.83	Significant	1.61	Not Significant
$SiO_2.TiO_2$	0.69	Not Significant	-2.30	Significant	1.06	Not Significant
$Al_2O_3.TiO_2$	2.43	Significant	1.41	Not Significant	0.29	Not Significant

Predictor is significant if $|t| > t_{\alpha,DF(error)}$ ($t_{0.05,11} = 1.796$)

Table 5.7.7 Analysis of regression coefficients of weld responses (%Cr, %Ni, Ferrite number) using t-test

Predictor	%Cr		%Ni		Ferrite number	
	t value	Status	t value	Status	t value	Status
CaO	22.52	Significant	3.50	Significant	5.95	Significant
SiO_2	18.33	Significant	5.19	Significant	3.09	Significant
Al_2O_3	3.51	Significant	2.43	Significant	0.38	Not Significant
TiO_2	27.26	Significant	10.63	Significant	2.32	Significant
$CaO.SiO_2$	-3.92	Significant	4.72	Significant	-5.26	Significant
$CaO.Al_2O_3$	-1.37	Not Significant	-0.30	Not Significant	-0.97	Not Significant
$CaO.TiO_2$	-2.27	Significant	2.05	Significant	-1.85	Significant
$SiO_2.Al_2O_3$	-1.13	Not Significant	-0.12	Not Significant	-0.84	Not Significant
$SiO_2.TiO_2$	-2.36	Significant	2.99	Significant	-2.74	Significant
$Al_2O_3.TiO_2$	0.41	Not Significant	-1.84	Significant	0.31	Not Significant

Predictor is significant if $|t| > t_{\alpha,DF(error)}$ ($t_{0.05,11} = 1.796$)

Table 5.7.8 t-test analysis of regression coefficients of mechanical properties

Predictor	Ultimate tensile strength		Impact toughness		Microhardness	
	t value	Status	t value	Status	t value	Status
CaO	7.25	Significant	13.16	Significant	11.99	Significant
SiO_2	7.70	Significant	9.39	Significant	11.23	Significant
Al_2O_3	2.42	Significant	-0.82	Not Significant	1.77	Not Significant
TiO_2	8.01	Significant	7.57	Significant	19.40	Significant
$CaO.SiO_2$	2.39	Significant	-2.18	Significant	-1.81	Significant
$CaO.Al_2O_3$	-0.15	Not Significant	2.72	Significant	-1.16	Not Significant
$CaO.TiO_2$	6.44	Significant	7.46	Significant	-5.60	Significant
$SiO_2.Al_2O_3$	-1.80	Significant	3.84	Significant	1.26	Not Significant
$SiO_2.TiO_2$	0.31	Not Significant	5.45	Significant	1.26	Not Significant
$Al_2O_3.TiO_2$	-0.17	Not Significant	2.35	Significant	-0.57	Not Significant

Predictor is significant if $|t| > t_{\alpha,DF(error)}$ ($t_{0.05,11} = 1.796$)

The values of R-square for the developed regression models are nearly equal or greater than 90% which indicate that predicted values of various weld responses are in close agreement with their actual values as shown in Figures 5.7.1 (a) to (f) and 5.7.2 (a) to (c).

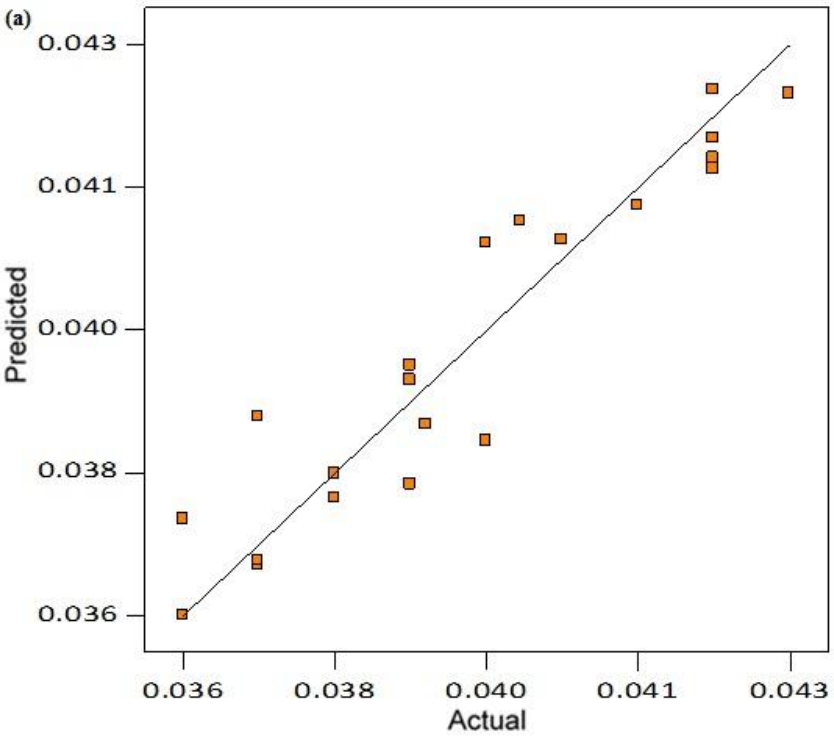
(a)
0.043
0.041
0.040
0.038
0.036
Predicted
0.036
0.038
0.040
0.041
0.043
Actual

(a) %C

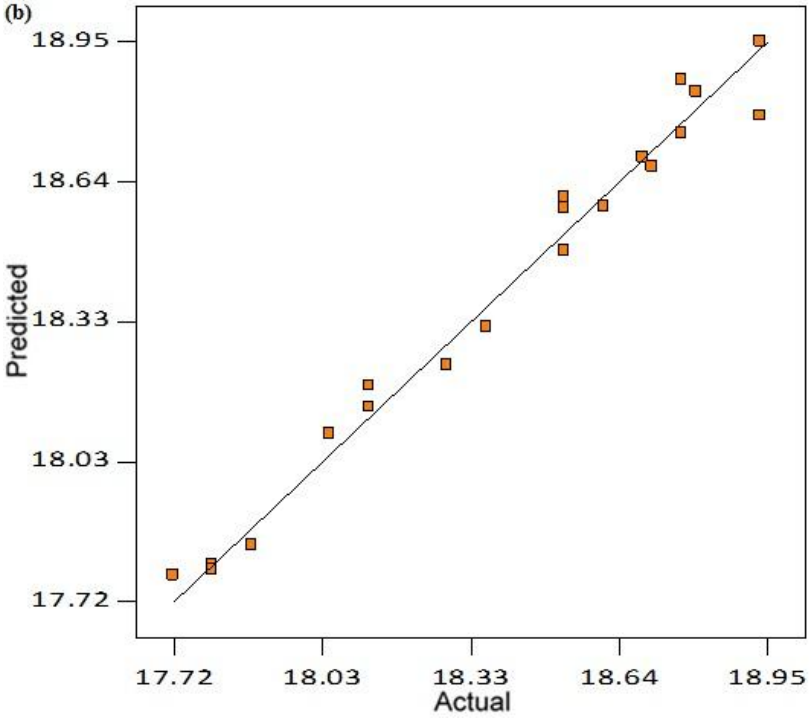
(b)
18.95
18.64
18.33
18.03
17.72
Predicted
17.72
18.03
18.33
18.64
18.95
Actual

(b) %Cr

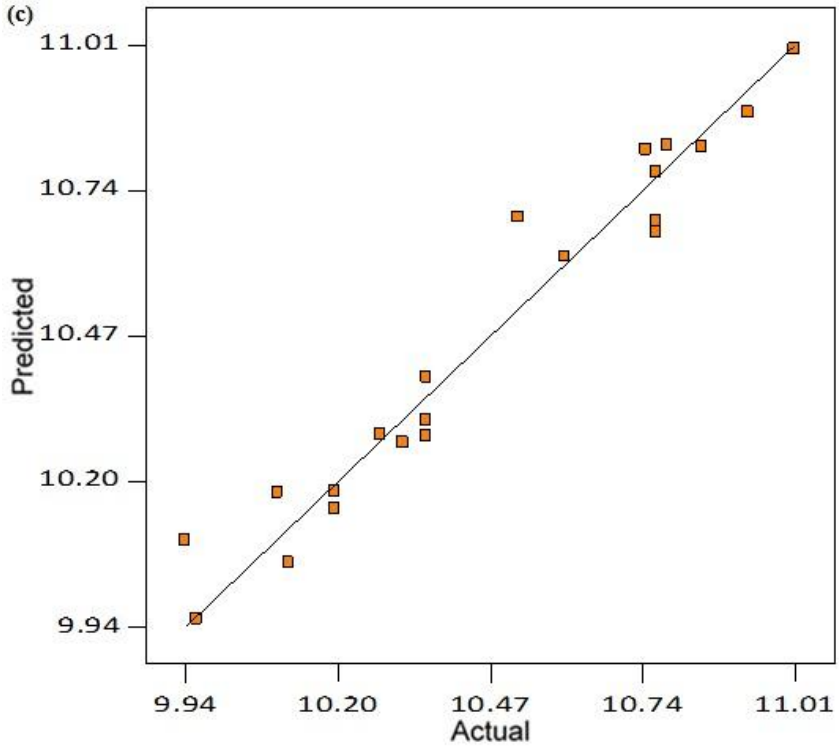
(c)
11.01
10.74
10.47
10.20
9.94
Predicted
9.94
10.20
10.47
10.74
11.01
Actual

(c) %Ni

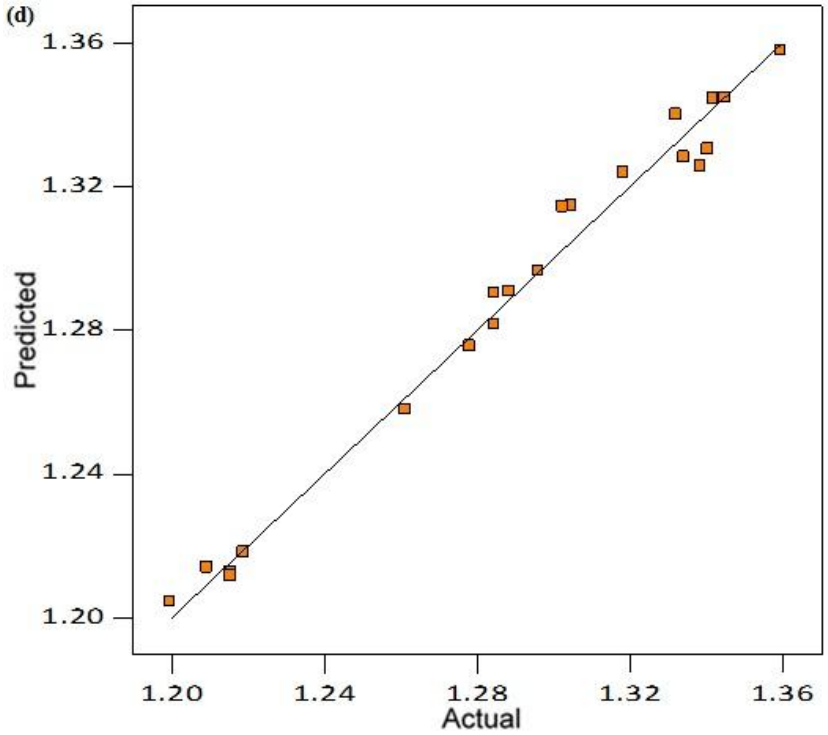
(d)
1.36
1.32
1.28
1.24
1.20
Predicted
1.20
1.24
1.28
1.32
1.36
Actual

(d) %Mn

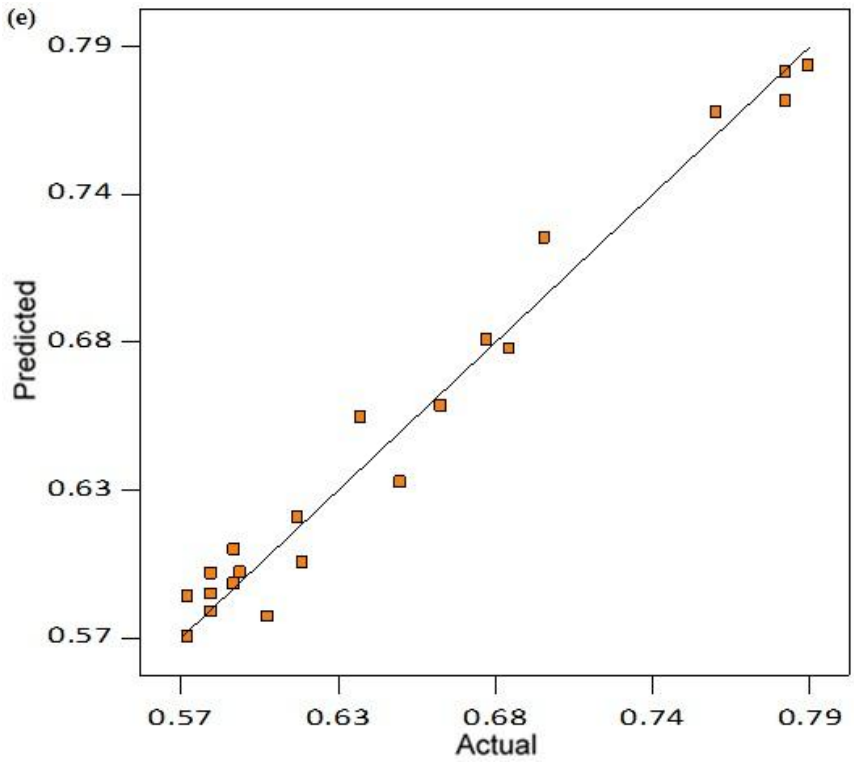

(e) % Si

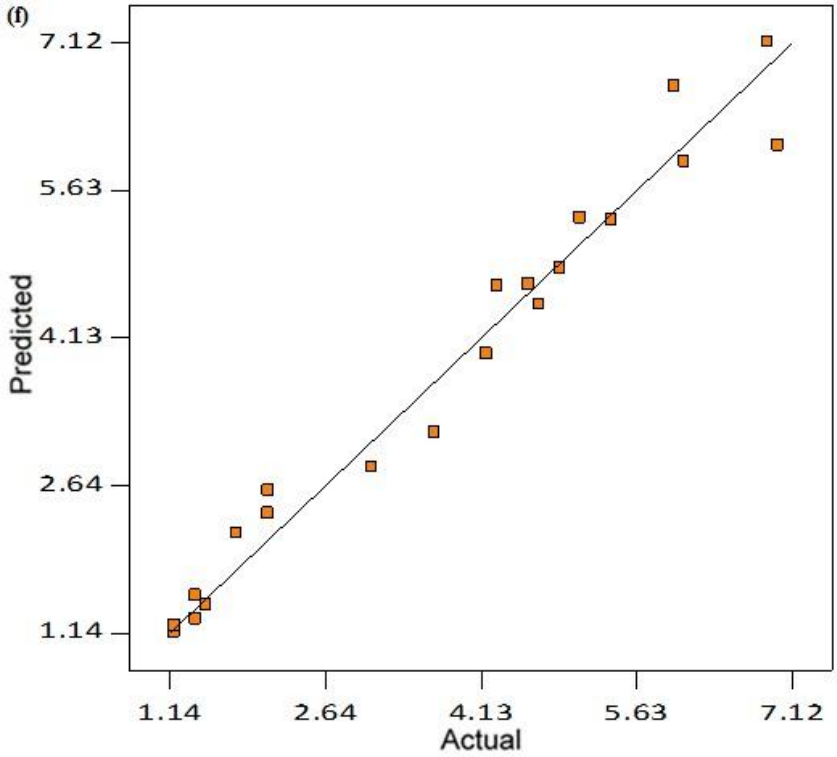

(f) Ferrite number

Figure 5.7.1 Predicted versus actual values of various weld responses of bimetallic welds (a) %C, (b) %Cr, (c) %Ni, (d) %Mn, (e) %Si and (f) ferrite number.

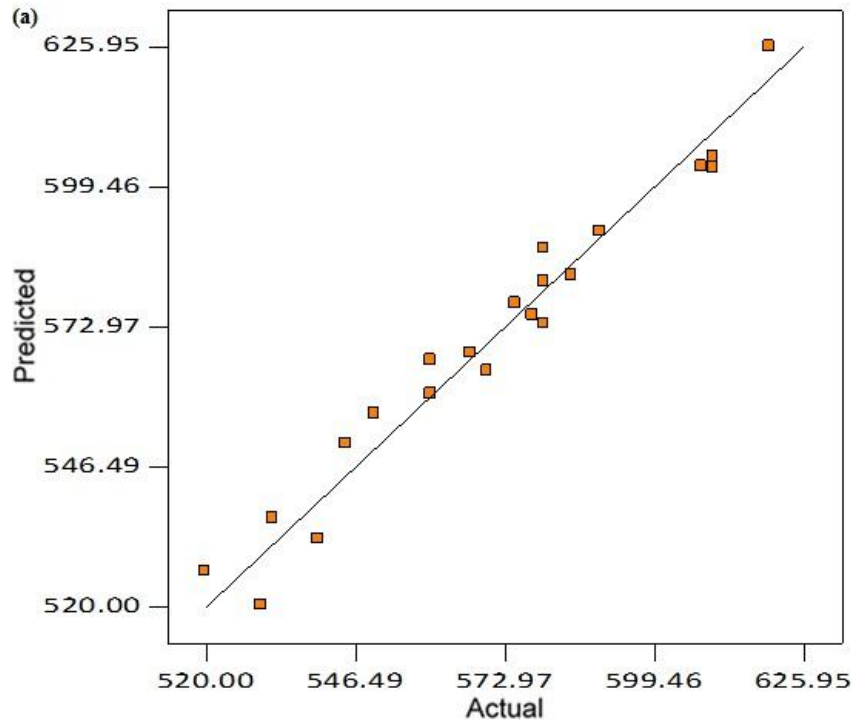

(a) Ultimate tensile strength

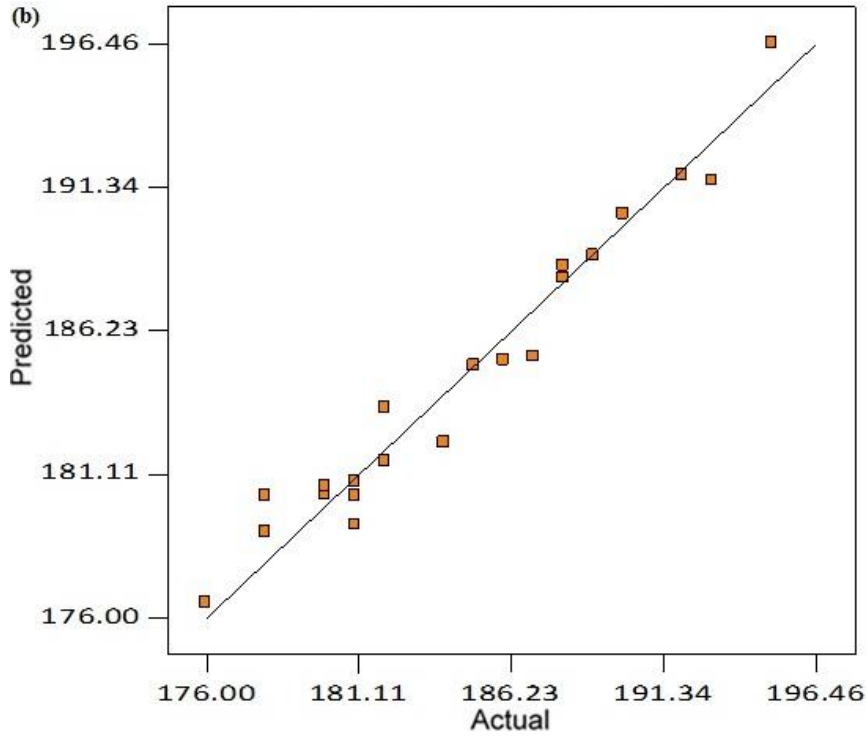

(b) Impact toughness

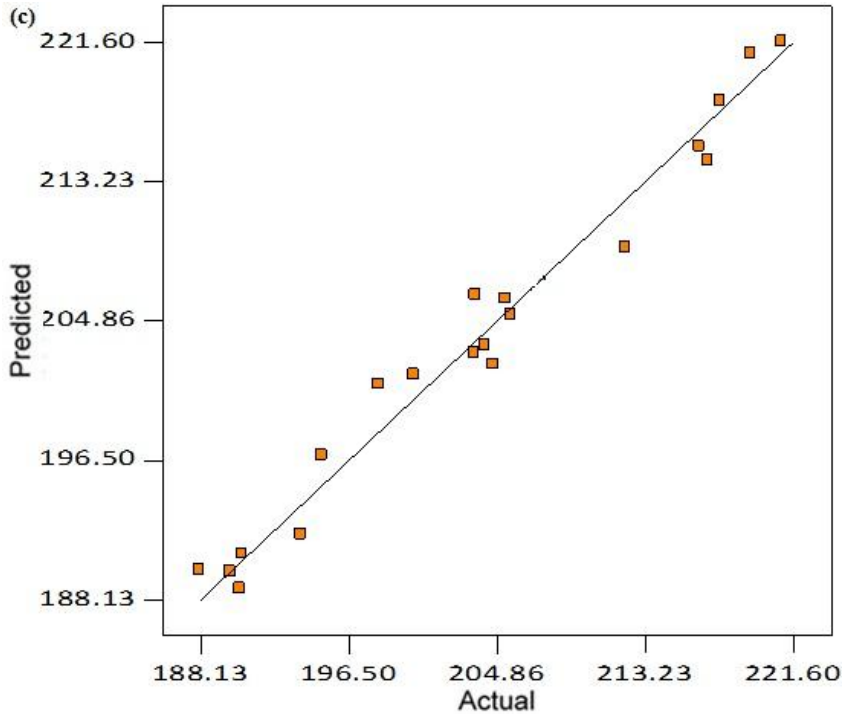

(c) Microhardness

Figure 5.7.2 Predicted versus actual values of mechanical properties of bimetallic welds (a) ultimate tensile strength, (b) impact toughness and (c) microhardness.

5.8 Discussion of Two Layer Bimetallic Welds Fabricated with Stainless Steel Electrodes based on $CaO\text{-}SiO_2\text{-}Al_2O_3\text{-}TiO_2$ System

5.8.1 Effect of electrode coating ingredients on weld metal composition

The results from this work show that silicon percentage in weld metal has significantly increased with the increase in SiO_2 content in electrode coatings. SiO_2 dissociates into silicon and oxygen during slag-metal reactions and thereby raises the silicon content in the weld (Kou, 2002 [86]). Al_2O_3 tends to decrease the silicon content in weld metal as it reacts with the fluorides present in the electrode coatings to form AlF_4 compound which further reacts with silicon according to the following reaction (Lau, 1986 [95]):

$$4AlF_3+3Si \rightarrow 3SiF_4+4Al \qquad (5.8.1)$$

The individual electrode coating ingredients CaO and TiO_2 show increasing effect on weld metal silicon content. The effect of binary mixture $CaO.SiO_2$ is to decrease the silicon content as the CaO has a tendency to decrease the activity of SiO_2 in slag-metal reactions and thus decrease the silicon content in weld metal composition.

The individual effect of all the ingredients of electrode coatings i.e. CaO, SiO_2, Al_2O_3 and TiO_2 is increasing on the manganese content of weld metal. The effect of TiO_2 could be explained from the fact that it decreases the viscosity of slag during slag-metal reactions and hence promotes the transfer of manganese to weld metal. All the binary mixtures of SiO_2 show the reversing trend on manganese content of weld metal which can be attributed to the increase in the concentration of MnO in slag resulting in the lower level of manganese content in the weld (Mitra and Eagar,1984 [105]).

The individual electrode coating ingredients except Al_2O_3 show the increasing effect on the carbon content of weld metal. $CaO.SiO_2$ shows the single significant decreasing effect on weld metal carbon content whereas the interaction effects of other binary mixtures are not significant as shown in Table 5.7.6.

The regression analysis shows that interaction effects of all the ingredients are to decrease the chromium content of weld metal. The free oxygen available during the slag-metal reactions combines with chromium so as to form chromium oxide, resulting in decrease in chromium content of weld metal. From the regression analysis it is observed that the electrode coating ingredients and the binary mixtures $CaO.SiO_2$, $CaO.TiO_2$, $SiO_2.TiO_2$ increase the nickle content of the weld metal while the interaction effect of binary mixture $Al_2O_{3.}TiO_2$ is significantly decreasing.

5.8.2 Effect of electrode coating ingredients on solidification behaviour

The electrode coating ingredients promote the delta ferrite with vermicular morphology in welds as compared to sigma phase as is clear from the microstructures (as explained later in the microstructure analysis section). The solidification modes predicted from WRC diagram and evaluated from the weld metal microstructures are either ferritic–austenitic (FA) or austenitic–ferritic (AF) as shown in Table 5.7.2.

5.8.3 Effect of electrode coating ingredients on weld metal mechanical properties

The regression analysis reveals that all electrode coating ingredients have significant increasing effect on the ultimate tensile strength of weld (Table 5.7.8). The electrode coating ingredients tend to promote inclusions in the form of metal sulfides and oxides in weld which may further assist in the ferrite nucleation at the interface between austenite matrix and inclusions. The plasticity of the material improved with

the finely dispersed spheroid-shaped inclusions. The binary effect of $CaO.SiO_2$ is to increase the UTS as the activity of SiO_2 reduced duo to the formation of SiO_4^{4-} complex ion. Therefore, the excessive dissociation of SiO_2 reduced and the amount of dissolved oxygen remains limited. The binary mixture $SiO_2.Al_2O_3$ shows significant decreasing effect on ultimate tensile strength due to their combined increasing effect on O_2 in the weld.

CaO increases the impact toughness of welds by increasing the basicity of the electrode coatings also reported in literature (De Rissone et al., 2002 [35]). The impact toughness increased with TiO_2 as it acts as a grain refiner and also reduces the oxygen content of weld metal which is also reported by Kohno et al., 1982 [83]. The interaction effects of all binary mixtures except $CaO.SiO_2$ show the increasing trend on impact toughness.

It is observed from regression analysis that the electrode coating ingredients CaO, SiO_2 and TiO_2 increase the microhardness of weld while the effect of Al_2O_3 is not significant. The decreasing interaction effect of binary mixtures $CaO.SiO_2$ and $CaO.TiO_2$ indicates that CaO tends to pick carbon from the weld metal during slag-metal reactions.

5.8.4 Contour surface plots for various properties

The contour surface plots depicting predicted values of chemical composition of various elements of bimetallic welds for different proportions of electrode coating ingredients CaO, SiO_2, Al_2O_3 and constant TiO_2= 18.83% are shown in Figure 5.8.1 (a) to (f). The variation of a particular weld response with respect to electrode coating ingredients can be easily observed from these contour curves as each curve on the surface plot shows the constant value of that weld response.

The Figure 5.8.2 (a) to (c) shows the contour surface plots of various mechanical properties of bimetallic welds i.e. ultimate tensile strength, impact toughness and microhardness for different proportions of electrode coating ingredients CaO, SiO_2, Al_2O_3 at the constant value of TiO_2= 18.83%.

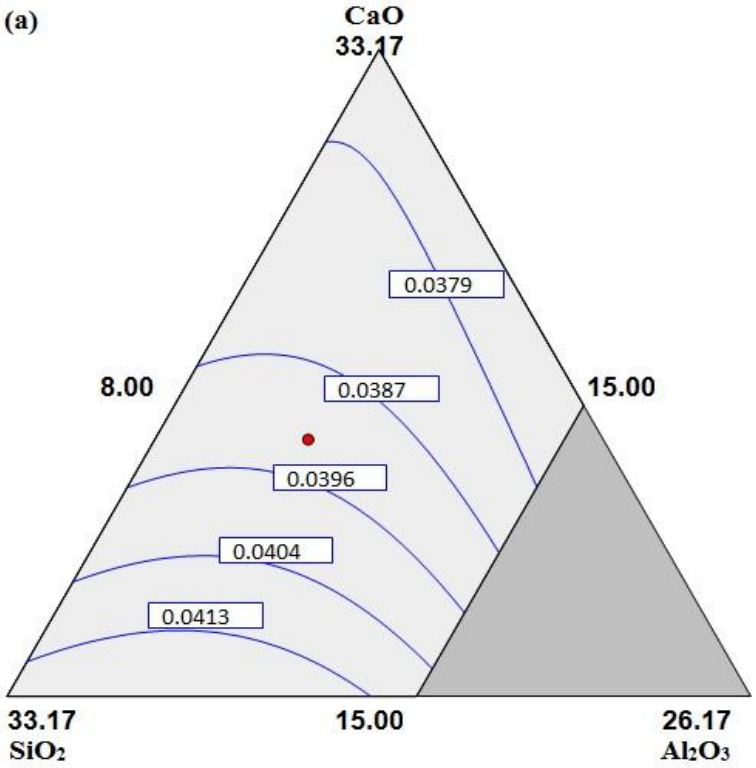
(a)
CaO
33.17
0.0379
8.00
0.0387
15.00
0.0396
0.0404
0.0413
33.17
SiO2
15.00
26.17
Al2O3

(a) %C

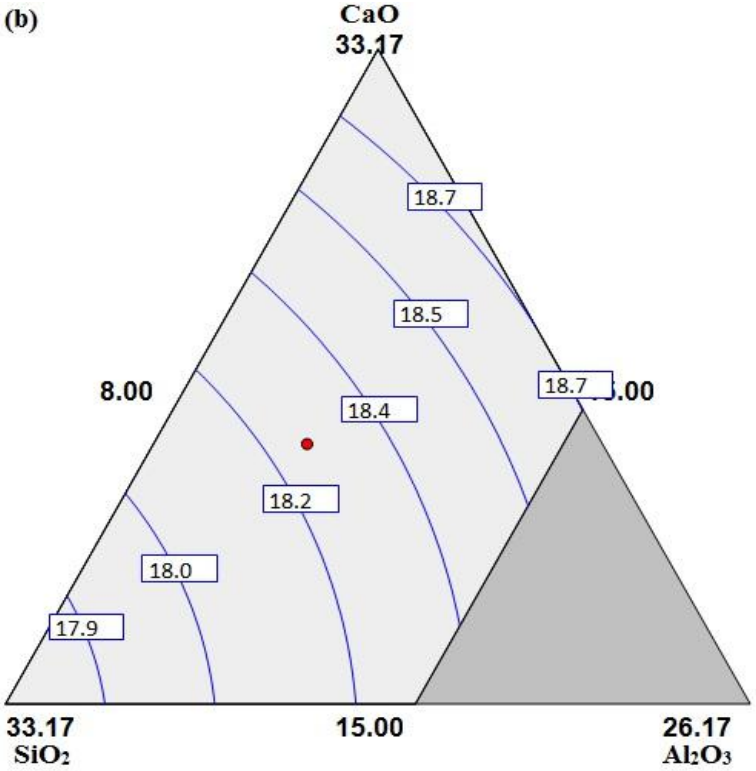
(b)
CaO
33.17
18.7
18.5
8.00
18.7
18.4
18.2
18.0
17.9
33.17
SiO2
15.00
26.17
Al2O3

(b) %Cr

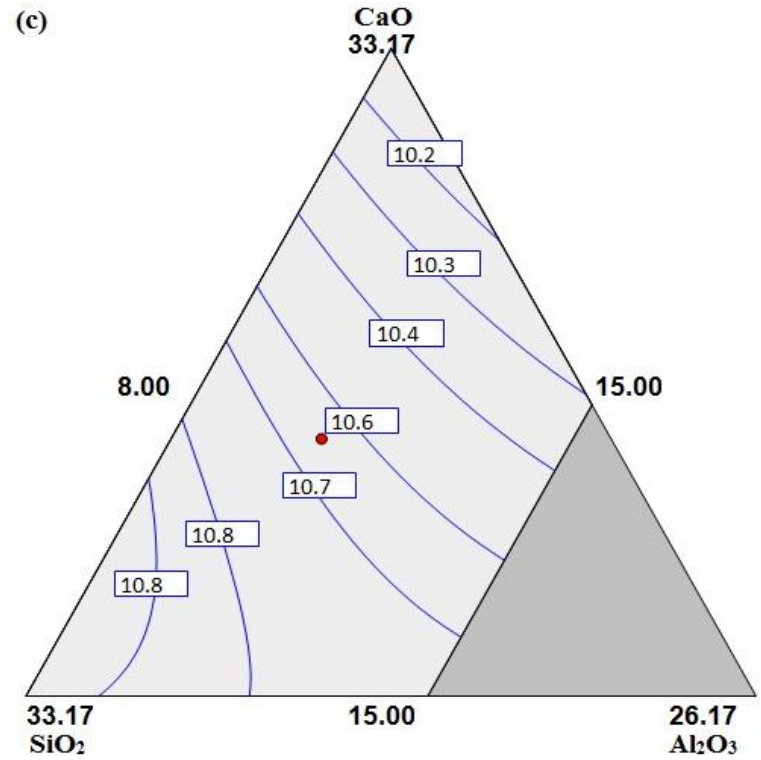
(c)
CaO
33.17
10.2
10.3
10.4
8.00
15.00
10.6
10.7
10.8
10.8
33.17
SiO2
15.00
26.17
Al2O3

(c) %Ni

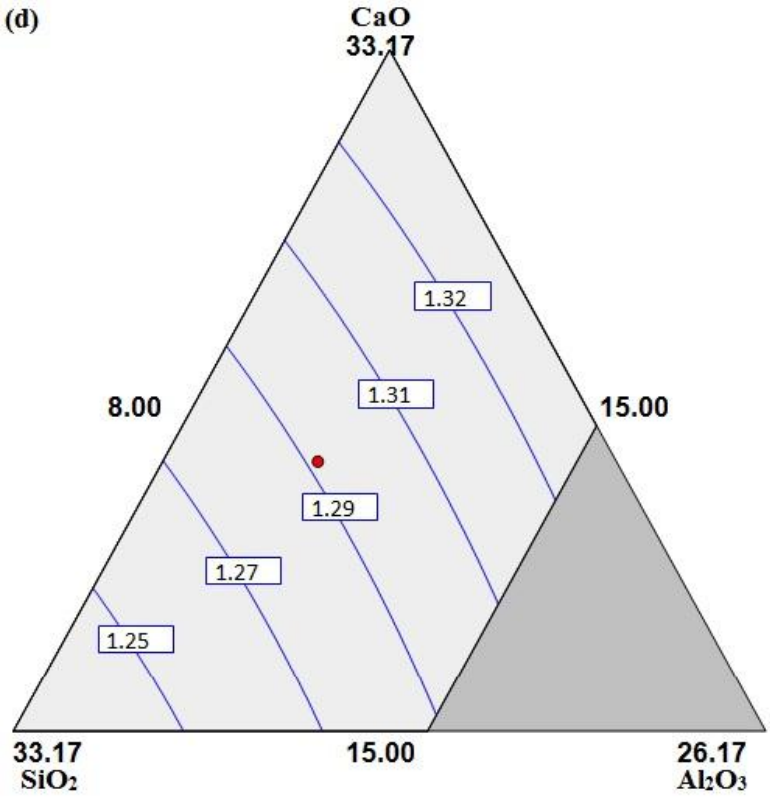
(d)
CaO
33.17
1.32
1.31
8.00
15.00
1.29
1.27
1.25
33.17
SiO2
15.00
26.17
Al2O3

(d) %Mn

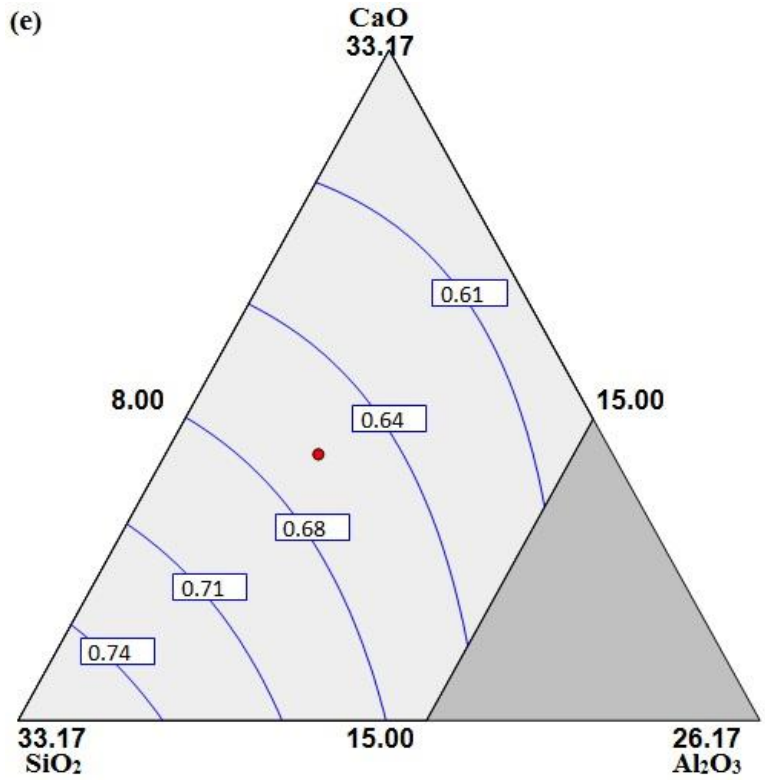

(e) %Si

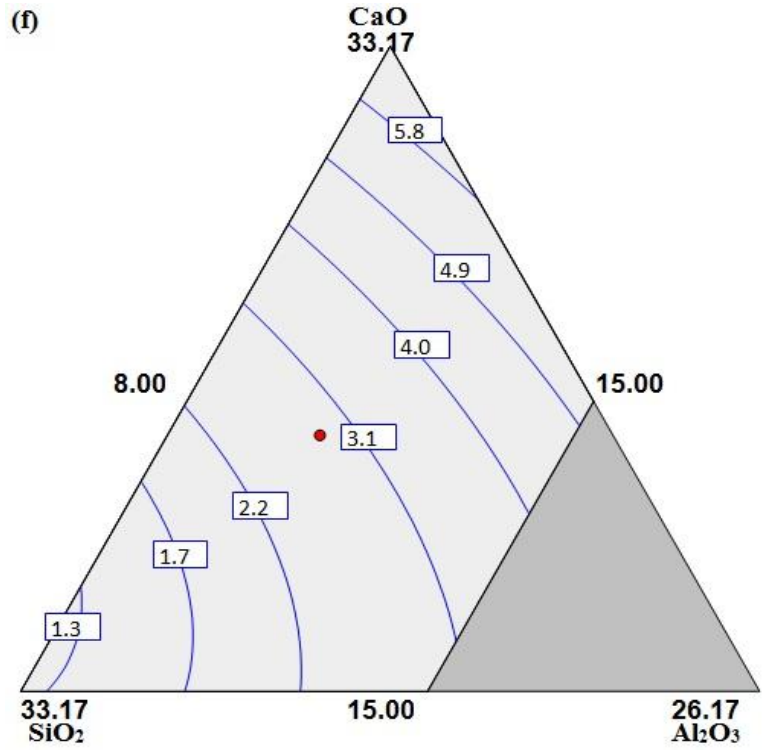

(f) Ferrite number

Figure 5.8.1 Contour surface plots of bimetallic weld responses (a) %C, (b) %Cr, (c) %Ni, (d) %Mn, (e) %Si and (f) ferrite number.

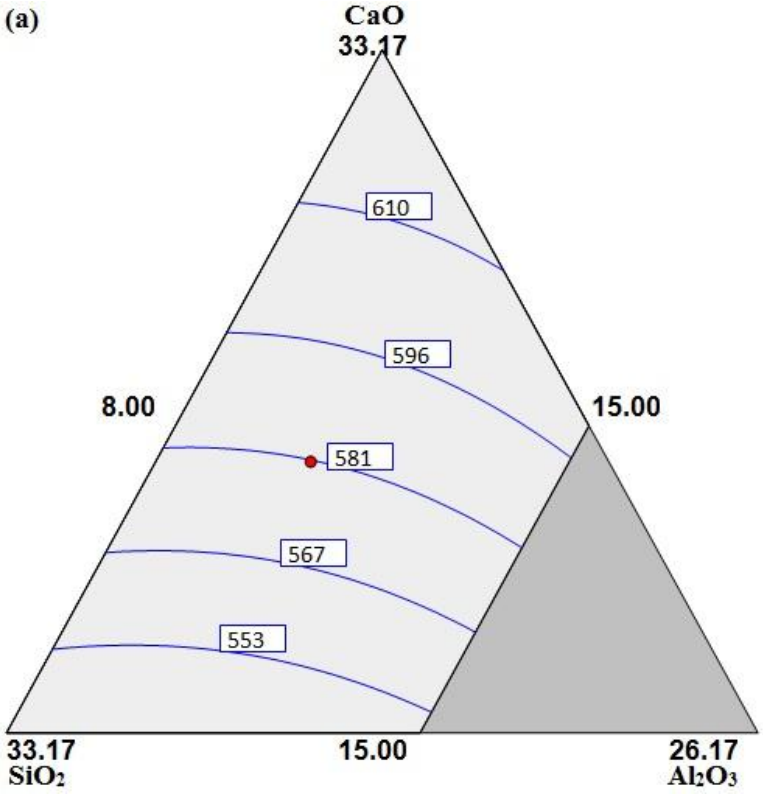

(a) Ultimate tensile strength

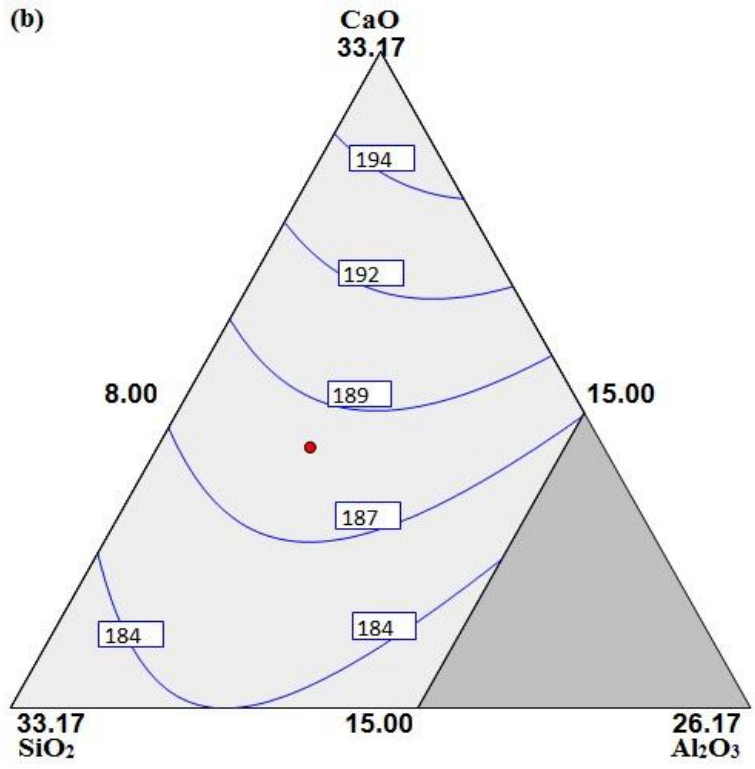

(b) Impact toughness

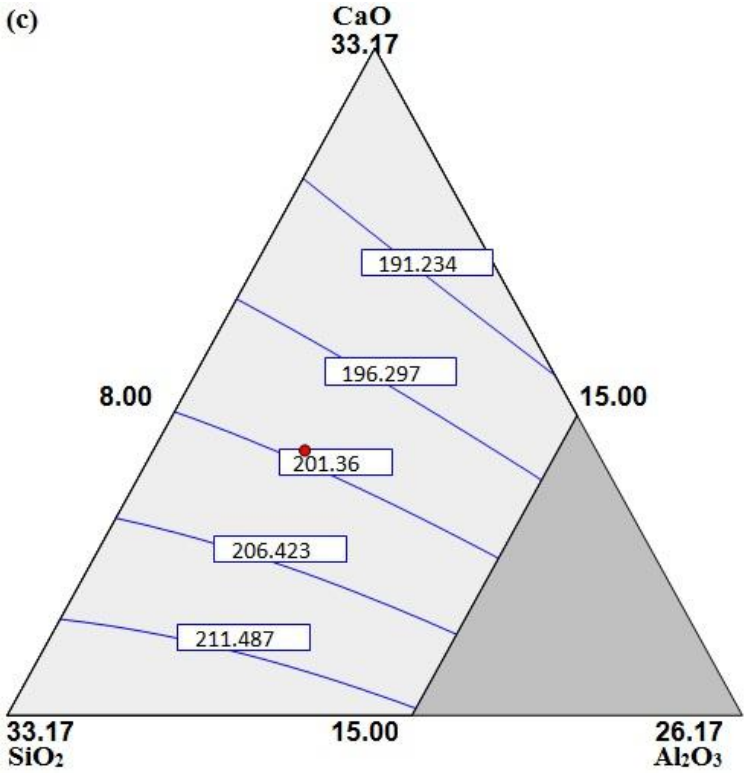

(c) Microhardess

Figure 5.8.2 Contour surface plots of various mechanical properties of bimetallic welds (a) ultimate tensile strength, (b) impact toughness and (c) microhardness.

5.8.5 Microstructure analysis

Figure 5.8.3(a) to (c) shows the typical microstructures of various weld metal specimens. The microstructures comprise of austenite (fcc) with varying amount of delta ferrite (bcc) indicating the primarily solidifications mode as ferritic–austenitic (FA). The delta ferrite at the dendrite cores also known as skeletal ferrite or vermicular ferrite (VF) is clearly visible in the microstructures of welds.

A few large inclusions (I) of size nearly 6μm are present on grain boundaries in microstructure of experiment no. 1 as shown in Figure 5.8.3(a). This electrode coating formulation contains higher amount of SiO_2 and Al_2O_3 (Table 4.5.1) and their binary interaction promotes the large size inclusions which adversely affects the mechanical strength and impact toughness of weld whereas increased average microhardness value is obtained (Table 5.7.3). The delta ferrite may also transform to lathy ferrite (LF) in addition to vermicular ferrite as shown in the weld microstructure derived from experiment no. 2 (Figure 5.8.3(b)). It shows dispersed structure of very small

size spherical-shaped inclusions of maximum size 0.4μm inside the grains that increased the ultimate tensile strength, impact toughness and average microhardness values as observed from mechanical property test data (Table 5.7.3). This can be attributed to relative higher amount of TiO_2 and CaO in the electrode coating formulation which further assists in promoting the small size inclusions in weld metal.

The Figure 5.8.3(c) shows sparcely distributed intermediate size inclusions (maximum size 2μm) in the microstructure of weld sample of experiment no. 7. The intermediate ultimate tensile strength and impact toughness values were observed for these weld samples. The changes in the weld microstructures and the resultant mechanical peoperties can be attributed to the slag-metal reactions occuring due to the interaction of different ingredients with the weld metal resulting in element transfer and different weld chemistry.

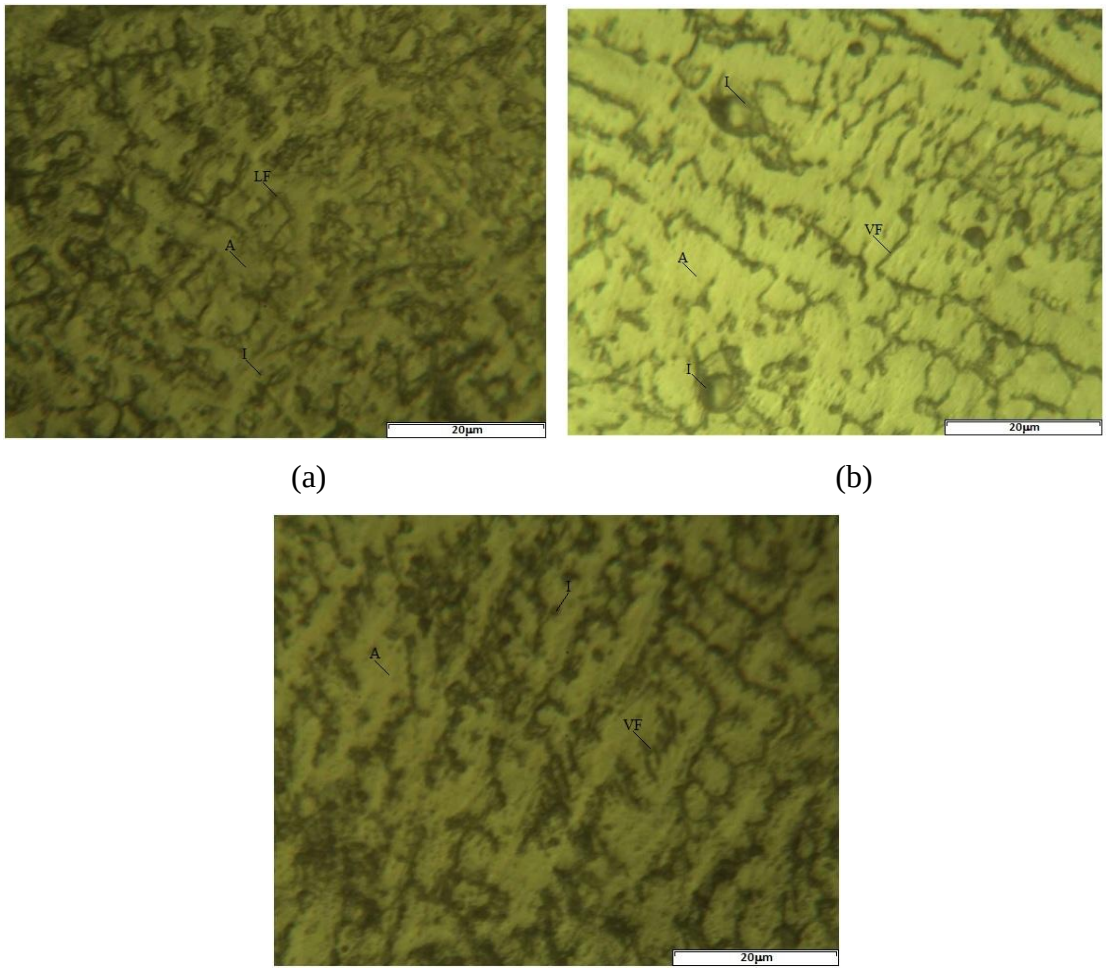

(a) (b)

(c)

Figure 5.8.3 Microstructure of weld specimen (a) expt. no. 1, (b) expt. no. 2 and (c) expt. no. 7.

5.8.6 Model validation

The developed regression models of various weld responses were validated by using three randomly selected welding electrode coating formulations for conducting the confirmatory experiments. The experimental results along with predicted values are summarized in Table 5.8.1 and it is observed that percentage error (%) for weld responses is nearly 5% in almost all the cases.

5.8.7 Multi objective optimization

Table 5.8.2 shows the three multi objective optimized solutions with equal weights to ultimate tensile strength, impact toughness and microhardness along with the target value of ferrite number. The target value of ferrite number was decided on the observation that the ferrite number in the range from 3 to 8 helps in minimizing the hot cracking of austenitic stainless steel matrix. The graphical demonstration of desirability of optimized solution no.1 is shown in Figure 5.8.4. It clearly indicates that the desirability of all the electrode coating ingredients along with ferrite number is one while the composite desirability of complete solution is 0.91.

The best optimum electrode coating composition of stainless steel electrode (formulation no. 1) shown in Table 5.8.2 was then selected for the three layer bimetallic weld approach.

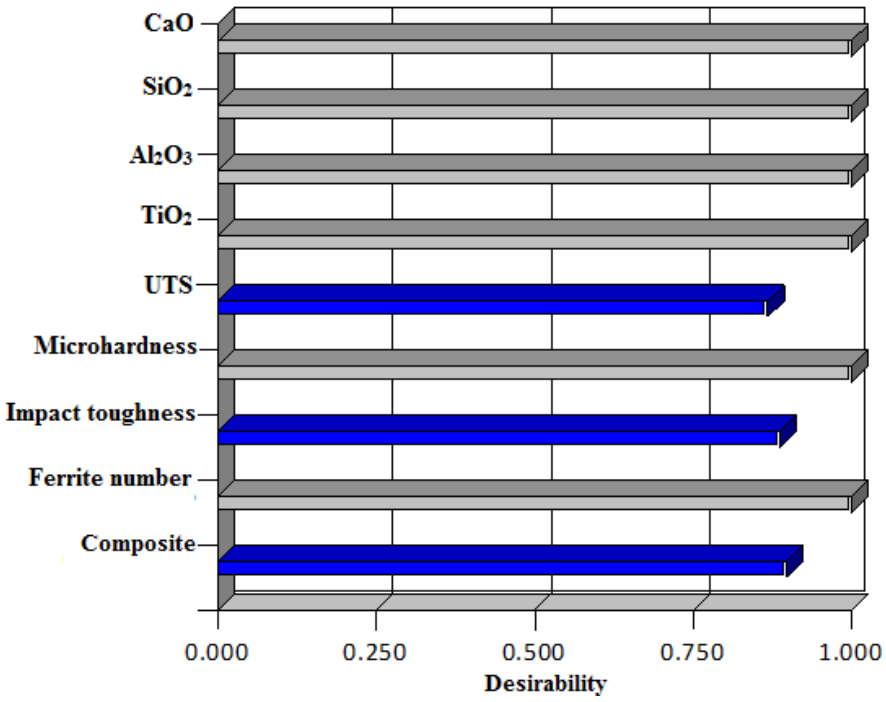

Figure 5.8.4 Graphical demonstration of variation of desirability of optimized solution

Table 5.8.1 Percentage error during confirmatory experiments in weld responses

Electrode coating formulation				Predicted value			Actual value			Error (%)		
CaO	SiO_2	Al_2O_3	TiO_2	UTS (MPa)	Impact toughness (Nm)	Microhardness (VHN)	UTS (MPa)	Impact toughness (Nm)	Microhardness (VHN)	UTS	Impact toughness	Microhardness
20	20	15	20	577.5	186.9	201.4	595	195	190	3.02	4.35	5.65
30	15	15	15	608.2	191.8	188.2	580	182	198	4.64	5.11	5.21
15	20	10	30	556.9	183.1	209.2	585	192	219	5.05	4.87	4.70

Error (%) = (Actual value- Predicted value) x100/(Actual value)

Table 5.8.2 Electrode coating formulations for optimized weld responses

S.No.	Electrode coating formulation				Ultimate tensile strength (MPa)	Impact toughness (Nm)	Microhardness (VHN)	Ferrite number	Composite Desirability
	CaO	SiO_2	Al_2O_3	TiO_2					
1	28.07	16.67	10.69	19.56	610	192	193	5.1	0.916609
2	32.73	17.72	9.39	15.16	610	190	193	5.5	0.875076
3	25.41	15.00	13.49	21.10	600	187	192	5.4	0.830636

5.9 Development of Regression Models of Buttering Layer (Stainless Steel Electrodes Based on $CaO\text{-}SiO_2\text{-}Al_2O_3\text{-}TiO_2$ System) with Two Layer Methodology

The results of buttering layer metal chemistry, ferrite number and microhardness tests were also conducted for the buttering layer (stainless steel electrodes based on $CaO\text{-}SiO_2\text{-}Al_2O_3\text{-}TiO_2$ system) of bimetallic welds are shown in Table 5.9.1.

Table 5.9.1 Results of metal chemistry, ferrite number and microhardness of buttering layer of bimetallic welds based on $CaO\text{-}SiO_2\text{-}Al_2O_3\text{-}TiO_2$ system

Expt. No.	%C	%Cr	%Ni	%Mn	%Si	Ferrite number	Microhardness (VHN)
1	0.077	18.40	9.80	1.24	0.59	2.0	241
2	0.0752	18.64	9.59	1.31	0.54	3.5	220
3	0.075	19.20	9.10	1.37	0.45	6.4	224
4	0.078	19.04	9.24	1.33	0.49	5.5	227
5	0.0785	18.24	9.73	1.24	0.63	1.6	239
6	0.0745	18.40	9.60	1.27	0.60	2.6	227
7	0.0752	19.20	9.10	1.37	0.46	6.6	211
8	0.0759	18.56	9.59	1.31	0.54	3.2	225
9	0.0745	19.44	8.89	1.37	0.45	8.0	206
10	0.0738	19.28	9.03	1.38	0.48	7.2	208
11	0.0731	19.44	8.95	1.34	0.48	8.0	212
12	0.0776	18.64	9.40	1.32	0.60	3.3	235
13	0.076	18.32	9.87	1.25	0.64	2.1	238
14	0.0738	18.88	9.38	1.31	0.51	5.0	220
15	0.0773	19.12	9.17	1.35	0.47	6.0	225
16	0.0752	18.80	9.45	1.31	0.55	4.4	223
17	0.0766	19.04	9.24	1.34	0.45	5.6	223
18	0.0759	18.32	9.52	1.26	0.63	2.6	237

With the help of observed values of test results, the regression equations developed in terms of percentage composition of individual electrode coating ingredients and their combined binary mixtures are shown below:

%C = +1.05644E-003 CaO +8.93581E-004SiO_2 -1.06124E-003Al_2O_3 +1.18649E-003TiO_2 -5.19289E-006CaO.SiO_2 +3.20350E-005CaO.Al_2O_3 -7.49294E-006CaO.TiO_2 +5.15286E-005SiO_2.Al_2O_3 -8.70254E-007SiO_2.TiO_2 +3.02701E-005Al_2O_3.TiO_2 (5.9.1)

%Cr = +0.32171CaO +0.26250SiO_2 +0.30709Al_2O_3 +0.26731TiO_2 -2.07974E-003CaO.SiO_2 -2.18045E-003CaO.Al_2O_3 -9.78499E-004CaO.TiO_2 -1.77904E-003SiO_2.Al_2O_3 -1.02359E-003SiO_2.TiO_2 +1.58543E-004Al_2O_3.TiO_2 (5.9.2)

%Ni = +0.070093CaO +0.10694SiO_2 +0.32163Al_2O_3 +0.11873TiO_2 +1.95730E-003CaO.SiO_2 -2.17382E-003CaO.Al_2O_3 +9.35617E-004CaO.TiO_2 -2.92076E-003SiO_2.Al_2O_3 +1.55649E-003SiO_2.TiO_2 -5.47860E-003Al_2O_3.TiO_2 (5.9.3)

%Mn = +0.018241CaO +0.017429SiO_2 -0.015510Al_2O_3 +0.015827TiO_2 -9.84004E-005CaO.SiO_2 +6.80489E-004CaO.Al_2O_3 +4.95201E-005CaO.TiO_2 +4.46130E-004SiO_2.Al_2O_3 -8.95975E-005SiO_2.TiO_2 +8.65530E-004Al_2O_3.TiO_2 (5.9.4)

%Si = +4.29710E-003CaO +7.68233E-003SiO_2 -0.029830Al_2O_3 -8.24249E-004TiO_2 -4.60520E-005CaO.SiO_2 +7.50215E-004CaO.Al_2O_3 -3.17424E-005CaO.TiO_2 +7.32445 E-004SiO_2.Al_2O_3 +3.73495E-004SiO_2.TiO_2 +6.30102E-004Al_2O_3.TiO_2 (5.9.5)

Ferrite number = +0.41542CaO +0.21006SiO_2 +0.17933Al_2O_3 +0.14674TiO_2 -0.012333CaO.SiO_2 -6.49514E-003CaO.Al_2O_3 -4.43486E-003CaO.TiO_2 -9.65055E-003SiO_2.Al_2O_3 -8.20159E-003SiO_2.TiO_2 +4.85270E-003Al_2O_3.TiO_2 (5.9.6)

Microhardness = +3.38041CaO +2.87443SiO_2 +0.72210Al_2O_3 +3.41992TiO_2 -0.014125CaO.SiO_2 +4.68139E-003CaO.Al_2O_3 -0.057830CaO.TiO_2 +0.087191SiO_2.Al_2O_3 +0.025921SiO_2.TiO_2 +0.030979Al_2O_3.TiO_2 (5.9.7)

5.9.1 Regression Analysis

The developed regression equations have been analyzed using analysis of variance (ANOVA) as shown in Tables 5.9.2 and 5.9.3. The coefficient of determination i.e. R-square values for the developed regression models are nearly equal or greater than 92% which indicate that predicted values are in close agreement with the actual values of various weld responses as shown in Figures 5.9.1 (a) to (g).

Table 5.9.2 Analysis of regression equations using ANOVA (F-test) of buttering layer metal chemistry of bimetallic welds

Weld response	Source	Sum of squares	DF	Mean square	F value	P value	R square
%C	Model	4.9E-05	9	5.44E-06	15.09493	< 0.0001	0.92
	Linear	3.77E-05	3	1.26E-05	34.84397	< 0.0001	
	$CaO.SiO_2$	4.99E-07	1	4.99E-07	1.383411	0.2643	
	$CaO.Al_2O_3$	2.17E-06	1	2.17E-06	6.012096	0.0321	
	$CaO.TiO_2$	1.15E-06	1	1.15E-06	3.178412	0.1022	
	$SiO_2.Al_2O_3$	5.61E-06	1	5.61E-06	15.55508	0.0023	
	$SiO_2.TiO_2$	1.55E-08	1	1.55E-08	0.042874	0.8397	
	$Al_2O_3.TiO_2$	1.86E-06	1	1.86E-06	5.150565	0.0443	
	Residual	3.97E-06	11	3.61E-07			
	Total	5.29E-05	20				
%Cr	Model	2.998495	9	0.333166	54.86227	< 0.0001	0.96
	Linear	2.86078	3	0.953593	157.0277	< 0.0001	
	$CaO.SiO_2$	0.080007	1	0.080007	13.17463	0.0040	
	$CaO.Al_2O_3$	0.010043	1	0.010043	1.653695	0.2249	
	$CaO.TiO_2$	0.019544	1	0.019544	3.218218	0.1003	
	$SiO_2.Al_2O_3$	0.006685	1	0.006685	1.100867	0.3166	
	$SiO_2.TiO_2$	0.021386	1	0.021386	3.521643	0.0873	
	$Al_2O_3.TiO_2$	5.09E-05	1	5.09E-05	0.008389	0.9287	
	Residual	0.0668	11	0.006073			
	Total	3.065295	20				
%Ni	Model	1.43874	9	0.15986	17.38382	< 0.0001	0.93
	Linear	1.211723	3	0.403908	43.92255	< 0.0001	
	$CaO.SiO_2$	0.070864	1	0.070864	7.705989	0.0180	
	$CaO.Al_2O_3$	0.009982	1	0.009982	1.085432	0.3198	
	$CaO.TiO_2$	0.017868	1	0.017868	1.943046	0.1909	
	$SiO_2.Al_2O_3$	0.018019	1	0.018019	1.959511	0.1891	
	$SiO_2.TiO_2$	0.049451	1	0.049451	5.377522	0.0407	
	$Al_2O_3.TiO_2$	0.060833	1	0.060833	6.615267	0.0260	
	Residual	0.101155	11	0.009196			
	Total	1.539895	20				

%Mn	Model	0.037004	9	0.004112	31.21406	< 0.0001	0.94
	Linear	0.033694	3	0.011231	85.26624	< 0.0001	
	$CaO.SiO_2$	0.000179	1	0.000179	1.359703	0.2682	
	$CaO.Al_2O_3$	0.000978	1	0.000978	7.425647	0.0198	
	$CaO.TiO_2$	5.01E-05	1	5.01E-05	0.380003	0.5501	
	$SiO_2.Al_2O_3$	0.00042	1	0.00042	3.191653	0.1016	
	$SiO_2.TiO_2$	0.000164	1	0.000164	1.243983	0.2885	
	$Al_2O_3.TiO_2$	0.001518	1	0.001518	11.52681	0.0060	
	Residual	0.001449	11	0.000132			
	Total	0.038453	20				
%Si	Model	0.086783	9	0.009643	147.8102	< 0.0001	0.97
	Linear	0.080749	3	0.026916	412.5992	< 0.0001	
	$CaO.SiO_2$	3.92E-05	1	3.92E-05	0.601338	0.4544	
	$CaO.Al_2O_3$	0.001189	1	0.001189	18.22365	0.0013	
	$CaO.TiO_2$	2.06E-05	1	2.06E-05	0.315264	0.5857	
	$SiO_2.Al_2O_3$	0.001133	1	0.001133	17.37058	0.0016	
	$SiO_2.TiO_2$	0.002847	1	0.002847	43.64807	< 0.0001	
	$Al_2O_3.TiO_2$	0.000805	1	0.000805	12.33497	0.0049	
	Residual	0.000718	11	6.52E-05			
	Total	0.0875	20				

DF- degree of freedom

Table 5.9.3 Analysis of regression equations using ANOVA (F-test) of buttering layer ferrite number and microhardness

Weld response	Source	Sum of squares	DF	Mean square	F value	P value	R square
Ferrite number	Model	82.23893	9	9.137658	45.27061	< 0.0001	0.96
	Linear	77.31732	3	25.77244	127.6841	< 0.0001	
	$CaO.SiO_2$	2.813562	1	2.813562	13.9392	0.0033	
	$CaO.Al_2O_3$	0.08911	1	0.08911	0.441478	0.5201	
	$CaO.TiO_2$	0.401458	1	0.401458	1.98894	0.1861	
	$SiO_2.Al_2O_3$	0.196723	1	0.196723	0.974622	0.3447	
	$SiO_2.TiO_2$	1.373021	1	1.373021	6.802342	0.0243	
	$Al_2O_3.TiO_2$	0.047728	1	0.047728	0.236456	0.6363	
	Residual	2.220298	11	0.201845			
	Total	84.45922	20				

Microhardness	Model	2187.128	9	243.0142	97.0699	< 0.0001	0.97
	Linear	2083.41	3	694.4699	277.3999	< 0.0001	
	$CaO.SiO_2$	3.690392	1	3.690392	1.474094	0.2501	
	$CaO.Al_2O_3$	0.046291	1	0.046291	0.018491	0.8943	
	$CaO.TiO_2$	68.264	1	68.264	27.26745	0.0003	
	$SiO_2.Al_2O_3$	16.05825	1	16.05825	6.414328	0.0278	
	$SiO_2.TiO_2$	13.71453	1	13.71453	5.47815	0.0391	
	$Al_2O_3.TiO_2$	1.945069	1	1.945069	0.776941	0.3969	
	Residual	27.53847	11	2.503497			
	Total	2214.667	20				

DF- degree of freedom

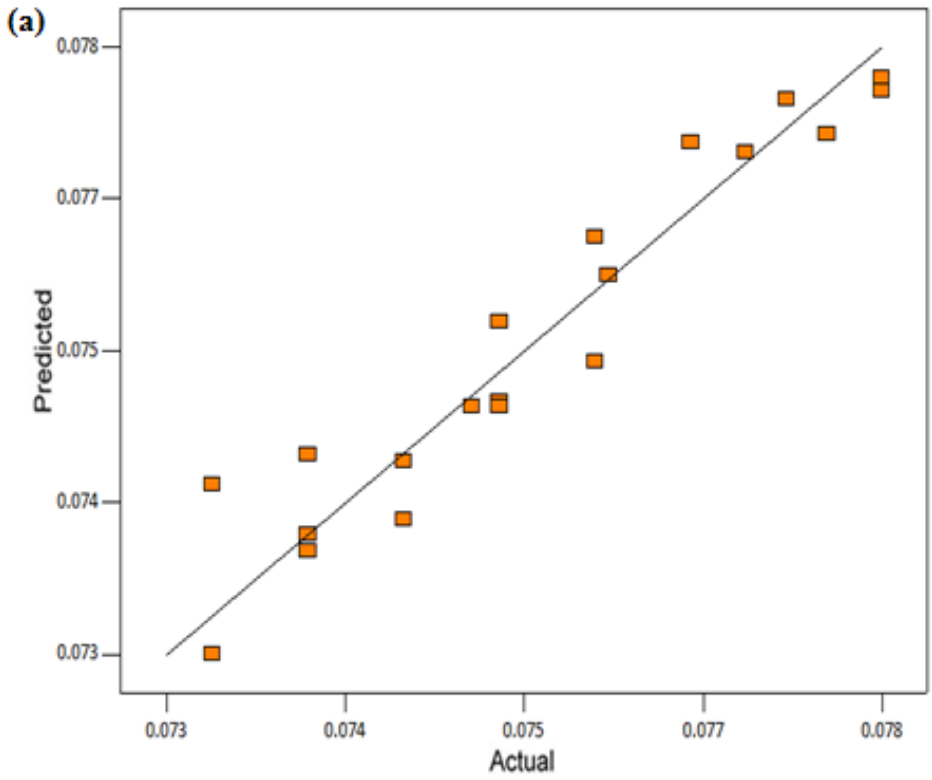

(a) %C

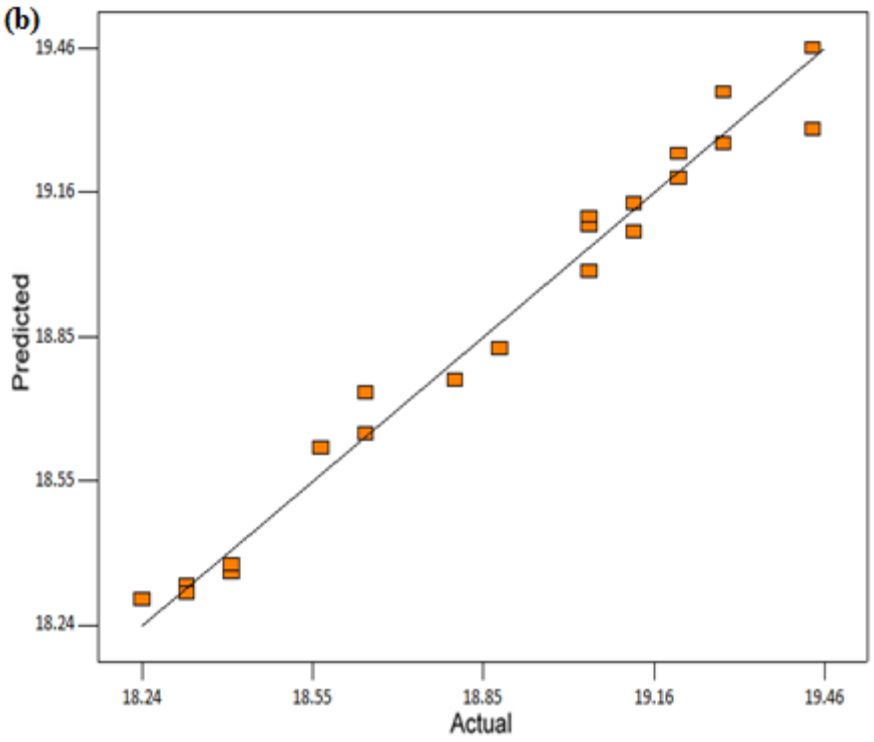
(b)
19.46
19.16
18.85
18.55
18.24
Predicted
18.24
18.55
18.85
19.16
19.46
Actual

(b) %Cr

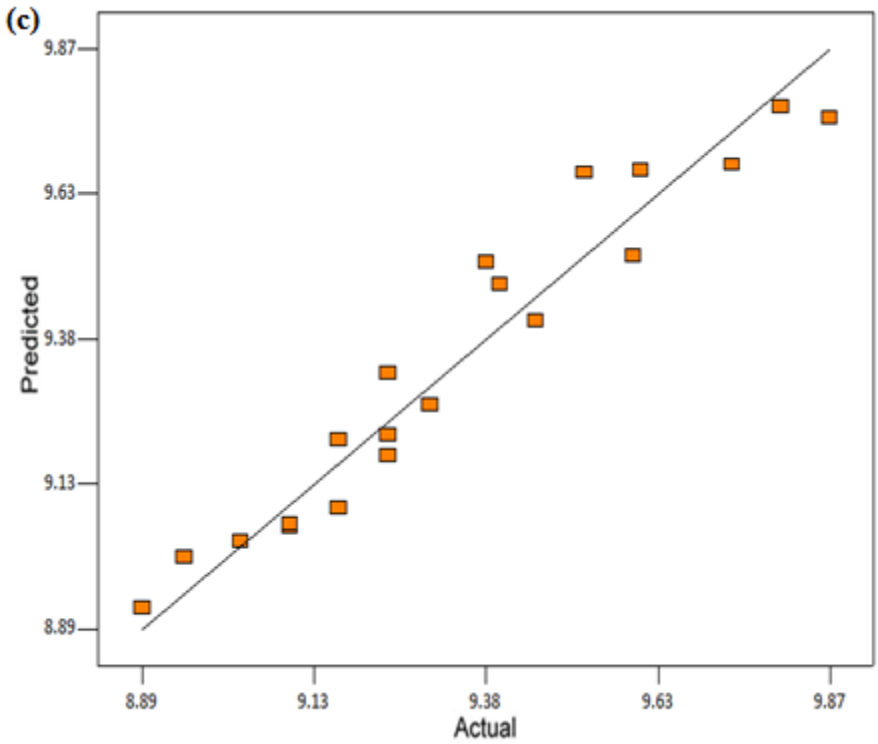
(c)
9.87
9.63
9.38
9.13
8.89
Predicted
8.89
9.13
9.38
9.63
9.87
Actual

(c) Ni

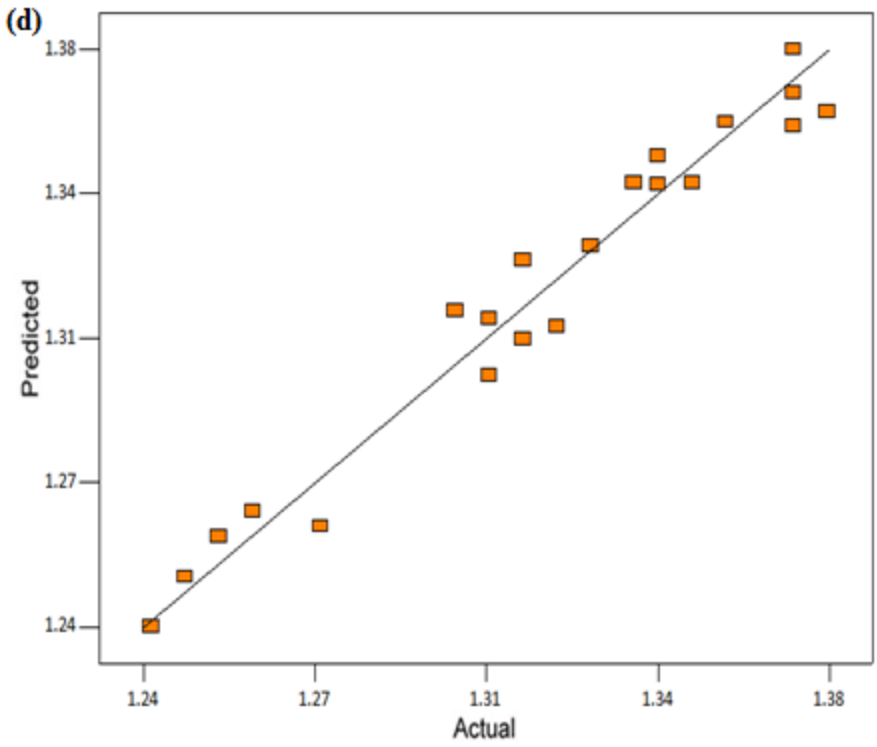
(d)
1.38
1.34
1.31
1.27
1.24
Predicted
1.24
1.27
1.31
1.34
1.38
Actual

(d) %Mn

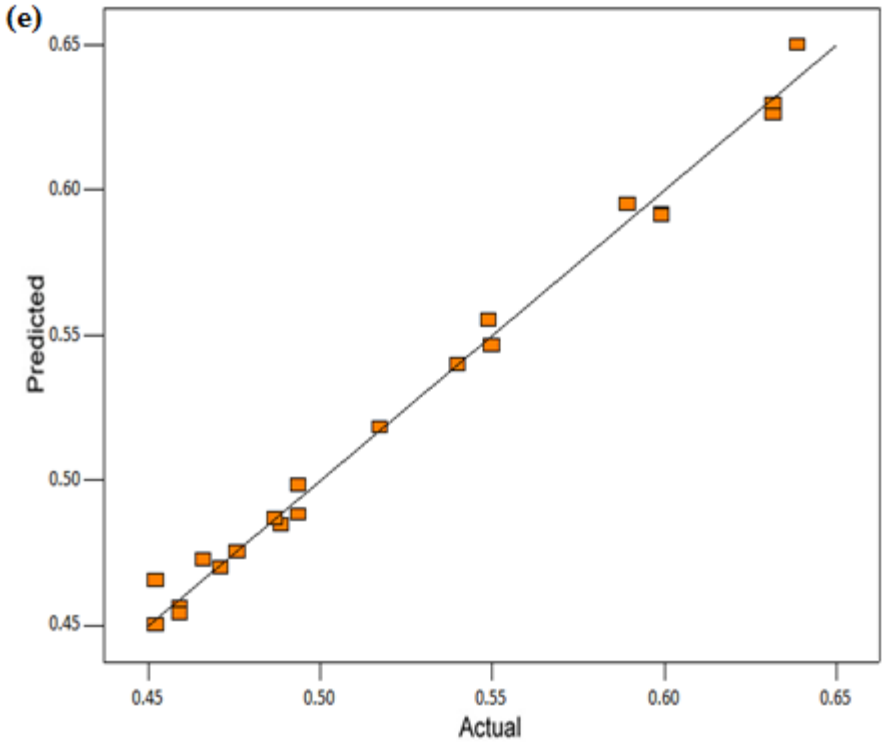
(e)
0.65
0.60
0.55
0.50
0.45
Predicted
0.45
0.50
0.55
0.60
0.65
Actual

(e) %Si

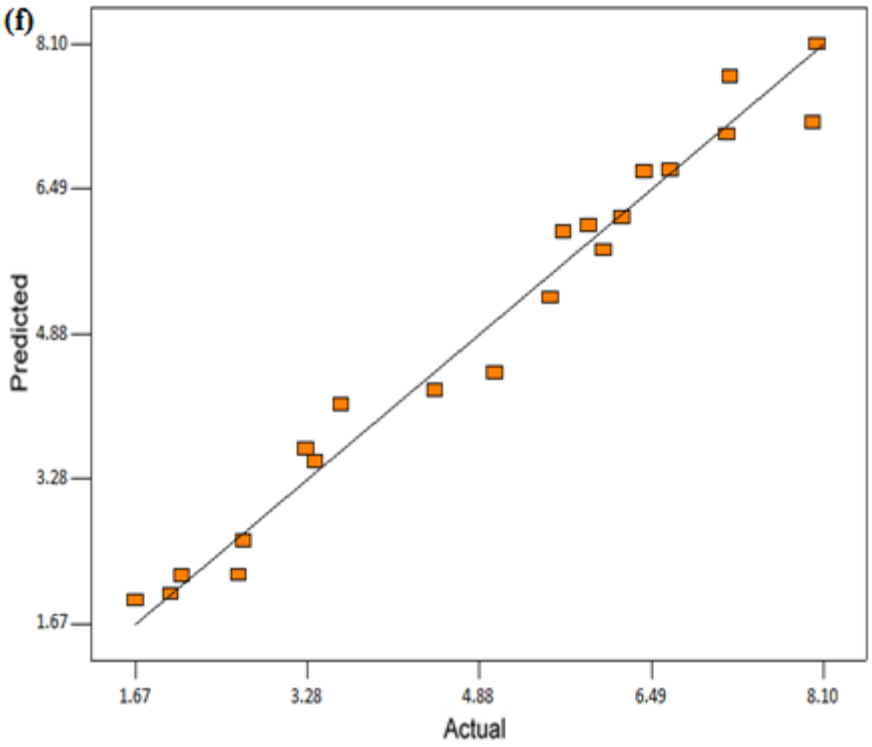

(f) Ferrite number

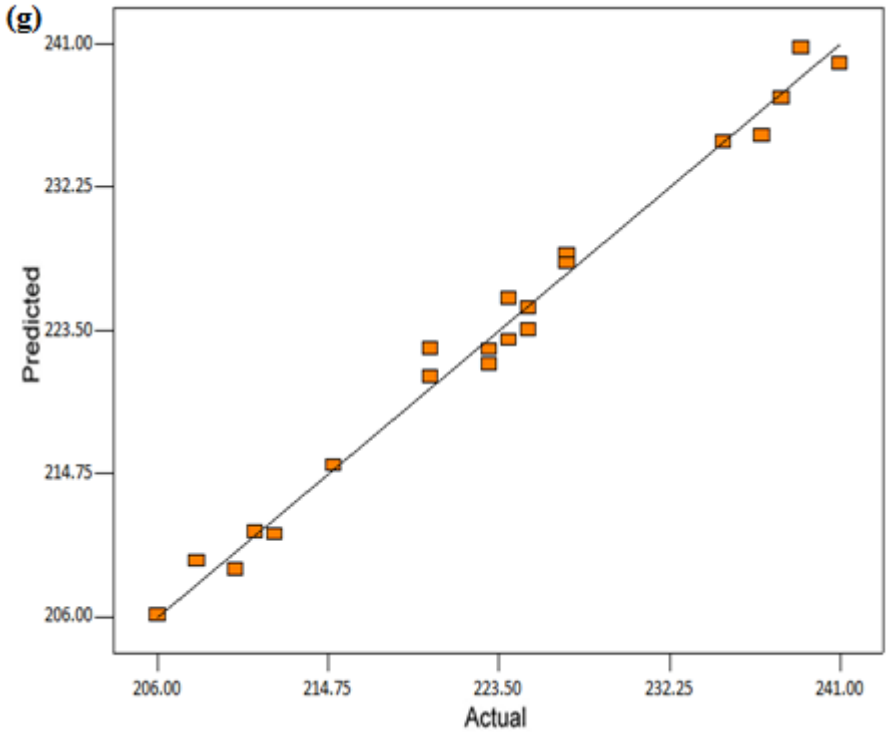

(g) Microhardness

Figure 5.9.1 Predicted versus actual values of various weld responses of buttering layer region (a) %C, (b) %Cr, (c) %Ni, (d) %Mn, (e) %Si, (f) ferrite number and (g) microhardness.

5.10 Discussion of Regression Models of Buttering Layer (Stainless Steel Electrodes Based on CaO-SiO_2-Al_2O_3-TiO_2 System) with Two Layer Methodology

5.10.1 Effect of electrode coating ingredients on weld responses of buttering layer

The regression analysis shows that silicon content in the buttering layer is significantly increased with the increase in SiO_2 content in electrode coatings which may be attributed to the dissociation of SiO_2 into silicon and oxygen during slag-metal reactions. Al_2O_3 shows the decreasing trend on the silicon content of buttering layer metal as it reacts with the fluorides present in the electrode coatings to form AlF_4 compound which further reacts with silicon. It has also been observed that the individual effect of TiO_2 and the interaction effects of CaO with SiO_2 and TiO_2 are also decreasing. The decreasing effect of binary mixture $CaO.SiO_2$ is due the decrease in activity of SiO_2 by the CaO in slag-metal reactions.

The individual effect of all the ingredients of electrode coatings i.e. CaO, SiO_2 and TiO_2 is on increasing the manganese content of buttering layer. TiO_2 decreases the viscosity of slag during slag-metal reactions and promotes the transfer of manganese to buttering layer. The decreasing effect of binary mixtures of SiO_2 on manganese content of buttering layer may be attributed to the increase in the concentration of MnO in slag resulting in the lower level of manganese content in the buttering layer (Mitra and Eagar, 1984 [105]).

The individual electrode coating ingredients except Al_2O_3 show the increasing effect on the carbon content of buttering layer. The binary mixtures of CaO, SiO_2 and TiO_2 with each other, show the decreasing effect on buttering layer carbon content.

The regression analysis shows that interaction effects of all the ingredients are to decrease the chromium content of buttering layer. It can be explained on the basis that the free oxygen available during the slag-metal reactions combines with chromium so as to form chromium oxide, resulting in decrease in chromium content of buttering layer. From the regression analysis it is observed that the electrode coating ingredients increase the nickle content of the buttering layer while the interaction effects of binary mixtures of Al_2O_3 are decreasing.

The regression analysis shows that the electrode coating ingredients promote the delta ferrite in buttering layer. It has been found from regression analysis that the electrode coating ingredients CaO, SiO_2 and TiO_2 significantly increase the microhardness of buttering layer. The binary mixture CaO.TiO_2 shows the significant decreasing effect on the buttering layer microhardness as is indicated by its lower p value in regression analysis (Table 5.9.3). It is also observed that the binary mixtures SiO_2.Al_2O_3 and SiO_2.TiO_2 show significant increasing effect on microhardness of buttering layer.

5.10.2 Contour surface plots for various properties

The contour surface plots showing predicted values of chemical composition of various elements, ferrite number and microhardness of buttering region for different proportions of electrode coating ingredients CaO, SiO_2, Al_2O_3 and constant TiO_2= 18.83% are shown in Figure 5.10.1 (a) to (g).

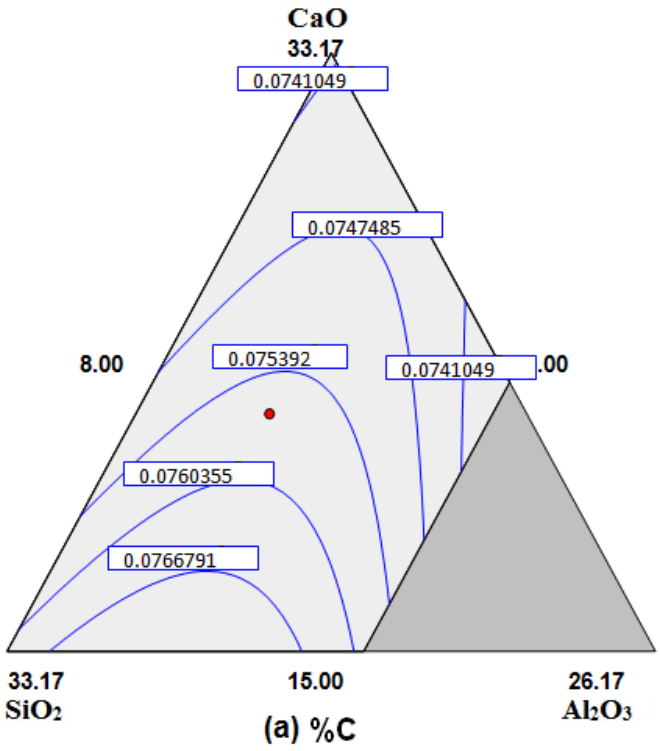

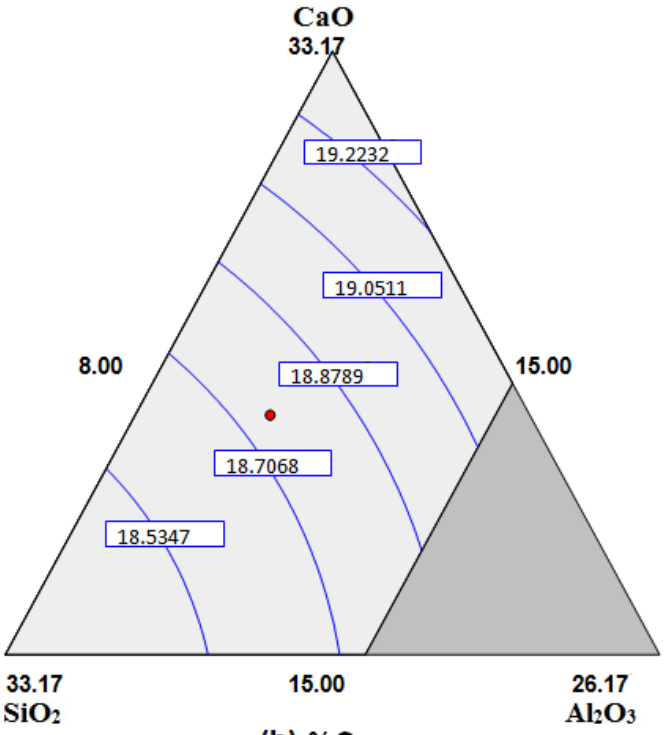
CaO
33.17
19.2232
19.0511
8.00
18.8789
15.00
18.7068
18.5347
33.17
SiO2
15.00
26.17
Al2O3

(b) %Cr

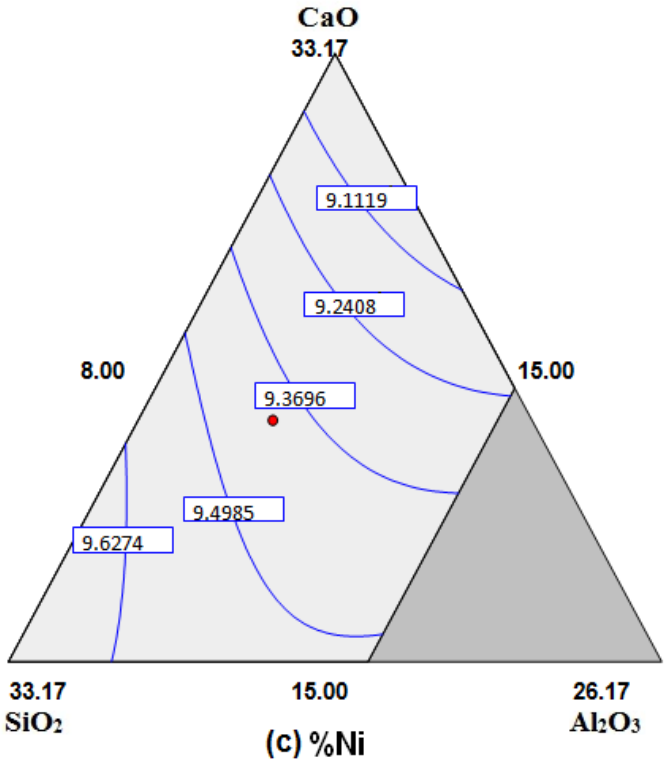
CaO
33.17
9.1119
9.2408
8.00
15.00
9.3696
9.4985
9.6274
33.17
SiO2
15.00
26.17
Al2O3

(c) %Ni

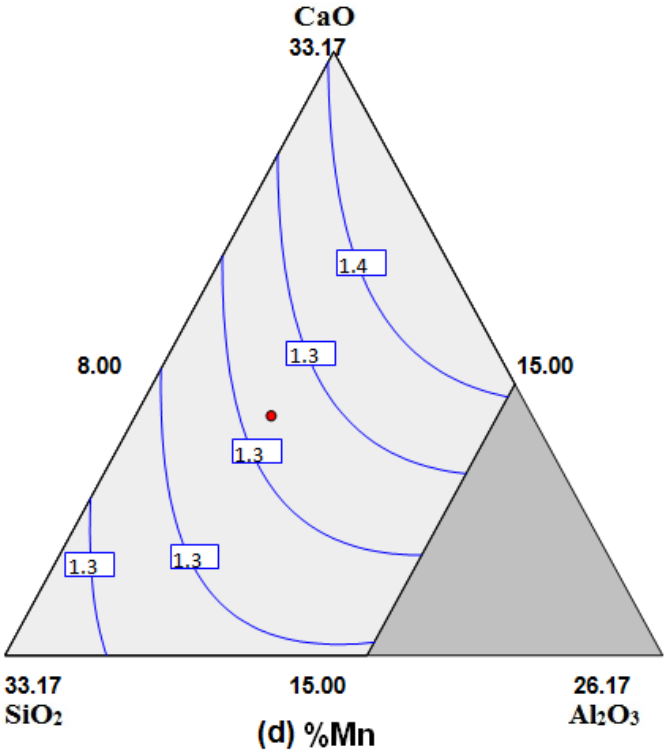
CaO
33.17
8.00
15.00
1.4
1.3
1.3
1.3
1.3
33.17
SiO2
15.00
26.17
Al2O3

(d) %Mn

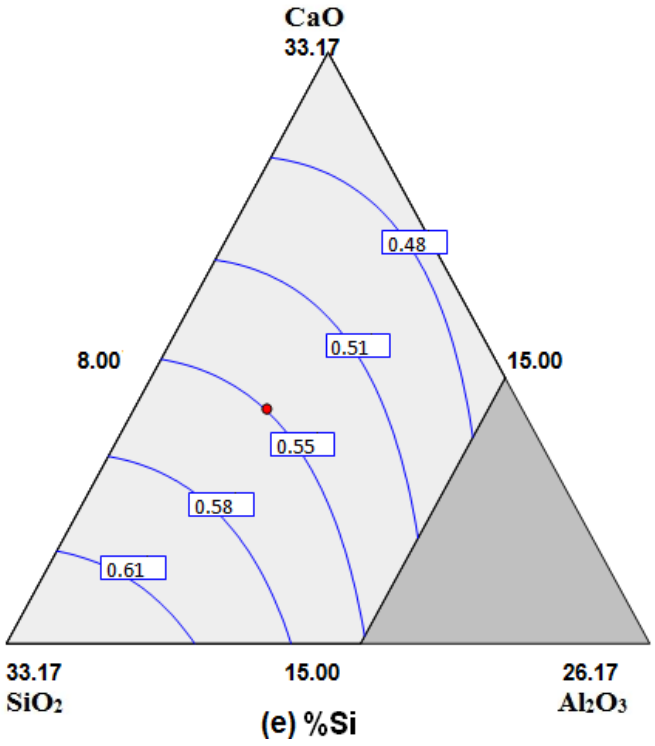
CaO
33.17
8.00
15.00
0.48
0.51
0.55
0.58
0.61
33.17
SiO2
15.00
26.17
Al2O3

(e) %Si

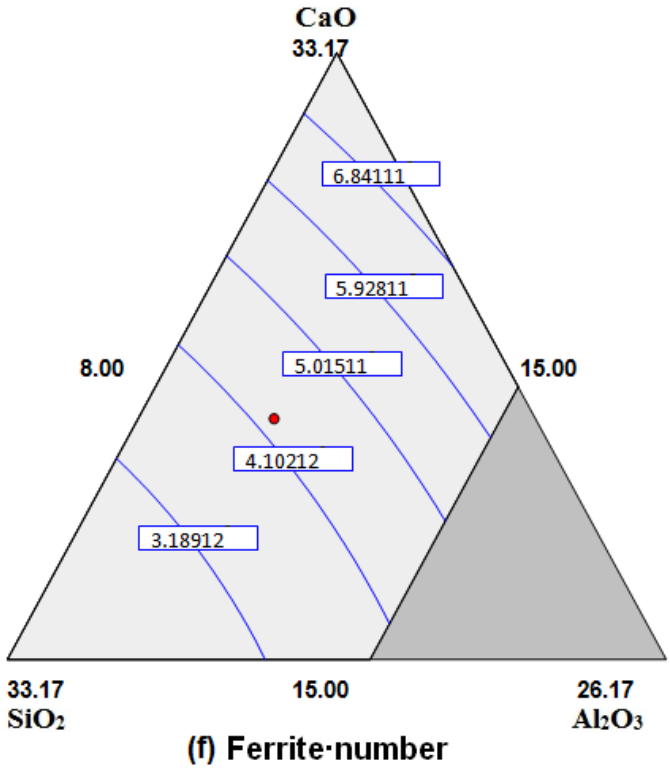

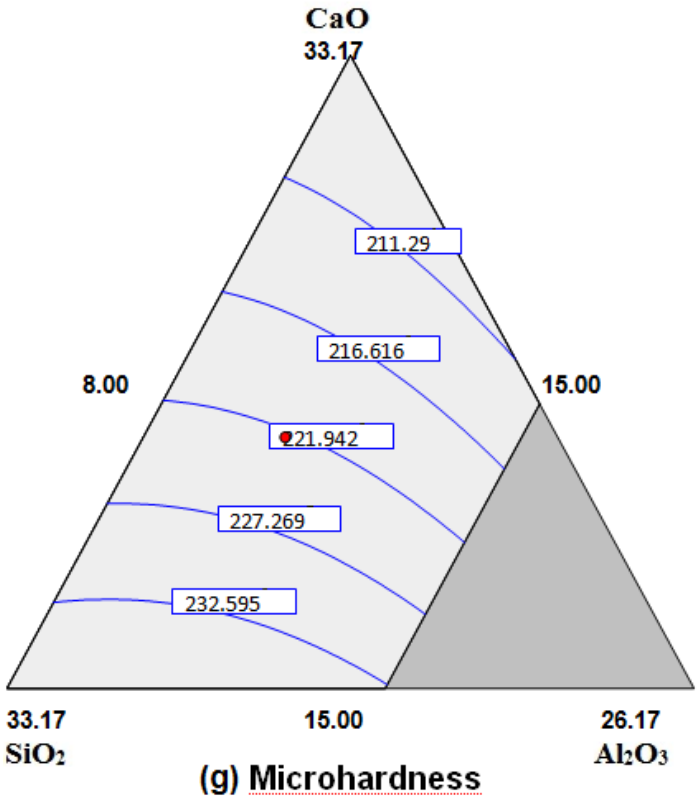

Figure 5.10.1 Contour surface plots of various weld responses of buttering region (a) %C, (b) %Cr, (c) %Ni, (d) %Mn, (e) %Si, (f) ferrite number and (g) microhardness.

5.10.3 Microstructural analysis

Figures 5.10.2 (a) and (b) show the microstructures of buttering layer of bimetallic welds of expt. no. 5 based on $CaO\text{-}SiO_2\text{-}Al_2O_3\text{-}TiO_2$ system with two different interfaces. The interface of SA516 and buttering layer is shown in Figure 5.10.2(a). Less carbide precipitates are seen as compared to the buttering region of bimetallic welds based on $CaO\text{-}TiO_2\text{-}SiO_2$ system (Figures 5.6.3(a) and (b)). The coarse grained region is also visible on the SA516 side. The interface of buttering layer and weld is seen in Figure 5.10.2(b). It has been observed that the microhardness of the buttering region (Table 5.9.1) as well as the bimetallic weld (Table 5.7.3) specimen fabricated with the electrode coating formulation or expt. no. 5 has increased probably due to the carbon migration.

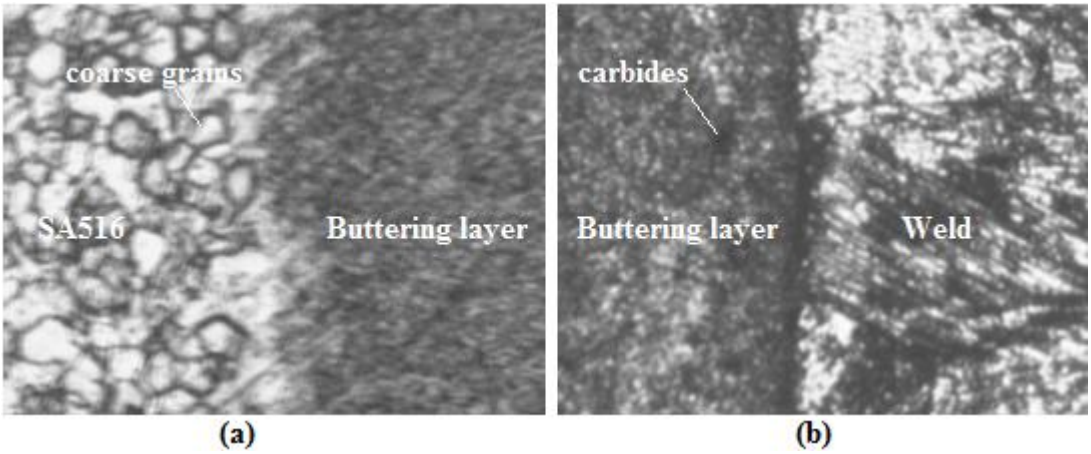

Figure 5.10.2 Microstructure of (a) SA516 and buttering layer interface and (b) Buttering layer and weld interface.

5.11 Discussion of three layer bimetallic welds

The three layer bimetallic weld methodology was then applied to fabricate bimetallic joints with the optimally designed three different types of electrodes as discussed in the previous sections. Two different set of weld coupons were fabricated. First set of bimetallic coupon was fabricated with mild steel electrodes and stainless steel electrodes based on $CaO\text{-}TiO_2\text{-}SiO_2$ system. The second set of weld coupons was fabricated with mild steel electrodes and stainless steel electrodes based on $CaO\text{-}SiO_2\text{-}Al_2O_3\text{-}TiO_2$ system. The mechanical property evaluation and weld chemistry characterisation was conducted on the test specimens prepared from the weld coupons, buttering layer pads; and the comparative evaluation of three layer and two layer bimetallic weld results has been shown in Table 5.11.1.

Table 5.11.1 Comparative evaluation of results of three layer and two layer bimetallic welds.

Description	Ultimate tensile strength (MPa)	Impact toughness (Nm)	Percentage elongation (%)	Microhardness (VHN)
MS core wire	560	166	31	145*
MS buttering	597.9	178.4	32	160*
SA516	580	154	24	172
SS304L	530	290	80	270
SS308L core wire	594	190	32	191
SS309L core wire	610	232	34	217
SS buttering (CaO-TiO_2-SiO_2 system) (using pad)	619	235	37	232
SS buttering (CaO-SiO_2-Al_2O_3-TiO_2 system) (using pad)	628	248	40	238
Three layer (CaO-TiO_2-SiO_2 system)	613	194	34	195
Three layer (CaO-SiO_2-Al_2O_3-TiO_2 system)	618	198	38	199
Two layer (CaO-TiO_2-SiO_2)	597	191	33	193
Two layer (CaO-SiO_2-Al_2O_3-TiO_2 system)	605	192	36	196

*-macrohardness

It has been observed from the comparative evaluation of mechanical property evaluation results (Table 5.11.1) that better mechanical properties are obtained with the three layer bimetallic methodology for both the phase diagram systems. Also the

electrodes based on $CaO\text{-}SiO_2\text{-}Al_2O_3\text{-}TiO_2$ seem to depict better results as compared to the electrodes designed on $CaO\text{-}TiO_2\text{-}SiO_2$ system.

The maximum ultimate tensile strength has been observed in the specimen made using buttering layer pads and the specimen prepared from the weld regions of three layer bimetallic welds fabricated using electrodes designed with $CaO\text{-}SiO_2\text{-}Al_2O_3\text{-}TiO_2$ flux system. It is found from the comparative results that the buttering layer deposits have much higher impact toughness, higher microhardness and percentage elongation than weld specimens fabricated using two and three layer approaches.

Table 5.11.2 and Figures 5.11.1 (a) to (d) show the various mechanical property variations with respect to the core wires. Higher overmatch for ultimate tensile strength, impact toughness and microhardness has been obtained for MS buttering/ MS core wire combination. The comparative evaluation of two layer and three layer bimetallic welds with different electrode coating flux systems reveals that maximum overmatch has been obtained for ultimate tensile strength, impact toughness, percentage elongation and microhardness for three layer ($CaO\text{-}SiO_2\text{-}Al_2O_3\text{-}TiO_2$ system)/ SS308L combination.

Table 5.11.2 Effect of flux systems on mechanical properties

Description	Ratio of ultimate tensile strength	Ratio of impact toughness	Ratio of percentage elongation	Ratio of microhardness
MS buttering/ MS core wire	1.068	1.075	1.032	1.103
Three layer ($CaO\text{-}TiO_2\text{-}SiO_2$ system)/ SS308L	1.032	1.021	1.063	1.021
Three layer ($CaO\text{-}SiO_2\text{-}Al_2O_3\text{-}TiO_2$ system)/ SS308L	1.040	1.042	1.188	1.042
Two layer ($CaO\text{-}TiO_2\text{-}SiO_2$ system)/ SS308L	1.005	1.005	1.031	1.010
Two layer ($CaO\text{-}SiO_2\text{-}Al_2O_3\text{-}TiO_2$ system)/ SS308L	1.019	1.011	1.125	1.026

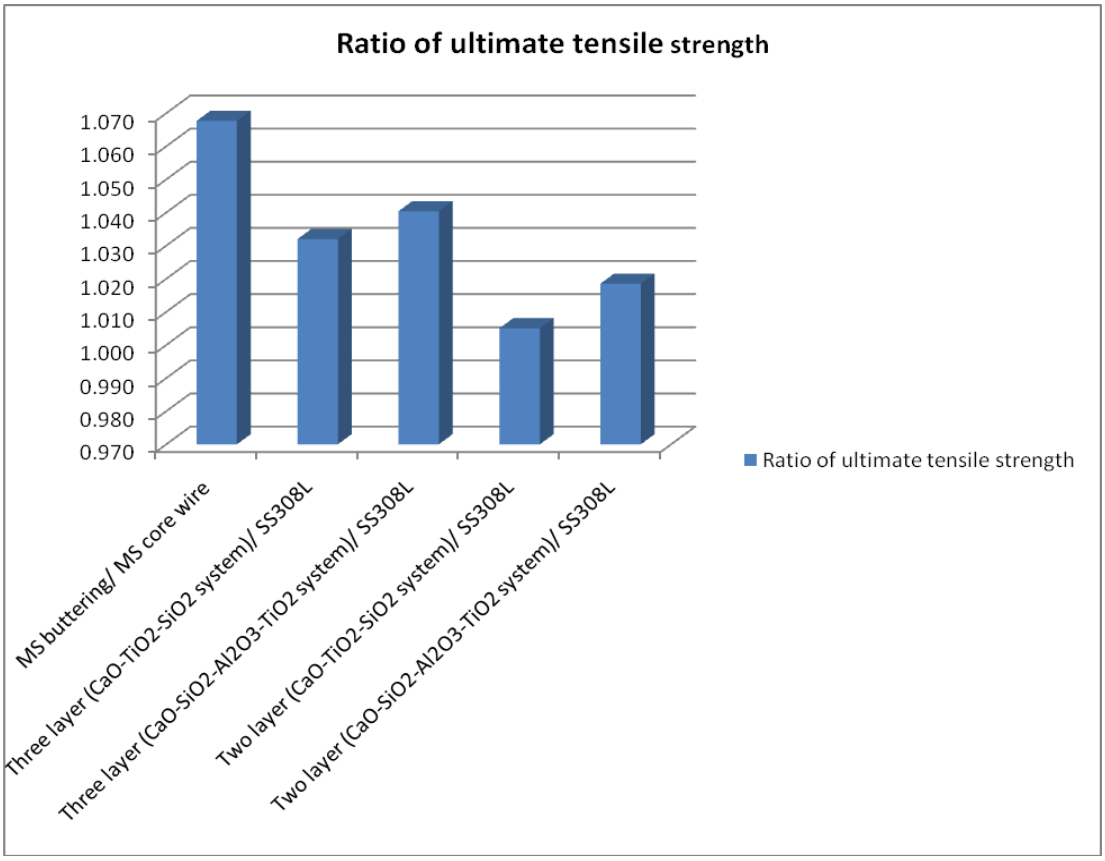
Ratio of ultimate tensile strength
1.070
1.060
1.050
1.040
1.030
1.020
1.010
1.000
0.990
0.980
0.970
MS buttering/ MS core wire
Three layer (CaO-TiO2-SiO2 system)/ SS308L
Three layer (CaO-SiO2-Al2O3-TiO2 system)/ SS308L
Two layer (CaO-TiO2-SiO2 system)/ SS308L
Two layer (CaO-SiO2-Al2O3-TiO2 system)/ SS308L
Ratio of ultimate tensile strength

(a)

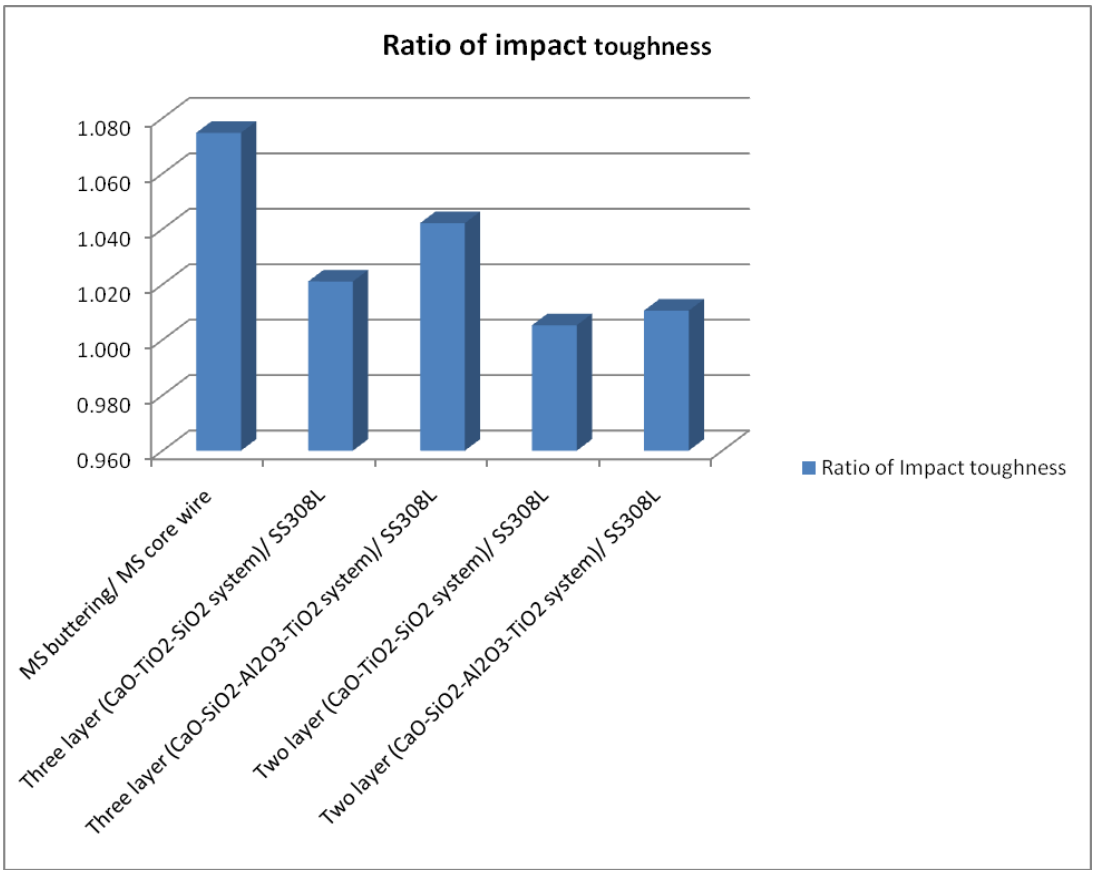
Ratio of impact toughness
1.080
1.060
1.040
1.020
1.000
0.980
0.960
MS buttering/ MS core wire
Three layer (CaO-TiO2-SiO2 system)/ SS308L
Three layer (CaO-SiO2-Al2O3-TiO2 system)/ SS308L
Two layer (CaO-TiO2-SiO2 system)/ SS308L
Two layer (CaO-SiO2-Al2O3-TiO2 system)/ SS308L
Ratio of Impact toughness

(b)

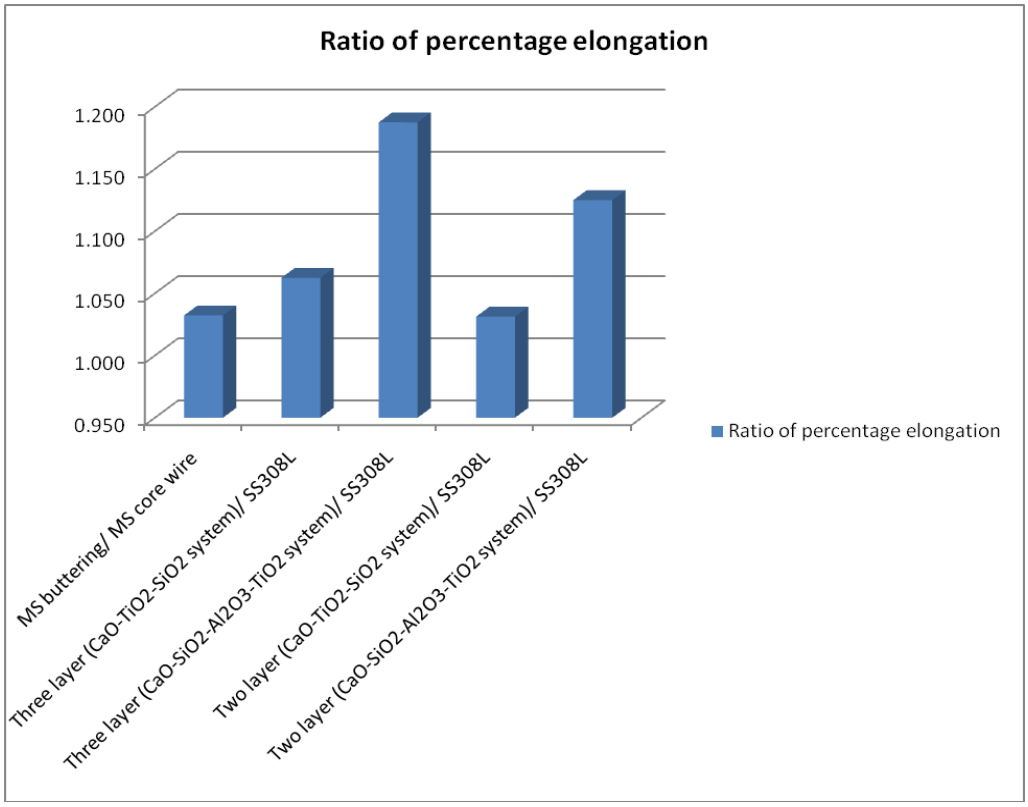

(c)

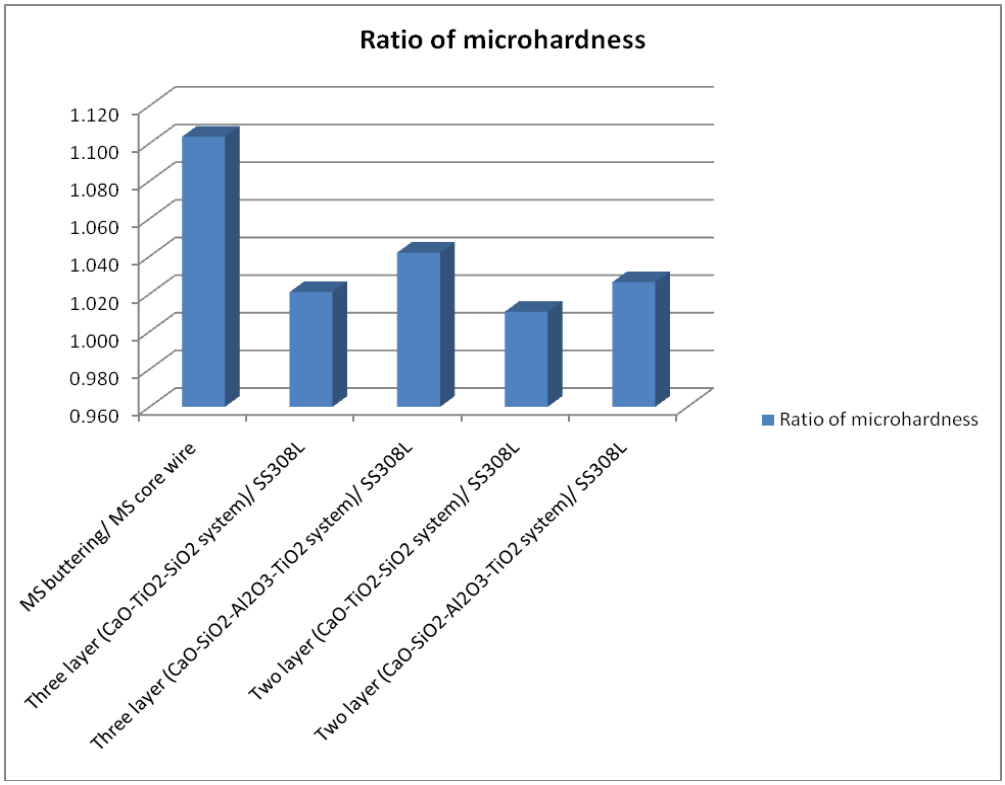

(d)

Figure 5.11.1 Effect of flux systems on the mechanical properties (a) ultimate tensile strength, (b) impact toughness, (c) percentage elongation and (d) microhardness.

Table 5.11.3 shows the elemental composition results while the percentage elemental pickup in welds for two layer and three layer bimetallic welds with different flux systems is shown in Table 5.11.5 and Figure 5.11.2(a) to (e). It is observed that highest chromium pickup and lowest carbon pickup are obtained with bimetallic welds fabricated with three layer methodology based on $CaO\text{-}SiO_2\text{-}Al_2O_3\text{-}TiO_2$ system. Nickel pickup for bimetallic welds fabricated with three layer methodology is found to be better as compared to the two layer methodology.

Table 5.11.3 Elemental composition results

Description	%C	%Mn	%Si	%Ni	%Cr
MS core wire	0.058	0.486	0.015	Nil	Nil
SA516	0.19	1.1	0.3	Nil	Nil
SS304L	0.025	1.6	0.5	8.5	18.2
SS308L	0.02	1.5	0.4	9.9	20
SS309L	0.02	1.7	0.4	13	23.5
SS buttering ($CaO\text{-}TiO_2\text{-}SiO_2$ system)	0.0766	1.331	0.462	9.31	19.12
SS buttering ($CaO\text{-}SiO_2\text{-}Al_2O_3\text{-}TiO_2$ system)	0.0738	1.38	0.488	9.03	19.28
Three layer ($CaO\text{-}TiO_2\text{-}SiO_2$ system)	0.036	1.26	0.59	10.5	18.6
Three layer ($CaO\text{-}SiO_2\text{-}Al_2O_3\text{-}TiO_2$ system)	0.035	1.32	0.57	10.4	19.1
Two layer ($CaO\text{-}TiO_2\text{-}SiO_2$ system)	0.04	1.28	0.6	10.2	18.4
Two layer ($CaO\text{-}SiO_2\text{-}Al_2O_3\text{-}TiO_2$ system)	0.038	1.34	0.58	10.1	18.8

Table 5.11.4 Elemental pickup during fabrication of bimetallic welds

Description	Ratio of %C	Ratio of %Mn	Ratio of %Si	Ratio of %Ni	Ratio of %Cr
Three layer (CaO-TiO_2-SiO_2 system)/SS 308L	1.8	0.84	1.18	1.06	0.93
Three layer (CaO-SiO_2-Al_2O_3-TiO_2 system)/SS308L	1.75	0.88	1.14	1.05	0.95
Two layer (CaO-TiO_2-SiO_2 system)/SS308L	2	0.85	1.2	1.03	0.92
Two layer (CaO-SiO_2-Al_2O_3-TiO_2 system)/SS308L	1.9	0.89	1.16	1.02	0.94

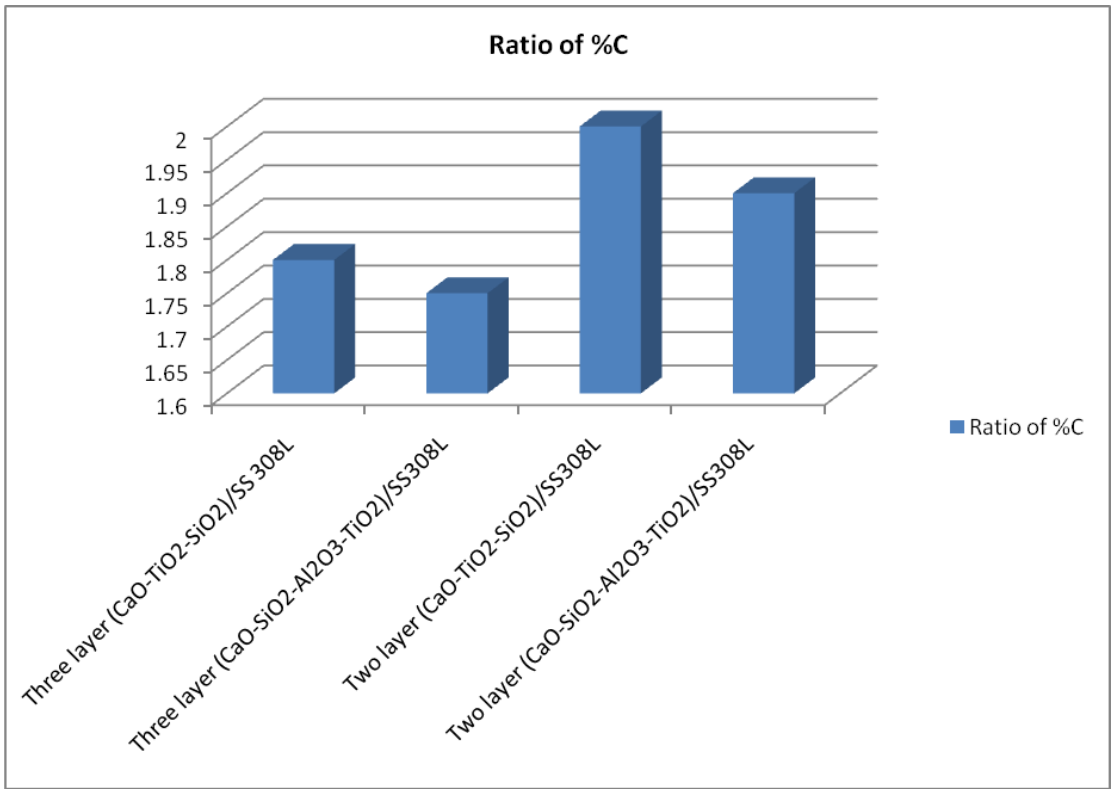

(a)

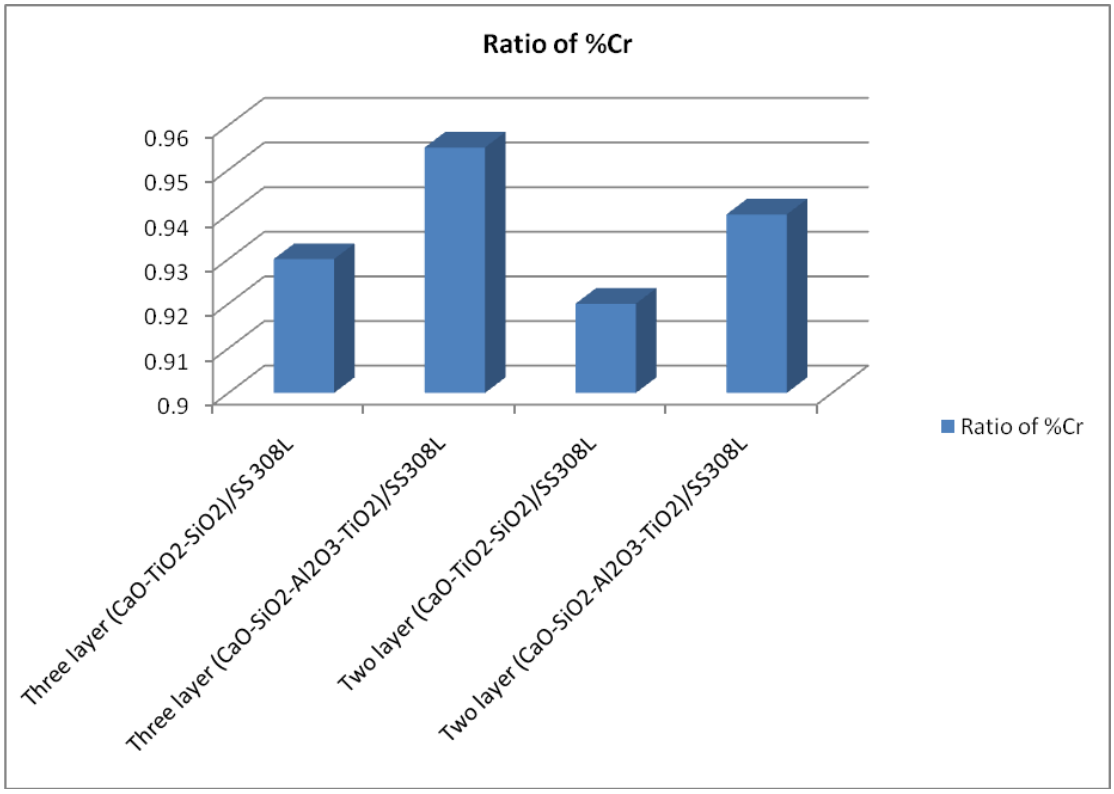
Ratio of %Cr
0.96
0.95
0.94
0.93
0.92
0.91
0.9
Three layer (CaO-TiO2-SiO2)/SS 308L
Three layer (CaO-SiO2-Al2O3-TiO2)/SS308L
Two layer (CaO-TiO2-SiO2)/SS308L
Two layer (CaO-SiO2-Al2O3-TiO2)/SS308L
Ratio of %Cr

(b)

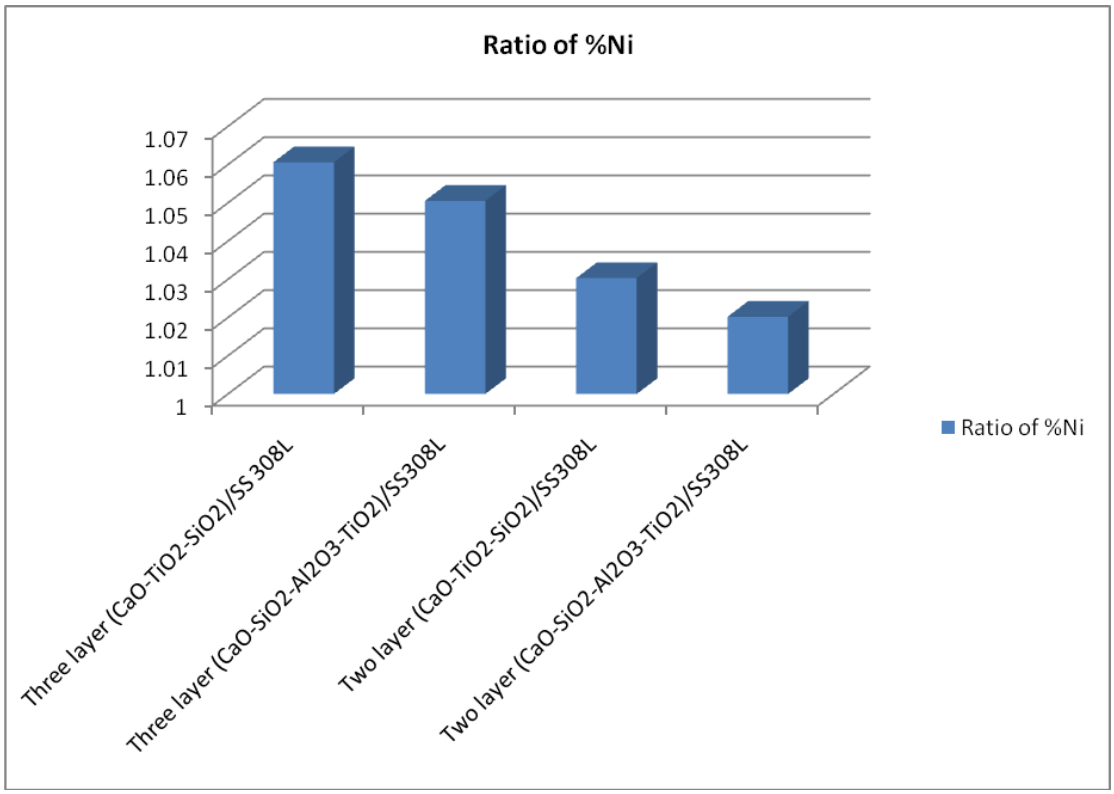
Ratio of %Ni
1.07
1.06
1.05
1.04
1.03
1.02
1.01
1
Three layer (CaO-TiO2-SiO2)/SS 308L
Three layer (CaO-SiO2-Al2O3-TiO2)/SS308L
Two layer (CaO-TiO2-SiO2)/SS308L
Two layer (CaO-SiO2-Al2O3-TiO2)/SS308L
Ratio of %Ni

(c)

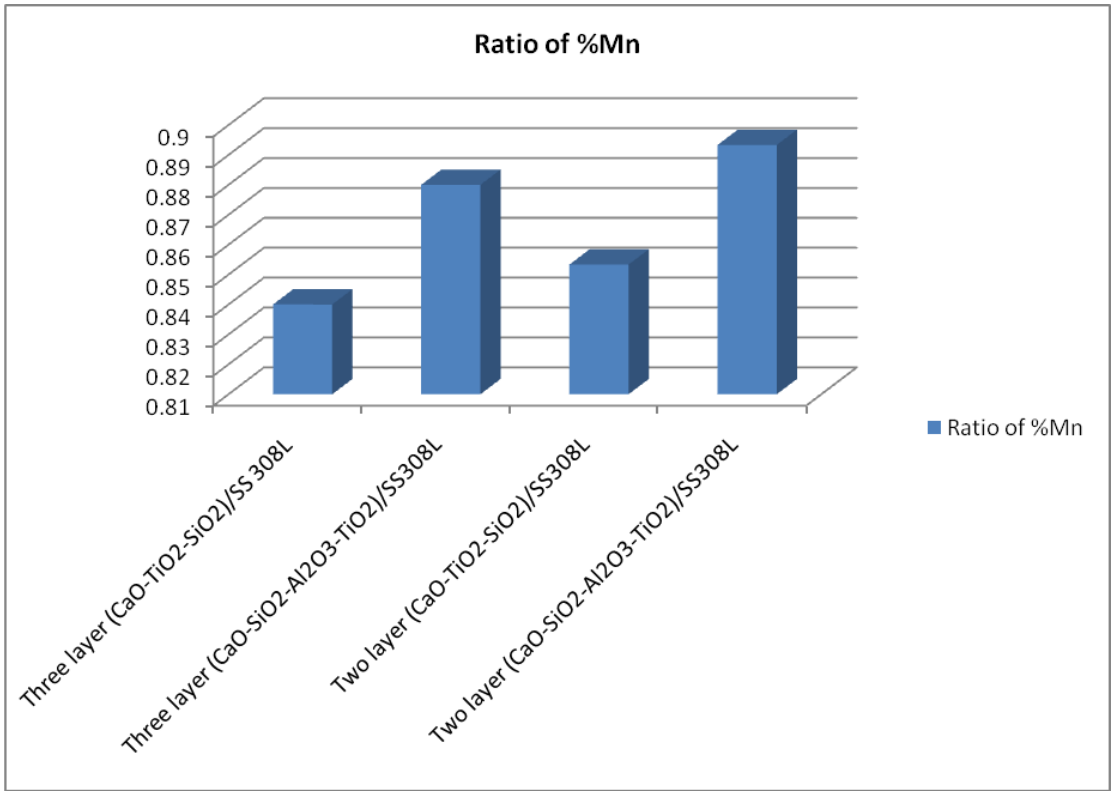

(d)

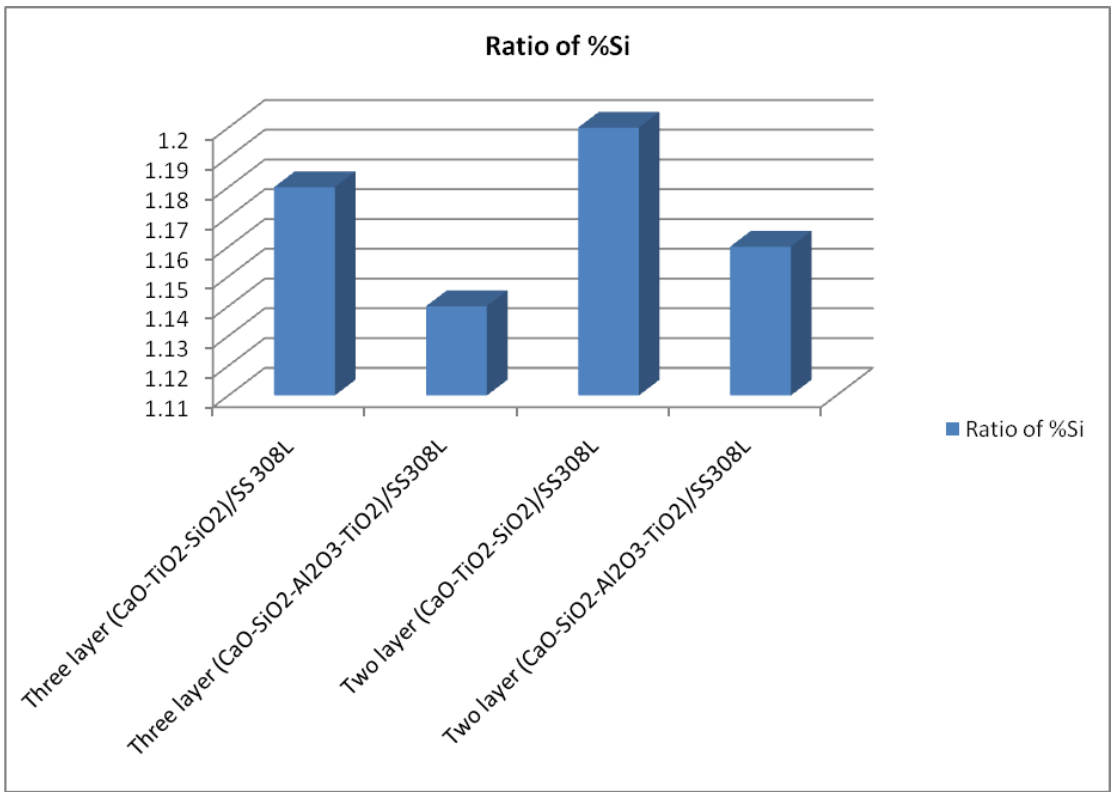

(e)

Figure 5.11.2 Elemental pickup (a) %C, (b) %Cr, (c) %Ni, (d) %Mn and (e) %Si.

CHAPTER 6
CONCLUSIONS AND SCOPE OF FUTURE WORK

6.1 Conclusions

In the work presented here, the welding electrodes have been designed and developed on the basis of ternary phase systems using MS and SS based fillers. The comparative evaluation of bimetallic welded joints has been done on the basis of two layer and three layer methodologies.

6.1.1 Based on mild steel electrodes

- Regression analysis of weld metal chemistry data shows that CaO, CaF_2 and SiO_2 content tends to decrease the nickel and phosphorous content in weld metal. All the interaction binary effects of electrode coating ingredients are negative on the weld metal sulphur content. SiO_2 and all the binary mixtures of CaO have significant decreasing effect on the carbon content of weld metal. The manganese content in weld is decreased with the increase in SiO_2 whereas CaO promotes transfer of manganese across the slag-metal interface thereby increasing its content. Silicon content in weld metal is increased with SiO_2 content in the electrode coating composition while the effect of all binary mixtures is decreasing.
- The ultimate tensile strength of weld has been increased with increase in individual electrode coating ingredients CaO, CaF_2 and Ni in electrode coatings. All the binary mixtures of nickel also show an increasing effect on UTS while the SiO_2 behaves in a negative manner.
- The addition of nickel and its binary mixtures show increasing effect on impact toughness due to grain refinement phenomenon. CaO and CaF_2 in electrode coatings also tend to increase the impact toughness of weld metal.
- The decreasing effect of binary mixtures $CaO.CaF_2$ and $CaO.SiO_2$ on macrohardness indicates that CaO tends to pick carbon from weld.
- All the individual electrode coating ingredients show decrease in the diffusible hydrogen content in weld metal whereas the effect of binary mixtures $CaO.CaF_2$, CaO.Ni, $CaF_2.SiO_2$ and SiO_2.Ni is increasing.

- Binary mixtures of Ni i.e. CaO.Ni, CaF_2.Ni and SiO_2.Ni improve the corrosion resistance of weld metal.
- The multi objective optimized solutions of various weld responses have been found out on the basis of composite desirability function and the most desirable electrode composition in terms of percentage of constituents was 20.9% CaO, 23.3 CaF_2, 12.8% SiO_2 and 8% Ni.

6.1.2 Two layer bimetallic welds based on stainless steel electrodes (CaO-TiO_2-SiO_2 system)

- The addition of SiO_2 content in the coating has an increasing effect on the weld metal silicon content while the CaO content tends to decrease it. Manganese as well as nickel content in the weld decreased with the increase in all the individual electrode coating ingredients.
- The additions of TiO_2, CaO and CaF_2 content in the coating have tendency to increase the chromium content of weld metal whereas addition of SiO_2 results in opposite behavior. The addition of individual flux ingredients CaO, CaF_2 and SiO_2 tend to decrease the carbon in weld metal composition.
- The ultimate tensile strength of welds is increased with the TiO_2, SiO_2 and CaF_2 content in the coating whereas the interaction effects of CaO, SiO_2 and CaF_2 cause significant decrease in the ultimate tensile strength of the welds.
- The increase of SiO_2 content in the electrode coatings results in higher dissolved oxygen content of weld which further has a negative effect on impact toughness and micro hardness values of the weld.
- The microstructures of welds comprise of austenite with varying amount of delta ferrite indicating the primarily solidification mode as ferritic–austenitic. The delta ferrite at the dendrite cores with vermicular morphology is clearly visible in the microstructures of welds.
- The microstructures of the welds obtained from different experiments show presence of small size inclusions (0.4μm) intermediate size inclusions (max size 3μm) and large size inclusions (6μm) which are responsible for varying mechanical properties.
- The most desirable electrode composition in terms of percentage of constituents based on the composite desirability function was 50.2% TiO_2, 9.2% CaO, 10% SiO_2 and 10% CaF_2.

6.1.3 Two layer bimetallic welds based on stainless steel electrodes (CaO-SiO_2-Al_2O_3-TiO_2 system)

- SiO_2 shows an increasing effect on the weld metal silicon content whereas Al_2O_3 tends to decrease it. The silicon content is decreased with the binary mixture $CaO.SiO_2$ due to decrease in activity of silica by the basic oxide CaO.
- TiO_2 assists in the transfer of manganese to weld metal by decreasing the viscosity of slag during slag metal reactions. Al_2O_3 releases O^{-2} ions that react with carbon thereby reducing its composition. The interaction effect of coating ingredients on the weld metal chromium content is decreasing.
- The mechanical behavior of the bimetallic welds largely depends on the individual electrode coating ingredients and their binary interaction effects. The microstructures of the weld samples obtained from different experiments show the presence of inclusions of varying size (0.3μm to 6μm) and are responsible for varying mechanical properties. The delta ferrite at the dendrite cores with vermicular morphology can be seen in the microstructures of welds.
- The better mechanical properties were observed as compared to the stainless steel electrodes based on CaO-TiO_2-SiO_2 system.
- The most desirable electrode composition in terms of percentage of coating ingredients on the basis of composite desirability function was 28.07% CaO, 16.67% SiO_2, 10.69% Al_2O_3 and 19.56% TiO_2.

6.1.4 Three layer bimetallic welds

- Three layer bimetallic welds methodology has been evolved and the three optimized weld electrodes have been developed.
- The welds developed on the basis of three layer methodology have depicted better mechanical properties as compared to two layer method. The maximum overmatch have been obtained for ultimate tensile strength, impact toughness, percentage elongation and microhardness for bimetallic welds fabricated with three layer methodology based on CaO-SiO_2-Al_2O_3-TiO_2 system.
- The highest chromium pickup and lowest carbon pickup have been obtained with bimetallic welds fabricated with three layer methodology based on CaO-SiO_2-Al_2O_3-TiO_2 system.

6.2 Scope of Future Work

- The more phase diagram systems can be explored for the design and development of electrode coatings for bimetallic welds.
- In the present research work, the weld metal chemistry and mechanical property analysis has been done for three different electrode coating systems. The further scope includes the more mechanical tests like thermal fatigue under cyclic loading conditions and corrosion behavior at elevated temperatures so as to establish the complete evaluation and utility of stainless steel electrodes for bimetallic welds based on three layer methodology.

REFERENCES

1. **Anawa E.M.** and Olabia A.G. Using Taguchi method to optimize welding pool of dissimilar laser-welded components. Optics and Laser Technology 2008; 40 (2): 379-388.
2. **Anderson V.L.** and McLean R.A. Design of experiments: a realistic approach. New York: Marcell Dekker, 1974.
3. **Arora K.S.**, Ray A., Lester S. and Shome M. Laser cladding of continuous caster rolls: Microstructure, wear and corrosion characterization and on field performance evaluation. Journal of Materials Processing Technology 2014; 214(8): 1566-1575.
4. **Arora K.S.** and Viehrig H.W. Evaluation of the ASTM and ISO J Initiation Procedures by applying the unloading compliance technique to reactor pressure vessel steels. Journal of Testing and Evaluation 2011; 39(6): 1-10.
5. **Belton G.R.**, Moore T.J. and Tankins E.S. Slag metal reactions in submerged arc welding. Welding Journal 1963; 42(7): 289s-297s.
6. **Bennett A.P**. Using basic fluxes. Metal Construction1970: 523-527.
7. **Benyounisa K.Y.** and Olabib A.G. Optimization of different welding processes using statistical and numerical approaches– a reference guide. Advances in Engineering Software 2008; 39(6): 483-496.
8. **Bhaduri A.K.** and Venkadesan S. Effect of thermal cycling on the alloy 800/2.25 Cr-1 MO steel joint. Zeitschrift fur Metallkunde 1990; 82(2): 135-138.
9. **Bhaduri A.K.**, Venkadesan S., Rodriguez P. and Mukunda P.G. Transition metal joints for steam generators-An overview. International Journal of Pressure Vessel and Piping 1994; 58: 251-265.
10. **Bhaduri A.K.**, Gowrisankar I., Seetharaman V., Venkadesan, S. and Rodriguez, P., Development of transition metal joint for steam generator circuit of prototype fast breeder reactor. Materials Science and Technology 1988; 4(11): 1020-1029.
11. **Bhaduri A.K.**, Seetharaman V. and Venkadesan S. Effect of ageing on the interfacial microstructure and mechanical properties of a alloy 800/2.25 Cr-1 Mo steel joint. Zeitschrift fur Metallkunde 1989: 80(9): 630-634.

12. **Bhandari D.**, Chhibber R. and Arora N. Effect of electrode coatings on diffusible hydrogen content, hardness and microstructures of the ferritic heat affected zones in bimetallic welds. Advanced Materials Research 2012; 383-390: 4697-4701.
13. **Bhandari D.**, Chhibber R. and Arora N. Investigation of TiO_2–SiO_2–CaO–CaF_2 based electrode coatings on weld metal chemistry and mechanical behaviour of bimetallic welds. Journal of Manufacturing Processes 2016; 23: 61–74.
14. **Blander M.** and Olson D.L. Electrochemical effects on weld pool chemistry in submerged arc and DC electroslag welding. Proceedings International Conference on Trends in Welding Research 1986.
15. **Blumer U.**, Fricker H. and Amacher S. The use of bimetallic welds in the THTR steam generators. Proceedings of the IAEA Specialist's Meeting on the Heat Exchanging Components of Gas Cooled Reactors, Dusseldorf, 1984; Report No. 36: 1-2.
16. **Bracarense A.Q.** and Liu S. Chemical composition variations in shielded metal arc welds. Welding Research Supplement December 1993: 529s-536s.
17. **Brandi S.**, Taniguchi C., and Liu S. Analysis of metal transfer in shielded metal arc welding. Welding Journal 1991: 261-270.
18. **Buckthorpe D.**, Escaravage C., Neri P., Pierantozzi P. and Schmidt. Final report CSC-WGCS/AG2 study contract on bi-Metallic weldments (ETNU-CT94-0133UK). Document No C9731/ TR/002, Vol. 02.NNC Ltd, 1997
19. **Buckthorpe D.C.** High Temperature Reactor (HTR) materials. Conference, Materials for Advanced Power Engineering 2002.
20. **Butler C.A.** and C.E. Jackson, "Submerged-arc welding characteristics of the CaO–TiO_2–SiO_2 system. Welding Journal of Supplement Research 1967; 46: 448–456.
21. **Bystram M.C.T.** Consumable for fusion welding of dissimilar metals. Metal Construction and British Welding Journal 1969; 1:150.
22. **Castillo D.E.**, Montgomery D.C. and McCrville D.R. Modified desirability functions for multiple response optimization. Journal of Quality Technology 1996; 28: 337-345.
23. **Celik A.** and Alsaran A. Mechanical and structural properties of similar and dissimilar steel joints. Material Characterization 1999; 43: 311-318.

24. **Chai C.S.** and Eagar T.W. Slag metal reactions in binary CaF_2—metal oxide welding fluxes. Welding Journal 1982; 16(7): 229–232.

25. **Chai C.S.** and Eagar T.W. Slag–metal equilibrium during submerged arc welding. Metallurgical Transaction B 1981; 12B: 539–547.

26. **Chandel R.S**. The effect of process Variables on the flux consumption in submerged arc welding. Materials and Manufacturing Processes 1998; 13(2): 181-188.

27. **Chhibber R.**, Arora N., Gupta S.R. and Dutta B.K. Use of bimetallic welds in nuclear reactors: associated problems and structural integrity assessment issues. Journal of Mechanical Engineering Science C 2006; 220: 1121-1133.

28. **Christensen N.** and Chapman J. Slag metal interaction in arc welding. Welding Research Council Bulletin Series 1953; 15: 1-14.

29. **Cornell J.** Experiments with mixtures: designs, models, and the analysis of mixture data. John Wiley & Sons Inc. 2002.

30. **Das C.R.**, Bhaduri A.K., Srinivasan G., Shankar V. and Mathew S. Selection of filler wire for and effect of auto tempering on the mechanical properties of dissimilar metal joint between 403 and 304L(N) stainless steel. Journal of Materials Processing Technology 2009; 209: 1428–1435.

31. **Da Silva L.F.M.** et al. Characterization of composite bonded joints under pure mode II fatigue loading. Composite Structures 2013; 95: 222-226.

32. **Da Silva L.F.M.** et al. Sensitivity and optimization of peel strength based on composition of adhesives for footwear industry. Journal of Adhesion 2015; 91(10-11): 801-822.

33. **Davis M.L.E.** and Coe F.R. The chemistry of submerged arc welding fluxes. The Welding Institute Research Report, 39/1977/M, London, 1977: 1–61.

34. **De Rissone N.M.R.**, De Souza Bott I., Jorge J.C.F., Corvalan P. and Surian E. ANSI/AWS A5.1-91 E6013 rutile electrodes: the effect of wollastonite. Welding Research Supplement November 1997: 498s-507s.

35. **De Rissone N.M.R.**, Farias J.P., De Souza Bott I. and Surian E. ANSI/AWS A5.1-91 E6013 rutile electrodes: the effect of calcite. Supplement to the Welding Journal, July 2002: 113s-124s.

36. **De Vries R.C.**, Roy R. and Osborn E.F. Phase equilibria in the system CaO-TiO_2-SiO_2. Journal of the American Ceramic Society 1955; 38: 158-171.

37. **Dehmolaeia R.**, Shamanian M. and Kermanpura A. Microstructural characterization of dissimilar welds between alloy 800 and HP heat-resistant steel. Materials Characterization 2008; 59(10): 1447-1454.

38. **Du Plessis J.**, Du Toit M. and Pistorius P.C. Control of diffusible weld metal hydrogen through flux chemistry modification. Weld Journal 2007; 86(9): 273s-280s.

39. **Correa E.O.** et al. Influence of clad metal chemistry on stress corrosion cracking behaviour of stainless steels claddings in chloride solution. Scientific Research Publishing 2010; 2(5): 391-396.

40. **Correa E.O.** et al. Mechanical and microstrutural characterization of weldments of ferritic stainless steel AISI 444 using austenitic stainless steels filler metals. 18th International Federation for Heat Treatment and Surface Engineering, ASTM International 2012.

41. **Correa E.O.** et al. Effect of weld metal chemistry on stress corrosion cracking behavior of AISI 444 ferritic stainless steel weldments in boiling chloride solution. Materials and Corrosion 2013; 64 (5): 415-421.

42. **Eriksson G.** and Pelton A.D. Critical evaluation and optimization of the thermodynamic properties and phase diagrams of the $CaO–Al_2O_3$, $Al_2O_3–SiO_2$ and $CaO–SiO_2–Al_2O_3$ systems. Metallurgical and Materials Transactions B 1993; 24: 807-816.

43. **Evans G.M.** The effect of titanium in manganese-containing SMA weld deposits. Welding Journal 1993; 72(3): 123s-133s.

44. **Evans G.M.** The effect of titanium in SMA C-Mn steel multipass deposits. Welding Journal 1992; 71(12): 447s-454s.

45. **Farias J.P.**, Quites A.M. and Surian E.S. The effect of magnesium content on the arc stability of SMAW E7016-C2L/8016-C2 covered electrodes. Welding Research Supplement June 1997: 245s-250s.

46. **Ferrera K. P.** and Olson D.L. $MnO-SiO_2-CaO$ welding flux system. Welding Journal 1975; 54(7): 211-215.

47. **Fussel U.** et al. Visualization and optimization of shielding gas flows in arc welding. Welding in the World 2012; 56 (1): 54-61.

48. **Fussel U.** et al. Numerical investigations of the influence of metal vapor in GMA welding. Welding in the World 2011; 55(11): 114-120.

49. **Gaal B.** Development of a coating formulation procedure for Ni-base shielded metal arc electrodes with varying core wire composition. Thesis-Master of Science, The Ohio State University, 2012.

50. **Gunaraj V.**, and Murugan N. Application of response surface methodology for predicting weld bead quality in submerged arc welding of pipes. Journal of Materials Processing Technology 1999; 88: 266–275.

51. **Haas P.E.** Results of industry-wide survey on dissimilar metal welds in power plants. In Proc. A WS/EPRI Conf. Joining Dissimilar Metals, Pittsburg, PA 1982: 37-47.

52. **Hadraba H.** and Dlouhy I. Effect of thermal ageing on the impact fracture behaviour of Eurofer'97 steel. Journal of Nuclear Materials 2009; 386: 564-568.

53. **Hadraba H.** et al. Influence of microstructure on impact properties of 9–18% Cr ODS steels for fusion/fission applications. Journal of Nuclear Materials 2011a; 411(1): 112-118.

54. **Hadraba H.**, Stratil L., Bursik J. and Dlouhy I. Comparison of microstructural properties and charpy impact behaviour between different plates of the Eurofer97 steel and effect of isothermal ageing. Journal of Nuclear Materials 2011b; 416(3): 311-317.

55. **Harington J.** The desirability function. Industrial Quality Control 1965; 21: 494- 498.

56. **Hasanbasoglu A.** and Kacar R. Resistance spot weldability of dissimilar materials (AISI 316L–DIN EN 10130-99 steels). Materials and Design 2007; 28 (6): 1794-1800.

57. **Hazlett T.H.** and Parker E.R. Effect of individual coating ingredients on surface tension of iron electrodes. Welding Journal, 1956; 35: 113s-114s.

58. **Hazlett T.H.** Coating ingredients' influence on surface tension, arc stability and bead shape. Welding Journal 1957; 38(1): 18s-22s.

59. **IAEA Report**: TECDOC-1361. Assessment and management of ageing of major nuclear power plant components important to safety in primary piping in PWRs, July 2003.

60. **Jackson C.E.** Fluxes and slags in welding. Welding Research Bulletin 1973, No. 190, Welding Research Council, New York.

61. **Jang C.**, Lee J., Kim J.S. and Jin T.E. Mechanical property variation within Inconel 82/182 dissimilar metal weld between low alloy steel and 316 stainless steel. International Journal of Pressure Vessels and Piping; 85(9): 635-646.

62. **Jeng S.L.**, Lee H.T., Rehbach W.P., Kuo T.Y., Weirich T.E. and Mayer J.P. Effects of Nb on the microstructure and corrosive property in the Alloy 690–SUS 304L weldment. Materials Science and Engineering A 2005; 397(1-2): 229-238.

63. **Jindal S.**, Chhibber R. and Mehta N.P. Investigation on flux design for submerged arc welding of high-strength low-alloy steel. Journal of Engineering Manufacture 2013, 227: 383-395.

64. **Jindal S.** et al. Determination of flux consumption in submerged arc welding by the effect of welding parameters by using RSM techniques. Global Journal of Research in Engineering 2012; 12(2).

65. **Jindal S.** et al. Design and development of fluxes for submerged arc welding of HSLA steel. International Journal of Surface Engineering & Materials Technology 2013; 3(2): 52-58.

66. **Jindal S.** et al. To study the effect of welding parameters on weld bead geometry in SAW welding process. Elixir Mechanical Engineering 2011; 40: 5519-5524.

67. **Jindal S.** and Kumar D. Optimization of process parameters of gas metal arc welding by Taguchi's experimental design method. International Journal of Surface Engineering & Materials Technology 2014; 4(1): 24-27.

68. **Jindal S.**, Chhibber R. and Mehta N.P. Effect of flux constituents and basicity index on mechanical properties and microstructural evolution of submerged arc welded high strength low alloy steel. Materials Science Forum 2013; 738: 242-246.

69. **Jindal S.**, Chhibber R. and Mehta N.P. Effect of welding parameters on bead profile, microhardness and H_2 content in submerged arc welding of high-strength low-alloy steel. Proceedings of the Institution of Mechanical Engineers, Part B: Journal of Engineering Manufacture 2014a; 228(1): 82-94.

70. **Jindal S.**, Chhibber R. and Mehta N.P. Modeling flux chemistry for submerged arc weldments of high-strength low-alloy steel. Proceedings of the

Institution of Mechanical Engineers, Part B: Journal of Engineering Manufacture 2014b; 228(10): 1259–1272.

71. **Jindal S.**, Chhibber R. and Mehta N.P. Prediction of element transfer due to flux and optimization of chemical composition and mechanical properties in high-strength low-alloy steel weld. Proceedings of the Institution of Mechanical Engineers, Part B: Journal of Engineering Manufacture 2015; 229(5): 785-801.

72. **Joseph A.**, Rai S.K., Jayakumar T. and Murugan N. Evaluation of residual stresses in dissimilar weld joints. International Journal of Pressure Vessels and Piping 2005; 82: 700–705.

73. **Kacar R.** and Baylan O. An investigation of microstructure/property relationships in dissimilar welds between martensitic and austenitic stainless steels. Materials and Design 2004; 25, 317–329.

74. **Kalisz D.** Influence of casting mold slag on the progress of casting process. Archives of Metallurgy and Materials 2013; 58(1): 35-41.

75. **Kanjilal P.**, Pal T.K. and Majumdar S.K. Combined effect of flux and welding parameters on chemical composition and mechanical properties of submerged arc weld metal. Journal of Materials Processing Technology 2006; 171: 223–231.

76. **Kanjilal P.**, Pal T.K. and Majumdar S.K. Prediction of submerged arc weld metal composition from flux ingredients with the help of statistical design of experiment. Scandinavian Journal of Metallurgy 2004; 33: 146–159.

77. **Khan M.K.**, Pathak M., Suman S., Deo A. and Singh R. Burst investigation on Zircaloy-4 claddings in inert environment. Annals of Nuclear Energy, 2014; 69: 292–300.

78. **Khan M.K.**, Alam T., Pathak M., Ravi K., Singh R. and Gupta S.K. A review on the clad failure studies. Nuclear Engineering and Design 2011; 241(9): 3658-3677.

79. **King J.F.**, Sullivan M.D. and Slaughter G.M. Development of an improved stainless steel to ferritic steel transition joint. Welding Journal 1977; 56: 354s-358s.

80. **Kiyohoara M.**, Okada T., Wakino Y.and Yamamoto H. Why dissimilar metal welding is needed & how to select proper filler metals. Kobelco Welding Today 2002; 5: 9-10.

81. **Klueh R.L.** and King J.F. Austenitic–Ferritic weld joint failures. Weld Journal 1982; 61: 302s–311s.

82. **Klueh R.L.**, King J.F. and Griffith J.L. A simple test for dissimilar-metal welds. Weld Journal 1983; 62: 154s–159s.

83. **Kohno R.**, Takami T., Mori N. and Nagano K. New fluxes of improved weld metal toughness for HSLA steels. Welding Journal 1982; 61(12): 373s-380s.

84. **Komapov A.I.**, Khodakov V.D. and Volobuev Y. Effects of the surface tension of steels and fluxes on the shape of deposited metal. Automatic Welding 1983; 36 (3): 27-29.

85. **Kotecki D.J.** and Siewert T.A. WRC-1992 constitution diagram for stainless steel weld metals: A modification of the WRC-1988 diagram. Welding Journal 1992; 71: 171s-178s.

86. **Kou S.** Welding Metallurgy. A John Wiley & Sons, Inc., Publication, 2002.

87. **Kozyrev N.A.** et al. Some aspects of oxidation-reduction reactions under carbon bearing flux welding. IOP Conf. Series: Materials Science and Engineering 2015; 91: 012016.

88. **Kozyrev N.A.** et al. The Carbon-Fluorine additives for welding fluxes. Mechanics, Material Science and Engineering January 2016a; ISSN 2412-5954.

89. **Kozyrev N.A.** et al. Influence of Filler metals in welding wires on the phase and chemical composition of Weld Metal. IOP Conf. Series: Materials Science and Engineering 2016b; 125: 012027.

90. **Kumar R.,** Kumar S. and Kumar A. Some studies on heat affected zone (HAZ) toughness behavior of API 5L X52 steel. Indian Welding Journal 2015; 48(2): 68-75.

91. **Kumar R.,** Gupta S.K. and Pandey K.N. Multi-objective optimization of friction stir welding process parameters for joining of dissimilar AA5083/AA6063 aluminium alloys using hybrid approach. Proceedings of the Institution of Mechanical Engineers, Part L: Journal of Materials Design and Applications 2016.

92. **Kurt B.** The interface morphology of diffusion bonded dissimilar stainless steel and medium carbon steel couples. Journal of Materials Processing Technology 2007; 190 (1-3): 138-141.

93. **Kuzmenko V.G.** Effects of slag on formation of the surface of a weld. Automatic Welding 1985; 38(2): 32-35.

94. **Labanowski J.** Mechanical properties and corrosion resistance of dissimilar stainless steel welds. Archives of Material science and Engineering 2007; 28: 27-33.

95. **Lau T.**, Weatherly G.C. and McLean A. Gas/metal/slag reactions in submerged arc welding using $CaO\text{-}AI_2O_3$ based fluxes. Welding Research Supplement 1986: 31s-38s.

96. **Laukkanen A.**, Nevasmaa P., Ehrnstén U. and Rintamaa R. Mapping of characteristic features of bimetallic welds from the standpoint of engineering critical analysis. Transactions SMiRT 16, paper 1566, Washington DC, 2001.

97. **Lee C.S.**, Chandel R.S. and Seow H.P. Effect of welding parameters on the size of heat affected zone of submerged arc welding. Materials and Manufacturing Processes 2000; 15(5): 649-666.

98. **Leggatt R.H.** and Olden E.J. Variation of residual stresses in aged components (VORSAC), Final report, TWI report 88291/15/01, 2001.

99. **Liu S.** and Siewert T.A. Metal transfer in gas metal arc welding: Droplet rate. Welding Research Supplement February 1989: 53s-58s.

100. **Liu S.**, Frederickson G.L., Johnson M.Q. and Edwards G.R. Shielded Metal arc welding consumables for advanced high strength steels (HSLA-130 steel welding consumables). Center for Welding and Joining Research, Colorado School of Mines, 1994.

101. **Lundin C.D.** Dissimilar metal welds-transition joints literature review. Welding Journal 1982; 61(2): 58-63.

102. **Maruyama T.** Arc welding technology for dissimilar joint. Welding International 2003; 17(4): 276-281.

103. **Matsushita M.** and Liu S. Hydrogen control in steel weld metal by means of fluoride additions in welding flux. Welding Journal 2000; 79(10): 295s-303s.

104. **Meola C.**, Squillace A., Memola F., Minutolo C. and Morace R.E. Analysis of stainless steel welded joints a comparison between destructive and non-destructive techniques. Journal of Materials Processing Technology 2004; 155–156: 1893–1899.

105. **Mittal R.** and Sidhu B.S. Microstructures and mechanical properties of dissimilar T91/347H steel weldments. Journal of Materials Processing Technology 2015; 220: 76–86.

106. **Mitra U.** and Eagar T.W. Slag metal reactions during welding, Part: I, Evaluation and reassessment of existing theories. Metallurgical Transaction B 1991a; 22B: 65–71.

107. **Mitra U.** and Eagar T.W. Slag metal reactions during welding, Part: II, Theory. Metallurgical Transaction B 1991b; 22B: 73–81.

108. **Mitra U.** and Eagar T.W. Slag metal reactions during welding, Part: III, Verification of the theory. Metallurgical Transaction B 1991c; 22B: 83–100.

109. **Murugana N.** and Gunaraj V. Prediction and control of weld bead geometry and shape relationships in submerged arc welding of pipes. Journal of Materials Processing Technology 2005; 168: 478–487.

110. **Murugananth M.**, Babu S.S. and David S.A. Optimization of shielded metal arc weld metal composition for charpy toughness. Welding Journal October 2004: 267s-276s.

111. **Nadkarni S.V.** Modern arc welding technology, New Delhi: IBH publication, 1988.

112. **Naffakh H.**, Shamanian M. and Ashrafizadeh F. Dissimilar welding of AISI 310 austenitic stainless steel to nickel-based alloy Inconel 657. Journal of Materials Processing Technology 2009; 209: 3628–3639.

113. **Natalie C.A.**, Olson D.L. and Blande M. Physical and chemical behavior of welding fluxes. Annual review of Material Science 1986; 16: 389-413.

114. **Niagaj J.** An assessment of arc stability during welding with basic shielded electrodes. Welding International 2002; 16: 593-598.

115. **North T.H.**, Bell H.B., Nowicki A. and Craic I. Slag/Metal interaction, oxygen and toughness in submerged arc welding. Welding Journal 1978; 56(3): 63s-73s.

115a. **NPTEL** Lecture 35. Chemical reaction in welds I. http:// nptel.ac.in/courses/112107090/module8/lecture3/lecture3.pdf.

116. **Palm J.H.** How fluxes determine the metallurgical properties of submerged arc welds, Weld Journal 1972; 51(7): 358s-360s.

117. **Pan C.** and Zhang Z. Characteristics of weld interface in dissimilar austenitic-pearlitic steel welds. Material Characterization 1994; 33: 87-92.

118. **Pandey N.D.**, Bharti A. and Gupta S.R. Effect of submerged arc welding parameters and fluxes on element transfer behaviour and weld-metal chemistry. Journal of Materials Processing Technology 1994; 40: 195-211,

119. **Paniagua-Mercado A.M.** et al. Chemical and physical properties of fluxes for SAW of low carbon steels, 2011.

120. **Paniagua-Mercado A.M.** et al. Effect of active and non-active fluxes on the mechanical properties and microstructure in submerged arc weld of A-36 weld plates. Materials and Manufacturing Processes 2007; 22: 295-297.

121. **Paniagua-Mercado A.M.** et al. Influence of chemical composition of flux on the microstructure and tensile properties of submerged-arc welds. Journal of Materials Processing Technology 2005; 169: 346–351.

122. **Panigrahi S.K.**, Chakreverty S. and Saini H. Prediction of compressive strength using simplex lattice design for mix proportions in ternary systems of fly ash-cement-sand bricks. Indian Concrete Journal 2008; 82: 27-34.

123. **Panigrahi S.K.**, Chakreverty S. and Saini H. Prediction of product parameters of fly ash cement bricks using two dimensional orthogonal polynomials in the regression analysis. Computers and Concrete 2008; 5(5): 1-11.

124. **Parmar R.S.** Welding engineering and technology, Khanna Publisher, New Delhi.

125. **Patchett B.M.** and Yarmuch M.A.R. Hydrocarbon contamination and diffusible hydrogen levels in shielded metal arc weld deposits. Welding Journal 2010; 89: 262s-265s.

126. **Patchett B.M.** Some influences of slag composition on heat transfer and arc stability. Welding Journal 1974; 53(5): 203s-210s.

127. **Polar A.**, Indacochea J.E. and Blander M. Fundamentals of the chemical behaviour of selected welding fluxes. Welding Journal January 1991: 15–19.

128. **Price A.T.** CEGB experience with small diameter dissimilar metal welds in coal-fired boilers. In Proc. AWS/EPRI Conf. Joining Dissimilar Metals, Pittsburg, PA 1982: 48-79.

129. **Rathod D.W.**, Singh P.K., Pandey S. and Aravindan S. Effect of buffer-layered buttering on microstructure and mechanical properties of dissimilar metal weld joints for nuclear plant application. Materials Science & Engineering A 2016; 666: 100–113.

130. **Roberts D.I.**, Li C.C. and Nicholson R.D. Dissimilar-weld failure analysis and development program. Report CS-4252, Vol. 2, EPRI, Palo Alto, CA, 1985.

131. **Sacks R.J.** and Bohnart E.R. Welding: Principles and Practices/Edition 3. Publisher: McGraw-Hill Companies, 2004.

132. **Schwalbe K.H.**, Cornec A. and Lidbury D. Fracture mechanics analysis of the BIMET welded pipe tests. International Journal of Pressure Vessels and Piping 2004; 81: 251–277.

133. **Schwemmer D.D.** and Olson D.L. Relationship of weld penetration to welding fluxes. Welding Journal 1979; 58(5): 153s-160s.

134. **Sham K.** and Liu S. Flux coating development for SMAW consumable electrode of high nickel alloys. Welding Journal 2014; 8: 271s-281s.

135. **Sireesha M.**, Albert S.K. and Sundaresan S. Thermal cycling of joints between modified 9Cr-1Mo steel and Alloy 800 for steam generator application. International Journal of Pressure Vessels and Pipings 2002; 79: 819-827.

136. **Sireesha M.**, Albert S.K., Shankar V. and Sundaresan S. A comparative evaluation of welding consumables for dissimilar welds between 316LN austenitic stainless steel and Alloy 800. Journal of Nuclear Materials 2000; 279: 65-76.

137. **Sireesha M.**, Shankar V., Albert S.K. and Sundaresan S. Microstructural features of dissimilar welds between 316LN austenitic stainless steel and alloy 800. Materials Science and Engineering A 2000; 292(1): 74-82.

138. **Slaughter C.M.** and Housley T.R. The welding of ferritic steels to austenitic stainless steels. Welding Journal 1964; 43(10): 454s-460s.

139. **Srinivasan P.B.** and Satish Kumar M.P. Characterization of thin section dissimilar weld joint comprising austenitic and ferritic stainless steels. Materials Science and Technology 2008; 24 (4): 392-398.

140. **Srinivasan P.B.**, Muthupandi V., Dietzel W. and Sivan V. An assessment of impact strength and corrosion behaviour of shielded metal arc welded dissimilar weldments between UNS 31803 and IS 2062 steels. Materials and Design 2006; 27(3): 182-191.

141. **Suban M.** and Tusek J. Methods for the determination of arc stability. Journal of Materials Processing Technology 2003; 143–144: 430–437.

142. **Sudha C.**, Paul V.T., Terrance A.L.E., Saroja S. and Vijayalakshmi M. Microstructure and microchemistry of hard zone in dissimilar weldments of Cr-Mo steels. Welding Journal 2006; 85(4): 71s-80s.

143. **Sudha C.**, Terrance A.L.E., Albert S.K. and Vijayalakshmi M. Systematic study of formation of soft and hard zones in dissimilar weldments of Cr-Mo steels. Journal of Nuclear Materials 2002; 302: 193–205.

144. **Sun Z**. Feasibility of producing ferritic/austenitic dissimilar metal joints by high energy density laser beam process. International Journal of Pressure Vessel and Piping 1996; 68: 153-160.

145. **Surian E.** and Vedia L.A. All weld metal design for AWS E10018M, E11018M and E12018M type electrodes. Welding Research Supplement June 1999: 217s-228s.

146. **Surian E.** ANSI/AWS E7024 SMAW electrodes: The effect of coating magnesium additions. Welding Journal Research Supplement October 1997: 404s-411s.

147. **Surian E.** Influence of molybdenum on ferritic high strength SMAW all-weld-metal properties. Supplement to Welding Research; 2005: 53s-62s.

148. **Tarlinsku.** The effect of viscosity of slag on the welding and technological properties of electrodes. Svar. Proiz. 1980; 9: 21-22.

149. **Tucker J.T.** and Eberle F. Development of a ferritic-austenitic weld joint for steam plant applications. Welding Journal 1956, 35(11): 529s-540s.

150. **Tuliani S.S.**, Boniszewski T. and Eaton N.F. Carbonate fluxes for submerged arc welding of mild steel. Welding and Metal Fabrication 1972; 40(7): 247-250.

151. **TWI Connect No. 103**. Defects – solidification cracking, TWI Job knowledge for welders 44, 1999.

152. **Viswanathan R.**, Jaffee R.I. and Dimmer J. Dissimilar metal welds in power plants. In: Proceedings of AWS/EPRI Conference on Joining of dissimilar metals, Pittsburgh, PA, 1982: 7–27.

153. **Vornovitskii I.N.**, Malashonok V.A. and Cherkasskii, A.L. Procedure for quantitative evaluation of slag detachability. Svarochn. Proizvodstvo 1975; 2: 47–48.

154. **Vornovitskii I.N.**, Medvedev A.Z. and Cherkasskii, A.L. Influence of coefficient of thermal expansion of slag on its detachability from weld metal. Svarochn. Proizvodstvo 1973; 3:35–37.

155. **Wang S.**, Ma Q. and Li Y. Characterization of microstructure, mechanical properties and corrosion resistance of dissimilar welded joints between 2205 duplex stainless steel and 16MnR. Materials and Design 2011; 32(2): 831–837.

156. **Waszink J. H.** and Piena M. J. Thermal processes in covered electrodes. Welding Journal 1985; 64(2): 37s- 48s.

157. **Weymueller C.R.** Electrodes and fluxes needed: speed, quality. Welding Design and Fabrication 1981; 6: 56-64.

158. **Witting, L.** Some physical and chemical properties of welding slag and their influence on slag detachability. Proceedings of International Conference on Weld Pool Chemistry and Metallurgy, Cambridge, England, The Welding Institute. 1980: 83-90.

159. **Yusufzai M.Z.K.** and Dewangan R. Development of submerged arc welding flux using red mud. International Conference on Agile Manufacturing, IIT BHU, Varanasi, 2012.

160. **Yusufzai M.Z.K.,** Singh G. and Kumar V. Effect of process parameters of gas metal arc welding on dilution in cladding of stainless steel on mild Steel. International Journal of Mechanical Engineering 2012; 2: 127-131.

APPENDIX

(a) (b)

Figure A.1 Impact specimens of SA516.

(a) (b)

Figure A.2 Impact specimens of SS304L.

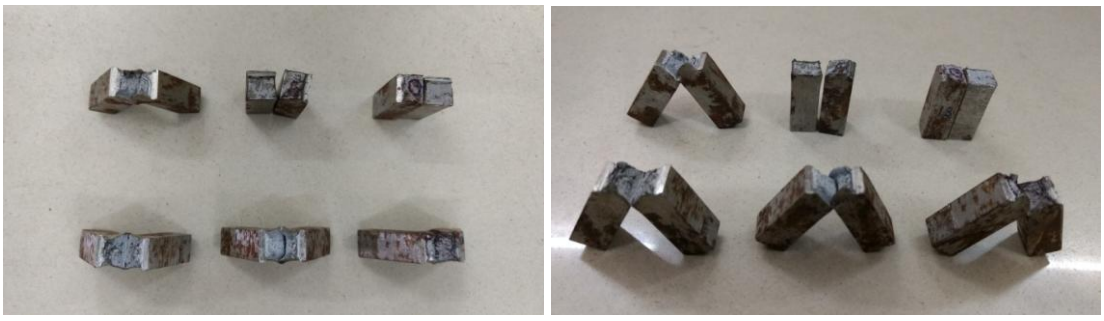

(a) (b)

Figure A.3 Impact specimens of MS buttering layer.

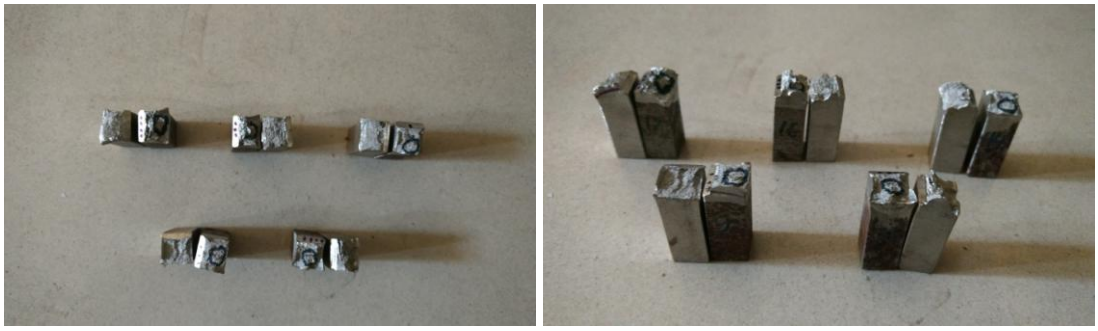

(a) (b)

Figure A.4 Impact specimens of welds (two layer methodology).

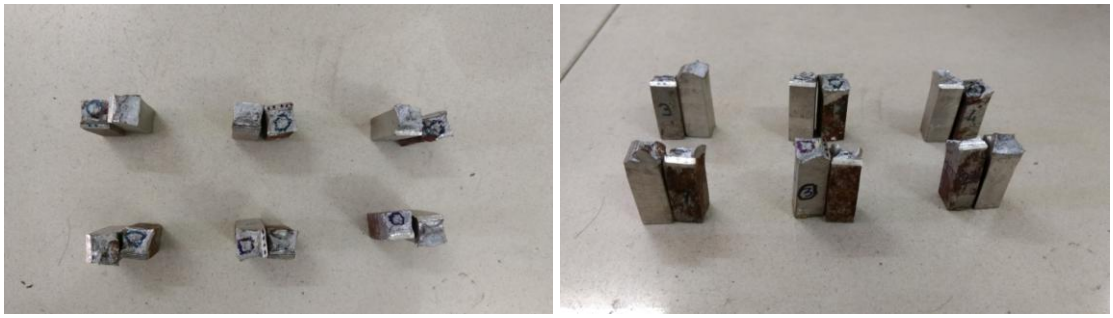

(a) (b)

Figure A.5 Impact specimens of welds (three layer methodology).

(a) (b)

Figure A.6 Tensile specimens of SA516.

Figure A.7 Tensile specimens of MS buttering electrode.

Figure A.8 Tensile specimens of SS304L.

Figure A.9 Tensile specimens of welds (three layer methodology).